DESY-THESIS-2012-039
Juli 2012

arXiv:1307.3887v1 [hep-ph] 15 Jul 2013

The $B-L$ Phase Transition

Implications for Cosmology and Neutrinos

Dissertation

zur Erlangung des Doktorgrades

des Departments Physik

der Universitt Hamburg

vorgelegt von

Kai Schmitz

aus Berlin

Hamburg

2012

Gutachter der Dissertation:	Prof. Dr. Wilfried Buchmüller Prof. Dr. Mark Hindmarsh Prof. Dr. Günter Sigl
Gutachter der Disputation:	Prof. Dr. Wilfried Buchmüller Prof. Dr. Jan Louis
Datum der Disputation:	9. Juli 2011
Vorsitzender des Prfungsausschusses:	Prof. Dr. Georg Steinbrück
Vorsitzender des Promotionsausschusses:	Prof. Dr. Peter Hauschildt
Dekan der Fakultt fr Mathematik, Informatik und Naturwissenschaften:	Prof. Dr. Heinrich Graener

Abstract

We investigate the possibility that the hot thermal phase of the early universe is ignited in consequence of the $B-L$ phase transition, which represents the cosmological realization of the spontaneous breaking of the Abelian gauge symmetry associated with $B-L$, the difference between baryon number B and lepton number L. Prior to the $B-L$ phase transition, the universe experiences a stage of hybrid inflation. Towards the end of inflation, the false vacuum of unbroken $B-L$ symmetry decays, which entails tachyonic preheating as well as the production of cosmic strings. Observational constraints on this scenario require the $B-L$ phase transition to take place at the scale of grand unification. The dynamics of the $B-L$ breaking Higgs field and the $B-L$ gauge degrees of freedom, in combination with thermal processes, generate an abundance of heavy (s)neutrinos. These (s)neutrinos decay into radiation, thereby reheating the universe, generating the baryon asymmetry of the universe and setting the stage for the thermal production of gravitinos. The $B-L$ phase transition along with the (s)neutrino-driven reheating process hence represents an intriguing and testable mechanism to generate the initial conditions of the hot early universe. We study the $B-L$ phase transition in the full supersymmetric Abelian Higgs model, for which we derive and discuss the Lagrangian in arbitrary and unitary gauge. As for the subsequent reheating process, we formulate the complete set of Boltzmann equations, the solutions of which enable us to give a detailed and time-resolved description of the evolution of all particle abundances during reheating. Assuming the gravitino to be the lightest superparticle (LSP), the requirement of consistency between hybrid inflation, leptogenesis and gravitino dark matter implies relations between neutrino parameters and superparticle masses, in particular a lower bound on the gravitino mass of 10 GeV. As an alternative to gravitino dark matter, we consider the case of very heavy gravitinos, which are motivated by hints for the Higgs boson at the LHC. We find that the nonthermal production of pure wino or higgsino LSPs, i.e. weakly interacting massive particles (WIMPs), in heavy gravitino decays can account for the observed amount of dark matter, while simultaneously fulfilling the constraints imposed by primordial nucleosynthesis and leptogenesis, within a range of LSP, gravitino and neutrino masses. Besides its cosmological implications, the spontaneous breaking of $B-L$ also naturally explains the small observed neutrino masses via the seesaw mechanism. Upon the seesaw model we impose a flavour structure of the Froggatt-Nielson type which, together with the known neutrino data, allows us to strongly constrain yet undetermined neutrino observables.

Zusammenfassung

Wir untersuchen die Möglichkeit, dass die heiße thermische Phase des frühen Universums in Folge des $B-L$ Phasenübergangs, welcher die kosmologische Umsetzung der spontanen Brechung der mit $B-L$, der Differenz von Baryonenzahl B und Leptonenzahl L, verknüpften Abelschen Eichsymmetrie darstellt, enzündet wird. Vor dem $B-L$ Phasenübergang durchlebt das Universum einen Abschnitt der Hybridinflation, gegen deren Ende das falsche Vakuum ungebrochener $B-L$ Symmetrie zerfällt, was tachyonisches Vorheizen sowie die Produktion kosmischer Strings nach sich zieht. Aus Beobachtungen gewonnene Einschränkungen dieses Szenarios erfordern es, dass der $B-L$ Phasenübergang bei der Skala der Großen Vereinheitlichung stattfindet. Die Dynamik des $B-L$ brechenden Higgsfeldes und der $B-L$ Eichfreiheitsgrade, zusammen mit thermischen Prozessen, generiert ein Vorkommen an schweren (S)neutrinos. Diese (S)neutrinos zerfallen in Strahlung, wodurch sie das Universum aufheizen, die Baryonenasymmetrie des Universums erzeugen und der thermischen Produktion von Gravitinos den Weg ebnen. Der $B-L$ Phasenübergang stellt folglich mitsamt dem (S)neutrinogetriebenen Aufheizprozess einen überzeugenden und testbaren Mechanismus zur Erzeugung der Anfangsbedingungen des heißen frühen Universums dar. Wir studieren den $B-L$ Phasenübergang im vollständigen supersymmetrischen Abelschen Higgsmodel, für welches wir die Lagrangedichte in beliebiger und unitärer Eichung herleiten und diskutieren. In Hinblick auf den anschließenden Aufheizprozess formulieren wir den kompletten Satz an Boltzmanngleichungen, deren Lösungen uns zu einer detaillierten und zeitaufgelösten Beschreibung aller Teilchenhäufigkeiten verhelfen. Angenommen, das Gravitino ist das leichteste Superteilchen (LSP), so impliziert die Forderung nach Konsistenz zwischen Hybridinflation, Leptogenese und Gravitino-Dunkler-Materie Beziehungen zwischen Neutrinoparametern und Superteilchenmassen, insbesondere eine untere Schranke an die Gravitinomasse von 10 GeV. Als Alternative zu Gravitino-Dunkler-Materie betrachten wir den Fall sehr schwerer Gravitinos, die durch Hinweise auf das Higgs-Boson am LHC motiviert sind. Wir stellen fest, dass die nichtthermische Produktion reiner Wino- oder Higgsino-LSPs, d.h. schwach wechselwirkender massereicher Teilchen (WIMPs), in den Zerfällen schwerer Gravitinos für die beobachtete Menge an Dunkler Materie innerhalb einer Bandbreite von LSP-, Gravitino- und Neutrinomassen aufkommen und zugleich den von primordialer Nukleosynthese und Leptogenese auferlegten Einschränkungen genügen kann. Abgesehen von ihren kosmologischen Auswirkungen, erklärt die spontane $B-L$ Brechung auch in natürlicher Weise die kleinen beobachteten Neutrinomassen vermöge des Seesaw-Mechanismus. Wir erlegen dem Seesaw-Model eine Flavour-Struktur vom Froggatt-Nielsen-Typ auf, welche es uns zusammen mit den bekannten Neutrinodaten erlaubt, bislang unbestimmte Neutrinoobservablen stark einzuschränken.

Contents

Abstract iii

Zusammenfassung v

Contents vii

List of Figures x

1 Introduction 1

2 Early Universe Cosmology 9

2.1 Composition of the Universe 10

2.1.1 CMB Photons 10

2.1.2 Relic Neutrinos 11

2.1.3 Baryonic Matter 13

2.1.4 Dark Matter 15

2.1.5 Dark Energy 17

2.1.6 Stages in the Expansion History 19

2.2 The Hot Thermal Phase 21

2.2.1 The Cosmic Microwave Background 21

2.2.2 Primordial Nucleosynthesis 25

2.2.3 Phase and Topological Transitions 28

3 Framework for a Consistent Cosmology 33

3.1 Beyond the Standard Model 34

3.1.1 Inflation . . . 34
3.1.2 Right-Handed Neutrinos and the Seesaw Mechanism . . . 40
3.1.3 Baryogenesis . . . 45
3.1.4 Particle Candidates for Dark Matter . . . 49
3.2 SSB of $B-L$ as the Origin of the Hot Early Universe . . . 54
3.2.1 Reheating through Heavy (S)neutrino Decays . . . 55
3.2.2 Froggatt-Nielsen Flavour Structure . . . 58

4 Neutrino Phenomenology **65**
4.1 Monte-Carlo Sampling of $\mathcal{O}(1)$ Factors . . . 66
4.2 Predictions for Neutrino Observables . . . 69
4.3 Analytic Derivation of the Majorana Phase α_{21} . . . 75

5 Supersymmetric Abelian Higgs Model **77**
5.1 Before Spontaneous Symmetry Breaking . . . 78
5.1.1 From Superspace to the Component Lagrangian . . . 78
5.1.2 General Lagrangian in Arbitrary Gauge . . . 86
5.1.3 Gauge and Mass Eigenstates . . . 87
5.2 During and After Spontaneous Symmetry Breaking . . . 92
5.2.1 Lagrangian of the SSB Sector in Unitary Gauge . . . 92
5.2.2 Physical Degrees of Freedom and Time-Dependent Masses . . . 93
5.2.3 Decay Rates and Branching Ratios . . . 98

6 Nonperturbative Dynamics **103**
6.1 Production of Cosmic Strings . . . 104
6.2 Tachyonic Preheating . . . 108

7 The Reheating Process **115**
7.1 Boltzmann Equations . . . 116
7.1.1 Symmetry-Breaking Sector . . . 117
7.1.2 Neutrino Sector . . . 119
7.1.3 MSSM Degrees of Freedom . . . 127

7.1.4 Gravitinos . . . 133
7.2 Time Evolution of the Particle Abundances . . . 134
7.2.1 Particle Masses and Couplings . . . 134
7.2.2 Decay of the Massive Particles . . . 135
7.2.3 Reheating and the Temperature of the Thermal Bath . . . 139
7.2.4 Small Departures from Thermal Equilibrium . . . 143
7.2.5 Robustness against Theory Uncertainties . . . 147
7.3 Scan of the Parameter Space . . . 151
7.3.1 Reheating Temperature . . . 153
7.3.2 Baryon Asymmetry . . . 155
7.3.3 Gravitino Dark Matter . . . 159

8 WIMP Dark Matter from Heavy Gravitino Decays 165
8.1 Thermal and Nonthermal Neutralino Production . . . 166
8.2 Relations between Neutralino, Gravitino and Neutrino Masses . . . 168
8.3 Prospects for Direct Detection and Collider Experiments . . . 172

9 Conclusions and Outlook 173

Acknowledgements 179

A Statistical Thermodynamics 181
A.1 Kinetic Theory in the Expanding Universe . . . 181
A.2 Kinetic and Thermal Equilibrium . . . 183

B *CP* Violation in 2-to-2 Scattering Processes 187

C Thermal Gravitino Production 191

Bibliography 197

List of Figures

2.1 Timeline of the hot thermal phase of the early universe 21

4.1 Neutrino mixing angles θ_{13} and θ_{23}. 70
4.2 Lightest neutrino mass m_1 and effective neutrino mass in tritium decay m_β . 71
4.3 Effective neutrino mass in $0\nu\beta\beta$ decay $m_{0\nu\beta\beta}$ and Majorana phase α_{21} 72
4.4 Effective neutrino mass $\widetilde{m}_1$ and CP violation parameter ϵ_1 73

5.1 Particle spectrum and interactions after spontaneous $B-L$ breaking 94

7.1 Comoving number and energy densities 136
7.2 Breakdown of the comoving number densities 138
7.3 Temperature of the thermal bath and lepton asymmetry 141
7.4 Comoving number densities after slight theoretical modifications 148
7.5 Contour plot of the reheating temperature 153
7.6 Contour plot of the baryon asymmetry 156
7.7 Relations between neutrino parameters and the gravitino mass 160

8.1 Lower bounds on M_1 and $T_{\rm RH}$ as functions of $\widetilde{m}_1$ 168
8.2 Upper and lower bounds on $T_{\rm RH}$ as functions of $\widetilde{m}_1$ and $m_{\widetilde{G}}$ 169
8.3 Upper and lower bounds on $m_{\rm LSP}$ and lower bounds on $m_{\widetilde{G}}$. 170
8.4 Upper bounds on $m_{\rm LSP}$ and lower bound on $m_{\widetilde{G}}$ as functions of $\widetilde{m}_1$ 171

C.1 C_1 and C_2 as functions of $T_{\rm RH}$ 193
C.2 Rescaling prescription for the gravitino mass 194

Chapter 1

Introduction

The cosmic microwave background (CMB) radiation [1] and the primordial abundances of the light nuclei [2] provide direct evidence for a hot thermal phase in the early universe. While the CMB represents a full-sky picture of the hot early universe close to its minimal temperature, primordial nucleosynthesis allows us to probe the history of the universe up to the first tenth of a second after the big bang. Going further back in time, beyond the generation of the light elements, the theoretical extrapolation becomes increasingly uncertain. Up to temperatures slightly above the electroweak scale, we are still able to make an educated guess about the evolution of the universe based on the established and well-tested physics of the standard model of particle physics. At temperatures around the scale of quantum chromodynamics (QCD), we thus expect the occurrence of a phase transition, in the course of which quarks and gluons become confined into hadrons. Similarly, one presumes a phase transition around the electroweak scale, which causes the Higgs boson, the electroweak gauge bosons as well as all fermions expect for neutrinos to acquire a mass via the Higgs mechanism. If indeed realized in the early universe, the electroweak phase transition would correspond to the cosmological implementation of electroweak symmetry breaking. Meanwhile, in anticipation of new insights from observations and experiments as to the physics beyond the standard model, we are at present merely able to speculate about the nature of the processes taking place at even higher energy scales. While the conclusive identification of a successor to the standard model is still pending, we know for sure that some processes must occur in the very early universe, which cannot be accounted for by the known laws of physics.

A clear indication for physics beyond the standard model is the present composition of the universe [2]. First of all, it is astonishing that all matter in the universe which can be more or less well described by standard model physics seems to be almost exclusively made out of baryons and hardly out of antibaryons. This cosmic asymmetry between matter and antimatter calls for a nonequilibrium process in the hot early universe, in which a primordial baryon asymmetry is generated before baryons and antibaryons decouple from the hot

plasma. Furthermore, as ordinary matter contributes with only 5 % to the energy budget of the universe, we are led to the conclusion that 95 % of the energy of the universe reside in unknown forms of matter and energy, *viz.* dark matter and dark energy. Dark matter, which encompasses 27 % of the total energy of the universe, is able to clump under the influence of the gravitational force and thus plays a crucial role in the theory of structure formation. Studies of the cosmic density perturbations, seen for instance in the CMB [1] or the distribution of galaxies in the neighbourhood of the Milky Way [3], imply that dark matter has to be present in the early universe long before the end of the hot thermal phase. Barring a modification of general relativity, the remaining 73 % of the energy of the universe have to be attributed to some form of dark energy, which is commonly identified as the energy of the vacuum and as such explained in terms of a cosmological constant Λ. Further evidence for new physics derives from the properties of the CMB. The minute temperature anisotropies of the CMB exhibit correlations on scales exceeding the sound horizon at the time of photon decoupling and thus point to a mechanism in the very early universe capable of generating primordial metric fluctuations with super-horizon correlations. Finally, on the particle physics side, the flavour oscillations among the three standard model neutrino species [4, 5] represent the clearest evidence for physics beyond the standard model. These oscillations indicate that neutrinos have tiny, but nonzero masses, although the standard model stipulates them to be massless.

The most popular solution to the problem of the primordial density perturbations as well to other puzzles related to the initial conditions of big bang cosmology is inflation [6–8]—a stage of accelerated expansion in the very early universe driven by the energy of the vacuum. During inflation, the quantum fluctuations of a scalar field, the so-called inflaton field, are stretched to super-horizon scales, whereupon they freeze, remaining basically unchanged in shape until the onset of structure formation. The dynamics of the inflaton field correspond to those of an ensemble of inflaton particles in a coherent quantum state at zero temperature. Assuming inflation to be the source of the primordial perturbations, one arrives at the question as to the origin of the entropy of the hot plasma filling the universe during the thermal phase. In summary, we conclude that contemporary particle cosmology faces the task to explain the origin of the hot early universe as well as its initial conditions, i.e. the entropy of the thermal bath, the primordial baryon asymmetry and the abundance of dark matter.

In this thesis, we put forward the idea that the emergence of the hot thermal universe might be closely related to the decay of a false vacuum of unbroken $B-L$ symmetry, where $B-L$ denotes the difference between baryon number B and lepton number L. In such a scenario, the energy of the false vacuum drives a stage of hybrid inflation [9, 10], ending in a phase transition, in the course of which the Abelian gauge symmetry $U(1)_{B-L}$ becomes spontaneously broken. Guided by the expectation that phase transitions might be in fact common phenomena in the early universe, we hence propose that also the very origin of the hot

thermal phase has to be attributed to a phase transition, *viz.* the $B-L$ phase transition as we shall refer to it from now on. To be very clear about this point, we stress that the $B-L$ phase transition represents the cosmological realization of spontaneous $B-L$ breaking, similarly as the electroweak phase transition represents the cosmological realization of electroweak symmetry breaking.

Hybrid inflation ending in the spontaneous breaking of a local symmetry is an attractive scenario of inflation, as it establishes a connection between cosmology and particle physics. The symmetry breaking at the end of inflation may, in particular, be identified as an intermediate stage in the breaking of the gauge group of some theory of grand unification (GUT) down to the gauge group of the standard model. In this sense, the $B-L$ phase transition may be easily embedded into a grander scheme based on a GUT theory featuring $B-L$ as an additional gauge symmetry. A prime example in this context are GUT theories with gauge group $SO(10)$ [11]. We also note that incorporating $B-L$ into the gauge group of the theory is an almost trivial extension of the standard model. As it turns out, the global $U(1)_{B-L}$ is already an anomaly-free symmetry of the standard model Lagrangian [12, 13]. Upon the introduction of three generations of right-handed neutrinos, it is then readily promoted to a local symmetry [14, 15]. Unfortunately, the statistical properties of the CMB temperature anisotropies rule out the simplest nonsupersymmetric version of hybrid inflation [1]. For this reason we will consider supersymmetric F-term hybrid inflation [16, 17] in this thesis. Apart from its usual inner-theoretical and aesthetic virtues, including supersymmetry into our analysis also has an important phenomenological advantage. Invoking a discrete symmetry such as matter [18] or R parity [19] renders the lightest superparticle (LSP) stable, turning it into an excellent particle candidate for dark matter [20–22]. Moreover, supersymmetry implies that each right-handed neutrino pairs up with a complex scalar to form a chiral multiplet. In the course of the $B-L$ phase transition, these neutrino multiplets acquire Majorana mass terms, such that after symmetry breaking the physical neutrino states consist of three heavy Majorana neutrinos N_i and three heavy complex sneutrinos $\tilde{N}_i$. The $B-L$ phase transition hence also sets the stage for the seesaw mechanism [23–27], which elegantly explains the tiny masses of the standard model neutrinos.

The decay of the false vacuum at the end of hybrid inflation is accompanied by tachyonic preheating [28, 29] and the production of topological defects in the form of cosmic strings [30–32]. Successful hybrid inflation in combination with the nonobservation of cosmic strings requires that the $B-L$ phase transition indeed has to take place at the GUT scale [33, 34]. Tachyonic preheating denotes the rapid transfer of the false vacuum energy into a gas of nonrelativistic $B-L$ Higgs bosons, entailing the nonadiabatic production of all particles coupled to the Higgs field [35]. After the $B-L$ phase transition the energy density of the universe is dominated by the abundance of Higgs bosons, which slowly decay into heavy neutrinos and sneutrinos. In combination with tachyonic preheating, the dynamics of the

$B-L$ gauge degrees of freedom (DOFs) as well as thermal processes, the decay of the Higgs boson and its superpartners produces an abundance of heavy (s)neutrinos. These (s)neutrinos subsequently decay into radiation, thereby generating the entropy of the hot thermal phase, i.e. reheating the universe.

Hence, an important consequence of the $B-L$ phase transition is that the reheating process is driven by the decay of the heavy (s)neutrinos. This in turn automatically yields baryogenesis via a mixture of nonthermal and thermal leptogenesis [36]. Our work is thus closely related to previous studies on thermal leptogenesis [37, 38] as well as on nonthermal leptogenesis via inflaton decay [39–42]. Furthermore, the fact that the reheating process is (s)neutrino-driven results in the temperature scale of reheating, i.e. the reheating temperature, being determined by the (s)neutrino lifetime and therefore directly related to (s)neutrino parameters. Of course, the final baryon asymmetry is also determined by (s)neutrino parameters and so we arrive at the remarkable conclusion that the initial conditions of the hot early universe cannot be freely chosen, but are fully controlled by the parameters of a Lagrangian, which could in principle be measured by particle physics experiments and astrophysical observations. The $B-L$ phase transition is hence not only a particularly simple mechanism for the generation of the initial conditions of the hot early universe, it is also testable in present-day and future experiments.

Assuming supersymmetry to be a local symmetry, the particle spectrum also features the gravitino—the spin-3/2 superpartner of the spin-2 graviton, which acts as the gauge field of local supersymmetry transformations. Due to the high reheating temperatures reached after the $B-L$ phase transition, thermal gravitino production during the reheating process is unavoidable [43, 44]. Depending on the superparticle mass spectrum, this may lead to various cosmological problems. As for a light stable gravitino, inelastic scatterings in the thermal bath may produce the gravitino so efficiently that it overcloses the universe. Meanwhile, the late-time decay of an unstable gravitino may alter the abundances of the light elements and thus spoil the successful theory of big bang nucleosynthesis (BBN) [45–49]. To avoid these problems, we will consider two particular superparticle mass spectra in this thesis. In the first case, we will assume the gravitino to be the LSP with a mass of $\mathcal{O}(10..100)\,\mathrm{GeV}$, as it typically arises in scenarios of gravity- or gaugino-mediated supersymmetry breaking. Gravitino dark matter can then be thermally produced at a reheating temperature compatible with leptogenesis [50]. In the second case, we will take the gravitino to be the heaviest superparticle with a mass of $\mathcal{O}(10..1000)\,\mathrm{TeV}$. Such large gravitino masses are realized in anomaly mediation, which is a promising scenario of supersymmetry breaking, given the recent hints by the LHC experiments ATLAS and CMS that the Higgs boson may have a mass of about 125 GeV [51, 52]. A gravitino heavier than roughly 10 TeV can be consistent with primordial nucleosynthesis and leptogenesis [45, 53, 54], thus allowing us to circumvent all cosmological gravitino problems. In our second scenario, the nonthermal production of pure wino or higgsino LSPs, i.e. weakly interacting massive particles (WIMPs), in the decay

of heavy, thermally produced gravitinos accounts for the relic density of dark matter.

In this thesis, we study the $B-L$ phase transition in the full supersymmetric Abelian Higgs model, for which derive the complete Lagrangian in arbitrary and unitary gauge. From this Lagrangian, we cannot only infer the decay rates of all particles under study, but also read off how the corresponding mass eigenvalues evolve with time in the course of spontaneous symmetry breaking. These time-dependent masses are an important input to the calculation of the particle abundances produced during tachyonic preheating. In order to describe the reheating process subsequent to the $B-L$ phase transition, we derive the Boltzmann equations for all particle species of interest. To facilitate our calculations, we treat the various contributions to the respective heavy (s)neutrino abundances separately, i.e. we formulate a separate Boltzmann equation for each contribution. Thanks to this novel technical procedure, we are able to solve a subset of Boltzmann equations analytically. Solving the remaining equations numerically, we obtain a detailed and time-resolved picture of the evolution of all particle abundances during reheating. An interesting result of our analysis is that the competition between cosmic expansion and entropy production leads to an intermediate period of constant reheating temperature, during which the baryon asymmetry as well as the thermal gravitino abundance are produced. The final results for these two quantities as well as the reheating temperature turn out to be rather insensitive to the influence of the extra superparticles not contained in the supersymmetric standard model. Likewise, the decay of the $B-L$ gauge DOFs shortly after preheating hardly affects the final outcomes of our calculations. Based on these observations, we conclude that the investigated scenario of reheating is quite robust against uncertainties in the underlying theoretical framework.

Successful hybrid inflation and leptogenesis constrain the viable range of neutrino mass parameters. Combining these constraints with the requirement that dark matter be made out of gravitinos, we find relations between neutrino parameters and superparticle masses, in particular a lower bound on the gravitino mass of 10 GeV. Similarly, we infer relations between the masses of the dark matter particle, the gravitino and the standard model neutrinos in the case of WIMP dark matter. Requiring consistency between hybrid inflation, leptogenesis, dark matter and BBN, we derive upper and lower bounds on the LSP mass as well as lower bounds on the gravitino mass, all of which depend on the lightest neutrino mass. For instance, given that the lightest neutrino has a mass of 0.05 eV, a higgsino LSP would have to be lighter than 900 GeV, while the gravitino would need to have a mass of at least 10 TeV.

Our quantitative analysis of the reheating process by means of Boltzmann equations is based on a flavour model [55] of the Froggatt-Nielsen type [56]. Generally speaking, Froggatt-Nielsen flavour models are able to reconcile the large quark and charged-lepton mass hierarchies and the small quark mixing angles with the observed small neutrino mass hierarchies and the large neutrino mixing angles in a natural way. In this thesis, we point out that the Froggatt-Nielsen flavour structure, which we employ for our analysis, together with the

known neutrino data, strongly constrains yet undetermined parameters of the neutrino sector. Treating unknown $\mathcal{O}(1)$ parameters as random variables, we obtain surprisingly sharp predictions for the smallest mixing angle, $\sin^2(2\theta_{13}) = 0.07^{+0.11}_{-0.05}$, the smallest neutrino mass, $m_1 = 2.2^{+1.7}_{-1.4} \times 10^{-3}$ eV, and one Majorana phase, $\alpha_{21}/\pi = 1.0^{+0.2}_{-0.2}$.

This thesis is organized as follows. In Ch. 2, we briefly review the basics of early universe cosmology, which we require as background material for our further discussion. We outline how the present composition of the universe calls for new physics beyond the standard model, discuss the main observational evidence for the hot thermal phase in the early universe, i.e. the CMB and BBN, and shortly touch on the other phase transitions, which we expect to take place in the early universe, i.e. the QCD and the electroweak phase transition. Finally, we review the electroweak sphaleron process, which is a crucial ingredient to leptogenesis. The reader acquainted with these rudiments of particle cosmology is invited to skip our introductory chapter and directly proceed with Ch. 3.

In Ch. 3, we develop a theoretical framework for a consistent cosmology, which addresses most of the problematic issues alluded to in Ch. 2. First, we motivate supersymmetric F-term hybrid inflation as an attractive inflationary scenario and compile several useful formulae, which we need for our later analysis of the production of cosmic strings. Then we turn to the seesaw mechanism and the right-handed neutrinos. We introduce the superpotential for all quark and lepton superfields and subsequently use it to derive the mass and mixing matrices in the lepton sector. Next, we motivate leptogenesis as the most promising scenario of baryogenesis and elaborate on the two superparticle mass spectra, which we consider in this thesis. In the latter part, we particularly emphasize how the spectra under study circumvent the cosmological gravitino problems. Finally, we assemble all pieces of the puzzle and outline how the $B-L$ phase transition at the end of inflation gives rise to a consistent cosmology. We summarize all mechanisms for the production of particles during preheating and reheating and illustrate how the fact that the reheating process is driven by the decay of heavy (s)neutrinos directly implies relations between neutrino and superparticle masses. In conclusion, we present our Froggatt-Nielsen flavour structure and parametrize our entire model in terms of flavour charges.

In Ch. 4, we employ Monte-Carlo techniques to study the dependence of yet undetermined neutrino observables on the unknown $\mathcal{O}(1)$ factors contained in the Froggatt-Nielsen model. After a few technical remarks on our procedure, we list the surprisingly precise predictions for the various parameters in the neutrino sector and demonstrate that we are partly even able to reproduce them analytically.

In Ch. 5, we lay the theoretical foundation for our study of the $B-L$ phase transition and the subsequent reheating process. To be able to describe the dynamics of all physical particle species after spontaneous symmetry breaking, we require the Lagrangian of the supersymmetric Abelian Higgs model in unitary gauge. In a first step, we therefore derive the Lagrangian

of a general supersymmetric Abelian gauge theory in arbitrary gauge. Then we evaluate this Lagrangian in unitary gauge for our specific field content, which readily provides us with all time-dependent mass eigenvalues and decay rates that we require for our further analysis.

In Ch. 6, we discuss the nonperturbative dynamics during the decay of the false vacuum of unbroken $B-L$. First, we estimate the abundance of cosmic strings produced during the $B-L$ phase transition and restrict the parameters of hybrid inflation based on the requirement of successful inflation and the fact that no observational indications of effects related to cosmic strings have been found so far. In the second section of Ch. 6, we introduce the quench approximation for the waterfall transition at the end of hybrid inflation and generalize the common waterfall conditions [10], which only apply to the original, nonsupersymmetric variant of hybrid inflation, to the supersymmetric case. Furthermore, we compute the particle abundances generated during preheating.

In Ch. 7, we study the reheating process subsequent to the $B-L$ phase transition by means of Boltzmann equations. For a series of particle species, we first formulate template Boltzmann equations serving as proxies for their actual Boltzmann equations. After solving these template equations analytically and in full generality, we then apply our findings to our actual scenario. Moreover, we develop techniques to describe the evolution of the gravitational background analytically and to track the evolution of the temperature of the hot plasma by means of its own Boltzmann equation. In the next section, assuming the gravitino to be the LSP, we present the solutions of the Boltzmann equations for a representative choice of parameter values. Apart from a comprehensive discussion of the evolution of all particle abundances, we motivate a particular definition of the reheating temperature and check the robustness of the reheating process against small changes in the theoretical setup. In the third section of Ch. 7, we finally carry out a scan of the parameter space, from which we infer relations between neutrino and superparticle masses. To some extent, we are again able to reproduce our results analytically. For all important quantities we provide useful fit formulae.

In Ch. 8, we consider the production of WIMP dark matter in the decay of heavy, thermally produced gravitinos. After a short comment on the competition between our nonthermal WIMP production mechanism and thermal WIMP freeze-out, we present constraints on the neutralino, gravitino and neutrino masses and sketch the prospects for the experimental confirmation of our scenario.

In Ch. 9, we conclude and summarize our results. Furthermore, we give an outlook as to the possible directions into which the analysis presented in this thesis could be extended. The three appendices contain important supplementary material. In App. A, we summarize the formalism of Boltzmann equations and discuss the properties of particle species in kinetic and thermal equilibrium. In App. B, we provide the proof for an important relation, which is needed in the derivation of the Boltzmann equation for the lepton asymmetry and which is related to the CP violation in 2-to-2 scattering processes with heavy (s)neutrinos in the

intermediate state. In App. C, we derive an analytical expression for the abundance of thermally produced gravitinos and illustrate how our quantitative discussion in Ch. 7 is easily generalized to gluino masses other than the one we employ in our analysis.

The discussion in Chs. 4, 7 and 8 is based on two projects in collaboration with Wilfried Buchmüller and Gilles Vertongen as well as on three projects in collaboration with Wilfried Buchmüller and Valerie Domcke, the results of which were respectively first published in Refs. [57, 58] and Refs. [59–61].

Chapter 2

Early Universe Cosmology

The main intention of this thesis is to motivate and investigate the $B-L$ phase transition as the possible origin for the thermal phase of the hot early universe. Before we are ready to do so, we have to acquaint ourselves with the observational evidence for this phase and understand which physical processes have or may have taken place in it. For this reason we shall provide a brief review of early universe cosmology in this chapter, thereby compiling the background material for the further discussion. We will first discuss the present composition of the universe (cf. Sec. 2.1) and then some of the main events in the thermal history of the universe in reverse chronological order (cf. Sec. 2.2). We would like to emphasize that in this introductory chapter we will crudely restrict ourselves to aspects which are relevant for our purposes. More balanced and comprehensive presentations of the topic are for instance provided in standard textbooks [62–64] or dedicated review articles [2, 65, 66].

2.1 Composition of the Universe

Over the last years the observational progress has marked the advent of the era of precision cosmology. The combined data exhibits an impressive consistency and is in very good agreement with the currently accepted concordance model of big bang cosmology, the Lambda-Cold Dark Matter (ΛCDM) model. Major evidence for this standard scenario of big bang cosmology derives from several cosmological observations, the most eminent being perhaps (i) the observed primordial abundances of the light elements, matching very well the theoretical prediction from BBN [2], (ii) the angular power spectrum of the temperature anisotropies in the CMB as measured by the Wilkinson Microwave Anisotropy Probe (WMAP) satellite [1], (iii) the imprint of baryonic acoustic oscillations (BAOs) in the local distribution of matter as seen in galaxy surveys [3], (iv) direct measurements of the cosmic expansion rate, i.e. the Hubble parameter H_0, by the Hubble Space Telescope [67], and (v) distance measurements based on type Ia supernovae (SNe) [68, 69].

All observed cosmological phenomena are consistent with the assumption that our universe is spatially flat [1, 70]. Indeed, combining the data on CMB anisotropies, BAOs and H_0 shows that presently, at 95 % CL, the total energy density of the universe ρ_{tot} does not deviate by more than 1 % from the critical energy density ρ_c that is required for exact spatial flatness. In the following we shall hence neglect the possibility of a small spatial curvature and assume that $\rho_{\mathrm{tot}} = \rho_c$, which is equivalent to saying that all density parameters Ω_i sum to unity,

$$\Omega_{\mathrm{tot}} = \sum_i \Omega_i = \sum_i \frac{\rho_i}{\rho_c} = \frac{\rho_{\mathrm{tot}}}{\rho_c} = 1\,. \tag{2.1}$$

This sum receives contributions from three different forms of energy or matter: radiation, matter and dark energy. In the present epoch the energy in radiation from beyond our galaxy is dominated by the photons of the CMB. Relic neutrinos which are presumed to be present in the current universe as a remnant of the hot early universe either belong to radiation or matter, depending on their absolute masses. The matter component splits into a small baryonic and a large dark nonbaryonic fraction. We shall now discuss in turn how photons, neutrinos, baryonic matter, dark matter and dark energy respectively contribute to Ω_{tot}.

2.1.1 CMB Photons

In the early 1990s the Cosmic Background Explorer (COBE) satellite experiment was the first precision measurement to confirm two key features of the CMB. Since COBE we know that the CMB has an almost perfect Planckian spectrum [71, 72] and that it is highly isotropic, with its temperature fluctuating across the sky only at the level of 10^{-5} [73]. Together, these findings provide strong evidence for a hot thermal phase in the early universe preceded by an inflationary era (cf. Sec. 2.2.1). The mean CMB temperature is $T_\gamma^0 = 2.7255(6)\,\mathrm{K}$ [74]. Given

the thermal black-body distribution of the CMB photons, this temperature directly implies the following entropy, number and energy densities

$$s_\gamma^0 \simeq 1500\,\mathrm{cm}^{-3}\,, \quad n_\gamma^0 \simeq 410\,\mathrm{cm}^{-3}\,, \quad \rho_\gamma^0 \simeq 260\,\mathrm{meV\,cm}^{-3}\,. \tag{2.2}$$

The present value of the critical energy density is determined by the current expansion rate. With the aid of the dimensionless Hubble parameter h, which is defined through the relation $H_0 = 100\,h\,\mathrm{km/s/Mpc}$, we are able to write ρ_c^0 as

$$\rho_c^0 = \frac{3M_P^2}{8\pi} H_0^2 \simeq 10.54\,h^2\,\mathrm{keVcm}^{-3}\,, \tag{2.3}$$

with $M_P \simeq 1.22 \times 10^{19}$ GeV denoting the Planck mass. The ΛCDM fit to the combined CMB, BAO and H_0 data gives $h \simeq 0.704$ [1], such that $\rho_c^0 \simeq 5200\,\mathrm{eV\,cm}^{-3}$, which results in a photon density parameter

$$\Omega_\gamma^0 \simeq 5 \times 10^{-5}\,. \tag{2.4}$$

Barring some unknown form of dark radiation [75], the only other significant contribution to the present-day entropy density in radiation comes from neutrinos.[1] We thus conclude that photons are responsible for a large fraction of the radiation entropy in the current universe, but contribute only to a negligible extent to the total energy density.

2.1.2 Relic Neutrinos

In the hot early universe neutrinos are produced and kept in thermal equilibrium via weak interactions. Around a temperature $T \sim 1\,\mathrm{MeV}$ the rate of these interactions drops below the Hubble rate, causing the neutrinos to decouple from the thermal bath and evolve independently of all other species afterwards. The presence of a relic abundance of primordial neutrinos in the current universe is hence a fundamental prediction of the hot big bang scenario. It is doubtful whether this cosmic neutrino background (CNB) will ever be directly observed, as the low-energetic CNB neutrinos interact only extremely weakly [77]. By contrast, a series of physical processes in the early universe such as BBN, the evolution of the CMB temperature anisotropies or the formation of matter structures on large scales are fortunately sensitive to the influence of primordial neutrinos, which provides us with compelling indirect evidence for their existence [78, 79].

The observed oscillations between the three neutrino flavours [4, 5] indicate that neutrinos have small masses[2]. This has a direct impact on their evolution after decoupling. If neutrinos

[1] Note that in the recent cosmic past, shortly after the onset of star formation, the entropy contained in black holes has come to dominate over the entropy in radiation [76].

[2] In the following discussion we shall restrict ourselves to the relic abundance of primordial neutrinos. If neutrinos are Dirac fermions, the abundance of antineutrinos should at each time be approximately the same as the abundance of neutrinos.

were massless, their temperature T_ν would decrease for the most part in parallel to the photon temperature T_γ as the universe continues to expand. Only at photon temperatures around the electron mass $m_e \simeq 511\,\mathrm{keV}$, T_γ and T_ν would behave slightly differently. Around $T_\gamma \sim m_e$, the thermal production of electrons and positrons begins to cease. e^+e^- annihilations into photons then deposit the entire energy formerly contained in electrons and positrons in the photon component, which slows down the decline of T_γ for a short time, but not the decline of T_ν. For massless neutrinos entropy conservation would imply $T_\nu^0 = (4/11)^{1/3}\, T_\gamma^0 \simeq 1.9\,\mathrm{K}$ and neutrinos would presently have a density $\Omega_\nu^0 \simeq 3 \times 10^{-5}$. The energy density of massive neutrinos, however, experiences a slower redshift due to the cosmic expansion than the energy density of massless neutrinos. While the energy of a massless neutrino goes to zero as the universe expands, the energy E_{ν_i} of a neutrino mass eigenstate with mass $m_{\nu_i} \neq 0$ asymptotically approaches m_{ν_i}. Once the energy of a massive neutrino is dominated by its mass rather its momentum, it becomes nonrelativistic. For sufficiently large neutrino masses, the energy contained in nonrelativistic neutrinos thus outweighs by far the energy of neutrinos that are still relativistic, such that the present neutrino density is well described by

$$\Omega_\nu^0 h^2 \simeq \frac{m_{\nu,\mathrm{tot}}}{94\,\mathrm{eV}}\,, \quad m_{\nu,\mathrm{tot}} = \sum_{\nu_i} m_{\nu_i}\,, \tag{2.5}$$

where the sum runs over all mass eigenstates that have turned nonrelativistic at some value of T_γ below 1 MeV, i.e., given the measured mass squared differences, over at least two out of three states. The lower bound on the sum of neutrino masses implied by the mass squared differences is roughly 0.05 eV, so that $\Omega_\nu^0 \gtrsim 1 \times 10^{-3}$. On the other hand, several cosmological observations constrain $m_{\nu,\mathrm{tot}}$ from above. Massive free-streaming neutrinos damp the growth of matter fluctuations and could thus leave an imprint in large-scale structure (LSS) observables [80, 81]. So far, no effects from neutrino masses have yet been observed. Instead, combining data from galaxy surveys, WMAP, BAO, H_0 and type Ia SNe, one is able to put an upper limit of 0.28 eV on $m_{\nu,\mathrm{tot}}$ [82], which corresponds to $\Omega_\nu^0 \lesssim 6 \times 10^{-3}$.

After leaving thermal equilibrium, most neutrinos never again interact with other particles. The entropy and total number of neutrinos hence remain practically unchanged after decoupling, which is why we speak of the neutrinos as being *frozen out*. At the time neutrinos decouple, they are relativistic. Their entropy and number densities thus subsequently always evolve as the corresponding densities of massless neutrinos would do, independently of the fact that neutrinos are actually massive, turning nonrelativistic at lower temperatures. Because of this peculiar thermal history, neutrinos represent a prime example for what is often referred to as *hot relics*. With the aid of the would-be temperature of massless neutrinos, $T_\nu^0 \simeq 1.9\,\mathrm{K}$, we then obtain $s_\nu^0 \simeq 1400\,\mathrm{cm}^{-3}$ and $n_\nu^0 \simeq 340\,\mathrm{cm}^{-3}$.

In conclusion, we find that also neutrinos contribute only to a negligibly small extent to the total energy density of the universe,

$$1 \times 10^{-3} \lesssim \Omega_\nu^0 \lesssim 6 \times 10^{-3}\,, \tag{2.6}$$

which follows from Eq. (2.5) and the bounds on the total neutrino mass,

$$0.05\,\mathrm{eV} \lesssim m_{\nu,\mathrm{tot}} \lesssim 0.28\,\mathrm{eV}\,. \tag{2.7}$$

In return, their entropy density is almost as large as the one of the CMB photons. The present radiation entropy density s_R^0, comprising the photon entropy density and the entropy densities of all hot relics, i.e. neutrinos in the standard hot big bang scenario, then turns out to be

$$s_R^0 = s_\gamma^0 + s_\nu^0 \simeq 2900\,\mathrm{cm}^{-3}\,. \tag{2.8}$$

Note that, by definition, s_R^0 can also be written as the entropy of a thermal bath with an effective number of degrees of freedom $g_{*,s}^0$ at temperature T_γ^0,

$$s_R^0 = \frac{2\pi^2}{45} g_{*,s}^0 \left(T_\gamma^0\right)^3\,, \quad g_{*,s}^0 = 2 + \frac{7}{8}\cdot 3\cdot 2\cdot\frac{4}{11} = \frac{43}{11}\,. \tag{2.9}$$

The entropy associated with this density directly corresponds to the entropy inherent in the thermal bath during the hot phase of the early universe. A conclusive explanation for its origin is still lacking and it is a major task of modern particle cosmology to explore possible sources for this primordial entropy. A key motivation of this thesis is to demonstrate that the spontaneous breaking of $B-L$ at the end of inflation represents a viable scenario for its generation.

2.1.3 Baryonic Matter

All forms of matter in the universe that can be more or less well described by standard particle physics, such as gas clouds, stars, planets, black holes, etc., are baryonic, i.e. made out of ordinary atoms, whose nuclei are composed of protons and neutrons.[3] The present abundance of these baryons, or more precisely nucleons, is conveniently parametrized in terms of the baryon-to-photon ratio η_b,

$$\Omega_b^0 h^2 = \frac{m_N}{\rho_c^0/h^2}\, n_\gamma^0\, \eta_b^0 \simeq \frac{1}{273}\left(\frac{\eta_b^0}{10^{-10}}\right)\,, \quad \eta_b^0 = \frac{n_b^0}{n_\gamma^0}\,. \tag{2.10}$$

where $m_N \simeq 940\,\mathrm{MeV}$ is the mass of a single nucleon, n_b^0 denotes the present number density of baryons, and where we have used the value for n_γ^0 stated in Eq. (2.2). In the standard BBN scenario with three generations of relativistic neutrinos, the primordial abundances of the light nuclei are solely controlled by the baryon-to-photon ratio (cf. Sec. 2.2.2). The measurement

[3] In order to ensure that the universe as a whole is electrically charge neutral, there has to be present one electron for each proton in the universe. As a single proton is, however, roughly 1800 times heavier than an electron, the contribution from electrons to the total energy presently stored in matter is negligibly small, which is why we will not consider it any further.

of these abundances hence provides us with an observational handle on η_b^0. Matching the observed abundances with the theoretical BBN prediction, one finds at 95 % CL [2]

$$\text{BBN:} \qquad 5.1 \times 10^{-10} \leq \eta_b^0 \leq 6.5 \times 10^{-10}\,, \quad 0.019 \leq \Omega_b^0 h^2 \leq 0.024\,. \tag{2.11}$$

One of the key predictions of standard cosmology is that between BBN and the decoupling of the CMB the number of baryons as well as the photon entropy are conserved such that the baryon-to-photon ratio remains unchanged between these two processes. This prediction can be observationally tested as the CMB power spectrum is fortunately very sensitive to the physical baryon density $\rho_b \propto \Omega_b h^2$ (cf. Sec. 2.2.1). Fitting the ΛCDM model to the CMB data yields [1]

$$\text{CMB:} \qquad \eta_b^0 \simeq (6.18 \pm 0.14) \times 10^{-10}\,, \quad \Omega_b^0 h^2 = 0.02260 \pm 0.00053\,, \tag{2.12}$$

which is consistent with the BBN result in Eq. (2.11) and hence serves as yet another endorsement of the standard picture. The agreement between the two determinations of η_b^0 is particular remarkable in so far as they probe completely different physical processes occurring in two widely separated epochs. Due to its high precision, we will from now on, after some additional rounding, use the CMB value as our estimate for the present baryon-to-photon ratio, $\eta_b^{\text{obs}} = 6.2 \times 10^{-10}$, which corresponds to a baryon density parameter $\Omega_b^0 \simeq 4.6 \times 10^{-2}$.

Depending on the perspective, we are led to the conclusion that the present abundance of baryons in the universe is either exceptionally low or high. First of all, it is surprising that BBN and the CMB concordantly imply that only a fraction of roughly 5 % of the total energy of the universe resides in baryons. In view of the fact that our universe appears to be spatially flat, one might rather expect a baryon density parameter $\Omega_b^0 \simeq 1$. The low abundance of baryons is hence an indication for the presence of other nonbaryonic forms of matter or energy, viz. dark matter and dark energy, that account for 95 % of the energy budget of the universe. On the other hand Ω_b^0 is remarkably large compared to the theoretical expectation.[4] In the early universe the baryon-to-photon ratio freezes out when the baryons decouple from the thermal bath at temperatures of $\mathcal{O}(10..100)\,\text{MeV}$. Assuming that the universe is locally baryon-antibaryon symmetric down to temperatures of this magnitude, the annihilation of baron-antibaryon pairs shortly before decoupling would dramatically reduce the abundances of both baryons and antibaryons. In consequence of this *annihilation catastrophe* the present baryon-to-photon would be nine orders of magnitude smaller than the observed value, $\eta_b^0 \simeq 5 \times 10^{-19}$ [62, 85]. The most reasonable way out of the annihilation catastrophe is the possibility that the universe possesses a baryon-antibaryon asymmetry at temperatures of $\mathcal{O}(100)\,\text{MeV}$. The excess of baryons over antibaryons at the time of annihilation would then explain the large observed baryon abundance.

[4] It is also large compared to the observed abundance of luminous matter. The density parameter of stars is smaller than Ω_b^0 by one order of magnitude, $\Omega_{\text{stars}} \simeq 2.7 \times 10^{-3}$ [83]. Most baryons are thus optically dark, probably contained in some diffuse intergalactic medium [84].

Further evidence for a primordial baryon asymmetry comes from the fact that the observable universe seems to contain almost exclusively matter and almost no antimatter.[5] If there were to exist large areas of antimatter in the universe, annihilation processes along the boundaries between the matter and antimatter domains would result in characteristic gamma ray signals. As no such signals have yet been observed, the local abundance of antimatter can be tightly constrained on a multitude of length scales, ranging from our solar system, to galaxies and clusters of galaxies. X- and gamma-ray observations of the Bullet Cluster, a system of two colliding galaxy clusters, put for instance an upper bound of 3×10^{-6} on the local antimatter fraction, thus ruling out serious amounts of antimatter on scales of $\mathcal{O}(20)\,\mathrm{Mpc}$, which are the largest scales directly probed so far [86]. Furthermore, assuming that matter and antimatter are present in equal shares on cosmological scales, one can show that the matter domain we inhabit virtually has to cover the entire visible universe [87].

The absence of antimatter in our universe thus allows for a different interpretation of the baryon-to-photon ratio η_b^0. As the ratio of photons to antibaryons is practically zero, η_b^0 can also be regarded as a measure for the baryon asymmetry of the universe (BAU),

$$\eta_b^0 = \frac{n_b^0}{n_\gamma^0} \to \frac{n_b^0 - n_{\bar{b}}^0}{n_\gamma^0}\,. \tag{2.13}$$

To emphasize this different interpretation of the baryon-to-photon ratio we will write η_B^0 instead of η_b^0 in the following, where the subscript B is supposed to refer to the total baryon number of the universe. Again, standard cosmology lacks an explanation for the origin of this primordial asymmetry. A second key motivation for this thesis is hence to identify a natural mechanism for the dynamical generation of the BAU that can be consistently embedded into an overall picture of the early universe. As we will demonstrate, leptogenesis after nonthermal neutrino production in the decay of $B-L$ Higgs bosons represents a viable and particularly attractive option.

2.1.4 Dark Matter

A plethora of astrophysical and cosmological observations indicates that next to ordinary matter some form of dark matter (DM), i.e. nonluminous and nonabsorbing matter which reveals its existence only through its gravitational influence on visible matter, is ubiquitously present in the universe.[6] Direct evidence for dark matter derives from all observable length scales. The rotation curves of spiral galaxies as well as the velocity dispersions of stars in elliptical

[5] Antiparticles of cosmic origin such as antiprotons and positrons are seen in cosmic rays. Their fluxes are, however, consistent with the assumption that they are merely secondaries produced in energetic collisions of cosmic rays with the interstellar medium rather than primordial relics.

[6] For recent reviews on dark matter, cf. for instance Refs. [88–91]. Another ansatz to account for the various observed, but unexplained gravitational effects is to modify the theory of general relativity. While modifications of gravity (cf. in particular Refs. [92, 93]) are often able to explain isolated phenomena, they

galaxies probe the abundance of dark matter on the scale of individual galaxies.[7] This applies in particular to our own galaxy, whose rotation curve in combination with other data allows to determine the fraction of dark matter in the neighborhood of our solar system quite precisely [96]. On the scale of clusters of galaxies, peculiar galaxy velocities in viralized galaxy clusters, X-ray observations of the hot intracluster gas and gravitational lensing effects on background galaxies point to large amounts of dark matter.[8] Especially compelling evidence for dark matter comes from detailed studies of the Bullet Cluster, whose dynamics can only be understood if it is assumed to be predominantly composed of very weakly self-interacting dark matter [98]. Finally, on cosmological scales the presence of dark matter is implied by the theory of structure formation. If the presently observed LSS of matter in the universe was to be traced back only to the density fluctuations of ordinary baryonic matter at the time of photon decoupling, the temperature anisotropies in the CMB would have to be at the level of 10^{-3}. However, the fact that they are actually two orders of magnitude smaller indicates that baryonic density perturbations can, in fact, not be the source of the required primordial wells of the gravitational potential. Instead these potential wells have to be attributed to some form of nonbaryonic dark matter that, unimpeded by photon pressure, is able to start clumping way before decoupling. Furthermore, numerical simulations of structure formation show that most dark matter has to be cold at the onset of structure formation, i.e. has to turn nonrelativistic long before the energy in matter begins to dominate over the energy in radiation.[9]

By now the overwhelming observational evidence has firmly established the notion that nonbaryonic cold dark matter (CDM) is the prevailing form of matter in the universe. It is thus one of the key ingredients to the ΛCDM model. Strong support for the CDM picture is again provided by the CMB power spectrum, which is next to the baryon density ρ_b also sensitive to the total matter density $\rho_m \propto \Omega_m h^2$ (cf. Sec. 2.2.1). Assuming dark matter to be cold and nonbaryonic, the combined CMB, BAO and H_0 data allow for a precise determination of $\Omega_m h^2$ [1],

$$\Omega_m^0 h^2 = 0.1349 \pm 0.0036\,, \tag{2.14}$$

usually struggle to give a consistent description of all observed phenomena, which is why we will not consider them any further in this thesis.

[7] Seminal works in this field have been the observations by Vera Rubin and Kent Ford, who measured the rotation curve of the Andromeda Nebula in 1970 [94], as well as by Sandra Faber and Robert Jackson, who studied stellar velocities in elliptical galaxies in 1976 [95].

[8] The first astronomer to stumble upon the problem of the *missing mass* in galaxy clusters was Fritz Zwicky. In 1933, observations of the Coma Cluster led him to conclude that the galaxies in the cluster should actually fly apart, if there were not large amounts of invisible matter present in it, holding them together [97]. Zwicky is hence usually credited as the discoverer of dark matter.

[9] As light neutrinos turn nonrelativistic only at very late times in the cosmological evolution, they represent, in fact, a form of hot dark matter in the current universe.

which is roughly six times larger than the present baryon density $\Omega_b^0 h^2$ as inferred from the primordial abundances of the light elements or the CMB power spectrum. With the aid of Eqs. (2.12) and (2.14), the present density parameter of dark matter then turns out to be[10]

$$\Omega_{\mathrm{DM}}^0 h^2 = \Omega_m^0 h^2 - \Omega_b^0 h^2 = 0.1123 \pm 0.0036\,, \quad \Omega_{\mathrm{DM}}^0 \simeq 0.227\,. \tag{2.15}$$

We thus know quite certainly that dark matter accounts for roughly 23 % of the energy budget of the universe. The nature and the origin of dark matter have, however, remained mysterious puzzles so far. At the present stage we are merely able to constrain to some extent its properties. First of all, the mismatch between determinations of $\Omega_b^0 h^2$ and $\Omega_m^0 h^2$, i.e. the present abundances of baryons in particular and of matter in general, as well as arguments based on the theory of structure formation indicate that dark matter has to be cold and nonbaryonic for the most part.[11] As it is *dark*, the particles constituting dark matter are usually assumed to be electrically neutral. Similarly, if these particles carried colour charge, they would strongly interact with baryons, thus altering, for instance, the predictions of BBN and the appearance of the CMB. Hence the dark matter particles are assumed to be colour-neutral. Finally, they have to be perfectly stable or at least sufficiently long-lived in order to explain the presence and influence of dark matter on cosmological time scales up to the current epoch. Interestingly, no known particle fulfills all these requirement and thus the existence of dark matter is one of the strongest indications for physics beyond the standard model. Particle cosmology now faces the task to identify which hypothetical new elementary particles could serve as dark matter particles, embed dark matter into a consistent picture of the cosmological evolution, and explain in particular how its present abundance is generated (cf. Eq. (2.15)). Therefore, the third key motivation of this thesis is to demonstrate that several well-motivated dark matter scenarios can actually be easily realized, if reheating after inflation is triggered by the $B-L$ phase transition. For the most part, we will consider a scenario in which thermally produced gravitinos account for dark matter. In Ch. 8, we will then turn to a setup in which either higgsinos or winos represent the constituents of dark matter.

2.1.5 Dark Energy

A crucial result of our discussion so far is that dark matter, baryonic matter, neutrinos and photons together account for only roughly 27 % of the energy budget of the universe. The remaining 73 % have to be attributed to some form of dark energy that, as opposed to dark

[10] Later on we shall use a rounded version of the value in Eq. (2.15), namely $\Omega_{\mathrm{DM}}^{\mathrm{obs}} h^2 = 0.11$.

[11] Certain scenarios of warm dark matter or mixed dark matter which is composed of a mixture of cold, warm and or hot components, are also admissible [99, 100]. Likewise, also small amounts of baryonic matter in the form of massive compact halo objects (MACHOs) [101, 102] and or cold molecular gas clouds [103] may well contribute to the dark matter in galaxy halos.

matter, does not cluster under the influence of gravity. At the present stage we almost do not know anything about the nature and the origin of dark energy, whereby dark energy represents one of the greatest mysteries of modern physics. At least some light on the properties of dark energy is shed by the fact that the expansion of our universe is currently accelerating.[12] As matter and radiation on their own always lead to either a decelerating expansion or an accelerated contraction, the dark energy has to be responsible for the observed acceleration. Assuming that dark energy can be described as a perfect fluid, just as all other forms of matter and energy in the universe, the requirement that it be the source of the accelerated expansion constrains its equation of state, $\omega = p_{\mathrm{DE}}/\rho_{\mathrm{DE}} < -1/3$, where p_{DE} and ρ_{DE} denote the pressure and the energy density of dark energy, respectively. In other words: the accelerated expansion indicates that dark energy has a negative pressure.

There are several attempts to explain the presence of dark energy. Many approaches assume, for instance, that dark energy corresponds to the energy of a scalar field moving in some specific potential. Depending on whether this field has a canonical kinetic term or not, dark energy is then often referred to as quintessence [106, 107] or k essence [108]. An alternative possibility is that dark energy is entirely illusory, being in fact an artifact of an incorrect treatment of gravity. In this view, general relativity has to be modified in such a way that the accelerated expansion can be accounted for without any recourse to dark energy [109, 110]. The simplest solution, however, is provided by Einstein's cosmological constant Λ. Including a Λ term in the field equations of general relativity corresponds to adding a constant vacuum energy density $\rho_\Lambda = \Lambda/\kappa$ with $\kappa = 8\pi/M_P^2$ and equation of state $\omega = -1$ to the energy budget of the universe. Although this ansatz is the least sophisticated one, it is consistent with all observations and thus, along the lines of Occam's razor, the explanation of choice for dark energy in the ΛCDM model.[13] Our earlier results for the density parameters of all other forms of matter and energy in the ΛCDM model then allow us to calculate the density parameter of dark energy [1],

$$\Omega_\Lambda^0 = \Omega_{\mathrm{tot}}^0 - \Omega_{\mathrm{DM}}^0 - \Omega_b^0 - \Omega_\nu^0 - \Omega_\gamma^0 = 0.728^{+0.015}_{-0.016}\,. \tag{2.16}$$

Finally, we remark that fitting the CMB, BAO and the SNe data from Ref. [68] to a relaxed version of the ΛCDM model, in which Ω_{tot} and ω are allowed to differ from 1 and -1, respectively, yields a dark matter equation of state $\omega = -0.999^{+0.057}_{-0.056}$ [1], which is in excellent agreement with the assumption of a cosmological constant. For the moment being, as long as there is no commonly accepted explanation of dark energy in sight, we thus settle for a rather pragmatic approach and adopt the notion of a cosmological constant in this thesis, keeping

[12] The accelerated expansion of our universe became evident for the first time in measurements of the distance-redshift relation of high-redshift type Ia SNe in 1998 [104, 105].

[13] Naively one might expect the energy density of the vacuum to be related to the Planck scale, $\rho_\Lambda \sim M_P^4$. Interpreting dark energy as the energy of the vacuum, one then has to explain why $\rho_\Lambda \simeq 0.73\rho_c^0 \sim 10^{-123} M_P^4$. For a classic discussion of this so far unsolved problem cf. Ref. [111].

in mind that it should be regarded as a placeholder for a future theory of dark energy that is still to come.

2.1.6 Stages in the Expansion History

The identification of the key items in the cosmic energy inventory as well as the determination of their respective contributions Ω_i^0 to the total energy density mark milestones of modern cosmology. Together with the current expansion rate H_0, the density parameters Ω_i^0 fully determine the present state of the universe on all scales on which the cosmological principle holds. On top of that, they also allow to trace the evolution of the universe back in time up to temperatures of $\mathcal{O}(1)\,\mathrm{MeV}$, i.e. until weak interactions begin to bring about interchanges between the abundances of the different species. Below the threshold for e^+e^- pair production, $T \ll m_e$, the energy densities of photons, matter and dark energy can, for instance, be written as functions of the cosmological redshift z in the following way,

$$T \ll m_e : \qquad \rho_i(z) = \rho_c^0\,\Omega_i^0\,(1+z)^{3(1+\omega_i)}\,, \quad i = \gamma, m, \Lambda\,, \tag{2.17}$$

with ω_i denoting the coefficient in the equation of state of species i. We respectively have $\omega_\gamma = 1/3$, $\omega_m = 0$ and $\omega_\Lambda = -1$. The energy density of a nonrelativistic neutrino species with typical momentum p_{ν_i} and mass m_{ν_i} evolves similarly to the matter energy density ρ_m,

$$p_{\nu_i}(z) \lesssim m_{\nu_i} : \qquad \omega_{\nu_i} \approx 0\,, \quad \rho_{\nu_i}(z) \approx \frac{\rho_c^0}{h^2}\frac{m_{\nu_i}}{94\,\mathrm{eV}}\,(1+z)^3\,. \tag{2.18}$$

Once the typical neutrino momenta p_{ν_i} begin to exceed m_{ν_i}, the respective neutrino species becomes relativistic,[14] so that its energy density henceforth runs in parallel to ρ_γ,

$$m_{\nu_i} \lesssim p_{\nu_i}(z) \ll m_e : \qquad \omega_{\nu_i} \approx 1/3\,, \quad \rho_{\nu_i}(z) \approx \frac{7}{8}\left(\frac{4}{11}\right)^{4/3}\rho_\gamma(z)\,. \tag{2.19}$$

The density of the total radiation energy is given as usual, $\rho_R(z) = g_{*,\rho}(z)/g_\gamma\,\rho_\gamma(z)$, with $g_{*,\rho}$ counting the effective number of relativistic degrees of freedom.

In the present epoch dark energy dominates the total energy of the universe, $\Omega_\Lambda^0 \gtrsim \Omega_m^0 \gg \Omega_\nu^0 \simeq \Omega_\gamma^0$. However, as the energy densities of radiation, matter and dark energy scale differently with redshift z, this changes as we go back in time. First, at $z = z_\Lambda$ the energy contained in matter catches up with dark energy, $\rho_m(z_\Lambda) = \rho_\Lambda(z_\Lambda)$. Then, at $z = z_\mathrm{eq}$ radiation takes eventually over as the dominant form of energy in the universe, $\rho_R(z_\mathrm{eq}) = \rho_m(z_\mathrm{eq})$. The above scaling relations for the energy densities ρ_i imply

$$z_\Lambda = \left(\frac{\Omega_\Lambda^0}{\Omega_m^0}\right)^{1/3} - 1 \simeq 0.39\,, \quad z_\mathrm{eq} = \frac{g_{*,\rho}^0}{g_{*,\rho}^{eq}}\frac{\Omega_m^0}{\Omega_\gamma^0} - 1 \simeq 3200\,, \tag{2.20}$$

[14] Given the allowed range of the total neutrino mass (cf. Eq. (2.7)), matching the two expressions for ρ_{ν_i} in Eqs. (2.18) and (2.19) and solving for z shows that the heaviest neutrino, which eventually contributes most to Ω_ν^0, turns nonrelativistic at a redshift of $\mathcal{O}(10..100)$.

where we have used that $g^0_{*,\rho} = 2$ and $g^{eq}_{*,\rho} = 2 + 7/8 \cdot 3 \cdot 2 \cdot (4/11)^{4/3} \simeq 3.36$. These two redshifts correspond to the following photon temperatures,

$$T_\Lambda = T_\gamma\left(z_\Lambda\right) \simeq 3.8\,\mathrm{K} \simeq 0.33\,\mathrm{meV}\,, \quad T_{eq} = T_\gamma\left(z_{\mathrm{eq}}\right) \simeq 8800\,\mathrm{K} \simeq 0.76\,\mathrm{eV}\,, \tag{2.21}$$

as well as to the following values of the cosmic time t,

$$t_\Lambda = t\left(z_\Lambda\right) \simeq 9.6\,\mathrm{Gyr}\,, \quad t_{eq} = t\left(z_{\mathrm{eq}}\right) \simeq 56\,\mathrm{kyr}\,, \tag{2.22}$$

which are to be compared to the age of the universe, $t_0 = 13.75 \pm 0.13$ Gyr [1].

In summary, we conclude that the universe experiences at least three dynamically different stages in its expansion history. (i) In the very recent cosmic past, $z < z_\Lambda$, the energy of the universe is dominated by the vacuum contribution, which, due to its negative pressure, causes the expansion to accelerate. (ii) Between $z = z_\Lambda$ and $z = z_{\mathrm{eq}}$ most energy is contained in pressureless matter. Note that it is in this epoch that matter structures are able to form in the universe.[15] (iii) For $z > z_{\mathrm{eq}}$ radiation is the most abundant form of energy in the universe. When speaking of the *hot thermal phase of the early universe* or the *hot early universe*, we actually refer to this phase of radiation domination. During the radiation-dominated era the universe is filled by a hot plasma in thermal equilibrium that becomes increasingly hotter and denser as one goes further back in time. In the approximation of a constant number of relativistic degrees of freedom $g_{*,\rho}$, the temperature $T \equiv T_\gamma$ of the thermal bath scales inversely proportional to $t^{1/2}$,

$$T(t) \approx \left(\frac{90 M_P^2}{32\pi^3 g_{*,\rho}\, t^2}\right)^{1/4} \simeq 0.86\,\mathrm{MeV}\left(\frac{43/4}{g_{*,\rho}}\right)^{1/4}\left(\frac{1\,\mathrm{s}}{t}\right)^{1/2}\,, \tag{2.23}$$

where we have normalized $g_{*,\rho}$ to its value at the time of neutrino decoupling. As the temperature continues to rise, more and more particle species reach thermal equilibrium with the bath, causing $g_{*,\rho}$ to increase. Turning this picture around, we may equivalently say that in the hot early universe various species decouple one after another from the thermal bath in consequence of the declining temperature. These departures from thermal equilibrium shape the present state of the universe. Up to now we have already discussed the decoupling of neutrinos at $T \sim 1\,\mathrm{MeV}$ and the decoupling of baryons at $T \sim 10..100\,\mathrm{MeV}$. As we will see later on, similar nonequilibrium processes at even higher temperatures may be responsible for the relic density of dark matter and the baryon asymmetry of the universe. In fact, the very aim of this thesis is to describe a possible origin for the hot thermal phase of the early universe, namely the spontaneous breaking of $B-L$ at the end of inflation, that naturally entails the simultaneous generation of entropy, baryon asymmetry and dark matter.

[15] Curiously enough, the matter-dominated era lasts sufficiently long to allow for the formation of such complex structures as galaxies, solar systems and human beings, which, from the perspective of mankind, appears to be a fortunate *cosmic coincidence*. The question of why dark energy becomes relevant exactly at the present time, i.e. why presently $\Omega_\Lambda \sim \Omega_m$ rather than $\Omega_\Lambda \ll \Omega_m$ or $\Omega_\Lambda \gg \Omega_m$, is one of the greatest puzzles of modern cosmology. Cf. e.g. Ref. [112].

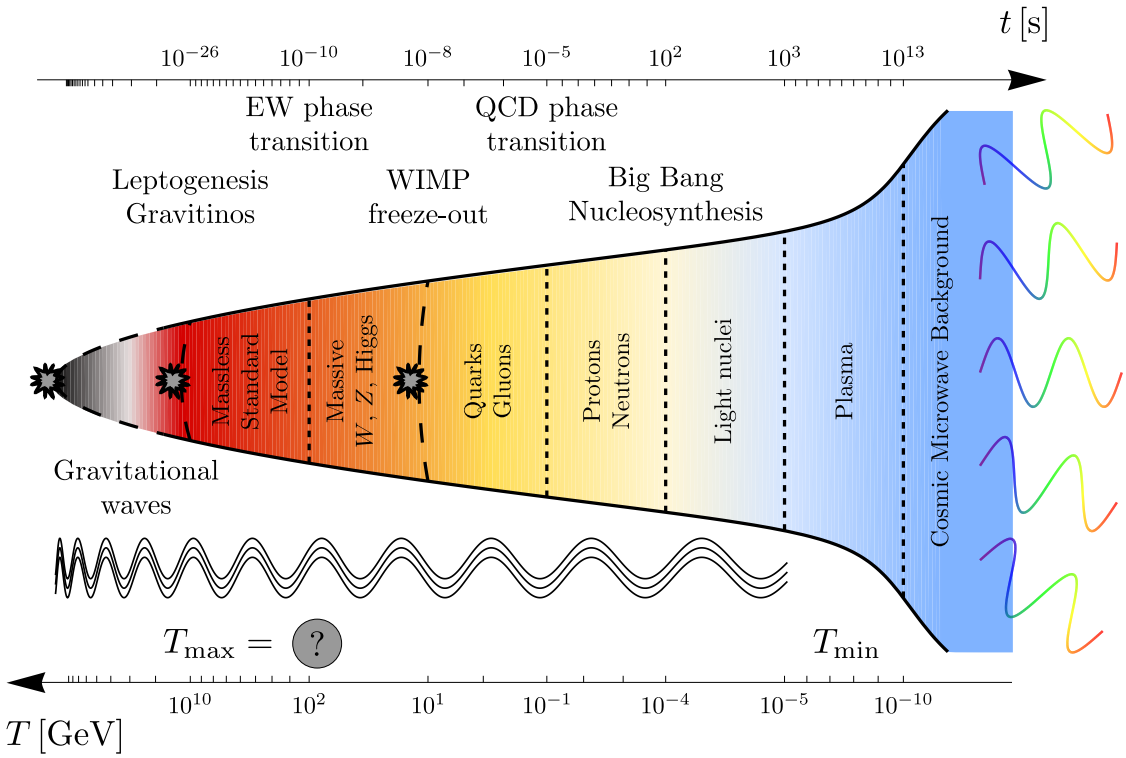

Figure 2.1: Timeline of the hot thermal phase of the early universe illustrating (i) the relation between the temperature of the thermal bath T and the cosmic time t (cf. Eq. (2.23)), (ii) the chronology of several important, partly hypothetical nonequilibrium processes, (iii) a representative selection of those forms of matter or energy that are respectively involved in these processes, and (iv) several possibilities for the reheating temperature after inflation (cf. Sec. 3.1).

2.2 The Hot Thermal Phase

The hot early universe represents the stage for a great variety of physical processes taking place over an enormous range of energy scales (cf. Fig. 2.1 for an overview of the main events in its thermal history). As a final preparation before turning to our own scenario, we shall now discuss in more detail the decoupling of the CMB, primordial nucleosynthesis, the QCD and the electroweak phase transition as well as electroweak sphalerons.

2.2.1 The Cosmic Microwave Background

Towards the end of the radiation-dominated phase, at temperatures of $\mathcal{O}(1)\,\mathrm{eV}$, protons, i.e. hydrogen nuclei, are kept in thermal equilibrium via the steady interplay of radiative recombination and photoionization processes. However, as the plasma cools in the course of the expansion, photoionization becomes less efficient, the hydrogen nuclei begin to bind

free electrons into neutral atoms and the ionization fraction of hydrogen freezes out at a vanishingly small value. This process is usually referred to as hydrogen recombination.[16] Due to the high abundance of thermal photons in the plasma it takes place at a temperature significantly below the binding energy of hydrogen, $B_{\rm H} = 13.6\,\text{eV}$. In fact, the temperature has to drop to $T_{\rm rec} \simeq 0.30\,\text{eV}$ until the fractional ionization reaches a value of 10 %. As the abundance of free electrons continues to decrease even further, the rate Γ_γ of Thomson scatterings between thermal photons and plasma electrons falls below the Hubble rate H. At $T_{\rm dec} \simeq 0.26\,\text{eV}$ the mean free photon path equals the Hubble radius H^{-1}, or equivalently $\Gamma_\gamma = H$, and most photons scatter for the last time. This moment of *last scattering* marks the time when the photons decouple and the universe becomes transparent to radiation. After decoupling the photons freely propagate until they eventually reach us in the form of CMB radiation. In this sense the CMB represents a full-sky picture of the early universe at a temperature of $T_{\rm dec} \simeq 0.26\,\text{eV}$, i.e. at a redshift $z_{\rm dec} \simeq 1100$ and a cosmic time $t_{\rm dec} \simeq 360\,\text{kyr}$.

To be precise, the decoupling of the CMB actually occurs during the matter-dominated era (cf. T_{eq} in Eq. (2.21)). But as its origin is inextricably linked with the thermal history of the universe, it represents nonetheless one of the main physical phenomena associated with the hot big bang [113]. In particular, the fact that the CMB has an almost perfect Planckian spectrum may be regarded as key evidence for an early stage during which the universe was filled by a hot plasma in thermal equilibrium. Alternative attempts to explain the origin of the CMB, such as the idea put forward by the proponents of the steady state theory proposing that the CMB may in fact be starlight thermalized by dust grains, typically end up with a superposition of blackbody spectra corresponding to different temperatures.

The CMB not only provides striking evidence for the hot thermal phase, as we have seen in Sec. 2.1, it also allows to precisely determine a multitude of cosmological parameters that enter into the theoretical description of the early universe.[17] The primary CMB observable encoding cosmological information is the variation of the CMB temperature across the sky, which is conveniently characterized by the angular power spectrum C_ℓ of the relative temperature fluctuations,

$$\frac{\delta T}{T_0}(\mathbf{n}) = \sum_{\ell=2}^{\infty} \sum_{m=-\ell}^{+\ell} a_{\ell m} Y_{\ell m}(\mathbf{n}) \,, \quad \langle a^*_{\ell m} a_{\ell' m'} \rangle = C_\ell \, \delta_{\ell\ell'} \delta_{mm'} \,. \tag{2.24}$$

Except for the dipole anisotropy, which is interpreted as being due to the motion of the earth relative to the absolute CMB rest frame, the CMB temperature anisotropies directly correspond to the density perturbations inherent in the baryon-photon fluid at the time of last scattering. Several physical processes leave their imprint in the observed power spectrum. (i)

[16] Prior to hydrogen recombination, at $T \sim 0.5\,\text{eV}$, helium decouples in a similar way. As hydrogen is still fully ionized at this time, the universe remains opaque after helium recombination.

[17] For reviews on the physics of the CMB and its potential to constrain cosmological models, cf. for instance Refs. [114, 115].

The tight coupling between photons and baryons leads to higher temperatures in regions of high baryon density. (ii) Photons that have to climb out of potential wells after decoupling are gravitationally redshifted. This translates into a shift of the observed with respect to the intrinsic temperature fluctuation, which is usually referred to as the Sachs-Wolfe effect [116]. Similarly, decaying gravitational potentials traversed by the CMB photons on their way from the surface of last scattering to the observer induce small boots in the observed CMB temperature. This is known as the integrated Sachs-Wolfe effect. (iii) The non-zero velocity of the plasma at decoupling results in a Doppler shift in the frequency of the CMB photons. (iv) Perturbations in the gravitational potential, induced by the growing density fluctuations of dark matter, as well as photon pressure drive acoustic oscillations in the photon-baryon fluid, which gives rise to a series of acoustic peaks in the CMB power spectrum.[18] These four effects, but in particular the acoustic peaks, are very sensitive to the parameters of the underlying cosmology. Barring a few degeneracies, the CMB power spectrum encodes information about at least ten basic cosmological parameters.

First of all, four parameters characterize the power spectra of primordial density fluctuations as well as primordial gravitational waves. These primordial scalar and tensor perturbations, as they are also referred to, eventually evolve into the CMB temperature fluctuations. The parameters characterizing their power spectra, P_s and P_t, hence determine the initial conditions for the evolution of the CMB anisotropies. Usually, P_s and P_t are taken to be power-laws,

$$P_s(k) = A_s \left(\frac{k}{k_*}\right)^{n_s-1}, \quad P_t(k) = A_t \left(\frac{k}{k_*}\right)^{n_t}, \quad r = \frac{A_t}{A_s}, \tag{2.25}$$

where k is the comoving momentum scale and k_* stands for an arbitrary reference scale. Technically, P_s denotes the power spectrum of the curvature perturbation $\mathcal{R}$, which measures the spatial curvature of a comoving slicing of spacetime. P_t represents in fact the sum of two power spectra, P_+ and $P_\times$, which respectively account for the two physical polarization modes h_+ and $h_\times$ of the general traceless and transverse spatial metric perturbation. Note that due to rotational invariance $P_+ = P_\times = P_t/2$. The great virtue of the three perturbations $\mathcal{R}$, h_+ and $h_\times$ is that they are time-independent at early times, i.e. as long as they extend over scales larger than the Hubble radius H^{-1}. So far, the CMB data has revealed no sign of tensor modes. Thus, only the curvature perturbation amplitude A_s as well as the scalar spectral index n_s have been measured up to now. Neglecting potential tensor contributions and using a reference scale $k_* = 0.002\,\mathrm{Mpc}^{-1}$, the combined WMAP, BAO and H_0 data yields [1],

$$A_s = \left(2.441^{+0.088}_{-0.092}\right) \times 10^{-9}, \quad n_s = 0.963 \pm 0.012, \tag{2.26}$$

[18] Perturbations in the photon-baryon fluid can only evolve causally as long as they extend over scales smaller than the sound horizon. This explains the position of the first acoustic peak in the CMB power spectrum. It is located at an angular scale of roughly 1° or equivalently at $\ell \sim 200$, which corresponds to the angular diameter of the sound horizon at last scattering.

For comparison, the COBE data implies an amplitude $A_s \simeq 2.28 \times 10^{-9}$ at roughly the same scale k_*. This result is usually referred to as the COBE normalization of the scalar power spectrum [117]. WMAP, BAO and the SNe data from Ref. [68] together yield a tight upper bound on the tensor-to-scalar ratio, $r < 0.20$ at 95 % CL. A measurement of the tensor spectral index n_t is beyond the scope of any experiment in the near future. In single-field slow-roll models of inflation (cf. Sec. 3.1) n_t does not represent an independent parameter in any case. It is rather directly related to the tensor-to-scalar ratio via the *consistency relation*, $n_t = -r/8$, which reduces the number of free parameters fixing the initial conditions of the CMB anisotropies to three. The background cosmology setting the stage for the evolution of the CMB anisotropies is described by at least five parameters: the expansion rate H_0, the energy densities of matter and baryons, or equivalently $\Omega_m^0 h^2$ and $\Omega_b^0 h^2$, the density parameter of dark energy Ω_{DE}^0, and the coefficient ω in the equation of state for dark energy. In Sec. 2.1, we discussed in detail the numerical values of these parameters according to the CMB data in combination with other cosmological observations. Finally, one astrophysical parameter influences the CMB power spectrum: the integrated optical depth τ, which characterizes the amount of CMB photons that undergo Thomson scattering owing to the reionization of the universe in the recent cosmic past. τ completes the set of standard parameters usually included in analyses of the CMB power spectrum. Beyond this set further parameters, such as the density of massive neutrinos $\Omega_\nu^0 h^2$ or the running of the scalar spectral index $d\, n_s / d \ln k$, may be taken into account as well.

While the CMB stands out as one of the main pillars of the picture of the big bang, it also shows very plainly some of the severe problems big bang cosmology is facing with regard to its initial conditions. First of all, the observation that presently Ω_{tot} does not deviate by more than 1 % from unity gives rise to the *flatness problem*. In a decelerating universe the deviation from exact flatness always grows as some power of the cosmic time.[19] The total density parameter Ω_{tot} of a universe exhibiting a small, but non-zero curvature in the present epoch must hence approach unity to arbitrary precision as one goes back in time. In other words, the initial value of Ω_{tot} must be unnaturally fine-tuned. Second, at the time of last scattering the past or particle horizon, i.e. the distance scale characterizing the radial extent of causally connected domains, is of $\mathcal{O}(100)\,\mathrm{Mpc}$ corresponding to an angular diameter of $\mathcal{O}(1^\circ)$ in the sky. By contrast, the CMB is highly isotropic across the entire sky, which is to say that at the time of decoupling the photon temperature is almost perfectly homogeneous over a huge number of causally disconnected regions. Again, this high degree of homogeneity can only be achieved by an unnatural fine-tuning of the initial conditions, a puzzle which is known as the *horizon problem*. Furthermore, the minute deviations from an exactly isotropic temperature, that we do observe in the CMB, finally lead to the third and perhaps most severe

[19] Given a scale factor $a \propto t^p$, $\Omega_{\mathrm{tot}} - 1$ scales like $\dot{a}^{-2} \propto t^{2(1-p)}$. During the phases of radiation and matter domination we respectively have $p = 1/2$ and $p = 2/3$.

problem. The mechanism responsible for the high degree of homogeneity over a multitude of causally disconnected regions also has to explain why the temperature fluctuations around the homogeneous background are precisely at the level of 10^{-5} and, in particular, why they are correlated over scales exceeding the causal horizon at decoupling. This problem may be translated into the following two fundamental questions: (i) what is the origin of the primordial scalar and tensor perturbations and (ii) which statistical properties do they have? As we will see in Sec. 3.1, all these three problems concerning the initial conditions of the hot big bang can be successfully solved in inflationary cosmology.

2.2.2 Primordial Nucleosynthesis

Primordial or big bang nucleosynthesis (BBN), i.e. the generation of the light elements during the first 20 min of the radiation-dominated era, represents the earliest testable nonequilibrium process in the history of the universe which can be accounted for by well-understood standard model physics only (cf. Fig. 2.1).[20] At present it hence provides the deepest reliable probe of the early universe. The overall agreement of the observed primordial abundances of the light elements with the predictions of BBN serves as a strong corroboration of hot big bang cosmology, underpinning our picture of the early universe to a similar extent as the anisotropies in the CMB.

Before the onset of BBN, at temperatures $T \gg 1\,\mathrm{MeV}$ or correspondingly at times $t \ll 1\,\mathrm{s}$, the weak interactions $n\,\nu_e \leftrightarrows p\,e^-$, $n\,e^+ \leftrightarrows p\,\bar{\nu}_e$, and $n \leftrightarrows p\,e^-\,\bar{\nu}_e$ keep the neutron-to-proton ratio n/p in thermal equilibrium, $n/p = e^{-Q/T}$ with $Q = m_n - m_p = 1.293\,\mathrm{MeV}$ denoting the neutron-proton mass difference. Around a temperature of 1 MeV the rate of neutron-proton interconversion processes Γ_{np} eventually drops below the Hubble rate H and the neutron-to-proton ratio freezes out at $n/p \simeq 1/6$. Subsequent to freeze-out, n/p still continues to decrease due to neutrons undergoing β^- decay, $n \to p\,e^-\,\bar{\nu}_e$. At the time the neutrons decouple from the thermal bath, the temperature has already fallen below the binding energy of deuterium, $T \sim 1\,\mathrm{MeV} < \Delta_\mathrm{D} \simeq 2.23\,\mathrm{MeV}$. The synthesis of deuterium, however, does not yet commence because of the large abundance of highly energetic photons that immediately dissociate each newly formed deuterium nucleus. This delay in the production of the light elements is referred to as the *deuterium bottleneck*. It is overcome once the number of photons per baryon above the deuterium photodissociation threshold has decreased below unity, which happens at a temperature $T \sim 0.1\,\mathrm{MeV}$ or roughly at the end of the first three minutes. The breaking of the deuterium bottleneck marks the onset of BBN. At last deuterium can be efficiently produced and further processed into heavier elements such as helium-3, helium-4 and lithium-7.

Independently of the nuclear reaction rates, virtually all free neutrons end up bound in

[20] For reviews on BBN, cf. for instance Refs. [118, 119].

helium-4, which is the most stable one among the light elements. At $T \sim 0.1\,\mathrm{MeV}$ the neutron-to-proton ratio has decreased to $n/p \simeq 1/7$ and the primordial mass fraction of helium-4 can be estimated as

$$Y_\mathrm{p} = \frac{4\,n_{^4\mathrm{He}}}{n_b} \approx \frac{4\,(n_n/2)}{n_p + n_n} = \frac{2\,n/p}{1 + n/p} \simeq 25\,\%\,, \tag{2.27}$$

which corresponds to a ratio by number of helium-4 to hydrogen of $^4\mathrm{He/H} \simeq 8\,\%$. Deuterium, helium-3 and lithium-7 are produced in much smaller numbers. At the end of BBN around $t \sim 20\,\mathrm{min}$, when the temperature has dropped to $T \sim 0.03\,\mathrm{MeV}$ and most nuclear reactions have become inefficient, D/H and $^3\mathrm{He/H}$ are of $\mathcal{O}\left(10^{-5}\right)$, while $^7\mathrm{Li/H}$ is of $\mathcal{O}\left(10^{-10}\right)$. The complicated network of nuclear reactions that lead to these primordial abundances is described by a coupled system of kinetic equations that needs to be solved numerically [120, 121]. Besides the temperature T or equivalently the cosmic time t, the Hubble rate and the nuclear reaction rates that enter into these equations are functions of only one cosmological parameter: the number density of baryons n_b during BBN. As n_b is directly related to the present value of the BAU, $n_b = n_\gamma\, g_{*,s}/g^0_{*,s}\, \eta^0_B$, this explains why the observed primordial abundances of the light elements give us a handle on η^0_B (cf. Sec. 2.1.3).

The abundance of primordial deuterium is inferred from spectra of high-redshift quasar absorption systems, while primordial helium-4 is observed in low-metallicity regions of ionized hydrogen. The spectra of old metal-poor, i.e. population II stars in the spheroid of our galaxy allow to determine the primordial abundance of lithium-7. All in all, the theoretical BBN predictions match the observed abundances of deuterium, helium-4 and lithium-7 quite well within the η^0_B range stated in Eq. (2.11).[21] An obvious curiosity, however, is that the lithium-7 abundance points to a value of η^0_B that is smaller by at least $4.2\,\sigma$ than the value jointly favoured by the abundances of deuterium and helium-4. This discrepancy is known as the *lithium problem* [122] and potentially indicates effects of new physics.

Leaving aside the lithium problem, we conclude that BBN is able to correctly predict the primordial abundances of the light elements over a range of nine orders magnitude. This success is a milestone of big bang cosmology, encouraging us to believe that the laws of physics which we are able to test in laboratory experiments also apply to the very first moments of the universe. We are thus confident that modern particle physics allows us to speculate about the history of the universe at still earlier times, $t \ll 1\,\mathrm{s}$, although as of now we have no means of observationally accessing them. Furthermore, the success of BBN provides us with a powerful tool to constrain deviations from the standard cosmology.

The helium-4 abundance, for instance, is very sensitive to the value of $g_{*,\rho}$ and thus the

[21] Data on helium-3 solely derives from the solar system and high-metallicity regions of ionized hydrogen in our galaxy, which makes it difficult to infer its primordial abundance. On top of that, the theory of stellar helium-3 synthesis is in conflict with observations. For these two reasons, helium-3 is usually not used as a cosmological probe.

presence of additional relativistic species during BBN [123]. Increasing $g_{*,\rho}$ above its standard value entails a faster Hubble expansion, which results in the neutrons decoupling at earlier times. The neutron-to-proton ratio then freezes out a correspondingly higher temperature, leading to a larger abundance of primordial helium-4 (cf. Eq. (2.27)). Deviations from the standard value of $g_{*,\rho}$ are usually parametrized in terms of an effective number of neutrino species $N_{\mathrm{eff}} = N_{\mathrm{eff}}^{\mathrm{st}} + \Delta N_{\mathrm{eff}}$. Before e^+e^- annihilation, $N_{\mathrm{eff}}^{\mathrm{st}}$ is given as $N_{\mathrm{eff}}^{\mathrm{st}} = 3.046$ [124] and $g_{*,\rho}$ is related to N_{eff} through $g_{*,\rho} = 2 + 7/8 \cdot (4 + N_{\mathrm{eff}} \cdot 2)$. In turns out that the primordial helium-4 mass fraction scales with ΔN_{eff} as $\Delta Y_{\mathrm{p}} \simeq 0.013 \Delta N_{\mathrm{eff}}$ [125], which allows to place limits on N_{eff} by means of the measured abundance of primordial helium-4. In combination with the seven-year WMAP data, one finds $N_{\mathrm{eff}} < 4.2$ at 95 % CL [126].

Likewise, the late-time decay of a massive nonrelativistic particle which is not included in the standard BBN scenario may as well alter the primordial abundances of the light elements. Similarly to additional relativistic species, the presence of such a particle modifies the expansion rate prior to its decay. On top of that, if the new particle dominates the energy density of the universe at the time of its decay, a significant amount of entropy is produced while its decay products thermalize. This changes the time-temperature relationship and results in a diluted baryon-to-photon ratio. Based on these effects, one can derive an upper bound on the lifetime of the decaying particle or equivalently a lower bound on the temperature of the thermal bath at the time the entropy production is completed [127]. If the process of entropy production shortly before BBN is identified with the reheating of the universe after inflation, this lower bound on the temperature corresponds to the lowest possible value of the reheating temperature $T_{\mathrm{RH}}^{\mathrm{min}}$ (cf. Sec. 3.1.1). Combining the observed primordial abundances of deuterium and helium-4 with CMB and LSS data, one obtains $T_{\mathrm{RH}}^{\mathrm{min}} \simeq 4\,\mathrm{MeV}$ at 95 % CL [128].

Independently of whether a long-lived massive particle dominates the energy density of the universe or not, it may after all spoil the success of standard BBN through the cascade processes induced by its decay. Charged particles or photons emitted in radiative decays of the long-lived particle entail electromagnetic showers [129]. Sufficiently energetic photons produced in these showers are then able to photodisintegrate previously formed light nuclei. Moreover, given appropriate couplings and on condition that they are kinematically allowed, decays into colour-charged particles trigger hadronic cascade processes [47]. These involve energetic pions, kaons, neutrons, protons as well as the corresponding antiparticles, all of which are able to react with the light nuclei in various ways. The hadrons emitted in the decays of the long-lived particle induce, for instance, extraordinary interconversion processes between the background nucleons. This leads to an enhancement of the neutron-to-proton ratio after neutron decoupling and thus to a larger abundance of helium-4. At the same time, the energetic hadrons are also able to dissociate background helium-4 nuclei and to produce the other light elements nonthermally. If the decaying particle is electrically charged, it can

form bound states with background nuclei, which again changes the nuclear reaction rates. Especially, the production of lithium-6 may be catalyzed in this way [130].

In order to determine the net effect of a long-lived massive particle on the primordial abundances of the light elements, it is necessary to compute the distributions of the various decay products of the decaying particle as functions of time. These spectra then allow to calculate the rates of the photo- and hadrodissociation, neutron-proton interconversion, and nonstandard production processes induced by the decay of the unstable particle. Requiring the impact of the decaying particle to remain small, such that the consistency between the theoretical BBN predictions and the astrophysical observations is maintained, one can derive constraints on the mass, lifetime and abundance of the unstable particle prior to its decay [48, 49]. In Ch. 8 we will in particular consider bounds on the properties of a very heavy gravitino decaying shortly before BBN [131].

2.2.3 Phase and Topological Transitions

The synthesis of the light elements marks the earliest process in the hot early universe that is firmly established on the basis of observations.[22] The exact nature of all nonequilibrium processes occurring prior to BBN, such as the generation of the BAU or the primordial metric perturbations, are currently still subject to speculations. On the other hand, the standard model of particle physics describes the interactions of elementary particles with great precision all the way up to the TeV scale. Based on standard model physics one is thus able to make an educated guess about the history of the universe up to $T \sim 1\,\mathrm{TeV}$ or equivalently $t \sim 10^{-13}\,\mathrm{s}$. In the following we shall in particular elaborate on the phase and topological transitions which presumably take place in the very early universe.

QCD Phase Transition

At temperatures well above the scale of quantum chromodynamics (QCD),[23] $T \gg \Lambda_{\mathrm{QCD}} \simeq 220\,\mathrm{MeV}$, most quarks, antiquarks and gluons interact only very weakly with each other. Instead of being bound in baryons or mesons, they freely propagate through the thermal bath as independent degrees of freedom, forming what is referred to as a quark-gluon plasma. However, as the temperature decreases, the strong force becomes increasingly stronger, until at a temperature $T \sim 100\,\mathrm{MeV}$ all colour-charged particles get confined in hadrons, i.e. pions for the most part. This transition from the quark-gluon plasma to hadronic matter is known as the QCD or quark-gluon phase transition (cf. Fig. 2.1). Its order parameter, ξ_{QCD},

[22] Recall that BBN enables us to trace the evolution of the hot thermal phase up to temperatures as high as $T_{\mathrm{RH}}^{\mathrm{min}} \simeq 4\,\mathrm{MeV}$ or equivalently cosmic times as early as $t \simeq 0.05\,\mathrm{s}$ (cf. Sec. 2.2.2).

[23] The QCD scale Λ_{QCD} corresponds to the energy scale at which, according to its renormalization group running in perturbative QCD, the strong coupling constant g_s formally diverges.

keeping track of the progress of the QCD transition as it unfolds, is given by the vacuum expectation value (VEV) of the quark condensate operator, $\xi_{\mathrm{QCD}} = \langle q_L q_R + \bar{q}_L \bar{q}_R \rangle$. While ξ_{QCD} initially vanishes, it is of $\mathcal{O}(\Lambda^3_{\mathrm{QCD}})$ at the end of the QCD phase transition. As the quark condensate operator transforms nontrivially under chiral transformations, we conclude that the QCD phase transition entails the spontaneous breaking of the global chiral symmetry in the quark sector. We also note that, according to numerical lattice calculations, the QCD phase transition is most likely a smooth crossover rather than a first or second order phase transition. One thus expects that it does not leave any observationally detectable imprint in the cosmic evolution.

Electroweak Phase Transition

The QCD phase transition is believed to be preceded by the electroweak (EW) phase transition, occurring close to the Fermi or electroweak scale $v_{\mathrm{EW}} \simeq 174\,\mathrm{GeV}$ (cf. Fig. 2.1). At temperatures $T \gg v_{\mathrm{EW}}$ all standard model particles are massless and the universe is said to be in the symmetric phase. The order parameter of the electroweak phase transition, ξ_{EW}, is identified with the VEV of the Higgs product operator $H^\dagger H$, with H denoting the standard model Higgs doublet, $\xi_{\mathrm{EW}} = \langle H^\dagger H \rangle$. By definition, ξ_{EW} vanishes in the symmetric phase. Once the temperature drops below a critical value T_{EW}, the Higgs boson $h \in H$, the electroweak gauge bosons and all fermions except for neutrinos acquire masses through the Higgs mechanism. This is reflected in the order parameter ξ_{EW} obtaining a nonzero value that approaches v^2_{EW} in the zero-temperature limit. Both the explicit value of T_{EW} as well as the order of the electroweak phase transition depend on the Higgs boson mass m_h. The LHC experiments ATLAS and CMS recently presented hints that the Higgs boson may have a relatively large mass, $m_h \simeq 125\,\mathrm{GeV}$ [51, 52]. Based on this value for m_h, one finds $T_{\mathrm{EW}} \simeq 170\,\mathrm{GeV}$ [64]. Furthermore, given $m_h \simeq 125\,\mathrm{GeV}$, the electroweak phase transition turns out to be a smooth crossover without any dramatic cosmological consequences.

After the phase transition the universe is in the Higgs phase and the electroweak symmetry is said to be spontaneously broken to the electromagnetic symmetry,

$$SU(2)_W \times U(1)_Y \to U(1)_{\mathrm{EM}}\,. \tag{2.28}$$

This terminology is, however, not quite correct as $H^\dagger H$ transforms as a singlet under all gauge transformations, so that the electroweak symmetry remains intact even after the electroweak phase transition. What happens instead is a rearrangement of the physical degrees of freedom, proceeding in such a way that after the phase transition the electroweak symmetry is realized in a nonlinear fashion. It would hence be more appropriate to speak of the electroweak symmetry as being *hidden* subsequent to the phase transition. However, as it is more common to refer to it as being *broken*, we will adopt this terminology in the following.[24] We note that

[24] Likewise, when referring to some Higgs product operator $s^\dagger s$ acquiring a VEV v, we will also sometimes

this discussion applies in particular also to the $B-L$ phase transition, during which the $B-L$ gauge symmetry actually becomes hidden rather than broken.

Electroweak Instanton and Sphaleron Transitions

As the temperature approaches the electroweak scale, also nonperturbative processes which simultaneously violate baryon number B and lepton number L gain in importance. Their emergence is a direct consequence of the fact that the electroweak dynamics are governed by a chiral and non-Abelian gauge theory. First of all, we note that both global $U(1)_B$ and $U(1)_L$ transformations represent accidental symmetries of the standard model Lagrangian. Hence, both B and L are conserved in the standard model at the classical level. Due to the chiral nature of the electroweak interactions, they are, however, violated at the quantum level through the triangle anomaly, which results in the divergences of the baryon and lepton number currents, J_B^μ and J_L^μ, being nonzero [12, 13],

$$\partial_\mu J_B^\mu = \partial_\mu J_L^\mu = \frac{N_f}{32\pi^2}\epsilon^{\mu\nu\sigma\tau}\left(-g_W^2 \operatorname{Tr} W_{\mu\nu}W_{\sigma\tau} + g_Y^2 B_{\mu\nu}B_{\sigma\tau}\right) . \tag{2.29}$$

Here, N_f counts the number of fermion families, $\epsilon^{\mu\nu\sigma\tau}$ represents the Levi-Civita symbol in four dimensions, $W_{\mu\nu}^a$ and $B_{\mu\nu}$ are the field strength tensors of the weak and hypercharge gauge fields, and g_W and g_Y denote the corresponding gauge couplings. The second ingredient to the nonconservation of B and L is the complicated structure of the vacuum of the $SU(2)_W$ gauge theory. As for any non-Abelian gauge theory, the $SU(2)_W$ vacuum manifests itself in infinitely many, homotopically distinct,[25] pure gauge configurations, each of which is characterized by a specific integer topological charge or Chern-Simons number $N_{\rm CS}$. An important observation is that distinct realizations of the $SU(2)_W$ vacuum differing by $\Delta N_{\rm CS} = 1$ are connected to each other via a non-contractible loop in field configuration space [132]. The field configuration of highest energy along this path is known as the sphaleron [133]. Corresponding to a saddle-point of the energy functional of the gauge-Higgs system, the sphaleron represents a classical, spatially localized and static, but unstable solution of the electroweak field equations. Its energy $E_{\rm sph}$ determines the height of the potential barrier by which two adjacent realizations of the $SU(2)_W$ vacuum are separated,

$$E_{\rm sph}(T) \simeq \frac{8\pi}{g_W}\sqrt{2}v_{\rm EW}(T) , \quad v_{\rm EW}(T) = \xi_{\rm EW}^{1/2}(T) . \tag{2.30}$$

Now combining the nontrivial topology of the $SU(2)_W$ vacuum with the fact that the currents J_B^μ and J_L^μ have nonzero divergences (cf. Eq. (2.29)), one can show that both B and

write $v = \langle s \rangle$, although we actually mean $v = \langle s^\dagger s \rangle^{1/2}$.

[25] Gauge configurations belonging to different homotopy classes are transformed into each other via *large* gauge transformations.

L are violated in topological vacuum transitions,

$$\Delta B = \Delta L = N_f \, \Delta N_{\mathrm{CS}} \, . \tag{2.31}$$

In the standard model, in which we have $N_f = 3$, the smallest jump in B and L is hence $\Delta B = \Delta L = \pm 3$. The difference between B and L is, by contrast, always conserved in topological transitions. This is also evident from the vanishing divergence of the $B-L$ current, $\partial_\mu J^\mu_{B-L} = \partial_\mu J^\mu_B - \partial_\mu J^\mu_L = 0$ (cf. Eq. (2.29)).

Topological transitions between different realizations of the $SU(2)_W$ vacuum come in two different varieties. One possibility is tunneling *through* the potential barrier via $SU(2)_W$ instantons. The instanton rate is, however, proportional to $\exp\left(-16\pi^2/g_W^2\right) \sim 10^{-170}$ and thus severely suppressed. This is to say that in the standard model B- and L-violating processes are completely negligible at low temperature. On the other hand, in the hot plasma filling the universe during the radiation-dominated era, thermal fluctuations can lead to sphaleron transitions *over* the potential barrier [134]. In the Higgs phase, the sphaleron rate is proportional to $\exp\left(-E_{\mathrm{sph}}/T\right)$ [135] and hence becomes unsuppressed as soon as $T \gtrsim E_{\mathrm{sph}}$. Although the barrier is large at zero temperature, $E_{\mathrm{sph}} \simeq 10\,\mathrm{TeV}$, it rapidly melts away as the temperature approaches the critical value T_{EW} from below (cf. Eq. (2.30)). That is why sphalerons already reach thermal equilibrium at a temperature slightly below the critical temperature, $T^{\mathrm{min}}_{\mathrm{sph}} \sim T_{\mathrm{EW}} - 10\,\mathrm{GeV}$ [136], rather than at temperatures as high as 10 TeV. Conversely, we may say that at $T^{\mathrm{min}}_{\mathrm{sph}}$ the sphaleron processes freeze-out, so that for $T \ll T^{\mathrm{min}}_{\mathrm{sph}}$ both B and L are conserved. This means in particular that at the latest around $T = T^{\mathrm{min}}_{\mathrm{sph}}$ the baryon asymmetry is fixed to its present value.

During the restoration of the electroweak symmetry the potential barrier vanishes completely. Hence, the actual sphaleron configuration in the sense of a saddle-point of the energy functional no longer exists in the symmetric phase. Instead, at $T > T_{\mathrm{EW}}$, topological transitions occur due to thermal fluctuations in the electroweak gauge fields. In the following we shall, however, refer to these transitions as sphaleron processes nonetheless. In the symmetric phase, sphaleron transitions occur at rate per unit volume $\Gamma_{\mathrm{sph}}/V \propto \alpha_W^5 T^4$ [137] where $\alpha_W = g_W^2/(4\pi)$. This result can be used to show that sphalerons are in thermal equilibrium up to a temperature $T^{\mathrm{max}}_{\mathrm{sph}} \sim 10^{12}\,\mathrm{GeV}$. At higher temperatures the sphaleron rate is again outweighed by the expansion rate.

Above the electroweak scale all standard model gauge and Yukawa interactions as well as the electroweak sphaleron and QCD instanton processes are in thermal equilibrium. This implies relations between the chemical potentials of all fermions and Higgs particles, which, together with the requirement that the total hypercharge of the thermal bath be zero, can be used to derive the sphaleron-driven equilibrium values of B and L [138],

$$B = C_{\mathrm{sph}}\,(B-L)\,, \quad L = (C_{\mathrm{sph}} - 1)\,(B-L)\,, \quad C_{\mathrm{sph}} = \frac{8N_f + 4N_H}{22N_f + 13N_H}\,, \tag{2.32}$$

with N_H denoting the number of Higgs doublets. The standard model (SM) only contains one Higgs doublet H, while in its minimal supersymmetric extension, the minimal supersymmetric standard model (MSSM), two Higgs doublets, H_u and H_d, are required in order to ensure anomaly freedom,

$$\text{SM:} \quad N_H = 1\,, \; C_{\text{sph}} = \frac{28}{79} \qquad \text{MSSM:} \quad N_H = 2\,, \; C_{\text{sph}} = \frac{8}{23}\,. \tag{2.33}$$

From Eq. (2.32) we conclude that if $B-L = 0$, sphaleron processes always completely wash out any baryon asymmetry, which is generated in some nonequilibrium process at $T \gg T_{\text{sph}}^{\text{min}}$. By contrast, as $B-L$ is conserved in topological transitions, any primordial $B-L$ asymmetry is guaranteed to survive until sphaleron freeze-out. From this perspective, the baryon asymmetry, which we presently observe in the universe, points to a nonequilibrium process above the electroweak scale that is responsible for the generation of a primordial $B-L$ asymmetry. As we will see in Sec. 3.1.3, leptogenesis is a prime candidate for such a process. Let us denote the time when the $B-L$-violating process, i.e. leptogenesis in our case, terminates by t_f. The present value of the baryon asymmetry or baryon-to-photon ratio η_B is then related to the primordial $B-L$ in the following way,

$$\eta_B^0 = \left.\frac{n_B}{n_\gamma}\right|_{t_0} = C_{\text{sph}} \left.\frac{n_{B-L}}{n_\gamma}\right|_{t_0} = C_{\text{sph}} \frac{g_{*,s}^0}{g_{*,s}} \left.\frac{n_{B-L}}{n_\gamma}\right|_{t_f}\,. \tag{2.34}$$

Chapter 3

Framework for a Consistent Cosmology

As we have seen in the previous chapter, a series of astrophysical and cosmological observations yields direct evidence for a hot thermal stage in the early history of our universe. Owing to the successful theory of BBN, our picture of this phase is rather well established up to times as early as $t \sim 0.1\,\mathrm{s}$. Beyond that, standard model physics allows us to make an educated guess about the further evolution of the universe up to temperatures of $\mathcal{O}(1)\,\mathrm{TeV}$, which are reached at $t \sim 10^{-13}\,\mathrm{s}$. However, we have also seen that, despite the impressive achievements in recent years, modern cosmology still faces a multitude of serious problems, all of which point to new physics beyond the standard model.

In this chapter, we shall thus contrive a consistent cosmological scenario, based on the idea that the hot early universe is ignited by the spontaneous breaking of $B-L$, which provides us with answers to several questions of early universe cosmology in one go. First, we will motivate various extensions of the standard model, each of which has respectively been put forward in order to address one of these questions individually (cf. Sec. 3.1). Then we will assemble all the pieces of the puzzle and outline how the $B-L$ phase transition at the end of inflation gives rise to a consistent cosmology (cf. Sec. 3.2). Finally, we will introduce a phenomenological flavour model based on an Abelian Froggatt-Nielsen flavour symmetry, which will enable us to study this cosmology in quantitative terms.

3.1 Beyond the Standard Model

The theoretical framework, within which we will develop a consistent cosmology, shall feature the following phenomena beyond the standard model: (i) supersymmetric F-term hybrid inflation as the key to resolving the flatness and horizon problems as well as to explaining the origin of the primordial metric fluctuations (cf. Sec. 2.2.1), (ii) the type I seesaw mechanism in order to account for the small masses of the standard model neutrinos (cf. Sec. 2.1.2), (iii) leptogenesis as the process generating the primordial $B-L$ asymmetry in the early universe (cf. Secs. 2.1.3 and 2.2.3), and (iv) gravitinos or other weakly interacting massive particles (WIMPs) as particle candidates for dark matter (cf. Sec. 2.1.4).[1] Let us now discuss each of these phenomena in turn.

3.1.1 Inflation

Basics of Inflation

Inflation denotes a stage of accelerated cosmic expansion taking place in the very early universe during which gravity acts as a repulsive force.[2] It provides viable solutions to the flatness and horizon problems, if during inflation physical scales are stretched by at least a factor of $\mathcal{O}\left(10^{29}\right)$. To see that, note that in an accelerating universe the total density parameter Ω_{tot} always asymptotically approaches unity. Hence, $\Omega_{\mathrm{tot}} = 1$ is a future attractor of any inflationary universe, irrespectively of its concrete initial conditions. After inflation the deviation from exact spatial flatness is, in particular, such small that even at present Ω_{tot} is still very close to unity, although the decelerated expansion during radiation and matter domination actually causes $|\Omega_{\mathrm{tot}} - 1|$ to grow again. Moreover, the inflationary paradigm implies that, as a result of the immense cosmic expansion, the entire observable universe in fact originates from a single homogeneous, causally connected patch.[3] Before the onset of inflation, the entire universe is hence in thermal contact after all, which resolves the horizon problem.

The requirement that the scale factor has to increase by at least a factor of $\mathcal{O}\left(10^{29}\right)$ during inflation can be translated into the condition that at the beginning of inflation the deviation from the vacuum equation of state must not exceed 1 %. In field theory such an

[1] Meanwhile, we will ignore the question as to the nature of dark energy, the coincidence problem (cf. Secs. 2.1.5 and 2.1.6) as well as the lithium problem in BBN (cf. Sec 2.2.2).

[2] The first inflationary model (*old inflation*) was proposed by Alan Guth in 1980 [6]. Subsequently, it was further developed (*new inflation*) by Andrei Linde [7] as well as Andreas Albrecht and Paul Steinhardt [8]. For reviews on inflation, cf. for instance Refs. [139, 140].

[3] The observable universe may as well emerge from an *inhomogeneous*, causally connected domain. Inflation would then simply have to last longer, so that initial inhomogeneities are stretched to physical scales which presently still exceed the size of the observable universe.

equation of state, $\omega \simeq -1$, can be easily realized by a homogeneous real scalar field, the *inflaton* field φ, which slowly rolls down its potential. The inflaton dynamics are governed by the Klein-Gordon equation in an expanding Friedmann-Lemaître background,

$$\ddot{\varphi} + 3H\dot{\varphi} + V'(\varphi) = 0\,, \quad V'(\varphi) = \frac{d}{d\varphi}V(\varphi)\,. \tag{3.1}$$

For a sufficiently flat scalar potential V, the two slow-roll conditions are satisfied: (i) the energy of the scalar field is dominated by its potential energy, $\frac{1}{2}\dot{\varphi}^2 \ll V$, and (ii) the acceleration of the scalar field is negligibly small compared to the friction as well as to the gradient term in its equation of motion, $\left|\ddot{\varphi}\right| \ll 3H\left|\dot{\varphi}\right|, \left|V'\right|$. Eq. (3.1) then reduces to

$$3H\dot{\varphi} + V'(\varphi) \approx 0\,, \tag{3.2}$$

and the equation of state approximately corresponds to the one of the vacuum. In the slow-roll approximation, the scale factor a grows exponentially fast,

$$a(t) \approx a_e \exp\left[H_I\left(t_e - t\right)\right] \approx e^{N_e}\,, \tag{3.3}$$

where H_I denotes the value of the Hubble parameter after neglecting all contributions to the total energy density ρ_{tot} except for the vacuum energy density ρ_0 and N_e stands for the number of *e-folds* by which the universe expands between a given time t and the end of inflation at time t_e,

$$H(t) \approx H_I = \left(\frac{8\pi}{3M_P^2}\rho_0\right)^{1/2}\,, \quad N_e = \int_t^{t_e} dt' H\left(t'\right) \approx H_I\left(t_e - t\right)\,. \tag{3.4}$$

A key argument for attributing inflation to a slowly-rolling scalar field is that it comes with a built-in mechanism to generate the primordial metric fluctuations imprinted in the CMB. Quantum fluctuations of the scalar field arising on scales below the Hubble horizon, $H^{-1} \approx H_I^{-1} = \text{const.}$, are stretched in the course of inflation to ever larger physical scales. As they cross the horizon, the fluctuations *freeze-in*, which means that their amplitudes remain preserved as soon as they become sensitive to curvature effects. Once inflation ends, the primordial fluctuations re-enter the horizon, now in the form of the classical scalar metric perturbations which lay the foundation of the CMB anisotropies. Similarly, tensor metric perturbations stretched to super-horizon scales during inflation give rise to the primordial gravitational waves which also affect the physics of the CMB.

Slow-roll inflation generally predicts nearly scale-invariant and almost perfectly Gaussian power spectra for both primordial scalar and tensor perturbations. In any model of slow-roll inflation, the inflationary observables A_s, n_s, r, and n_t can be conveniently calculated from the slow-roll parameters ϵ_V and η_V,

$$\epsilon_V = \frac{1}{2\kappa}\left(\frac{V'}{V}\right)^2\,, \quad \eta_V = \frac{1}{\kappa}\frac{V''}{V}\,, \quad \kappa = \frac{8\pi}{M_P^2}\,. \tag{3.5}$$

The two slow-roll conditions stated above are equivalent to the requirement that ϵ_V and η_V be very small, $\epsilon_V, |\eta_V| \ll 1$. If that requirement is fulfilled, one finds

$$P_s(k) \approx \left.\frac{\kappa^2 V}{24\pi^2\epsilon_V}\right|_{aH=k}, \quad P_t(k) \approx \left.\frac{2\kappa^2 V}{3\pi^2}\right|_{aH=k}, \tag{3.6}$$

where for a given scale k the right-hand sides of both equations are to be evaluated at the respective time when the scale exits the Hubble horizon during inflation. From Eq. (3.6) one can easily deduce:

$$A_s = P_s(k_*), \quad n_s = 1 + 2\eta_V - 6\epsilon_V, \quad r = 16\epsilon_V, \quad n_t = -2\epsilon_V, \tag{3.7}$$

where ϵ_V and η_V are understood to be evaluated at $k = k_*$.

At the end of inflation the universe is flat, homogeneous and isotropic. Its energy density only receives contributions from the vacuum as well as the homogeneous inflaton field φ, which may be regarded as a classical condensate of inflaton particles. The energy densities of other particles, any pre-existent baryon asymmetry, the abundance of topological defects as well as any primordial curvature are completely diluted during inflation.[4] Subsequent to inflation, the energy contained in the vacuum and the inflaton field is converted into the energy of a hot thermal plasma. This process, connecting the inflationary stage with the radiation-dominated era, is known as the *reheating* of the universe and a large fraction of this thesis is devoted to a detailed study of its dynamics. The characteristic temperature scale of reheating is referred to as the reheating temperature T_{RH}. It is a measure for the highest temperature ever reached in the hot early universe and thus represents one of the most important parameters of early universe cosmology. In the context of our cosmological framework, it is in particular closely related to the origin of the BAU and the nature of dark matter. Note that, in Fig. 2.1, we have indicated several possibilities for the actual value of the reheating temperature.

Supersymmetric *F*-Term Hybrid Inflation

Among the multitude of inflationary models present in the literature, we shall consider supersymmetric F-term hybrid inflation in thesis. In general, models of hybrid inflation feature next to the inflaton field φ at least one second scalar field, the *waterfall* field σ, which is stabilized during inflation due to its interactions with the inflaton field and whose potential energy dominates the total energy budget.[5] However, once φ drops below a critical value φ_c, the waterfall field σ becomes destabilized and inflation ends in a phase transition, during which φ and σ evolve from the unstable *false* vacuum to the stable *true* vacuum. Depending on the transformation behaviour of the field σ, this phase transition at the end of inflation

[4] The rigorous formulation of this statement goes by the name of the *no-hair* theorem [141].

[5] Note that hybrid inflation differs in this respect from ordinary single-field inflation, during which ρ_{tot} receives its largest contribution from the potential energy of the inflaton field itself.

may be accompanied by the spontaneous breakdown of some global or local symmetry of the Lagrangian. Hybrid inflation hence offers a natural setting for spontaneous symmetry breaking (SSB) in the course of the cosmic evolution. In this sense, it allows to establish a connection between cosmology and particle physics and thus represents a particularly attractive scenario of inflation. The symmetry breaking at the end of hybrid inflation may, in particular, be identified as an intermediate stage in the breaking of the gauge group G_{GUT} of some grand unified theory (GUT) down to the standard model gauge group G_{SM}. The scalar sector, containing among other fields the two scalars φ and σ, would then be determined by the particle content of the respective GUT theory and inflation would turn out to be a mere implication of particle physics. As we will discuss in more detail below, we shall, of course, presume that it is the difference between baryon and lepton number $B-L$ which is broken at the end of inflation.

The first and simplest model of hybrid inflation was proposed by Andrei Linde in the early 1990s [9, 10]. Rather than embedding SSB into a cosmological context, Linde's original motivation, however, was to construct a model in which inflation ends differently as compared to the standard scenarios featuring a first-order phase transition or a slow-roll motion gradually becoming faster and faster. Indeed, under quite generic conditions, the field σ evolves very rapidly, though continuously, towards the true vacuum during the phase transition (cf. Sec. 6.2). Hybrid inflation hence typically ends very abruptly, which is why the phase transition marking its end is usually referred to as a *waterfall* transition. Unfortunately, Linde's model predicts a scalar spectral index $n_s \geq 1$, with the deviation from an exactly flat spectrum, $n_s = 1$, generically being very small. As observations point to $n_s = 0.963 \pm 0.012$ (cf. Eq. (2.26)), it is therefore disfavoured at the level of at least $3\,\sigma$. This conflict with the observational data can, however, be resolved in supersymmetric versions of hybrid inflation.

Let us consider supersymmetric F-term hybrid inflation, which is implemented by the following superpotential [16, 17],

$$W_{B-L} = \frac{\sqrt{\lambda}}{2}\Phi\left(v_{B-L}^2 - 2S_1S_2\right) . \tag{3.8}$$

Here, λ is a dimensionless coupling constant, v_{B-L} represents a mass scale, and Φ, S_1 and S_2 are chiral superfields. W_{B-L} is the simplest renormalizable superpotential allowing for the spontaneous breaking of a $U(1)$ symmetry of the Lagrangian. We identify this $U(1)$ with the global $U(1)_{B-L}$, which is preserved in standard model interactions even at the quantum level (cf. Sec. 2.2.3),[6] and assign the following $B-L$ charges to the three chiral superfields: $q_\Phi = 0$ as well as $q_S \equiv q_{S_2} = -q_{S_1} = 2$. Hence, Φ represents a $B-L$ singlet, while the two fields S_1 and S_2 transform as conjugates of each other. The radial component φ of the complex scalar $\phi = \varphi/\sqrt{2}e^{i\theta}$ contained in Φ plays the role of the inflaton. The $B-L$ Higgs boson or waterfall field σ corresponds to one of the four real scalar degrees of freedom contained

[6] In Sec. 3.1.2, we will see that $U(1)_{B-L}$ can, in fact, also be promoted to a local symmetry.

in the superfields S_1 and S_2 (cf. Sec. 5.1). In the following, we shall collectively refer to all component fields of Φ, S_1 and S_2 as the symmetry breaking sector. Given the above $B-L$ charge assignments, we remark that W_{B-L} is *natural* in the strong sense that it is the most general renormalizable superpotential which is compatible with the $U(1)_{B-L}$ as well as with R symmetry. As the superpotential itself has to carry R charge $R(W_{B-L}) = 2$, we know that $R(\Phi) = 2$ and $R(S_1 S_2) = 0$, which means that $R(S_1) = R(S_2) = 0$ in the simplest case. These R charge assignment forbid all terms involving the inflaton field Φ except for the linear term in Eq. (3.8) and hence enforce the absence of undesirable inflaton couplings. Meanwhile, the $B-L$ charges ensure that S_1 and S_2 can only appear in the superpotential in the form of their product $S_1 S_2$.

During inflation the scalar mass eigenstates contained in S_1 and S_2 have masses $m_{s_\pm}^2 = \lambda/2\left(\varphi^2 \mp v_{B-L}^2\right)$ (cf. Sec. 5.1) and are thus stabilized at the origin for large inflaton field values. The inflaton-Higgs system is hence in the false vacuum state, $\langle\Phi\rangle \neq 0$ and $\langle S_1\rangle = \langle S_2\rangle = 0$, and the scalar potential energy is dominated by the vacuum energy density ρ_0,

$$S_{1,2} \to 0 : \quad V \to |W_{,\Phi}|^2 = \frac{1}{4}\lambda v_{B-L}^4 = \rho_0 \,, \quad W_{,\Phi} = \frac{\partial W}{\partial \phi} \tag{3.9}$$

As ρ_0 originates from the F-term contribution $|W_{,\Phi}|^2$ to the scalar potential, the model defined through Eq. (3.8) is known as F-term hybrid inflation. Correspondingly, models in which ρ_0 stems from a D-term contribution to the scalar potential are referred to as D-term hybrid inflation [142, 143]. Note that, while $B-L$ is conserved during inflation, supersymmetry is spontaneously broken by ρ_0. This situation is reversed at the end of inflation. Once the inflaton field φ drops below the critical value $\varphi_c = v_{B-L}$, the mass squared of the waterfall field turns negative, i.e. the waterfall field becomes tachyonically unstable, which triggers the transition to the true vacuum. In the true ground state, supersymmetry is no longer broken, but $B-L$ is broken spontaneously, $\langle\Phi\rangle = 0$ and $\langle S_1\rangle = \langle S_2\rangle = v_{B-L}/\sqrt{2}$. This phase transition entailing the breaking of $B-L$ gives this thesis its name. In Sec. 5.1, we will compute the full Lagrangian governing the $B-L$ phase transition; in Ch. 6, we will then elaborate in more detail on the various nonperturbative processes associated with it.

An appealing feature of supersymmetric hybrid inflation is that it comes with an intrinsically flat inflaton potential. Along the inflationary trajectory, $S_{1,2} = 0$, the ordinary tree-level scalar potential is constant (cf. Eq. (3.9)). Furthermore, assuming a canonical Kähler potential, one can show that, as W_{B-L} is linear in the inflaton field Φ, the supergravity (SUGRA) corrections to the inflaton mass m_φ exactly cancel at tree-level [16]. This provides a solution to the notorious *eta problem*, with which inflationary models based on supergravity usually have to struggle. As supergravity typically induces inflaton masses of order the Hubble rate, $m_\varphi^2 \sim H_I^2 = 8\pi\rho_0/\left(3M_P^2\right)$, the contribution from the inflaton mass to the slow-roll parameter η_V can become dangerously large, $\eta_V = m_\varphi^2 M_P^2/\left(8\pi V\right) + \ldots \sim 1$. Given the superpotential

W_{B-L}, together with a minimal Kähler potential, the eta problem is now partly resolved.[7] The actual slope of the inflaton potential, causing φ to roll towards its critical value φ_c, is induced at the one-loop level by the Coleman-Weinberg potential [144],

$$V_{\rm CW} = \frac{1}{64\pi^2}\mathrm{STr}\left[M^4 \ln\left(\frac{M^2}{\Lambda^2}\right)\right] , \quad \mathrm{STr}\, M^2 = \sum_s (-1)^{2s}\,(2s+1)\,\mathrm{Tr}\, M_s^2 , \tag{3.10}$$

where Λ is a renormalization scale and M^2 denotes the total mass matrix squared of our theory, which receives contributions from particles of all possible spins s, $M^2 = \bigoplus_s M_s^2$. Thanks to the spontaneous breaking of supersymmetry by the vacuum energy density ρ_0, the supertrace in Eq. (3.10) ends up being nonzero. The mass splitting among the mass eigenstates contained in S_1 and S_2 results in

$$V_{\rm CM} = \frac{\lambda\rho_0}{16\pi^2}\left[\ln\left(\frac{\lambda\varphi^2}{2\Lambda^2}\right) + \frac{1}{2}\sum_{n=\pm 1}\left(1+n\,x^2\right)^2 \ln\left(1+n\,\frac{1}{x^2}\right)\right] , \quad x = \frac{\varphi}{\varphi_c} . \tag{3.11}$$

Beyond the radiative Coleman-Weinberg correction, SUGRA induces further terms in the inflaton potential. As stated above, these are at least of fourth order in φ assuming a minimal Kähler potential, but also include an inflaton mass term, if the Kähler potential has a noncanonical form [145]. Anyway, since we are mainly interested in the transition from inflation to the hot thermal universe rather than in the exact inflationary dynamics, we may disregard all SUGRA corrections. More precisely, we can safely neglect all SUGRA effects in our analysis, as long as the $B-L$ phase transition takes place at a scale, which is much lower than the Planck scale. Moreover, there is a curvature-induced correction to the inflaton potential, which, however, turns out to be insignificant for all viable values of λ [33, 146].

Finally, let us analytically estimate the parameter dependence of the inflationary observables A_s and n_s. The scale k_*, on which these quantities are determined in CMB observations, leaves the Hubble horizon $N_e^* \simeq 50$ e-folds before the end of inflation [147]. For intermediate values of the coupling constant, $\lambda \sim 10^{-4}$, the inflaton field value φ_* at this time is much larger than the critical value, but still far below the Planck scale. To first approximation, the effective inflaton potential is then given as:

$$\varphi_c \ll \varphi \ll M_P : \quad V_{\rm eff}\,(\varphi) \approx \rho_0\left[1 + \frac{\lambda}{16\pi^2}\ln\left(\frac{\lambda\varphi^2}{2\Lambda^2}\right)\right] , \tag{3.12}$$

from which one easily deduces the two slow-roll parameters ϵ_V and η_V,

$$\epsilon_V \approx \frac{\lambda}{16\pi^2}\,|\eta_V| , \quad \eta_V \approx -\frac{1}{2N_e} , \quad N_e \approx \frac{32\pi^3}{\lambda M_P^2}\varphi^2 . \tag{3.13}$$

Hence, ϵ_V is always negligibly small compared to $|\eta_V|$. On the other hand, $|\eta_V|$ may become of order unity way before the inflaton field reaches φ_c. We conclude that inflation ends at

[7] Of course, other scalar fields present in the early universe and having values of $\mathcal{O}(M_P)$, such as moduli fields from string theory, could still spoil inflation through their contributions to η_V.

φ_e, which either corresponds to $\varphi_{\rm sr}$, the field value at which the slow-roll condition $|\eta_V| \ll 1$ becomes violated, or to φ_c, the critical field value,

$$\varphi_e = \max\left[\varphi_c, \varphi_{\rm sr}\right] , \quad \varphi_c = v_{B-L} , \quad \varphi_{\rm sr} \approx \sqrt{\frac{\lambda}{\pi}} \frac{M_P}{8\pi} . \tag{3.14}$$

According to Eqs. (3.6), (3.7) and (3.13), one finds for the amplitude of the scalar power spectrum and the scalar spectral index,

$$A_s \approx \frac{64\pi^2}{3} N_e^* \left(\frac{v_{B-L}}{M_P}\right)^4 , \quad n_s \approx 1 - \frac{1}{N_e^*} . \tag{3.15}$$

The measured value of A_s (cf. Eq. (2.26)) thus allows to estimate the scale v_{B-L},

$$v_{B-L} \approx \left(\frac{3A_s}{64\pi^2 N_e^*}\right)^{1/4} M_P \simeq 8 \times 10^{15}\ {\rm GeV} \left(\frac{A_s}{2.441 \times 10^{-9}}\right)^{1/4} \left(\frac{50}{N_e^*}\right)^{1/4} , \tag{3.16}$$

which is remarkably close to the GUT scale.[8] Similarly, given $N_e^* \simeq 50$, we obtain

$$n_s \simeq 0.98 . \tag{3.17}$$

This result for n_s, deviating from the best-fit value of $n_s \simeq 0.963$ by only $1.4\,\sigma$, may be regarded as a satisfactory improvement in comparison to Linde's original nonsupersymmetric prediction $n_s \geq 1$. However, one can show that for very small, $\lambda \lesssim 10^{-6}$, as well as for very large, $\lambda \gtrsim 10^{-2}$, values of the coupling constant λ, the spectral index increases above the naive estimate in Eq. (3.17) [147]. $n_s \simeq 0.98$ should, hence, rather be considered as a lower bound on n_s. One possibility to improve on the predicted n_s value is to allow nonminimal terms in the Kähler potential, which, however, requires the tuning of at least one additional dimensionless parameter to an unnaturally small value. Again, as we wish to focus on the $B-L$ phase transition instead of the inflationary dynamics in this thesis, we shall content ourselves with the result in Eq. (3.17) and forget about possible SUGRA corrections in the following.

3.1.2 Right-Handed Neutrinos and the Seesaw Mechanism

Observations of atmospheric, solar, reactor, and accelerator neutrinos clearly indicate flavour oscillations, i.e. in-flight flavour transitions, among the three standard model neutrino species [4, 5, 148–150].[9] These oscillations are attributed to small mass-squared differences, $\Delta m^2_{\rm atm}$ and $\Delta m^2_{\rm sol}$, between the three known neutrino states, and hence point to new physics beyond

[8] GUT theories are characterized by the fact that, as a result of renormalization group running, all gauge couplings g_i unify, i.e. obtain the same value $g_{\rm GUT}$, at some scale $\Lambda_{\rm GUT}$. In the MSSM, the GUT coupling is expected to be $g_{\rm GUT} \simeq \sqrt{\pi/6} \simeq 0.72$, while the GUT scale $\Lambda_{\rm GUT}$ turns out to be of $\mathcal{O}\left(10^{16}\right)$ GeV.

[9] For reviews on neutrino physics, cf. for instance Refs. [2, 151, 152].

the standard model. At the $3\,\sigma$ CL, $\left|\Delta m^2_{\text{atm}}\right|$ and Δm^2_{sol} are constrained to lie within the following ranges [2],

$$2.07 \times 10^{-3}\,\text{eV}^2 \leq \left|\Delta m^2_{\text{atm}}\right| \leq 2.75 \times 10^{-3}\,\text{eV}^2\,, \tag{3.18}$$

$$7.05 \times 10^{-5}\,\text{eV}^2 \leq \Delta m^2_{\text{sol}} \leq 8.34 \times 10^{-5}\,\text{eV}^2\,. \tag{3.19}$$

In the standard model, neutrinos are considered to be massless left-handed Weyl fermions. In order to account for the small neutrino masses, we supplement the standard model particle content by three right-handed neutrinos, so that neutrinos can either acquire Dirac or Majorana mass terms.[10] Which of these two possibilities is realized in nature is unknown at present and represents one of the greatest questions of modern neutrino physics. In this thesis, we shall assume that neutrinos are Majorana fermions. A minimal mechanism capable of generating neutrino masses of the right magnitude is then provided by the type I seesaw mechanism [23–27][11].

Superpotential for the Quark and Lepton Superfields

The superpotential setting the stage for the type I seesaw mechanism may be cast in the following form,

$$W_{\text{Seesaw}} = \frac{1}{\sqrt{2}} h^n_i n^c_i n^c_i S_1 + h^\nu_{ij} \mathbf{5}^*_i n^c_j H_u\,. \tag{3.20}$$

It combines with the MSSM superpotential W_{MSSM} to give the total superpotential for all chiral quark and lepton superfields present in our theoretical framework,

$$W_{\text{QL}} = W_{\text{Seesaw}} + W_{\text{MSSM}}\,, \tag{3.21}$$

$$W_{\text{MSSM}} = h^u_{ij} \mathbf{10}_i \mathbf{10}_j H_u + h^d_{ij} \mathbf{5}^*_i \mathbf{10}_j H_d\,. \tag{3.22}$$

In Eqs. (3.20) and (3.22), all superfields have been arranged in $SU(5)$ multiplets,[12] the indices $i, j = 1, 2, 3$ label the different fermion generations,

$$S_1 \sim \mathbf{1}\,, \quad n^c \sim \mathbf{1}\,, \quad H_u \sim \mathbf{5}\,, \quad H_d \sim \mathbf{5}^*\,, \quad \mathbf{5}^* = (d^c, \ell)\,, \quad \mathbf{10} = (q, u^c, e^c)\,. \tag{3.23}$$

[10] As current neutrino data is still consistent with one standard model neutrino being massless, one is only forced to introduce two right-handed neutrinos. We shall, however, assume that each left-handed neutrino is complemented by a corresponding right-handed neutrino.

[11] The type II and III variants of the seesaw mechanism feature couplings of the left-handed neutrinos to weak isospin Higgs or fermion triplets rather than to right-handed neutrino singlets.

[12] This $SU(5)$ structure of the superpotential implies mass unification of down-type quarks and charged leptons at the GUT scale, which may indeed be accomplished, if nonrenormalizable terms in the Lagrangian are arranged such that they yield appropriate mass corrections [153]. Also, note that we do not take $SU(5)$ to be the gauge group of our model (cf. Eq. (3.24)).

The left-handed Weyl fermions $\nu_{R,i}$ contained in the neutrino superfields n_i^c are the antiparticles of the right-handed neutrinos $\bar{\nu}_{R,i}$ required by the seesaw mechanism. The superfields n_i^c hence carry $B-L$ charge $q_{n^c} = 1$, which explains why they couple to the negatively charged Higgs superfield S_1 rather than to the positively charged Higgs superfield S_2. Similarly, as can be seen from the superpotential in Eq. (3.20), the superfields n_i^c have R charge $R(n_i^c) = 1$, which forces the R charges of S_1 and S_2 to vanish (cf. Sec. 3.1.1). Furthermore, including three right-handed neutrinos into the particle spectrum of our model allows us to promote the *global* $U(1)_{B-L}$, which is a symmetry of the standard model Lagrangian even at the quantum level, to an anomaly-free *local* symmetry [14, 15]. Before the $B-L$ phase transition, the full gauge group G of our model is hence given as

$$G = G_{\mathrm{SM}} \times U(1)_{B-L}\,, \quad G_{\mathrm{SM}} = SU(3)_C \times SU(2)_W \times U(1)_Y\,. \tag{3.24}$$

It is an intriguing possibility that, allowing for a rescaling of the $B-L$ coupling strength, the group G may in fact represent an intermediate stage in the breaking of some GUT gauge group such as $SO(10)$ down to the standard model gauge group G_{SM} [11]. A hint towards such a scenario might be that one quark-lepton family of the standard model plus one right-handed neutrino exactly fits into the smallest complex representation of $SO(10)$.

The Higgs superfields H_u and H_d in Eqs. (3.20) and (3.22) transform in the fundamental and anti-fundamental representation of $SU(5)$, respectively, and thus both consistent of a colour triplet as well as a weak isospin doublet. While the Higgs doublets are supposed to obtain masses of order the electroweak scale, the masses of the Higgs triplets have to exceed the GUT scale in order to avoid too rapid proton decay. This dilemma is known as the *doublet-triplet splitting problem* [154]. We assume one of the many mechanisms proposed in the literature and capable of solving this problem (cf. Ref. [155] and references therein) to be at work and thus regard the Higgs triplets as being projected out of the superpotential W_{QL}. Correspondingly, we shall denote with H_u and H_d the doublet components of the respective Higgs multiplets from now on. During the electroweak phase transition, the electrically neutral components of these two doublets acquire nonzero VEVs, $v_u = \langle H_u^0 \rangle$ and $v_d = \langle H_d^0 \rangle$, which leads to the spontaneous breakdown of the electroweak symmetry.[13] Adding v_u and v_d in quadrature yields the electroweak scale, $v_{\mathrm{EW}} = \left(v_u^2 + v_d^2\right)^{1/2}$, while the ratio v_u/v_d defines the mixing angle β via $\tan\beta = v_u/v_d$. In the following, we will assume large $\tan\beta$, implying that $v_d \ll v_u \simeq v_{\mathrm{EW}}$.

Finally, h^n, h^ν, h^u, and h^d denote Yukawa matrices. In general, h^n is an arbitrary complex symmetric matrix. By means of a Takagi diagonalization it can, however, always be brought into a diagonal form with real and nonnegative entries h_i^n on the diagonal such that $h_i^n \leq$

[13] The description of the electroweak phase transition in the MSSM is conceptually similar to the standard model description, which we outlined in Sec. 2.2.3. Also in the MSSM, the phase transition is typically governed by the evolution of a single light scalar degree of freedom, so that the same effective finite-temperature theory is applicable as in the standard case [156].

h^n_{i+1} [157]. Eq. (3.20) presents W_{Seesaw} in a form which assumes that such a diagonalization has previously been performed.

Neutrino Masses from $B-L$ and Electroweak Symmetry Breaking

During the $B-L$ phase transition at the end of hybrid inflation (cf. Sec. 3.1.1), the Higgs superfield S_1 acquires a nonzero VEV, which spontaneously breaks $B-L$ and generates a Majorana masses for the neutrino superfields n^c_i,

$$S_1 \to \frac{v_{B-L}}{\sqrt{2}} + S_1 \; : \quad \frac{1}{\sqrt{2}} h^n_i n^c_i n^c_i S_1 \to \frac{1}{2} M_i n^c_i n^c_i + \frac{1}{\sqrt{2}} h^n_i n^c_i n^c_i S_1 \,. \tag{3.25}$$

Consequently, the massless right-handed Weyl neutrinos $\bar{\nu}_{R,i}$ combine with the massless left-handed Weyl antineutrinos $\nu_{R,i}$ to form heavy Majorana neutrinos,[14]

$$N_i = \begin{pmatrix} \nu_{R,i} \\ \bar{\nu}_{R,i} \end{pmatrix} \,. \tag{3.26}$$

From this relation between the Majorana neutrinos N_i and the Weyl fermions $\nu_{R,i}$ and $\bar{\nu}_{R,i}$ it is evident that the N_i, rather than being uncharged under $B-L$, do not carry any definite $B-L$ charge at all. As we shall see in the next section, this property of the heavy Majorana neutrinos is a crucial ingredient for the generation of the primordial $B-L$ asymmetry in the early universe. Each of the heavy Majorana neutrinos N_i is accompanied by a superpartner, with which it shares a common mass M_i. These *sneutrinos* $\tilde{N}_i$ directly correspond to the complex scalars contained in the neutrino superfields n^c_i. In the true vacuum reached at the end of the $B-L$ phase transition, the heavy-(s)neutrino mass matrix is given as

$$M = v_{B-L} h^n = \text{diag}\,(M_1, M_2, M_3) \,, \quad M_1 \leq M_2 \leq M_3 \,, \tag{3.27}$$

and the seesaw superpotential contains, next to the Yukawa interaction with the Higgs superfield S_1, the following two terms,

$$W_{\text{Seesaw}} \supset \frac{1}{2} M_i n^c_i n^c_i + h^\nu_{ij} \ell_i n^c_j H_u \,. \tag{3.28}$$

The fermionic Lagrangian derived from Eq. (3.28) accounts for the interaction of the heavy Majorana neutrinos with the standard model lepton-Higgs pairs $\ell_i H_u$. Considering processes at energies far below the neutrino masses M_i, it is at our discretion to integrate the heavy neutrinos out of the Lagrangian. In the low-energy effective theory below the neutrino mass threshold, the $\ell_i \nu_{R,j} H_u$ interaction term then mutates into the dimension-5 Weinberg operator [158],

$$\mathcal{L}_{(5)} = \frac{1}{2} \left[h^\nu M^{-1} (h^\nu)^T \right]_{ij} (H_u \ell)_i (H_u \ell)_j + \text{h.c.} \,. \tag{3.29}$$

[14] Here, $\nu_{R,i}$ and $\bar{\nu}_{R,i}$ denote two-component spinors, while the N_i are four-component spinors.

In the course of electroweak symmetry breaking, the Higgs doublet H_u acquires a nonzero VEV, $\langle H_u \rangle = (0, v_u)^T$, so that $\mathcal{L}_{(5)}$ assumes the form of a Majorana mass term for the standard model neutrinos $\nu_{L,i}$ contained in $\ell_i = (\nu_{L,i}, e_{L,i})^T$,

$$H_u \to (0, v_u)^T \; : \quad \mathcal{L}_{(5)} \to -\frac{1}{2} \left(m_\nu\right)_{ij} \nu_{L,i} \nu_{L,j} + \text{h.c.}\,, \tag{3.30}$$

where the light-neutrino mass matrix m_ν is given by the *seesaw formula*

$$m_\nu = -m_D M^{-1} m_D^T\,, \quad m_D = v_u h^\nu\,, \tag{3.31}$$

with m_D denoting the neutrino Dirac mass matrix. m_ν is again a complex symmetric matrix that is Takagi-diagonalized by a unitary transformation Ω,

$$\Omega^T m_\nu \Omega = m_\nu^{\text{diag}} = \text{diag}\left(m_1, m_2, m_3\right)\,. \tag{3.32}$$

According to the measured differences of the masses-squared, $\Delta m_{ij}^2 = m_i^2 - m_j^2$, the light-neutrino mass spectrum may either exhibit a *normal* (NH) or an *inverted hierarchy* (IH). For definiteness, i.e. in order to fix the column ordering of Ω, one conventionally numbers the light-neutrino mass eigenstates such that

$$\text{normal hierarchy:} \quad 0 \leq m_1 < m_2 \ll m_3\,, \tag{3.33}$$

$$\text{inverted hierarchy:} \quad 0 \leq m_3 \ll m_1 < m_2\,. \tag{3.34}$$

Since the atmospheric neutrino oscillations are predominantly sourced by the largest Δm_{ij}^2 in the neutrino mass spectrum, while the solar neutrino oscillations are driven by the smallest Δm_{ij}^2, we may now identify Δm_{sol}^2 and Δm_{atm}^2 as

$$\Delta m_{\text{sol}}^2 = \Delta m_{21}^2\,, \quad \Delta m_{\text{atm}}^2 = \Delta m_{31}^2\,(\text{NH})\,, \Delta m_{32}^2\,(\text{IH})\,. \tag{3.35}$$

For very small m_1 (NH) or m_3 (IH), the light-neutrino mass spectrum features one (NH) or two (IH) neutrinos with a mass of roughly $\left(\Delta m_{\text{atm}}^2\right)^{1/2} \simeq 0.05\,\text{eV}$. Assuming Dirac masses of order the electroweak scale, $\left(m_D\right)_{ij} \sim v_{\text{EW}}$, such small light-neutrino masses readily follow from the seesaw formula (cf. Eq. (3.31)), given a heavy-neutrino mass scale of $\mathcal{O}\left(10^{15}\right)$ GeV. We hence conclude that the observed neutrino oscillations strongly suggest the existence of heavy Majorana neutrinos whose masses are generated in the course of $B-L$ breaking close to the GUT scale.

The weak isospin partners of the standard model neutrinos, the charged leptons $e_{L,i}$, acquire Dirac masses due to their Yukawa coupling to the down-type Higgs doublet H_d (cf. the second term of W_{MSSM} in Eq. (3.22)). During the electroweak phase transition H_d obtains a nonzero VEV, $\langle H_d \rangle = (v_d, 0)^T$, which gives rise to the charged-lepton Dirac mass matrix $m_{\text{cl}} = v_d h^d$. In general, m_{cl} is an arbitrary complex matrix that can be diagonalized by means of a singular value decomposition. For appropriate unitary matrices L and R, one has

$$L^T m_{\text{cl}} R = m_{\text{cl}}^{\text{diag}} = \text{diag}\left(m_e, m_\mu, m_\tau\right)\,, \quad m_{\text{cl}} = v_d h^d\,. \tag{3.36}$$

The fact that neutrinos are massive entails flavour-changing charged-current interactions in the lepton sector, accounted for by the following Lagrangian,

$$\mathcal{L}_{\mathrm{CC}} \supset -\frac{g}{\sqrt{2}} U_{ij} \hat{\bar{e}}_{L,i} \bar{\sigma}^{\mu} \hat{\nu}_{L,j} W_{\mu}^{-} + \mathrm{h.c.}\,, \quad U = L^{\dagger}\Omega\,. \tag{3.37}$$

Here, U denotes the Pontecorvo-Maki-Nakagawa-Sakata (PMNS) or lepton mixing matrix [159–161] and $\hat{e}_{L,i}$ and $\hat{\nu}_{L,i}$ represent the charged-lepton and light-neutrino fields in the mass eigenbasis. A priori, the PMNS matrix is an arbitrary unitary matrix, which may be parametrized in terms of three mixing angles $\theta_{12}, \theta_{13}, \theta_{23} \in [0, \pi/2]$ and six complex phases. However, due to the freedom of redefining the phases of the charged-lepton fields, the number of physical complex phases in U reduces to three: $\delta, \alpha_{21}, \alpha_{31} \in [0, 2\pi)$, where δ is referred to as the *Dirac phase* and α_{21} and α_{31} are the two *Majorana phases*.[15] In the standard parametrization U is given as [2]

$$U = \begin{pmatrix} c_{12}c_{13} & s_{12}c_{13}e^{i\frac{\alpha_{21}}{2}} & s_{13}e^{i(\frac{\alpha_{31}}{2}-\delta)} \\ -s_{12}c_{23} - c_{12}s_{23}s_{13}e^{i\delta} & \left(c_{12}c_{23} - s_{12}s_{23}s_{13}e^{i\delta}\right)e^{i\frac{\alpha_{21}}{2}} & s_{23}c_{13}e^{i\frac{\alpha_{31}}{2}} \\ s_{12}s_{23} - c_{12}c_{23}s_{13}e^{i\delta} & \left(-c_{12}s_{23} - s_{12}c_{23}s_{13}e^{i\delta}\right)e^{i\frac{\alpha_{21}}{2}} & c_{23}c_{13}e^{i\frac{\alpha_{31}}{2}} \end{pmatrix}, \tag{3.38}$$

where $c_{ij} = \cos\theta_{ij}$ and $s_{ij} = \sin\theta_{ij}$. Note that owing to its complex phases δ, α_{21} and α_{31}, the PMNS matrix is in general not real, $U \neq U^*$, which implies the nonconservation of CP in the charged-current interactions governed by the Lagrangian in Eq. (3.37). The phases δ, α_{21} and α_{31} are consequently also known as the CP violation phases of the PMNS matrix.

3.1.3 Baryogenesis

According to the seminal work of Andrei Sakharov in 1967 [162], any process in the early universe which might come into question for the dynamical generation of the primordial baryon asymmetry, i.e. which might provide a viable scenario of *baryogenesis*, has to satisfy three necessary conditions. It has to (i) violate the conservation of baryon number B, (ii) violate C as well as CP invariance, and (iii) involve a departure from thermal equilibrium.[16] Interestingly, all ingredients for successful baryogenesis are therefore in principle inherent in the standard model [134]: B is violated in $SU(2)_W$ sphaleron processes; due to their chiral nature, all electroweak interactions maximally violate C; the presence of a complex phase in the quark mixing matrix implies CP violation; and the out-of-equilibrium condition is satisfied during the EWPT, if it is of first order. However, as it turns out, the amount of CP violation in flavour-changing interactions in the quark sector is too small to account for the observed baryon asymmetry [163] and, more importantly, given a Higgs mass of roughly

[15] If neutrinos were Dirac fermions, α_{21} and α_{31} could be absorbed in the light-neutrino fields and would hence be unphysical as well, i.e. δ would remain as the sole physical phase in U.

[16] As an obvious 'zeroth' condition, we have to require the process in question to take place between the end of inflation and the freeze-out of baryons and antibaryons at $T \sim 10..100\,\mathrm{MeV}$.

125 GeV, the EWPT is a smooth crossover rather than a first-order phase transition [164] (cf. Sec. 2.2.3). The standard scenario of *electroweak baryogenesis* is hence ruled out and the observed BAU calls for new physics beyond the standard model.

Baryogenesis in Extensions of the Standard Model

One might presume that supersymmetry could rescue electroweak baryogenesis. The MSSM contains additional sources of CP violation and the contributions to the effective potential from scalar top quarks could render the EWPT first order after all [165]. However, the combined data from the Higgs searches, which have been carried out by the LHC experiments ATLAS and CMS up to now, exclude almost completely the fraction of the MSSM parameter space, which is consistent with electroweak baryogenesis [166]. Besides including supersymmetry, there are several alternative attempts to successfully generate the BAU at the electroweak scale. A viable option, for instance, is to extend the particle content of the standard model by one real scalar gauge singlet [167], which might appear as a pseudo-Nambu-Goldstone boson in the low-energy spectrum of composite-Higgs models [168]. Possible drawbacks of such models are that they are often quite speculative or might lack a connection to other observable phenomena, which can presently be tested in experiments.

From the historical perspective, the first baryogenesis scenarios were developed in the context of theories of grand unification [169–171]. In *GUT baryogenesis*, the primordial baryon asymmetry is generated in the out-of-equilibrium decay of superheavy GUT particles. But, as the GUT interactions preserve $B-L$, notably when the $U(1)_{B-L}$ is part of the gauge group, no net $B-L$ asymmetry is produced during GUT baryogenesis. Consequently, subsequent to its generation, the primordial baryon asymmetry is completely washed out in electroweak sphaleron processes (cf. Sec. 2.2.3).[17] Moreover, models of GUT baryogenesis typically predict too rapid proton decay, which represents the second major reason why GUT baryogenesis is nowadays considered less attractive.

A third scenario for the generation of the baryon asymmetry is provided by the *Affleck-Dine mechanism* [172], which is based on the dynamics of flat directions in the scalar potential of supersymmetric theories. If these flat directions have large initial values, they begin to oscillate in the early universe due to the soft masses, which they receive from spontaneous supersymmetry breaking. Furthermore, if the flat directions contain scalar quarks and thus carry baryon number, the primordial baryon asymmetry can be created in the course of their coherent oscillations.

[17] The fact that the actual success of GUT baryogenesis is spoiled by the influence of sphaleron processes shows that the first Sakharov condition should, in fact, be replaced by the requirement that any potential baryogenesis process has to violate $B-L$ rather than B.

Baryogenesis via Leptogenesis

One of the currently most favoured scenarios for the generation of the baryon asymmetry is *leptogenesis* [36],[18] which traces the observed BAU back to a primordial *lepton asymmetry* and which emerges as a direct consequence of the seesaw explanation for the observed neutrino masses and mixings. Recall that the key ingredient of the seesaw mechanism are the heavy Majorana neutrinos N_i, whose large masses lead to a suppression of the light-neutrino masses in the low-energy effective theory. Because the N_i neutrinos do not carry definite $B-L$ charges (cf. Eq. (3.26)), they can decay into final states containing leptons as well as into final states containing antileptons. Hence, heavy Majorana neutrinos decaying in the early universe allow for the generation of a primordial $B-L$ asymmetry, in the form of a pure lepton asymmetry, if their decays occur out of thermal equilibrium and violate CP invariance.[19] Electroweak sphalerons, rather than washing out the primordial asymmetry as in the case of GUT baryogenesis, then process the initial lepton asymmetry into the observed BAU (cf. Eq. (2.34)).

Leptogenesis represents a very attractive and well motivated scenario of baryogenesis, as it identifies the masses and mixings in the neutrino sector on the one hand and the BAU on the other hand as two related phenomena. This connection implies, in particular, that the baryon asymmetry generated during leptogenesis is sensitive to the light-neutrino mass spectrum [38, 174]. Thus, leptogenesis is falsifiable in neutrino experiments aiming at determining the absolute neutrino mass scale. Furthermore, leptogenesis heavily relies on the assumption that neutrinos are Majorana fermions. It hence predicts the presence of three physical complex phases in the PMNS matrix [175] and the existence of neutrinoless double-beta decay [176]. The detection of neutrinoless double-beta decay would therefore provide further evidence for the validity of the seesaw mechanism and leptogenesis.

One distinguishes between several variants of the central leptogenesis paradigm outlined above, differing from each other, for instance, in terms of the mechanism responsible for the generation of the heavy Majorana neutrinos in the early universe. In the original and most extensively studied scenario, known as *thermal leptogenesis* [36–38],[20] the N_i neutrinos are simply thermally produced at temperatures exceeding the heavy-neutrino masses, $T \gg M_i$. To guarantee the successful generation of the baryon asymmetry, thermal leptogenesis requires the reheating temperature after inflation $T_{\rm RH}$ to be at least of $\mathcal{O}\left(10^9\right)$ GeV. In locally supersymmetric theories such a high reheating temperature may, however, lead to a dangerously large abundance of thermally produced gravitinos, which, depending on the

[18] For reviews on leptogenesis, cf. for instance Refs. [85, 173].

[19] Whether the first condition can be satisfied depends on the production mechanism for the N_i neutrinos and on the strength of their coupling to the thermal bath. The second condition merely requires that the Yukawa matrix h^ν has to contain CP-violating complex phases.

[20] In the following, we shall refer to thermal leptogenesis also as *standard leptogenesis*.

superparticle mass spectrum, potentially entail various cosmological problems (cf. Sec. 3.1.4). As a possible way out of the *gravitino problems*, nonthermal leptogenesis via inflaton decay [39–42] has been proposed. In this scenario, the N_i neutrinos are nonthermally produced in the decay of the inflaton after inflation. The inflaton lifetime determines the temperature scale of reheating and may be adjusted such that leptogenesis takes place at a significantly smaller temperature than in the standard case. Furthermore, in supersymmetric scenarios with global $B-L$ symmetry, the $\tilde{N}_1$ sneutrino can play the role of the inflaton in models of chaotic [177, 178] or hybrid [179, 180] inflation. After the end of inflation, the $\tilde{N}_1$ sneutrino field coherently oscillates around the minimum of its potential[21] and leptogenesis directly proceeds via its decay. Finally, leptogenesis may be based on the Affleck-Dine mechanism, if the scalar potential features a flat direction which carries lepton number. The most interesting candidate for such a flat direction is related to the scalar component of the chiral superfield ℓH_u, which represents a flat direction of the MSSM scalar potential [182, 183].

Since we rely on the seesaw mechanism to account for neutrino oscillations, leptogenesis appears as a natural feature of our cosmological framework. In our scenario, as we will discuss in more detail in Sec. 3.2, thermal as well as nonthermal processes contribute to the production of the heavy (s)neutrinos. For now, let us summarize the most important quantities characterizing the decay of the heavy (s)neutrinos. The total decay rates of the N_i neutrinos and $\tilde{N}_i$ sneutrinos,[22]

$$\Gamma^0_{N_i} = \Gamma^0\big(N_i \to \ell H_u, \bar{\ell} H_u^*, \tilde{\ell} \tilde{H}_u, \tilde{\ell}^* \bar{\tilde{H}}_u\big)\,, \quad \Gamma^0_{\tilde{N}_i} = \Gamma^0\big(\tilde{N}_i \to \tilde{\ell} H_u, \bar{\ell} \bar{\tilde{H}}_u\big)\,, \tag{3.39}$$

are readily calculated from W_{Seesaw} (cf. Eq. (3.28)). At tree-level and summing over all final-state lepton flavours and weak isospin doublet components, one finds

$$\Gamma^0_{N_i} = \Gamma^0_{\tilde{N}_i} = \frac{1}{4\pi}\big[(h^\nu)^\dagger h^\nu\big]_{ii} M_i = \frac{1}{4\pi}\frac{\widetilde{m}_i M_i}{v_u^2} M_i\,, \tag{3.40}$$

with $\widetilde{m}_i$ denoting the effective neutrino mass of the i^{th} neutrino generation,

$$\widetilde{m}_i = \frac{\big[m_D^\dagger m_D\big]_{ii}}{M_i} = \big[(h^\nu)^\dagger h^\nu\big]_{ii}\frac{v_u^2}{M_i}\,. \tag{3.41}$$

These effective neutrino masses determine the coupling strengths of the heavy (s)neutrinos to the thermal bath and thus control, *inter alia*, the significance of washout effects. As an important detail, we note that $\widetilde{m}_1$ is bounded from below by the lightest neutrino mass, $m_1 < \widetilde{m}_1$ [184]. Consequently, constraints on $\widetilde{m}_1$ directly translate into constraints on the light-neutrino mass spectrum. Moreover, if the Yukawa matrix h^ν contains complex phases, the heavy (s)neutrino decays violate CP invariance, resulting in a violation of lepton number L at the quantum level. As a convenient measure for the amount of CP violation in the heavy

[21] The $\tilde{N}_1$ oscillations may even dominate the energy density of the universe after inflation [181].

[22] The superscript 0 indicates that the respective decay rates are evaluated at zero temperature.

(s)neutrino decays, one introduces the CP violation parameters ϵ_i, which indicate the lepton asymmetries produced *per* decay of a (s)neutrino from the i^{th} generation,

$$\epsilon_i = \frac{\Gamma^0\big(N_i \to L\big) - \Gamma^0\big(N_i \to \bar{L}\big)}{\Gamma^0_{N_i}} = \frac{\Gamma^0\big(\tilde{N}_i \to L\big) - \Gamma^0\big(\tilde{N}_i \to \bar{L}\big)}{\Gamma^0_{\tilde{N}_i}}\,, \tag{3.42}$$

where we have symbolically subsumed all partial rates for decays into final states with positive and negative lepton number, respectively. To lowest order, one obtains the CP violation parameter ϵ_i from the interference of the respective tree-level decay amplitude with the one-loop vertex as well as with the one-loop neutrino self-energy correction [185, 186],

$$\epsilon_i = -\sum_{j\neq i} \frac{\mathrm{Im}\big\{\big[(h^\nu)^\dagger\, h^\nu\big]^2_{ij}\big\}}{8\pi\big[(h^\nu)^\dagger\, h^\nu\big]_{ii}} F\left(\frac{M_j^2}{M_i^2}\right)\,. \tag{3.43}$$

In the MSSM supplemented by three heavy (s)neutrino generations, F is given as

$$F(x) = \sqrt{x}\left[\ln\left(\frac{1+x}{x}\right) + \frac{2}{x-1}\right]\,. \tag{3.44}$$

Throughout this thesis, we shall assume a hierarchical heavy-(s)neutrino mass spectrum, $M_1 \ll M_2 \lesssim M_3$. Therefore, the first (s)neutrino generation has the smallest decay rate and hence decays last (cf. Eq. (3.40)). Typically, the lepton asymmetry generated in the decay of the two heavier generations then gets washed out before the first generation begins to decay, or it is eventually outweighed by the asymmetry generated in the decay of the first generation. In either case, the final baryon asymmetry ends up being solely sensitive to the parameter ϵ_1. One can show that the absolute value of ϵ_1 is bounded from above [181, 187],

$$\epsilon_1 = \delta_1^{\text{eff}}\epsilon_1^{\max}\,, \quad \left|\delta_1^{\text{eff}}\right| \leq 1\,, \tag{3.45}$$

where δ_1^{eff} denotes an effective CP-violating phase of the Yukawa matrix h^ν [181]. Barring a conspiracy among the Yukawa couplings h^ν_{ij}, we expect δ_1^{eff} to be of $\mathcal{O}(1)$. Meanwhile, the maximal CP violation parameter $\epsilon_1^{\max}$ is given as

$$\epsilon_1^{\max} \approx \frac{3}{8\pi}\frac{\left|\Delta m^2_{\text{atm}}\right|^{1/2} M_1}{v^2_{\text{EW}}\sin^2\beta} \simeq 2.1\times 10^{-6}\left(\frac{1}{\sin^2\beta}\right)\left(\frac{M_1}{10^{10}\,\text{GeV}}\right)\,. \tag{3.46}$$

3.1.4 Particle Candidates for Dark Matter

In our cosmological framework, $B-L$ as well as R symmetry are spontaneously broken in the vacuum that we presently live in.[23] However, both symmetries leave behind a residual discrete $\mathbb{Z}_2$ subgroup, respectively referred to as matter parity P_M [18] and R parity P_R [19],

[23] Recall that $B-L$ is spontaneously broken during the $B-L$ phase transition. The spontaneous breaking of local supersymmetry in some hidden sector implies the breaking of R symmetry.

under which the Lagrangian is still invariant. One can show that matter and R parity are exactly equivalent to each other [188], so that we may restrict our discussion to R parity in the following. All ordinary particles have even R parity, $P_R = 1$, while all superparticles have odd R parity, $P_R = -1$. The fact that R parity remains as a residual symmetry in the low-energy effective theory prevents the appearance of B- and L-violating terms in the MSSM superpotential and hence guarantees the stability of the proton. A further, similarly important phenomenological consequence of R parity is that it renders the lightest superparticle (LSP) stable. If the LSP does not participate in electromagnetic or strong interactions, it is thus an excellent candidate for dark matter [20–22]. Meanwhile, all heavier superparticles are unstable, so that they eventually decay into final states featuring odd numbers of LSPs. Most often, the decay of a heavy superparticle yields one LSP and several ordinary particles.

The stability of the LSP in supersymmetric theories with conserved R parity and its ability to form dark matter represent the main phenomenological arguments in favour of supersymmetry. Also in this thesis, we shall adopt the notion that the LSP accounts for dark matter. The nature of the LSP depends on the superparticle mass spectrum and hence on the mechanism for the spontaneous breaking of supersymmetry. In many cases the lightest among the MSSM neutralinos ends up being the LSP. Neutralinos are the archetypes of weakly interacting massive particles (WIMPs) and so WIMP dark matter in the form of neutralinos is a popular and thoroughly studied scenario. However, if supersymmetry is assumed to be local, the particle spectrum also features the gravitino,[24] whose decays may render the WIMP dark matter scenario inconsistent with, for instance, leptogenesis or BBN. This problem can potentially be solved by promoting the gravitino itself to the LSP. We are thus led to consider two different, in a sense quite opposite scenarios in this thesis: For the most part (cf. Ch. 7), we will assume that the gravitino is the LSP and hence constitutes dark matter. By contrast, in Ch. 8 we will take it to be the heaviest superparticle and consider dark matter in the form of neutralinos. Both scenarios are only consistent within certain parameter bounds, since stable as well as unstable gravitinos can lead to various cosmological problems. As a preparation for the further investigation, let us now discuss these *cosmological gravitino problems* in turn and highlight for which parameter choices they are respectively circumvented.

Stable Gravitino and Gravitino Dark Matter

Any gravitino abundance existing prior to the $B-L$ phase transition is completely diluted in the course of the exponential expansion during inflation. Primordial gravitinos, hence, do not cause any cosmological problems [189]. After inflation, the gravitino abundance is,

[24] The gravitino is the spin-3/2 superpartner of the spin-2 graviton and may be regarded as the 'gauge' field of local supersymmetry transformations. Its mass represents the order parameter of the super-Higgs mechanism responsible for the spontaneous breaking of local supersymmetry.

however, regenerated by various mechanisms,[25] which gives rise to several restrictions on the cosmological scenario [190, 191].

Typically, the dominant mechanism for the production of gravitinos after inflation are inelastic 2-to-2 scatterings in the thermal bath. Assuming the gluino to be the heaviest gaugino, the thermal gravitino production is in turn dominated by QCD processes, while electroweak processes give only subleading contributions. The thermal gravitino abundance $\Omega_{\widetilde{G}}^{\mathrm{th}} h^2$ is then solely controlled by the reheating temperature T_{RH}, the gravitino mass $m_{\widetilde{G}}$ and the gluino mass $m_{\tilde{g}}$. In the limit $m_{\widetilde{G}} \ll m_{\tilde{g}}$, mainly the longitudinal, i.e. *goldstino* degrees of freedom of the gravitino with helicity $\pm 1/2$ are excited and one finds [43, 44],

$$\Omega_{\widetilde{G}}^{\mathrm{th}} h^2 = C \left(\frac{T_{RH}}{10^9 \text{ GeV}} \right) \left(\frac{10 \text{ GeV}}{m_{\widetilde{G}}} \right) \left(\frac{m_{\tilde{g}}}{1 \text{ TeV}} \right)^2 , \tag{3.47}$$

where the coefficient $C \simeq 0.26$ to leading order in the strong coupling constant.[26] For fixed superparticle masses, a too high reheating temperature results in the overproduction of gravitinos, such that $\Omega_{\widetilde{G}}^{\mathrm{th}}$ exceeds the presently observed abundance of dark matter, $\Omega_{\widetilde{G}}^{\mathrm{th}} > \Omega_{\mathrm{DM}}^0$, or, even worse, gravitinos *overclose*[27] the universe, $\Omega_{\widetilde{G}}^{\mathrm{th}} > 1$. Hence, for given $m_{\widetilde{G}}$ and $m_{\tilde{g}}$, the requirement that $\Omega_{\widetilde{G}}^{\mathrm{th}} \leq \Omega_{\mathrm{DM}}^0$ provides us with an upper bound on the reheating temperature. In particular, the reheating temperature has to be rather low, $T_{\mathrm{RH}} \ll 10^9$ GeV, for a very light gravitino, $m_{\widetilde{G}} \ll 10$ GeV, which excludes thermal leptogenesis as the possible origin of the BAU (cf. Sec. 3.1.3). On the other hand, it is well known that the high temperatures characteristic for thermal leptogenesis, $T_{\mathrm{RH}} \sim 10^9..10^{10}$ GeV, can become a virtue, if the gravitino is the LSP and has a mass of $\mathcal{O}(10...100)$ GeV. Given a gluino mass in the TeV range, thermally produced gravitinos can then successfully explain the observed amount of dark matter [50].[28] It is exactly this scenario, featuring a gravitino LSP with a mass around the electroweak scale, which we will further investigate in Ch. 7.

In addition to the scatterings in the thermal bath, gravitinos may be produced by a multitude of nonthermal mechanisms. For instance, the decays of heavier superparticles, in particular, the decay of the next-to-lightest superparticle (NLSP) may yield a sizable contribution $\Omega_{\widetilde{G}}^{\mathrm{NLSP}}$ to the gravitino abundance [198, 199]. The relative importance of $\Omega_{\widetilde{G}}^{\mathrm{NLSP}}$ compared to $\Omega_{\widetilde{G}}^{\mathrm{th}}$ depends on the nature of the NLSP as well as the details of the superparti-

[25] Notice that the production of gravitinos subsequent to inflation is also indicated in Fig. 2.1.

[26] C has an $\mathcal{O}(1)$ uncertainty due to unknown higher-order contributions and nonperturbative effects [43]. Resummation of thermal masses increases C by about a factor of two [192].

[27] If a particle species i is produced so abundantly that it overcloses the universe, $\Omega_i^0 > 1$, the spatial curvature of the universe remains, of course, unchanged. Overclosure merely refers to the fact that the presumed production mechanism in combination with the presumed parameter values is inconsistent with the measured value of the expansion rate H_0 and thus physically not viable.

[28] Note that superparticle mass spectra of the required form, i.e. containing a gravitino LSP with $m_{\widetilde{G}} \sim 10..100$ GeV alongside a heavy gluino with $m_{\tilde{g}} \sim 1$ TeV, naturally arise in gravity- [193–195] and gaugino-mediated [196, 197] scenarios of supersymmetry breaking.

cle mass spectrum. For a variety of popular NLSP candidates, the superparticle masses, that we shall consider in this thesis, however imply that $\Omega_{\widetilde{G}}^{\mathrm{NLSP}}$ is negligibly small [200, 201]. Furthermore, the particles from the symmetry breaking sector [202, 203] decay into the gravitino, thereby yielding a contribution $\Omega_{\widetilde{G}}^{S}$ to the total gravitino abundance. But as these particles also couple to the heavy (s)neutrinos, the decay into the gravitino is vastly outweighed by the much faster decay into N_i neutrinos and $\tilde{N}_i$ sneutrinos. Besides that, $\Omega_{\widetilde{G}}^{S}$ scales inversely proportional to the reheating temperature [34]. In view of the high temperatures, which we will eventually encounter after the $B-L$ phase transition, we thus expect $\Omega_{\widetilde{G}}^{S}$ to be negligible as well. We conclude that for our purposes it will suffice to approximate the total gravitino abundance $\Omega_{\widetilde{G}}$ by its thermal contribution $\Omega_{\widetilde{G}}^{\mathrm{th}}$,

$$\Omega_{\widetilde{G}} = \Omega_{\widetilde{G}}^{\mathrm{th}} + \Omega_{\widetilde{G}}^{\mathrm{NLSP}} + \Omega_{\widetilde{G}}^{S} + \ldots \approx \Omega_{\widetilde{G}}^{\mathrm{th}} \,. \tag{3.48}$$

Independently of its exact production mechanism and forgetting about possible constraints from leptogenesis for a moment, we may ask whether or not the gravitino is ever able to reach thermal equilibrium in the early universe. As it turns out, the gravitino equilibrium abundance always overcloses the universe, as long as the gravitino has a mass above the keV scale [20]. Conversely, a thermalized gravitino with $m_{\widetilde{G}} \sim 1\,\mathrm{keV}$ does not imply overclosure and thus allows for arbitrarily high reheating temperatures. However, it is excluded nonetheless by constraints on warm dark matter [99]. Only for a gravitino mass $m_{\widetilde{G}} \lesssim 1\,\mathrm{eV}$, a thermalized gravitino becomes cosmologically viable. But this scenario is less attractive, since then all of the MSSM superparticles would decay into the gravitino and none of them nor the gravitino could form dark matter. All in all, it hence seems rather unlikely that the gravitino was ever in thermal equilibrium after inflation.

Identifying the gravitino as the LSP may provide an attractive scenario for the nature of dark matter as well as the origin of the baryon asymmetry. Yet, it does not come without any further restrictions. Most notably, the decay of the NLSP into the gravitino and standard model particles potentially spoils the success of BBN (cf. Sec. 2.2.2) [204, 205].[29] Gravitino masses compatible with thermal leptogenesis, $m_{\widetilde{G}} \gtrsim 10\,\mathrm{GeV}$, imply a long NLSP lifetime, so that the NLSP decays way after BBN, thereby changing the theoretical predictions for the primordial abundances of the light elements. Requiring these changes to be insignificant, one is able to derive constraints on the abundance of the NLSP at the time of its decay as well as on its lifetime. These constraints may partly be translated into bounds on the masses of the NLSP and the gravitino. Assuming a gravitino mass $m_{\widetilde{G}} \sim 10..100\,\mathrm{GeV}$, a neutralino NLSP, for instance, must definitely be heavier than 1 TeV [206]. Similarly restrictive constraints apply to a scalar top quark NLSP [207, 208] as well as to a scalar tau lepton NLSP [130, 209]. Meanwhile, a scalar neutrino NLSP with a mass much below 1 TeV is not in conflict with BBN, thanks to the large branching ratio of its invisible decay mode, $\tilde{\nu} \to \widetilde{G}\nu$ [210].

[29] This threat to the gravitino dark matter scenario is known as the *NLSP decay problem*.

Several solutions to the NLSP decay problem have been proposed. The NLSP abundance could, for instance, be sufficiently diluted prior to BBN in the course of late-time entropy production [211, 212]. Alternatively, the lifetime of the NLSP could be shortened due to additional decay channels into particles of some hidden sector [213, 214]. A third option, which we consider particularly attractive, is that R parity is slightly broken after all [215, 216]. In such a scenario, given a sufficient strength of the R parity-violating interactions, the NLSP decays into standard model particles before the onset of BBN, hence resolving all tension with the BBN predictions. At the same time, the NLSP hardly decays into gravitinos anymore, so that the total gravitino abundance ceases to receive contributions from NLSP decays, $\Omega_{\widetilde{G}}^{\mathrm{NLSP}} \approx 0$. Meanwhile, the violation of R parity also renders the gravitino unstable. The decay rate of the gravitino, however, ends up being suppressed by the Planck scale as well as by the tiny coupling strength of the R parity-violating interactions. This results in very long-lived gravitino dark matter with a lifetime exceeding the present age of the universe by several orders of magnitude [216]. Interestingly, the possibility that dark matter in the form of gravitinos is, in fact, unstable leads to a rich phenomenology, which might be tested in experiments aiming at the indirect detection of dark matter [217–220]. Similarly, the R parity-violating couplings of the NLSP can be probed in collider experiments [221–224].

A slight violation of R parity hence represents an appealing solution to the NLSP decay problem. For clarity, we however emphasize that our further investigation will not depend on how exactly the NLSP decay problem is solved. When discussing gravitino dark matter in the following, the decay of the NLSP will not play any further role.

Unstable Gravitino and WIMP Dark Matter

While gravitino dark matter faces the NLSP decay problem, it is the decay of the gravitino itself, which might spoil the success of BBN in other dark matter scenarios [45–49].[30] Since its couplings are gravitationally suppressed, the gravitino typically decays very late, i.e. during or after BBN. In particular, for small gravitino masses $m_{\widetilde{G}}$ it has a long lifetime $\tau_{\widetilde{G}}$,

$$\tau_{\widetilde{G}} = \left[\frac{1}{4}\left(n_v + \frac{n_m}{12}\right)\frac{m_{\widetilde{G}}^3}{M_P^2}\right]^{-1} \simeq 280\,\mathrm{d}\left(\frac{100\,\mathrm{GeV}}{m_{\widetilde{G}}}\right)^3 . \tag{3.49}$$

Here, $n_v = 12$ and $n_m = 49$ respectively denote the number of vector and chiral multiplets the gravitino can decay into. In most cases, the decay of a gravitino yields one LSP and several standard model particles. Decaying gravitinos hence induce electromagnetic and hadronic showers, increase the entropy of the thermal bath and give rise to a nonthermal contribution $\Omega_{\mathrm{LSP}}^{\widetilde{G}}$ to the LSP abundance. Again, requiring the theoretical BBN predictions not to change too drastically allows one to derive constraints on the abundance of the gravitino at the time

[30] In analogy to the NLSP decay problem, we may now speak of the *gravitino decay problem*.

of its decay as well as on its lifetime. On top of that, one has to ensure that the LSP is not overproduced in gravitino decays, $\Omega^{\widetilde{G}}_{\mathrm{LSP}} \leq \Omega^0_{\mathrm{DM}}$. In the case of thermally produced gravitinos, these constraints can then be translated into bounds on the gravitino mass and the reheating temperature [131]. For a gravitino mass below 1 TeV, the reheating temperature must, for instance, not be higher than $\mathcal{O}\left(10^5..10^6\right)$ GeV, which rules out baryogenesis via thermal leptogenesis.[31] On the other hand, a gravitino heavier than about 10 TeV can be consistent with primordial nucleosynthesis and leptogenesis [45, 53, 54, 131]. In such a scenario, the gravitino then represents the heaviest superparticle—a possibility, which is in fact realized in models of anomaly-mediated supersymmetry breaking [227, 228] and which has recently been reconsidered in the case of wino [229], higgsino [230] and bino [231] LSP, because it nicely fits together with a Higgs boson mass of about 125 GeV. In Ch. 8, we shall thus consider WIMP dark matter in the form of a neutralino LSP, which is partly produced in the decay of a very heavy gravitino.

3.2 Spontaneous Breaking of $B-L$ as the Origin of the Hot Early Universe

A multitude of observed phenomena calls for new physics beyond the standard model. In the previous section, we have in particular addressed the apparent flatness of our universe, the high isotropy of the CMB temperature and the statistical properties of its tiny fluctuations, neutrino flavour oscillations, the cosmic baryon asymmetry as well as dark matter. We have also argued that the supersymmetric standard model supplemented by three generations of right-handed (s)neutrinos and spontaneously broken $B-L$ provides the necessary ingredients to account for all these phenomena.[32] The dynamical breaking of $B-L$ requires an extended scalar sector, which automatically yields hybrid inflation, thereby resolving the flatness and horizon problems as well as explaining the origin of the primordial metric fluctuations. Likewise, $B-L$ breaking at the GUT scale leads to an elegant explanation of the small neutrino masses via the seesaw mechanism and implies baryogenesis via leptogenesis. Finally, assuming R parity to be exactly conserved or at most only slightly violated, the LSP represents an excellent candidate for dark matter.

The main goal of this thesis now is to demonstrate that all these pieces of the puzzle naturally fit together, yielding a consistent cosmology, which is in accord with cosmological and astrophysical observations as well as with the data from neutrino and collider experiments.

[31] This bound on the reheating temperature is significantly alleviated, if the gravitino predominantly decays into a neutrino-sneutrino pair [225] or into particles that are completely decoupled from the thermal bath [226]. Similarly, it is also relaxed if late-time entropy production leads to a dilution of the gravitino abundance subsequent to its generation, but prior to its decay.

[32] Note that our framework can be naturally embedded in supersymmetric GUT models [232].

Our key insight is that the $B-L$ phase transition at the end of hybrid inflation, i.e. the *cosmological realization* of $B-L$ breaking, successfully generates the initial conditions of the hot early universe. After inflation, nonthermal and thermal processes produce an abundance of heavy (s)neutrinos, whose decays generate the primordial entropy of the thermal bath and the primordial $B-L$ asymmetry. At the same time, gravitinos are produced through inelastic scatterings in the thermal bath. If the gravitino is the LSP, it ends up being the dominant component of dark matter. Conversely, if the gravitino is the heaviest superparticle and one of the neutralinos plays the role of the LSP, the decay of the gravitino into the LSP gives rise to WIMP dark matter.

In this section, we will first outline how the energy of the false vacuum of unbroken $B-L$ is successively transferred into the energy of thermal radiation.[33] In doing so, we will pay special attention to the fact after inflation the universe is reheated through the decays of the heavy (s)neutrinos. As we will see, this characteristic feature of our scenario implies a nontrivial connection between the neutrino parameters $\widetilde{m}_1$ and M_1 on the one hand and the superparticle masses $m_{\widetilde{G}}$ and $m_{\widetilde{g}}$ on the other hand. In the second part of this section, we will then introduce the Froggatt-Nielsen flavour structure, on which we will base our analysis.

3.2.1 Reheating through Heavy (S)neutrino Decays

Particle Production during (P)reheating

The $B-L$ phase transition at the end of hybrid inflation is triggered by a tachyonic instability in the scalar potential (cf. Sec. 3.1.1). Once the inflaton φ reaches the critical field value $\varphi_c = v_{B-L}$, the mass-squared of the waterfall field σ turns negative, so that its long-wavelength modes begin to grow exponentially fast. This leads to the breaking of $B-L$ as well as to the massive production of nonrelativistic $B-L$ Higgs bosons. In fact, almost the entire energy initially stored in the false vacuum is converted into Higgs bosons during the $B-L$ phase transition. This nonperturbative energy transfer into Higgs bosons may be regarded as the first step towards reheating the universe after inflation and is thus referred to as *tachyonic preheating* [28, 29] (cf. Sec. 6.2). It is so efficient that symmetry breaking typically completes within a single oscillation of the scalar field distribution as it rolls towards the true vacuum. Meanwhile, particles coupled to the $B-L$ Higgs field are nonadiabatically produced as well [35]. In the context of our theoretical framework, these are in particular the $B-L$ gauge DOFs, the particles from the symmetry breaking sector as well as all three generations of heavy (s)neutrinos. However, due their strong coupling and their large masses, the gauge particles immediately decay after their production into heavy (s)neutrinos and the MSSM (s)quarks and (s)leptons. The initial conditions for the further cosmic evolution after inflation are hence determined by tachyonic preheating *and* the decay of the gauge multiplet.

[33] We will present a much more detailed discussion of this process in Chs. 6 and 7.

Since tachyonic preheating transfers most of the false vacuum energy into nonrelativistic Higgs bosons, the universe first undergoes a phase of matter-dominated expansion after inflation.[34] During this phase, the particles from the symmetry breaking sector decay in principle into all three generations of heavy (s)neutrinos. In our further analysis, we will however restrict ourselves to a mass spectrum that only allows for decays into the lightest heavy (s)neutrinos. While this special case promises to be less cluttered than the most general scenario, hence permitting a clear and unobstructed presentation of our findings, we expect it to fully feature all phenomenological aspects that we are interested in. Furthermore, in addition to the decay of the particles from the symmetry breaking sector, the N_1 neutrinos and $\tilde{N}_1$ sneutrino are also produced through scattering processes in the thermal bath. In view of the temperatures typically reached after inflation, the thermal production of the two heavier (s)neutrino generations is by contrast always negligible.

All heavy (s)neutrinos decay into the components of the MSSM superfields $\ell_i H_u$ as well as into the corresponding antiparticles (cf. Eq. (3.39)). In consequence of the strong standard model gauge interactions, the heavy-(s)neutrino decay products immediately thermalize, so that the energy of a decaying (s)neutrino is always quickly distributed among all MSSM degrees of freedom. This energy transfer from the heavy (s)neutrinos, most notably from the the heavy (s)neutrinos of the first generation, to the thermal bath is thus responsible for the reheating of the universe. On top of that, it also gives rise to the primordial lepton asymmetry, which is processed by the electroweak sphalerons into the observed baryon asymmetry. Finally, 2-to-2 scatterings in the thermal bath generate an abundance of gravitinos.

Connection Between the Neutrino Sector and Supergravity

Let us assume for now that the gravitino is the LSP, having a mass as it typically arises in gravity or gaugino mediation, $m_{\widetilde{G}} \sim 10..100\,\mathrm{GeV}$. According to Eq. (3.47), the reheating temperature T_{RH} then has to be of $\mathcal{O}\left(10^9..10^{10}\right)$ GeV, so that the thermal production of gravitinos just yields the observed relic density of dark matter. Remarkably, temperatures of the required magnitude are indeed realized, if the universe is reheated through the decays of the heavy (s)neutrinos.[35] Due to their dominant abundance, the reheating process is mainly driven by the decay of the lightest heavy (s)neutrinos. The reheating temperature is consequently reached, once the Hubble rate H has dropped to the value of the N_1 decay rate. Because of their relativistic motion with respect to the thermal plasma, the heavy (s)neutrinos actually decay at a lower rate as they would do at rest. Omitting this fact for a moment, we

[34] In Ch. 7, we will track the cosmic evolution during this era by means of Boltzmann equations.

[35] This observation initially stimulated our interest in the $B-L$ phase transition and prompted us to carry out the research program, the results of which are presented in this thesis. We reported on it for the first time in Ref. [57] and further expanded on it in Refs. [58, 60].

may approximate the N_1 decay rate by the vacuum decay rate $\Gamma^0_{N_1}$,

$$T = T_{\rm RH}: \quad H \approx \Gamma^0_{N_1}\,. \tag{3.50}$$

For values of the neutrino mass parameters $\widetilde{m}_1$ and M_1 compatible with thermal leptogenesis, $\widetilde{m}_1 \sim 0.01$ eV and $M_1 \sim 10^{10}$ GeV, one obtains (cf. Eq. (3.40))

$$\Gamma^0_{N_1} = \frac{1}{4\pi}\frac{\widetilde{m}_1 M_1}{v_u^2} M_1 \sim 10^3\,{\rm GeV}\,, \quad v_u \simeq v_{\rm EW} \simeq 174\,{\rm GeV}\,. \tag{3.51}$$

Furthermore, assuming that at $T = T_{\rm RH}$ the entire available energy has already been converted into radiation, the Friedmann equation tells us that,

$$T = T_{\rm RH}: \quad \rho_{\rm tot} \approx \rho_R\,, \quad H^2 = \frac{8\pi}{3M_P^2}\rho_{\rm tot} \approx \frac{8\pi}{3M_P^2}\frac{\pi^2}{30} g_{*,\rho} T^4_{\rm RH}\,. \tag{3.52}$$

In combination with Eqs. (3.50) and (3.51), this relation provides us with the following rough estimate for the reheating temperature,[36]

$$T_{\rm RH} \approx \left(\frac{90}{8\pi^3 g_{*,\rho}}\right)^{1/4} \sqrt{\Gamma^0_{N_1} M_P} \sim 10^{10}\,{\rm GeV}\,, \tag{3.53}$$

where we have used the MSSM value for the effective number of relativistic degrees of freedom contributing to the total radiation energy density, $g_{*,\rho} = 915/4$. This result confirms our claim that the decay of the heavy (s)neutrinos itself might account for the high temperatures required for leptogenesis and gravitino dark matter. Together with the observation that the dynamics of the symmetry breaking sector can give rise to a sizable abundance of heavy (s)neutrinos after inflation, it serves us as a key motivation for our study of the $B-L$ phase transition.

Since the reheating temperature depends on the N_1 decay rate and hence on $\widetilde{m}_1$ and M_1, the requirement that gravitinos be the constituents of dark matter yields a connection between neutrino and superparticle mass parameters (cf. Eq. (3.47)),

$$\Omega^0_{\widetilde{G}} h^2 = \Omega^0_{\widetilde{G}} h^2\left(\widetilde{m}_1, M_1, m_{\widetilde{G}}, m_{\tilde{g}}\right) = \Omega^0_{\rm DM} h^2 \simeq 0.11\,. \tag{3.54}$$

The neutrino masses $\widetilde{m}_1$ and M_1 are in turn constrained by the condition that the maximal baryon asymmetry, generated in the decay of the heavy (s)neutrinos if $\epsilon_1 = \epsilon_1^{\rm max}$ (cf. Sec. 3.1.3), must not be smaller than the observed one, $\eta_B^{\rm max} \geq \eta_B^{\rm obs} = 6.2 \times 10^{-10}$. As we will show in Sec. 7.3, this condition directly implies a lower bound on the gravitino mass $m_{\widetilde{G}}$ as a function of the effective neutrino mass $\widetilde{m}_1$.

[36] As we shall see in Ch. 7, including all effects neglected in the above discussion, the actual reheating temperature obtained for $\widetilde{m}_1 \sim 0.01\,{\rm eV}$ and $M_1 \sim 10^{10}\,{\rm GeV}$ turns out to be a bit lower than this estimate. Our main point, however, remains valid: reheating through the decays of heavy (s)neutrinos results in a reheating temperature, which is controlled by neutrino parameters.

In conclusion, we emphasize that the decay of the heavy (s)neutrinos after the $B-L$ phase transition entirely fixes the initial conditions of the hot early universe. The initial baryon asymmetry, dark matter density and reheating temperature cannot be freely chosen, but are determined by the parameters of the underlying Lagrangian, which can in principle be measured by particle physics experiments and astrophysical observations.

3.2.2 Froggatt-Nielsen Flavour Structure

Eventually, we wish to study the physical processes outlined in the previous section by means of Boltzmann equations. But before we are ready to carry out any quantitative calculations, we need to find a way to estimate the values of the dimensionless couplings λ and $h_{ij}^{n,\nu}$ in the superpotential (cf. Secs. 3.1.1 and 3.1.2). More precisely, we have to specify a flavour model, which correctly describes the masses and mixings of quarks, charged leptons and neutrinos, and which can at the same time be consistently extended to the symmetry-breaking sector as well as to the sector of the heavy (s)neutrinos. Since we would like to study our scenario for a broad spectrum of reheating temperatures, we seek a model which is flexible enough to allow the neutrino masses $\widetilde{m}_1$ and M_1 to vary within large ranges.

As of today, it poses a major theoretical challenge of particle physics to explain the observed patterns of quark and lepton masses and mixings, in particular the striking differences between the quark sector and the neutrino sector. Promising elements of a theory of flavour are grand unification based on the groups $SU(5)$, $SO(10)$ or E_6, supersymmetry, the seesaw mechanism and additional flavour symmetries [232]. A successful example is the Froggatt-Nielsen mechanism [56] based on spontaneously broken Abelian symmetries, which parametrizes quark and lepton mass ratios and mixings by powers of a small *hierarchy parameter* η. Interestingly, the resulting structure of mass matrices also arises in compactifications of higher-dimensional field and string theories, where the parameter η is related to the location of matter fields in the compact dimensions or to VEVs of moduli fields [233–235]. In this thesis, we shall consider a Froggatt-Nielsen symmetry which commutes with the GUT group $SU(5)$. Our model is a variant of the model discussed in Ref. [55]. It naturally explains the large atmospheric neutrino mixing angle [236, 237], satisfies all constraints from flavour-changing processes [238] and predicts Dirac and Majorana neutrino mass matrices which are consistent with thermal leptogenesis [55].

Yukawa Couplings from Nonrenormalizable Interactions

Evolving the masses of quarks and charged leptons to the scale of grand unification, $\Lambda_{\mathrm{GUT}} \sim 10^{16}$ GeV, they approximately satisfy the following relations,

$$m_t : m_c : m_u \sim 1 : \eta^2 : \eta^4 \,, \quad m_b : m_s : m_d \sim m_\tau : m_\mu : m_e \sim 1 : \eta : \eta^3 \,, \tag{3.55}$$

ψ_i	$\mathbf{10}_3$	$\mathbf{10}_2$	$\mathbf{10}_1$	$\mathbf{5}^*_3$	$\mathbf{5}^*_2$	$\mathbf{5}^*_1$	n^c_3	n^c_2	n^c_1	H_u	H_d	S_1	S_2	Φ
Q_i	0	1	2	a	a	$a+1$	b	c	d	0	0	0	0	e

Table 3.1: Chiral flavour charges Q_i of the $SU(5)$ matter multiplets ψ_i.

with $\eta^2 \simeq 1/300$. This hierarchy pattern can be well reproduced by a simple Abelian flavour symmetry, which we will denote by $U(1)_{\rm FN}$ in the following. Let us assign nonnegative flavour charges Q_i to all $SU(5)$ multiplets ψ_i which are contained in our superpotential and let us also introduce an extra $SU(5)$ singlet field Σ, the *flavon*, carrying negative flavour charge, $Q_\Sigma = -1$. In the effective theory below some high energy scale $\Lambda > \Lambda_{\rm GUT}$, the interactions of the matter fields ψ_i with the flavon Σ are described by nonrenormalizable terms in the superpotential,

$$W_{\rm nr} \supset C_{ijk} \left(\frac{\Sigma}{\Lambda}\right)^{Q_i+Q_j+Q_k} \psi_i\, \psi_j\, \psi_k\,, \tag{3.56}$$

where the coefficients C_{ijk} are unknown parameters, which are expected to be of $\mathcal{O}(1)$. Assigning a nonzero VEV $\langle\Sigma\rangle$ to the scalar component of the flavon field spontaneously breaks the $U(1)_{\rm FN}$ flavour symmetry and turns the nonrenormalizable terms in Eq. (3.56) into the Yukawa interactions of our superpotential. We shall assume that the Higgs fields $S_{1,2}$ and $H_{u,d}$ carry no flavour charge. Suppressing the $\mathcal{O}(1)$ coefficients in Eq. (3.56), we obtain

$$h_{ij} \sim \eta^{Q_i+Q_j}\,, \quad \sqrt{\lambda} \sim \eta^{Q_\Phi}\,, \quad \eta = \frac{\langle\Sigma\rangle}{\Lambda}\,. \tag{3.57}$$

The hierarchies of the quark and charged-lepton masses given in Eq. (3.55) are then naturally obtained for $\eta^2 \simeq 1/300$ and the chiral charges Q_i listed in Tab. 3.1. Note that Eq. (3.57) captures the key essence of our flavour model: up to $\mathcal{O}(1)$ factors, all dimensionless couplings in the superpotential are given as certain powers of a common hierarchy parameter η.

Parametrization of our Model

Eq. (3.57) in combination with Tab. 3.1 allows us to parametrize our entire model in terms of flavour charges and Higgs VEVs. The heavy-(s)neutrino mass matrix M, for instance, can now be estimated as (cf. Eq. (3.27)),

$$M = v_{B-L} h^n \sim v_{B-L}\, {\rm diag}\left(\eta^{2d}, \eta^{2c}, \eta^{2b}\right)\,. \tag{3.58}$$

We shall restrict our analysis to the case of a hierarchical heavy-(s)neutrino mass spectrum, $M_1 \ll M_2 \lesssim M_3$, which we readily obtain by imposing the following condition on the flavour charges of the heavy (s)neutrinos,[37]

$$b = c = d - 1\,. \tag{3.59}$$

[37] Notice that, although we require $b = c$, the $\mathcal{O}(1)$ uncertainties in M still allow the mass ratio M_3/M_2 to vary within one order of magnitude, $1 \lesssim M_3/M_2 \lesssim 10$.

While this restriction facilitates our investigation, it still preserves all characteristic features of our scenario, in particular the anticipated connection between neutrino parameters and superparticle masses. One of the simplifications implied by Eq. (3.59), for instance, is that the lepton asymmetry will be mostly generated by the decay of the lightest heavy-(s)neutrino generation (cf. Sec. 3.1.3). Having eliminated b and c, the remaining free charges are a, d and e. As we will shortly see, these can be related to the physical parameters v_{B-L}, M_1 and m_S, where the last quantity denotes the common mass of all particles from the symmetry-breaking sector in the true vacuum (cf. Ch. 5).

The neutrino Dirac mass matrix m_D may now be written as (cf. Eq. (3.31))

$$m_D = v_u\, h^\nu \sim v_u\, \eta^a \begin{pmatrix} \eta^{d+1} & \eta^{c+1} & \eta^{b+1} \\ \eta^d & \eta^c & \eta^b \\ \eta^d & \eta^c & \eta^b \end{pmatrix} . \tag{3.60}$$

Together with the heavy-(s)neutrino mass matrix M, it yields the light-neutrino Majorana mass matrix m_ν via the seesaw formula (cf. Eq. (3.31)),

$$m_\nu \sim \frac{v_u^2}{v_{B-L}}\, \eta^{2a} \begin{pmatrix} \eta^2 & \eta & \eta \\ \eta & 1 & 1 \\ \eta & 1 & 1 \end{pmatrix} . \tag{3.61}$$

Interestingly, the dependence on the heavy-(s)neutrino charges drops out in the calculation of m_ν, so that it ends up being solely controlled by the charge a. In fact, taking into account that $v_u = v_{\text{EW}} \sin\beta$ and apart from the unspecified $\mathcal{O}(1)$ coefficients, the light-neutrino mass matrix only depends one specific combination of parameters, namely the effective mass scale $\bar{v}_{B-L}$,

$$\bar{v}_{B-L} = \frac{v_{B-L}}{\eta^{2a} \sin^2\beta} . \tag{3.62}$$

We point out that the specific hierarchy pattern inherent in m_ν directly feeds into the lepton mixing matrix U and hence has a large impact on the low-energy observables in the neutrino sector. In Ch. 4, we will further elaborate on the neutrino phenomenology implied by the hierarchy structure of m_ν. Finally, diagonalizing the light-neutrino mass matrix yields the light-neutrino masses m_i,

$$m_1 \sim \eta^{2a+2} \frac{v_u^2}{v_{B-L}} , \quad m_2 \sim m_3 \sim \eta^{2a} \frac{v_u^2}{v_{B-L}} . \tag{3.63}$$

The second matrix which we have to diagonalize in order to obtain the PMNS matrix U is the charged-lepton mass matrix m_{cl} (cf. Eq. (3.37)). It is given by

$$m_{\text{cl}} = v_d\, h^d \sim v_d\, \eta^a \begin{pmatrix} \eta^3 & \eta^2 & \eta \\ \eta^2 & \eta & 1 \\ \eta^2 & \eta & 1 \end{pmatrix} . \tag{3.64}$$

As an important detail, we note that the second and the third row of the matrix $m_{\rm cl}$ have the same hierarchy pattern. This is a consequence of the same flavour charges for the second and the third charged-lepton generation, which is in turn the origin of the large atmospheric mixing angle. Hence, diagonalizing $m_{\rm cl}$ can in principle give a sizable contribution to the mixing in the lepton sector.

The light-neutrino mass scale is conveniently characterized by $\overline{m}_\nu = \sqrt{m_2 m_3}$, the geometric mean of the two light-neutrino masses m_2 and m_3. In the case of a normal mass ordering of the light neutrinos, we may estimate it as (cf. Eq. (3.19))

$$\overline{m}_\nu \approx \left[\left(\Delta m^2_{\rm sol}\right)^{1/2} \left|\Delta m^2_{\rm atm}\right|^{1/2}\right]^{1/2} \sim 3 \times 10^{-2}\,{\rm eV}\,. \tag{3.65}$$

On the other hand, estimating $\overline{m}_\nu$ with the aid of Eq. (3.63) provides us with

$$\overline{m}_\nu \sim \eta^{2a} \frac{v_u^2}{v_{B-L}}\,, \quad v_{B-L} \sim \eta^{2a} \frac{v_u^2}{\overline{m}_\nu} = \eta^{2a} M_0\,, \tag{3.66}$$

where we have introduced the heavy-neutrino mass scale M_0 through the relation

$$M_0 = \frac{v_u^2}{\overline{m}_\nu} \sim \frac{(174\,{\rm GeV})^2}{3 \times 10^{-2}\,{\rm eV}} \sim 1 \times 10^{15}\,{\rm GeV}\,. \tag{3.67}$$

Note that, as M_0 follows from the seesaw formula, triple products of $\mathcal{O}(1)$ coefficients enter into its calculation. Hence, it may in fact be easily as large as the GUT scale, $\Lambda_{\rm GUT} \sim 10^{16}$ GeV. Meanwhile, Eq. (3.66) illustrates that there is a one-to-one correspondence between the $B-L$ scale v_{B-L} and the charge a. Consequently, once v_{B-L} is fixed, M_1 is directly related to the charge d through Eq. (3.58),

$$v_{B-L} \sim \eta^{2a} M_0\,, \quad M_1 \sim \eta^{2d} v_{B-L}\,. \tag{3.68}$$

Furthermore, cosmology may impose a relation between a and d. Thermal leptogenesis, for instance, requires $M_1 \sim 10^{10}$ GeV, which translates into $a + d = 2$ [55].

The results obtained so far enable us to estimate the effective neutrino masses $\widetilde{m}_i$ as well as the CP violation parameters ϵ_i. First of all, we find (cf. Eq. (3.41))

$$\widetilde{m}_i = \frac{\left[m_D^\dagger m_D\right]_{ii}}{M_i} \sim \eta^{2a} \frac{v_u^2}{v_{B-L}} \sim \overline{m}_\nu\,. \tag{3.69}$$

Since the light-neutrino mass matrix is not hierarchical, the $\mathcal{O}(1)$ uncertainties in the Yukawa matrix h^ν can lead to large deviations from the relation between $\widetilde{m}_1$ and $\overline{m}_\nu$. The only rigorous inequality is $\widetilde{m}_1 > m_1$ [184]. We take these uncertainties into account by varying the effective neutrino mass $\widetilde{m}_1$ within the range

$$10^{-5}\,{\rm eV} \leq \widetilde{m}_1 \leq 1\,{\rm eV}\,. \tag{3.70}$$

Because the two heavier (s)neutrino generations will turn out to play a less prominent role in our scenario, we decide to ignore possible deviations of $\widetilde{m}_{2,3}$ from $\overline{m}_\nu$ and simply set $\widetilde{m}_{2,3} = \overline{m}_\nu$. Assuming that the complex phases in the Yukawa matrix h^ν are not accidentally suppressed, the CP violation parameter ϵ_1 is expected to have a value close to its upper bound (cf. Eq. (3.46)),

$$|\epsilon_1| \sim \frac{3}{8\pi}\eta^{2(a+d)} \sim \frac{3}{8\pi}\frac{M_1}{M_0} \sim 1 \times 10^{-6} \left(\frac{M_1}{10^{10}\,\text{GeV}}\right) \sim \epsilon_1^{\max} \tag{3.71}$$

The CP violation parameters $\epsilon_{2,3}$ are enhanced compared to ϵ_1 by a factor η^{-2}, so that our results for the parameters ϵ_i can be brought into the following neat form,

$$|\epsilon_{2,3}| \sim \eta^{-2}\,|\epsilon_1|\,, \quad |\epsilon_i| \sim \frac{1}{10}\frac{M_i}{M_0}\,. \tag{3.72}$$

Last but not least, let us turn to the implications of our estimate for the coupling constant λ (cf. Eq. (3.57)). As we will see in the next chapter, λ determines the mass of the particles from the symmetry-breaking sector m_S. At the same time, it also controls the initial false vacuum energy density ρ_0 (cf. Eq. 3.9),

$$m_S = \sqrt{\lambda} v_{B-L}\,, \quad \rho_0 = \frac{1}{4}\lambda v_{B-L}^4\,. \tag{3.73}$$

Within our flavour model these two quantities are thus estimated as

$$m_S \sim \eta^{2a+e} M_0\,, \quad \rho_0 \sim \frac{1}{4}\eta^{8a+2e} M_0^4\,, \tag{3.74}$$

where we have used that $Q_\Phi = e$. We shall assume m_S to be of the same order of magnitude as the heavy-(s)neutrino masses M_2 and M_3. This leads us to imposing the condition $e = 2b = 2c$, which, together with Eq. (3.59), results in

$$e = 2b = 2c = 2(d-1)\,. \tag{3.75}$$

In Chs. 7 and 8, we will set $m_S = M_3 = M_2$ for definiteness. Given such a mass spectrum, the particles from the symmetry-breaking sector only decay into the first heavy (s)neutrino-generation. Again, this restriction simplifies our analysis, but still preserves all aspects that we are interested in (cf. Sec. 3.2.1).

Owing to the two conditions in Eqs. (3.59) and Eq. (3.75), we have left over only two free flavour charges, a and d. According to Eq. (3.68), these can be traded for the more physical quantities v_{B-L} and M_1. The ranges over which a and d, and hence v_{B-L} and M_1, are allowed to vary are restricted by the requirement of perturbativity of all coupling constant as well as the lower bound on $\tan\beta$. First, to ensure that no coupling constant significantly exceeds the top-Yukawa coupling, we require that $a \geq 0$ and $d \geq 1$. Second, $\tan\beta > \mathcal{O}(1)$ implies $a \leq 1$, whereas there is no corresponding upper bound on d. On top of that, in Sec. 6.1

we will discuss further restrictions on a and d that follow from requiring a viable realization of hybrid inflation as well as a not too strong production of cosmic strings during the $B-L$ phase transition. Meanwhile, as the leptogenesis process after the $B-L$ phase transition is mainly driven by nonthermally produced (s)neutrinos, we do not have to worry about the constraint from thermal leptogenesis, $a + d = 2$. We also remark that bounds on a and d directly correspond to extremal values for v_{B-L} and M_1. In the following, we will assume that v_{B-L} and M_1 can continuously vary within the ranges bounded by their extremal values. With respect to a and d, such a variation may be effectively realized in terms of fractional flavour charges.

To sum up, our model is parametrized by five dimensionful parameters, the $B-L$ breaking scale v_{B-L}, the heavy (s)neutrino mass M_1, the effective neutrino mass $\widetilde{m}_1$, the gravitino mass $m_{\widetilde{G}}$, and the gluino mass $m_{\tilde{g}}$, as well as by the dimensionless $\mathcal{O}(1)$ coefficients in the Yukawa matrices, which we have left out of consideration up to now. We will turn our attention to the $\mathcal{O}(1)$ uncertainties of our flavour model in the next chapter, in which we will perform a numerical Monte-Carlo study to assess the impact of the unspecified $\mathcal{O}(1)$ factors in the lepton mass matrices on the various observables of the neutrino sector. This analysis will demonstrate that our Froggatt-Nielsen flavour model has a rather strong predictive power after all and that it in fact implies parameter predictions, which are in many cases much more precise than the rough order-of-magnitude estimates derived in the present section. In the subsequent chapters, we will then proceed employing the best-guess estimates obtained in Ch. 4, while henceforth ignoring the $\mathcal{O}(1)$ uncertainties of our flavour model. This means in particular that in Chs. 7 and 8 we will simply set all $\mathcal{O}(1)$ factors to one.

Chapter 4

Neutrino Phenomenology

In Sec. 3.2.2, we motivated the Froggatt-Nielsen mechanism as a promising prototype for a fundamental theory of flavour, allowing us to parametrize our entire model in terms of flavour charges and Higgs VEVs. Generally speaking, flavour symmetries of the Froggatt-Nielsen type provide a natural means to reconcile the large quark and charged-lepton mass hierarchies and small quark mixing angles on the one hand with the observed small neutrino mass hierarchies and large neutrino mixing angles on the other hand. But despite these virtues, the predictive power of the Froggatt-Nielsen mechanism is understood to be rather limited due to unknown coefficients of $\mathcal{O}(1)$ in the superpotential (cf. Eq. (3.56)), directly implying $\mathcal{O}(1)$ uncertainties in all entries of the mass matrices. The explicit model introduced in Sec. 3.2.2, for instance, is not able to make a precise prediction of the solar neutrino mixing angle θ_{12}, as it can accommodate both a small as well as a large value for this observable [236, 237, 239].

To get an idea of the range of possible predictions for a given flavour structure, it is instructive to treat the $\mathcal{O}(1)$ parameters as random variables [240–242]. In this chapter, we shall therefore employ Monte-Carlo techniques (cf. Sec. 4.1) to quantitatively study the dependence of yet undetermined, but soon testable parameters of the neutrino sector on the unknown $\mathcal{O}(1)$ factors. Using the already measured neutrino masses and mixings as input, we find surprisingly sharp predictions (cf. Sec. 4.2), which we are even able to reproduce analytically in the case of one observable, *viz.* the Majorana CP violation phase α_{21} (cf. Sec. 4.3).

The results presented in this chapter were first published in Ref. [59].

4.1 Monte-Carlo Sampling of $\mathcal{O}(1)$ Factors

In view of the $\mathcal{O}(1)$ factors in all mass matrices, one might expect the predictions for the observables of the neutrino sector to be quite uncertain. The light-neutrino mass matrix m_ν, for instance, is calculated as the product of three other matrices, the entries of which are all determined only up to coefficients of $\mathcal{O}(1)$ (cf. Eq. (3.31)). Hence, one may be led to the conclusion that the predictions for all observables deriving from m_ν should have an uncertainty of roughly three orders of magnitude. In principle, the Froggatt-Nielsen model allows, of course, for such large variations. This is the reason why we stated in Sec. 3.2.2 that the heavy-neutrino mass scale M_0 may be as large as the GUT scale Λ_{GUT} (cf. Eq. (3.67)) as well as the reason why we allow the effective neutrino mass $\widetilde{m}_1$ to vary over as much as five orders of magnitude (cf. Eq. (3.70)). As we shall demonstrate now by means of a numerical Monte-Carlo study, such a large dispersion is, however, not characteristic for the Froggatt-Nielsen model. In fact, quite the opposite is the case. For many observables, the predicted values turn out to be mostly confined to narrow ranges, extending over less than an order of magnitude.

Random Mass Matrices Compatible with all Experimental Constraints

All observables of the neutrino sector eventually derive from the mass matrices M, m_D and m_{cl} (cf. Eqs. (3.27), (3.31) and (3.36)) or equivalently from the Yukawa matrices h^n, h^ν and h^d (cf. Eqs. (3.20) and (3.22)). Postponing the discussion of the individual observables to Sec. 4.2, let us now focus on our numerical method to find mass matrices which are compatible with all experimental constraints.

The unknown $\mathcal{O}(1)$ coefficients of the Yukawa matrices h^d, h^ν and h^n are constrained by the experimental data on neutrino masses and mixings, with the $3\,\sigma$ confidence ranges of the respective measurable quantities being given by [2]

$$\begin{aligned} &2.07 \times 10^{-3}\,\text{eV}^2 \leq |\Delta m^2_{\text{atm}}| \leq 2.75 \times 10^{-3}\,\text{eV}^2\,, \\ &7.05 \times 10^{-5}\,\text{eV}^2 \leq \Delta m^2_{\text{sol}} \leq 8.34 \times 10^{-5}\,\text{eV}^2\,, \\ &0.75 \leq \sin^2(2\theta_{12}) \leq 0.93\,, \\ &0.88 \leq \sin^2(2\theta_{23}) \leq 1\,. \end{aligned} \tag{4.1}$$

We explicitly do not use the current bound on the smallest mixing angle, $\theta_{13} < 0.21$ at $3\,\sigma$ [2], to constrain the $\mathcal{O}(1)$ factors. This allows us to demonstrate that nearly all values we obtain for θ_{13} automatically obey the experimental bound, cf. Fig. 4.1.

Each of the Yukawa matrices h^ν and h^d contains nine complex $\mathcal{O}(1)$ factors, C^ν_{ij} and C^d_{ij}, respectively, while the Yukawa matrix h^n features three real $\mathcal{O}(1)$ factors C^n_i. In a numerical Monte-Carlo study, we now generate random numbers to model these in total 39 real

parameters.[1] The absolute values $|C_{ij}|$ are taken to be uniformly distributed on a logarithmic scale, while the phases in h^ν and h^d are chosen to be uniformly distributed on a linear scale,

$$-\frac{1}{2} \leq \log_{10} |C_{ij}| \leq \frac{1}{2}\,, \quad 0 \leq \arg C_{ij} < 2\pi\,. \tag{4.2}$$

In the following, we shall refer to those sets of coefficients which yield mass matrices that are consistent with the experimental constraints in Eq. (4.1) as *hits*.

In a preliminary run of our Monte-Carlo code, we solely take into account the neutrino mixing matrix Ω (cf. Eq. (3.32)) to calculate the PMNS matrix (cf. Eq. (3.37)) as well as the set of observables encoded in it. Meanwhile, we treat the effective scale $\bar{v}_{B-L}$ (cf. Eq. (3.62)) as a random variable in the interval $[1/\sqrt{10}, \sqrt{10}] \times 10^{15}$ GeV. We find that the percentage of hits strongly peaks at $\bar{v}_{B-L} \simeq 1 \times 10^{15}$ GeV. This is interesting for two reasons. First, it entails that given $0 \leq a \leq 1$ (cf. Sec. 3.2.2), the $B-L$ breaking scale v_{B-L} lies in the range

$$3 \times 10^{12}\ \text{GeV}\, \sin^2\beta \lesssim v_{B-L} \lesssim 1 \times 10^{15}\ \text{GeV}\, \sin^2\beta\,. \tag{4.3}$$

Recall that we assume large $\tan\beta$ (cf. Sec. 3.1.2). The upper boundary of this mass range is hence close to the GUT scale. In particular, it deviates by less than an order of magnitude from the rough estimate of v_{B-L} based on the amplitude of the scalar power spectrum A_s (cf. Eq. (3.16)). With regard to the great flexibility of the Froggatt-Nielsen model, we may thus regard the upper bound on v_{B-L} in Eq. (4.3) as being consistent with the estimate implied by hybrid inflation. Second, the fact that the $\bar{v}_{B-L}$ distribution exhibits a strong peak allows us to fix $\bar{v}_{B-L}$ to 10^{15} GeV in the following computations without introducing a significant bias.

In the main run of our code, in which $\bar{v}_{B-L}$ is now fixed, we include the charged-lepton mixing matrix L (cf. Eq. (3.36)) in the calculation of the PMNS matrix. We require the mass ratios of the charged leptons to fulfill the corresponding experimental constraints up to an accuracy of 5 % and allow for $1 \leq \tan\beta \leq 60$ to achieve the correct normalization of the charged-lepton mass spectrum. Imposing the $3\,\sigma$ constraints on the two large mixing angles inferred from the full PMNS matrix, $U = L^\dagger \Omega$, along with the constraints on $|\Delta m^2_{\text{atm}}|$ and Δm^2_{sol}, we then find the searched-for samples of $\mathcal{O}(1)$ factors, which yield random mass matrices that are compatible with the neutrino data in Eq. (4.1). Our final results are based on roughly 20 000 such hits. For each hit, we calculate the observables in the neutrino sector as well as two parameters relevant for leptogenesis, *viz.* $\widetilde{m}_1$ and ϵ_1. This provides us with distributions for the possible values of the respective observables. Before presenting our results, let us first elaborate on the statistical method with which we shall analyze these distributions.

[1] Note that it is the the low-energy Yukawa couplings which we treat as random variables. These are related to the couplings at higher energy scales, i.e. the couplings the Froggatt-Nielsen model is actually concerned with, via renormalization group equations. We however expect that the effect of renormalization group running can be absorbed into a redefinition of the effective scale $\bar{v}_{B-L}$ (cf. Eq. (3.62)), hence leaving the results presented in the following unchanged.

Statistical Analysis

The relative frequency with which we encounter a certain value for an observable might indicate the probability that this value is actually realized within the large class of concrete flavour models covered by our analysis. In the following, we shall therefore treat the distributions for the various observables as *probability densities* for continuous random variables, i.e. our predictions for the respective observables represent best-guess estimates according to a probabilistic interpretation of the relative frequencies. For each observable, we would like to deduce measures for its central tendency and statistical dispersion from the respective probability distribution. Unfortunately, it is infeasible to fit all obtained distributions with one common template distribution. Such a procedure would lack a clear statistical justification, and it also appears impractical, as the distributions that we obtain differ substantially in their shapes. We therefore choose a different approach.

We consider the *median* of a distribution as its center and we use the 68 % *confidence interval* around it as a measure for its spread. Of course, this range of the confidence interval is reminiscent of the $1\,\sigma$ range of a normal distribution. More precisely, for an observable x with probability density f, we will summarize its central tendency and variability in the following form [243],

$$x = \hat{x}^{\Delta_+}_{\Delta_-}\,, \quad \Delta_\pm = x_\pm - \hat{x}\,. \tag{4.4}$$

Here, x_- and x_+ denote the 16 % and 84 % quantiles with respect to the density function f. The central value $\hat{x}$ is the median of f and thus corresponds to its 50 % quantile. All three values can be calculated from the quantile function Q,

$$Q(p) = \inf\{x \in [x_{\min}, x_{\max}] : p \leq F(x)\}\,, \quad F(x) = \int_{x_{\min}}^{x} dt\, f(t)\,, \tag{4.5}$$

where F stands for the cumulative distribution function of x. We then have

$$x_- = Q(0.16)\,, \quad \hat{x} = Q(0.50)\,, \quad x_+ = Q(0.84)\,. \tag{4.6}$$

Intuitively, the intervals from $x_{\min}$ to x_-, $\hat{x}$, and x_+, respectively, correspond to the x ranges into which 16 %, 50 % or 84 % of all hits fall. This is also illustrated in the histogram for $\sin^2 2\theta_{13}$ in Fig. 1. Moreover, we have included vertical lines into each plot, indicating the respective positions of x_-, $\hat{x}$, and x_+.

In our case, the median is a particularly useful measure of location. First of all, it is resistant against outliers and hence an appropriate statistic for such skewed distributions, as we observe them. But more importantly, the average absolute deviation from the median is minimal in comparison to any other reference point. The median is thus the best guess for the outcome of a measurement, if one is interested in being as close as possible to the actual result, irrespectively of the sign of the error. On the technical side, the definition of

the median fits nicely together with our method of assessing statistical dispersion. The 68 % confidence interval as introduced above is just constructed in such a way, that equal numbers of hits lie in the intervals from x_- to $\hat{x}$ and from $\hat{x}$ to x_+, respectively. In this sense, our confidence interval represents a symmetric error with respect to the median.

To test the robustness of our results, we check the dependence of our distributions on the precise choice of the experimental error intervals. Our results, however, turn out to be insensitive to small variations of the error margins. For definiteness, we therefore stick to the $3\,\sigma$ ranges listed in Eq. (4.1). Furthermore, we also check the effect of taking the absolute values $|C_{ij}|$ of the $\mathcal{O}(1)$ factors to be uniformly distributed on a linear instead of a logarithmic scale (cf. Eq. (4.2)). Again, our results prove to be robust.

4.2 Predictions for Neutrino Observables

Finally, we present the results of our numerical Monte-Carlo study. Out of the findings which we obtain three particularly interesting ones deserve to be highlighted: (i) a large value for the smallest mixing angle θ_{13} in accordance with recent results from the T2K [244], Minos [245], Double Chooz [246], Daya Bay [247], and Reno [248] experiments, (ii) a value for the lightest neutrino mass of $\mathcal{O}\left(10^{-3}\right)$ eV, and (iii) one Majorana CP-violating phase in the PMNS matrix peaked at $\alpha_{21} \simeq \pi$.

Mass Hierarchy

An important unsolved puzzle of modern neutrino physics, which is closely connected to the flavour physics of the neutrino sector, is the question as to the hierarchy of the light-neutrino mass eigenstates. Since up to now the sign of Δm^2_{atm} has remained undetermined, the current experimental data is still consistent with a normal as well as with an inverted hierarchy (cf. Eq. (3.34)).[2] As a first result of our Monte-Carlo study, we find that all hits come with a normal mass ordering. We obtain no hits at all corresponding to an inverted hierarchy. It is, however, notable that merely imposing the hierarchy pattern of the neutrino mass matrix m_ν (cf. Eq. (3.61)) does *not* exclude the inverted mass ordering. Only if the bounds on the mixing angles are taken into account as well, this possibility is ruled out.

Mixing Angles

The flavour composition of the three neutrino mass eigenstates is characterized the three mixing angles θ_{12}, θ_{13}, and θ_{23} of the PMNS matrix (cf. Eq. (3.38)). Two of these angles are

[2] A measurement of the Mikheyev-Smirnov-Wolfenstein (MSW) effect of the earth on the neutrino oscillation probabilities could resolve this ambiguity (cf. Ref. [2] and references therein).

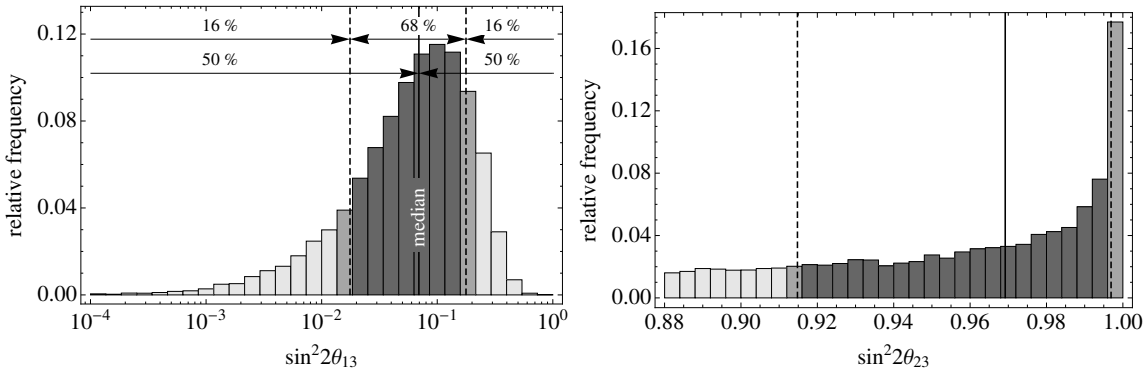

Figure 4.1: Neutrino mixing angles θ_{13} and θ_{23}. The vertical lines denote the positions of the medians (solid lines) and the boundaries of the 68 % confidence regions (dashed lines) of the respective distributions.

solely bounded from one side by experiment: for the largest mixing angle θ_{23} there merely exists a lower bound, whereas the smallest mixing angle θ_{13} is so far only bounded from above. Recent results from the T2K [244], Minos [245], Double Chooz [246], Daya Bay [247], and Reno [248] experiments point to a value of θ_{13} just below the current experimental bound.[3] The respective best-fit points, assuming a normal hierarchy, are $\sin^2 2\theta_{13} = 0.11$ (T2K), $2\sin^2\theta_{23}\sin^2 2\theta_{13} = 0.041$ (Minos), $\sin^2 2\theta_{13} = 0.085$ (Double Chooz), $\sin^2 2\theta_{13} = 0.092$ (Daya Bay), and $\sin^2 2\theta_{13} = 0.113$ (Reno). The 90 % or 68 % confidence intervals respectively read

$$\begin{aligned}
&0.03 < \sin^2 2\theta_{13} < 0.28 && \text{T2K, 90 % CL, } \delta_{CP} = 0, \\
&2\sin^2\theta_{23}\sin^2 2\theta_{13} < 0.12 && \text{Minos, 90 % CL, } \delta_{CP} = 0, \\
&0.01 < \sin^2 2\theta_{13} < 0.16 && \text{Double Chooz, 68 % CL,} \\
&0.07 < \sin^2 2\theta_{13} < 0.11 && \text{Daya Bay, 68 % CL,} \\
&0.09 < \sin^2 2\theta_{13} < 0.14 && \text{Reno, 68 % CL.}
\end{aligned} \tag{4.7}$$

We find sharp predictions for θ_{13} and θ_{23} within the experimental bounds,

$$\sin^2 2\theta_{13} = 0.07^{+0.11}_{-0.05}\,, \quad \sin^2 2\theta_{23} = 0.97^{+0.03}_{-0.05}\,, \tag{4.8}$$

with the corresponding distributions being shown in Fig. 4.1. These results are quite remarkable: our prediction for θ_{23} points to maximal mixing of atmospheric neutrinos, while the rather large value for θ_{13} is consistent with the recent T2K, Minos, Double Chooz, Daya Bay and Reno results.

Finally, we remark that the strong mixing in the lepton sector apparently derives for the most part from the peculiar hierarchy pattern of the neutrino mass matrix m_ν (cf. Eq. (3.61)).

[3] The Daya Bay and Reno experiments, whose results are the newest ones, claim that their measurements are indicative of $\theta_{13} \neq 0$ with a significance of $5.2\,\sigma$ and $4.9\,\sigma$, respectively.

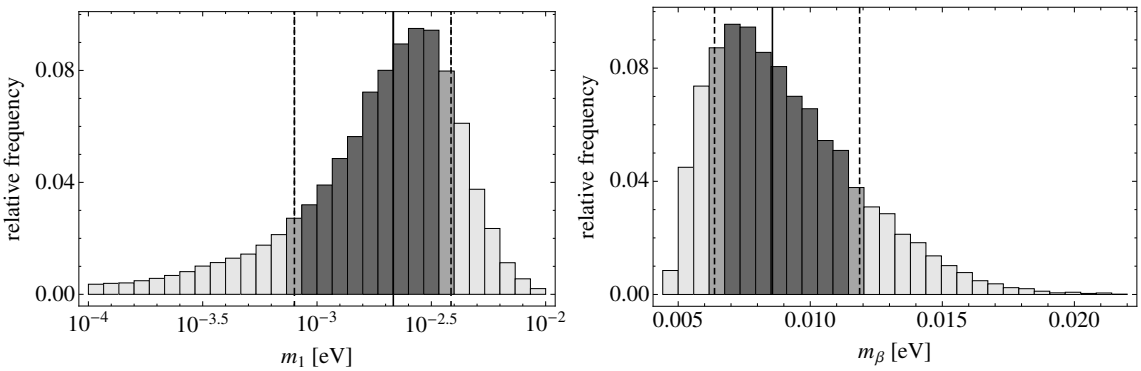

Figure 4.2: Lightest neutrino mass m_1 and effective neutrino mass in tritium decay m_β. Vertical lines and shadings as in Fig. 4.1.

In our Monte-Carlo study, we observe that our results for the mixing angles are not much affected when omitting the charged-lepton mixing matrix L in the calculation of the PMNS matrix. We hence conclude that the PMNS matrix is approximately given by Ω, the matrix which diagonalizes m_ν.

Absolute Mass Scale

The absolute neutrino mass scale determines the impact of cosmic neutrinos on the formation of matter structure in the early universe (cf. Sec. 2.1.2), represents a crucial parameter of leptogenesis (cf. Sec. 3.1.3) and enters into the description of various low-energy neutrino phenomena. Neutrino oscillation experiments are unfortunately insensitive to the absolute neutrino mass scale. But thanks to its influence on cosmology and low-energy neutrino processes, it is experimentally accessible nonetheless. Recall that the combination of several cosmological data sets allows to put an upper bound on $m_{\rm tot}$ (cf. Eq. (2.7)),

$$m_{\rm tot} = \sum_i m_i \lesssim 0.28\,{\rm eV}\,. \tag{4.9}$$

The Planck satellite is expected to be sensitive to values of $m_{\rm tot}$ as low as roughly 0.1 eV [249]. A further constraint on the absolute neutrino mass scale arises from measurements of the electron spectrum induced by the β^- decay of tritium. Such experiments are able to provide information on the effective neutrino mass m_β, for which there only exists an upper bound at present [2],

$$m_\beta^2 = \sum_i |U_{ei}|^2\, m_i^2 < 4\,{\rm eV}^2\,. \tag{4.10}$$

By comparison, the Katrin experiment, which will start taking data soon, aims at reaching a sensitivity of $0.04\,{\rm eV}^2$ [250]. Finally, the absolute neutrino mass scale also enters into the

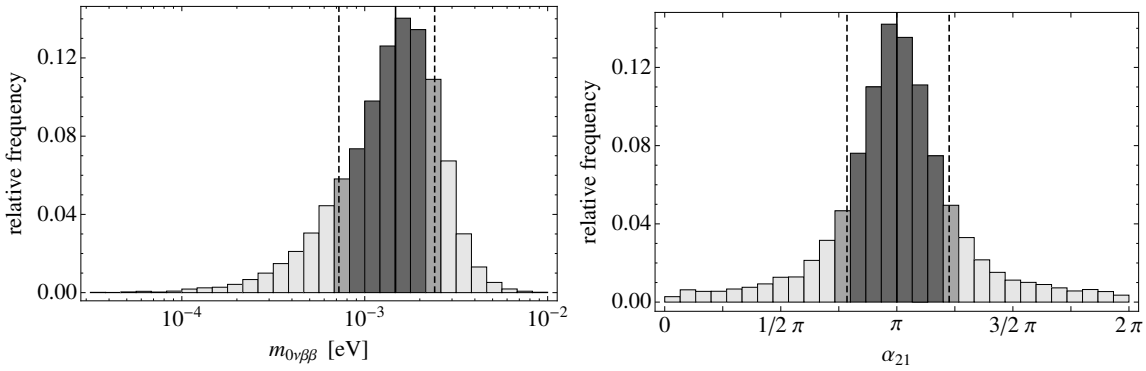

Figure 4.3: Effective neutrino mass in neutrinoless double-beta decay $m_{0\nu\beta\beta}$ and CP-violating Majorana phase α_{21}. Vertical lines and shadings as in Fig. 4.1.

decay amplitude of neutrinoless double-beta decay, *viz.* through the effective neutrino mass $m_{0\nu\beta\beta}$,

$$m_{0\nu\beta\beta} = \left| \sum_i U_{ei}^2 \, m_i \right| . \tag{4.11}$$

The authors of Ref. [251] claim to have a measured a value of 0.11..0.56 eV for this effective mass. Dedicated experiments searching for neutrinoless double-beta decay and capable of scrutinizing this claim, such as Gerda [252] with a design sensitivity of 0.09..0.20 eV, are on the way. Note that $m_{0\nu\beta\beta}$ does not only depend on the absolute neutrino mass scale and the mixing angles θ_{12} and θ_{13}, but also on the CP-violating phases $(\alpha_{31} - 2\delta)$ and α_{21}.

Again, our Monte-Carlo study provides us with sharp predictions. Our best-guess estimates for the neutrino masses listed in Eqs. (4.9), (4.10) and (4.11) as well as for the lightest neutrino mass m_1 are (cf. Figs. 4.2 and 4.3)

$$\begin{aligned} m_{\rm tot} &= 6.0^{+0.3}_{-0.3} \times 10^{-2}\,{\rm eV}\,, \quad & m_\beta &= 8.6^{+3.3}_{-2.2} \times 10^{-3}\,{\rm eV}\,, \\ m_{0\nu\beta\beta} &= 1.5^{+0.9}_{-0.8} \times 10^{-3}\,{\rm eV}\,, \quad & m_1 &= 2.2^{+1.7}_{-1.4} \times 10^{-3}\,{\rm eV}\,. \end{aligned} \tag{4.12}$$

The fact that m_1 turns out to be merely of $\mathcal{O}\left(10^{-3}\right)$ eV implies a low neutrino mass scale, unfortunately beyond the reach of current and upcoming experiments.

CP Violation Phases

The small value of our prediction for $m_{0\nu\beta\beta}$ can be traced back to a relative minus sign between the m_1 and m_2 terms in Eq. (4.11), which is caused by a strong peak in the distribution of the Majorana phase α_{21} at $\alpha_{21} \simeq \pi$ (cf. Fig. 4.3),

$$\frac{\alpha_{21}}{\pi} = 1.0^{+0.2}_{-0.2}\,. \tag{4.13}$$

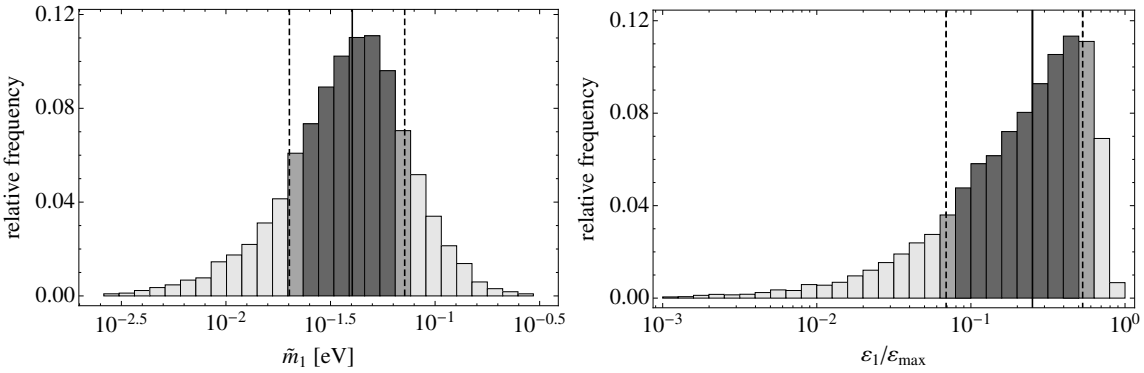

Figure 4.4: Effective neutrino mass of the first generation $\widetilde{m}_1$ and CP violation parameter ϵ_1. Vertical lines and shadings as in Fig. 4.1.

In the next section, we will demonstrate by means of a simplified analytic calculation how this preference for α_{21} values close to π directly emerges as a consequence of the hierarchy structure of the the neutrino mass matrix m_ν. For the other phases of the PMNS matrix, the Majorana phase α_{31} as well as the Dirac phase δ, we find no such distinct behaviour, but approximately flat distributions.

Leptogenesis Parameters

Leptogenesis links the low-energy neutrino physics to the high-energy physics of the early universe (cf. Sec. 3.1.3). The parameters which capture this connection are the effective neutrino mass $\widetilde{m}_1$ (cf. Eq. (3.41)) and the CP violation parameter ϵ_1 (cf. Eq. (3.43)). Our best-guess estimates are (cf. Fig. 4.4)

$$\widetilde{m}_1 = 4.0^{+3.1}_{-2.0} \times 10^{-2}\,\text{eV}\,, \qquad \frac{\epsilon_1}{\epsilon_1^{\max}} = 0.25^{+0.28}_{-0.18}\,. \tag{4.14}$$

The large value for $\widetilde{m}_1$ indicates a clear preference for the strong washout regime [85, 173]. Note that there is typically a hierarchy between $\widetilde{m}_1$ and the lightest neutrino mass m_1 of about one order of magnitude. Generally speaking, we observe that all $\widetilde{m}_1$ values generated in our Monte-Carlo study fall into a range extending over roughly two orders of magnitude (cf. Fig. 4.4). This result renders our decision to allow for a variation of $\widetilde{m}_1$ over *five* orders of magnitude quite conservative. In other words, it assures us that varying $\widetilde{m}_1$ as indicated in Eq. (3.70) will certainly suffice to cover all $\widetilde{m}_1$ values compatible with the Froggatt-Nielsen model. In particular, the chosen range of $\widetilde{m}_1$ values easily covers our best-guess estimate for $\widetilde{m}_1$ (cf. Eq. (4.14)).

The relative frequency of possible ϵ_1 values peaks close to the upper bound $\epsilon_1^{\max}$, with most of the hits lying one order of magnitude or less below $\epsilon_1^{\max}$. This confirms our earlier expectation that the effective CP-violating phase $\delta_1^{\text{eff}} = \epsilon_1/\epsilon_1^{\max}$ should be of $\mathcal{O}(1)$. Hence,

when using $\epsilon_1^{\max}$ to estimate the produced lepton asymmetry in leptogenesis, we should expect that the *actually* produced asymmetry, corresponding to the *actual* value of ϵ_1, is only slightly smaller than our estimate, i.e. the maximum possible asymmetry.

Theoretical versus Experimental Input

The results presented in this section are obtained from the combination of two conceptually different inputs: the hierarchy pattern of the neutrino mass matrix m_ν (cf. Eq. (3.61)) on the one hand and the experimental constraints listed in Eq. (4.1) on the other hand. For most neutrino observables, the distributions indeed arise from the interplay between both of these ingredients. To give an example, the hierarchy structure alone does *not* favour a large solar mixing angle θ_{12}, nor does it typically yield a ratio $r = \Delta m^2_{\rm sol}/\Delta m^2_{\rm atm}$ of about 1/30. Given the hierarchy structure in Eq. (3.61), r rather tends to be too large instead [253–256].[4] Only the requirement of consistency with the experimental data eventually singles out the subset of random mass matrices which we are able to use for our analysis. As another example, consider the smallest mixing angle θ_{13} and the smallest neutrino mass m_1. In the case of these observables, the hierarchy structure of the neutrino mass matrix automatically implies small values, similar to those in Figs. 4.1 and 4.2. However, the exact distributions, including the precise position of the peaks, only arise after implementing the experimental constraints. A notable exception to this scheme is the Majorana phase α_{21}. As we shall see in the next section, the peak in the α_{21} distribution at $\alpha_{21} \simeq \pi$ is a result of the hierarchy structure of the neutrino matrix alone.

In conclusion, we remark that we expect our results also to hold beyond flavour models of the Froggatt-Nielsen type. An obvious example are extradimensional models which lead to the same type of light neutrino mass matrix [257]. On the other hand, quark-lepton mass hierarchies and the presently available neutrino data cannot determine the remaining observables in a model-independent way. This is, for instance, illustrated by the fact that our present knowledge about quark and lepton masses and mixings is still consistent with an inverted neutrino mass hierarchy. As a consequence, further measurements of neutrino parameters will be able to falsify certain patterns of flavour mixing and thereby provide valuable guidance for the theoretical origin of quark and lepton mass matrices.

[4] In fact, in our case, this discrepancy is not as severe as we do not directly generate random coefficients for the entries of m_ν, but rather calculate m_ν from the seesaw formula (cf. Eq. (3.31)) after generating random coefficients for the entries of the matrices m_D and M.

4.3 Analytic Derivation of the Majorana Phase α_{21}

The complex phases of the $\mathcal{O}(1)$ coefficients in the neutrino mass matrix m_ν and the charged-lepton mass matrix $m_{\rm cl}$ are randomly distributed. One would thus naively expect that also the Majorana phases α_{21} and α_{31} in the PMNS matrix can take arbitrary values. By contrast, the distribution of values for α_{21} that we obtain from our numerical Monte-Carlo study (cf. Fig. 4.3) clearly features a prominent peak at $\alpha_{21} \simeq \pi$. In this section we shall demonstrate by means of a simplified example how the structure of the neutrino mass matrix m_ν may partly fix the phases of the corresponding mixing matrix U.

Consider the following simplified light-neutrino Majorana mass matrix m_ν,

$$m_\nu = \hat{v} \begin{pmatrix} \eta^2 & \eta e^{i\beta} & \eta \\ \eta e^{i\beta} & 1 & 1 \\ \eta & 1 & 1 \end{pmatrix} , \quad \hat{v} = \frac{v_{\rm EW}^2}{\bar{v}_{B-L}} , \tag{4.15}$$

where $\beta \in [0, 2\pi)$ is an arbitrary complex phase. For simplicity, let us neglect any effects on the mixing matrix U from the diagonalization of $m_{\rm cl}$. That is, we define U such that $U^T m_\nu U = {\rm diag}\,(m_i)$, with m_i^2 denoting the eigenvalues of $m_\nu^\dagger m_\nu$,

$$\begin{aligned} \frac{m_{1,2}^2}{\hat{v}^2} &= \eta^2 \sin^2(\beta/2) \left[2 \mp \eta \left(5 + 3\cos(\beta)\right)^{1/2}\right] + \mathcal{O}\left(\eta^4\right) , \\ \frac{m_3^2}{\hat{v}^2} &= 4\left(1 + \eta^2 \left[1 - \sin^2(\beta/2)\right]\right) + \mathcal{O}\left(\eta^4\right) . \end{aligned} \tag{4.16}$$

The first two mass eigenvalues are nearly degenerate. This is a consequence of the particular hierarchy pattern of the matrix m_ν, which originally stems from the equal flavour charges of the $\mathbf{5}_2^*$ and $\mathbf{5}_3^*$ multiplets. The relative sign of the $\mathcal{O}\left(\eta^3\right)$ contributions to m_1^2 and m_2^2 eventually shows up again in entries of U, for instance,

$$U_{11,12} = \mp \frac{2\left(5 + 3\cos(\beta)\right)^{1/2}}{3 + e^{i\beta}} \exp\left(-\frac{i}{2}{\rm Arg}\left[\mp z\right]\right) + \mathcal{O}(\eta) . \tag{4.17}$$

with $z = 1 - \cos(\beta) - 2i\sin(\beta)$. The phase $\alpha_{21} = 2\left({\rm Arg}\left[U_{12}/U_{11}\right] \bmod \pi\right)$ in the matrix U represents the analog of the Majorana phase α_{21} in the PMNS matrix, cf. Eq. (3.38). According to our explicit results for U_{11} and U_{12}, it is independent of the arbitrary phase β to leading order in η,

$$\alpha_{21} \simeq 2\left({\rm Arg}\left[-\exp\left(-\frac{i}{2}{\rm Arg}\left[+z\right] + \frac{i}{2}{\rm Arg}\left[-z\right]\right)\right] \bmod \pi\right) = \pi . \tag{4.18}$$

In a similar way, we may determine the phase analogous to the Majorana phase α_{31}. However, due to the hierarchy between the mass eigenvalues m_1 and m_3, the first and third column of the matrix U differ significantly from each other, thus leading to a phase that depends on β at all orders of η.

Including corrections to all orders in η and scanning over the phase β numerically shows that the maximum possible deviation of α_{21} from π is, in fact, of $\mathcal{O}\left(\eta^4\right)$. Adding more complex phases to the matrix m_ν in Eq. (4.15) gradually smears out the peak in the distribution of α_{21} values. The distribution which is reached in the case of six different phases is already very similar to the one in Fig. 4.3. We conclude that, despite the need for corrections, the rough picture sketched in this section remains valid: the hierarchy pattern of the neutrino mass matrix directly implies that α_{21} tends to be close to $\alpha_{21} = \pi$.

Chapter 5

Supersymmetric Abelian Higgs Model

In order to incorporate hybrid inflation as well as the $B-L$ phase transition into our cosmological scenario, we introduced the superpotential W_{B-L} (cf. Eq. (3.8)) in Ch. 3. The chiral superfields contained in this superpotential, the inflaton field Φ and the two Higgs fields $S_{1,2}$, partly carry $B-L$ charge, but all transform as standard model gauge singlets. Their dynamics are hence fully accounted for by a supersymmetric Abelian gauge theory with gauge group $U(1)_{B-L}$. The field-theoretic description of $B-L$ breaking at the end of inflation represents in particular a variant of the *supersymmetric Abelian Higgs model*.

The goal of this chapter now is to derive the full supersymmetric Lagrangian for the Abelian Higgs model describing the $B-L$ phase transition in unitary gauge. We will first consider $B-L$ to be unbroken and compute the Lagrangian of a general supersymmetric Abelian gauge theory in arbitrary gauge (cf. Sec. 5.1). Then, after going to unitary gauge, we will evaluate this general Lagrangian for the specific field content of our model in the broken phase (cf. Sec. 5.2). This will allow us to calculate the masses, decay rates and branching ratios of all particles coupling to the $B-L$ Higgs boson. One important result of our analysis at this point will be that during the $B-L$ phase transition the mass eigenvalues under study are time-dependent, which gives rise to nonperturbative particle production.

5.1 Before Spontaneous Symmetry Breaking

As a first step towards the supersymmetric Abelian Higgs model of the $B-L$ phase transition, we derive the Lagrangian of a general $U(1)$ gauge theory featuring N chiral superfields Φ_i and one massless vector superfield V. By virtue of its particular transformation law, the vector superfield V ensures the invariance of the Lagrangian under super-gauge transformations. In addition to the fields Φ_i and V, the theory also contains the gravity multiplet, consisting of the graviton G and the gravitino $\widetilde{G}$, which gives rise to further, Planck-suppressed operators in the Lagrangian. As the $B-L$ phase transition takes place around the GUT scale, $v_{B-L} \sim \Lambda_{\text{GUT}} \ll M_P$, these SUGRA corrections are however irrelevant, so that we may neglect them in the following (cf. Sec. 3.1.1). More precisely, for the purposes of this thesis, it will suffice to compute the Lagrangian of the Abelian Higgs model for the case of global supersymmetry. By contrast, we are not allowed to facilitate our calculation by choosing a specific gauge.[1] During the $B-L$ phase transition, the vector superfield turns massive, which is best described in unitary gauge, where the physical DOFs are manifest. To be able to evaluate the Lagrangian in unitary gauge later on, we now first have to calculate it in arbitrary gauge. In doing so, we will closely follow the notation of Ref. [258].

5.1.1 From Superspace to the Component Lagrangian

The total Lagrangian $\mathcal{L}$ of our Abelian gauge theory splits into three pieces,

$$\mathcal{L} = \mathcal{L}_G + \mathcal{L}_K + \mathcal{L}_W \,. \tag{5.1}$$

Here, $\mathcal{L}_G$ encompasses the gauge-kinetic terms, $\mathcal{L}_K$ takes care of the kinetic terms and gauge interactions of the chiral superfields Φ_i and $\mathcal{L}_W$ contains all interactions stemming from the superpotential W. Let us now calculate each of these contributions to $\mathcal{L}$ in terms of the components of the superfields Φ_i and V.

Expansion of the Superfields in Superspace Coordinates

The supersymmetric Abelian Higgs model may be formulated as a theory on *superspace*. In four spacetime dimensions and assuming the number of generators of supersymmetry transformations to be minimal, i.e. $\mathcal{N} = 1$ supersymmetry, superspace is spanned by four bosonic, commuting coordinates x^μ, where $\mu = 0, 1, 2, 3$, as well as four fermionic, anticommuting coordinates θ_α and $\bar{\theta}^{\dot{\alpha}}$, where $\alpha, \dot{\alpha} = 1, 2$. The superfields Φ_i and V are nothing but functions of these superspace coordinates and should be understood in terms of their power series

[1] The Lagrangian of the Abelian Higgs model in *Wess-Zumino gauge*, for instance, is well known and listed in all standard textbooks on supersymmetry and supergravity [258–260].

expansion in θ and $\bar{\theta}$ [258]. The chiral superfields Φ_i are expanded as follows,

$$\Phi_i = \phi_i + i\theta\sigma^\mu\bar{\theta}\partial_\mu\phi_i + \frac{1}{4}\theta\theta\bar{\theta}\bar{\theta}\Box\phi_i + \sqrt{2}\theta\psi_i - \frac{i}{\sqrt{2}}\theta\theta\partial_\mu\psi_i\sigma^\mu\bar{\theta} + \theta\theta F_i\,, \tag{5.2}$$

where we have introduced ϕ_i, ψ_i and F_i as the components of Φ_i, all of which are fields on spacetime. ϕ_i and F_i are complex scalars, having mass dimension 1 and 2, respectively, while ψ_i is an ordinary left-chiral Weyl fermion. As we will shortly see, F_i is not dynamical, i.e. an auxiliary field, and can therefore be integrated out. Under hermitian conjugation, the superfield in Eq. (5.2) turns into

$$\Phi_i^\dagger = \phi_i^* - i\theta\sigma^\mu\bar{\theta}\partial_\mu\phi_i^* + \frac{1}{4}\theta\theta\bar{\theta}\bar{\theta}\Box\phi_i^* + \sqrt{2}\bar{\theta}\bar{\psi}_i + \frac{i}{\sqrt{2}}\bar{\theta}\bar{\theta}\theta\sigma^\mu\partial_\mu\bar{\psi}_i + \bar{\theta}\bar{\theta}F_i^*\,. \tag{5.3}$$

The vector superfield V satisfies the reality condition $V^\dagger = V$ and is given by

$$\begin{aligned}\text{Arbitrary gauge:}\qquad V &= C + i\theta\chi - i\bar{\theta}\bar{\chi} + \frac{i}{2}\theta\theta\,(M + iN) - \frac{i}{2}\bar{\theta}\bar{\theta}\,(M - iN) \\ &- \theta\sigma^\mu\bar{\theta}A_\mu + i\theta\theta\bar{\theta}\left(\bar{\xi} + \frac{i}{2}\bar{\sigma}^\mu\partial_\mu\chi\right) - i\bar{\theta}\bar{\theta}\theta\left(\xi + \frac{i}{2}\sigma^\mu\partial_\mu\bar{\chi}\right) + \frac{1}{2}\theta\theta\bar{\theta}\bar{\theta}\left(D + \frac{1}{2}\Box C\right)\,.\end{aligned} \tag{5.4}$$

C, χ, M, N, A^μ, ξ, and D are the spacetime-dependent component fields of V, where C, M, N, and D are real scalars of mass dimension 0, 1, 1 and 2, respectively, while χ and ξ are left-chiral Weyl fermions of mass dimension 1/2 and 3/2, respectively. A^μ is an ordinary real four-vector. C, χ, M, N, and D are auxiliary fields, the latter three of which we will eventually integrate out, whereas C and χ will become dynamical during the $B-L$ phase transition. By performing an appropriate super-gauge transformation on V, one can eliminate all auxiliary fields in V except for D, such that V reduces to

$$\text{Wess-Zumino gauge:}\qquad V = -\theta\sigma^\mu\bar{\theta}A_\mu + i\theta\theta\bar{\theta}\bar{\xi} - i\bar{\theta}\bar{\theta}\theta\xi + \frac{1}{2}\theta\theta\bar{\theta}\bar{\theta}D\,. \tag{5.5}$$

The gauge in which V takes this form is referred to as the Wess-Zumino gauge. Compared to other gauge choices, it allows for the technically simplest treatment of the vector superfield V. After gauge-fixing to Wess-Zumino gauge, the Lagrangian is no longer manifestly invariant under supersymmetry transformations, but still gauge-invariant under ordinary $U(1)$ transformations. A slight relaxation of the Wess-Zumino gauge consists in merely gauging away χ, M and N, which corresponds to fixing the gauge only up to complexified $U(1)$ transformations, i.e. transformations featuring a complex gauge transformation parameter. In this *complex gauge*, C remains as an auxiliary field in V,

$$\text{Complex gauge:}\qquad V = C - \theta\sigma^\mu\bar{\theta}A_\mu + i\theta\theta\bar{\theta}\bar{\xi} - i\bar{\theta}\bar{\theta}\theta\xi + \frac{1}{2}\theta\theta\bar{\theta}\bar{\theta}D\,. \tag{5.6}$$

It is easy to construct the Lagrangian of the Abelian Higgs model from the chiral superfields Φ_i and $\Phi_i^\dagger$ as well as the vector superfield V in Wess-Zumino gauge (cf. Eq. (5.5))

[258–260]. However, since we wish to eventually describe the $B-L$ phase transition in unitary gauge, we now face the task to generalize the result commonly quoted in the literature to arbitrary gauge. Instead of V as given in Eq. (5.5), we now have to calculate the Lagrangian of the Abelian Higgs model using V as given in Eq. (5.4), thereby taking into account *all* auxiliary fields.

Gauge-Kinetic Terms and Terms Deriving from the Superpotential

$\mathcal{L}_G$ and $\mathcal{L}_W$ are solely constructed from gauge-invariant quantities. While the Lagrangian $\mathcal{L}_G$ is obtained from the gauge-invariant chiral superfield $\mathcal{W}_\alpha$, the supersymmetric generalization of the Abelian field strength tensor $F_{\mu\nu} = \partial_\mu A_\nu - \partial_\nu A_\mu$, the Lagrangian $\mathcal{L}_W$ follows straightforwardly from the gauge-invariant superpotential W. These two contributions to the total Lagrangian $\mathcal{L}$ hence look the same in all gauges, so that we may simply adopt the standard expressions for $\mathcal{L}_G$ and $\mathcal{L}_W$, which one readily finds in Wess-Zumino gauge,

$$\mathcal{L}_G = -\frac{1}{4}F_{\mu\nu}F^{\mu\nu} - i\bar{\xi}\bar{\sigma}^\mu\partial_\mu\xi + \frac{1}{2}D^2\,, \tag{5.7}$$

$$\mathcal{L}_W = -\frac{1}{2}\sum_{i,j} W_{ij}\psi_i\psi_j + \sum_i W_i F_i + \text{h.c.}\,. \tag{5.8}$$

Of course, the superpotential is actually a holomorphic function of the chiral superfields, $W = W(\{\Phi_k\})$. In Eq. (5.8), to the benefit of a convenient notation, it is, however, interpreted as a function of the corresponding complex scalars, $W = W(\{\phi_k\})$. The functions W_i and W_{ij} then stand for

$$W_i = \frac{\partial}{\partial\phi_i}W(\{\phi_k\})\,, \quad W_{ij} = \frac{\partial^2}{\partial\phi_i\partial\phi_j}W(\{\phi_k\})\,. \tag{5.9}$$

Kinetic Terms and Gauge Interactions of the Chiral Superfields

$\mathcal{L}_K$ receives a contribution $\mathcal{L}_K^i$ for each chiral superfield Φ_i. Assuming canonical kinetic terms for the Φ_i component fields, $\mathcal{L}_K$ is uniquely given as

$$\mathcal{L}_K = \sum_i \mathcal{L}_K^i\,, \quad \mathcal{L}_K^i = \left[\Phi_i^\dagger e^{p_i V}\Phi_i\right]_D\,, \quad p_i = 2gq_i\,. \tag{5.10}$$

Here, the subscript D indicates that only the $\theta\theta\bar{\theta}\bar{\theta}$ component, i.e. the D-term, of the field product $\Phi_i^\dagger e^{p_i V}\Phi_i$ is to be included in $\mathcal{L}_K^i$. Meanwhile, g is the $U(1)$ gauge coupling and q_i denotes the $U(1)$ gauge charge of the chiral superfield Φ_i. In Chs. 6, 7 and 8, we will take g to be the GUT gauge coupling, $g = g_{\text{GUT}} \simeq \sqrt{\pi/6}$. Expanding the exponential in Eq. (5.10)

in powers of $(V-C)$, the Lagrangian $\mathcal{L}_K^i$ turns into

$$\mathcal{L}_K^i = e^{p_i C}\left[\Phi_i^\dagger\left\{1 + p_i\,(V-C) + \frac{p_i^2}{2}\,(V-C)^2 + \frac{p_i^3}{6}\,(V-C)^3 + \frac{p_i^4}{24}\,(V-C)^4\right\}\Phi_i\right]_D . \tag{5.11}$$

All higher powers of $(V-C)$ vanish, as they only involve products of at least five Grassmannian superspace coordinates, which are all zero.

In a first step towards $\mathcal{L}_K^i$, we calculate $(V-C)^n$ for $n=2,3,4$. Given the component expansion of V in Eq. (5.4) and making heavy use of the following spinor identities [258],

$$\begin{aligned}
(\chi\theta)\,(\psi\theta) &= -\frac{1}{2}\,(\chi\psi)\,(\theta\theta)\,, & \left(\bar\chi\bar\theta\right)\left(\bar\psi\bar\theta\right) &= -\frac{1}{2}\left(\bar\chi\bar\psi\right)\left(\bar\theta\bar\theta\right)\,, \\
(\chi\theta)\,\bar\theta\bar\sigma^\mu\theta &= -\frac{1}{2}\bar\theta\bar\sigma^\mu\chi\,(\theta\theta)\,, & \left(\bar\chi\bar\theta\right)\bar\theta\bar\sigma^\mu\theta &= -\frac{1}{2}\bar\chi\bar\sigma^\mu\theta\left(\bar\theta\bar\theta\right)\,, \\
\chi\sigma^\mu\bar\psi &= -\bar\psi\bar\sigma^\mu\chi\,, & \left(\chi\sigma^\mu\bar\psi\right)^\dagger &= \psi\sigma^\mu\bar\chi\,, \\
\bar\theta\bar\sigma^\mu\theta\bar\theta\bar\sigma^\nu\theta &= -\frac{1}{2}\eta^{\mu\nu}\,(\theta\theta)\left(\bar\theta\bar\theta\right)\,, & \theta^\alpha\theta^\beta\theta^\gamma &= \bar\theta_{\dot\alpha}\bar\theta_{\dot\beta}\bar\theta_{\dot\gamma} = 0\,,
\end{aligned} \tag{5.12}$$

we find

$$\begin{aligned}
(V-C)^2 =\ & \frac{1}{2}\chi^2\theta\theta + \frac{1}{2}\bar\chi^2\bar\theta\bar\theta + 2\chi\theta\bar\chi\bar\theta + \chi\theta\bar\theta\bar\theta\,(M-iN) + \bar\chi\bar\theta\theta\theta\,(M+iN) \\
& + 2i\left(\chi\theta - \bar\chi\bar\theta\right)\bar\theta\bar\sigma^\mu\theta A_\mu + \Big[-\frac{1}{2}A_\mu A^\mu + \frac{1}{2}\left(M^2+N^2\right) \\
& - \chi\xi - \bar\chi\bar\xi - \frac{i}{2}\bar\chi\bar\sigma^\mu\partial_\mu\chi + \frac{i}{2}\partial_\mu\bar\chi\bar\sigma^\mu\chi\Big]\theta\theta\bar\theta\bar\theta
\end{aligned} \tag{5.13}$$

$$\begin{aligned}
(V-C)^3 =\ & \frac{3i}{2}\bar\chi^2\chi\theta\bar\theta\bar\theta - \frac{3i}{2}\chi^2\bar\chi\bar\theta\theta\theta + \Big[\frac{3i}{4}\bar\chi^2\,(M+iN) - \frac{3i}{4}\chi^2\,(M-iN) \\
& + \frac{3}{2}\bar\chi\bar\sigma^\mu\chi A_\mu\Big]\theta\theta\bar\theta\bar\theta
\end{aligned} \tag{5.14}$$

$$(V-C)^4 = \frac{3}{2}\chi^2\bar\chi^2\theta\theta\bar\theta\bar\theta\,. \tag{5.15}$$

These expressions allow us to work out the field products $\left[\Phi_i^\dagger\,(V-C)^n\,\Phi_i\right]_D$, where $n = 0,\ldots,4$, constituting the Lagrangian $\mathcal{L}_K^i$ in Eq. (5.11),

$$\begin{aligned}
\left[\Phi_i^\dagger\Phi_i\right]_D =\ & -\frac{1}{2}\partial_\mu\phi_i^*\partial^\mu\phi_i + \frac{1}{4}\phi_i^*\Box\phi_i + \frac{1}{4}\phi_i\Box\phi_i^* + \frac{i}{2}\partial_\mu\bar\psi_i\bar\sigma^\mu\psi_i \\
& - \frac{i}{2}\bar\psi_i\bar\sigma^\mu\partial_\mu\psi_i + F_i^*F_i\,,
\end{aligned} \tag{5.16}$$

$$\begin{aligned}
\left[\Phi_i^\dagger\,(V-C)\,\Phi_i\right]_D =\ & \frac{1}{2}\phi_i^*\phi_i\left(D + \frac{1}{2}\Box C\right) + \frac{1}{2}\bar\psi_i\bar\sigma^\mu\psi_i A_\mu + \Big\{\frac{i}{2}\phi_i^*\partial^\mu\phi_i A_\mu \\
& + \frac{i}{\sqrt{2}}\phi_i^*\psi_i\left(\xi + \frac{i}{2}\sigma^\mu\partial_\mu\bar\chi\right) - \frac{1}{2\sqrt{2}}\phi_i^*\bar\chi\bar\sigma^\mu\partial_\mu\psi_i
\end{aligned} \tag{5.17}$$

$$
\begin{aligned}
&- \frac{i}{2}\phi_i^* F_i\,(M - iN) + \frac{1}{2\sqrt{2}}\bar{\chi}\bar{\sigma}^\mu\psi_i\partial_\mu\phi_i^* + \frac{i}{\sqrt{2}}\bar{\psi}_i\bar{\chi}F_i + \text{h.c.}\Big\}\,, \\
\left[\Phi_i^\dagger\,(V-C)^2\,\Phi_i\right]_D &= \phi_i^*\phi_i\Big(-\frac{1}{2}A_\mu A^\mu + \frac{1}{2}\left(M^2+N^2\right) - \chi\xi - \bar{\chi}\bar{\xi} \\
&- \frac{i}{2}\bar{\chi}\bar{\sigma}^\mu\partial_\mu\chi + \frac{i}{2}\partial_\mu\bar{\chi}\bar{\sigma}^\mu\chi\Big) + \chi\psi_i\bar{\chi}\bar{\psi}_i + \Big\{-\frac{i}{2}\phi_i^*\bar{\chi}\bar{\sigma}^\mu\chi\partial_\mu\phi_i \\
&- \frac{1}{\sqrt{2}}\phi_i^*\psi_i\chi\,(M - iN) - \frac{i}{\sqrt{2}}\phi_i^*\bar{\chi}\bar{\sigma}^\mu\psi_i A_\mu + \frac{1}{2}\phi_i^*\bar{\chi}^2 F_i + \text{h.c.}\Big\}\,, \qquad (5.18) \\
\left[\Phi_i^\dagger\,(V-C)^3\,\Phi_i\right]_D &= \frac{3}{2}\phi_i^*\phi_i\bar{\chi}\bar{\sigma}^\mu\chi A_\mu + \Big\{\frac{3i}{4}\phi_i^*\phi_i\bar{\chi}^2\,(M + iN) \\
&+ \frac{3i}{2\sqrt{2}}\bar{\chi}\bar{\psi}_i\chi^2\phi_i + \text{h.c}\Big\}\,, \qquad (5.19) \\
\left[\Phi_i^\dagger\,(V-C)^4\,\Phi_i\right]_D &= \frac{3}{2}\phi_i^*\phi_i\chi^2\bar{\chi}^2\,. \qquad (5.20)
\end{aligned}
$$

By shifting around spacetime derivatives with the aid of integrations by parts, we are able to combine several terms in the above field products. We shall use that

$$
\begin{aligned}
e^{p_iC}\left(\frac{1}{4}\phi_i^*\Box\phi_i + \frac{1}{4}\phi_i\Box\phi_i^*\right) &= e^{p_iC}\Big(-\frac{1}{2}\partial_\mu\phi_i^*\partial^\mu\phi_i - \frac{p_i}{4}\phi_i^*\partial_\mu C\partial^\mu\phi_i \qquad (5.21) \\
&- \frac{p_i}{4}\phi_i\partial_\mu C\partial^\mu\phi_i^*\Big) + d\,, \\
\frac{i}{2}e^{p_iC}\partial_\mu\bar{\psi}_i\bar{\sigma}^\mu\psi_i &= -\frac{i}{2}e^{p_iC}\left(\bar{\psi}_i\bar{\sigma}^\mu\partial_\mu\psi_i + p_i\bar{\psi}_i\bar{\sigma}^\mu\psi_i\partial_\mu C\right) + d\,, \qquad (5.22) \\
\frac{ip_i^2}{4}e^{p_iC}\phi_i^*\phi_i\partial_\mu\bar{\chi}\bar{\sigma}^\mu\chi &= \frac{ip_i^2}{4}e^{p_iC}(-\phi_i^*\phi_i\bar{\chi}\bar{\sigma}^\mu\partial_\mu\chi - \phi_i^*\partial_\mu\phi_i\bar{\chi}\bar{\sigma}^\mu\chi \qquad (5.23) \\
&- \phi_i\partial_\mu\phi_i^*\bar{\chi}\bar{\sigma}^\mu\chi - p_i\phi_i^*\phi_i\partial_\mu C\bar{\chi}\bar{\sigma}^\mu\chi) + d\,, \\
-\frac{p_i}{2\sqrt{2}}e^{p_iC}\phi_i^*\psi_i\sigma^\mu\partial_\mu\bar{\chi} &= -\frac{p_i}{2\sqrt{2}}e^{p_iC}(\phi_i^*\bar{\chi}\bar{\sigma}^\mu\partial_\mu\psi_i + \partial_\mu\phi_i^*\bar{\chi}\bar{\sigma}^\mu\psi_i \qquad (5.24) \\
&+ p_i\phi_i^*\partial_\mu C\bar{\chi}\bar{\sigma}^\mu\psi_i) + d\,.
\end{aligned}
$$

Here, d denotes total derivatives, which we do not need to include into the Lagrangian. Inserting these relations into Eqs. (5.16), (5.17) and (5.18), we obtain

$$
\begin{aligned}
\left[\Phi_i^\dagger\Phi_i\right]_D &= -\partial_\mu\phi_i^*\partial^\mu\phi_i - i\bar{\psi}_i\bar{\sigma}^\mu\partial_\mu\psi_i + F_i^*F_i \qquad (5.25) \\
&- \frac{p_i}{4}\phi_i^*\partial_\mu C\partial^\mu\phi_i - \frac{p_i}{4}\phi_i\partial_\mu C\partial^\mu\phi_i^* - \frac{ip_i}{2}\bar{\psi}_i\bar{\sigma}^\mu\psi_i\partial_\mu C\,, \\
\left[\Phi_i^\dagger\,(V-C)\,\Phi_i\right]_D &= \frac{1}{2}\phi_i^*\phi_i\left(D + \frac{1}{2}\Box C\right) + \frac{1}{2}\bar{\psi}_i\bar{\sigma}^\mu\psi_i A_\mu + \Big\{\frac{i}{2}\phi_i^*\partial^\mu\phi_i A_\mu \qquad (5.26) \\
&+ \frac{i}{\sqrt{2}}\phi_i^*\psi_i\xi - \frac{1}{\sqrt{2}}\phi_i^*\bar{\chi}\bar{\sigma}^\mu\partial_\mu\psi_i - \frac{p_i}{2\sqrt{2}}\phi_i^*\bar{\chi}\bar{\sigma}^\mu\psi_i\partial_\mu C \\
&- \frac{i}{2}\phi_i^*F_i\,(M - iN) + \frac{i}{\sqrt{2}}\bar{\psi}_i\bar{\chi}F_i + \text{h.c.}\Big\}\,,
\end{aligned}
$$

$$\begin{aligned}\left[\Phi_i^\dagger \left(V-C\right)^2 \Phi_i\right]_D = \phi_i^* \phi_i \Bigg(&- \frac{1}{2} A_\mu A^\mu + \frac{1}{2}\left(M^2+N^2\right) - \chi\xi - \bar{\chi}\bar{\xi} \\ &- \frac{i p_i}{2} \bar{\chi}\bar{\sigma}^\mu \chi \partial_\mu C \Bigg) - i\phi_i^* \bar{\chi}\bar{\sigma}^\mu \partial_\mu \left(\phi_i \chi\right) + \chi\psi_i \bar{\chi}\bar{\psi}_i \\ &+ \Bigg\{ - \frac{1}{\sqrt{2}} \phi_i^* \psi_i \chi \left(M - iN\right) - \frac{i}{\sqrt{2}} \phi_i^* \bar{\chi}\bar{\sigma}^\mu \psi_i A_\mu \\ &+ \frac{1}{2} \phi_i^* \bar{\chi}^2 F_i + \text{h.c.} \Bigg\} .\end{aligned} \tag{5.27}$$

Note the newly emerged couplings to $\partial_\mu C$, which have been generated by the various integrations by parts. Our results in Eqs. (5.19) and (5.20) remain unchanged, so that we are able to construct a preliminary expression for $\mathcal{L}_K^i$ (cf. Eq. (5.11)) by assembling the field products in Eqs. (5.19), (5.20), (5.25), (5.26), and (5.27).

Eliminating the Auxiliary Fields

Our calculation thus far has provided us with kinetic terms for the gauge fields A_μ and ξ (cf. Eq. (5.7)) as well as for the scalar and fermionic components ϕ_i and ψ_i of the chiral superfields Φ_i (cf. Eq. (5.25)). The fields F_i, C, χ, M, N, and D are, by contrast, not dynamical and may hence be integrated out. An important observation, however, is that the Lagrangian $\mathcal{L}_K^i$ contains two terms (cf. Eq. (5.26), and (5.27)) which turn into kinetic terms for C and χ, once the scalar field ϕ_i acquires a nonzero VEV. As exactly this happens during the $B-L$ phase transition, we shall keep the auxiliary fields C and χ in the Lagrangian, anticipating them to become dynamical in the course of $B-L$ breaking. Meanwhile, no term in the total Lagrangian features a derivative of F_i, M, N, or D, i.e. no term could possibly give rise to a kinetic term for any of these fields, and hence all of them always remain auxiliary. Let us now integrate them out of the Lagrangian.

The auxiliary gauge field D only appears in two terms in the total Lagrangian (cf. Eqs. (5.7) and (5.26)), which we collect in the Lagrangian $\mathcal{L}_D$,

$$\mathcal{L}_D = \frac{1}{2} D^2 + \frac{1}{2} \sum_i p_i e^{p_i C} \phi_i^* \phi_i D \,. \tag{5.28}$$

The equation of motion of the field D is hence given as

$$\frac{\partial \mathcal{L}}{\partial D} = D + \frac{1}{2} \sum_i p_i e^{p_i C} \phi_i^* \phi_i = 0 \,, \quad D = -\frac{1}{2} \sum_i p_i e^{p_i C} \phi_i^* \phi_i \,. \tag{5.29}$$

Substituting the solution for D back into Eq. (5.28) yields

$$\mathcal{L}_D = \frac{1}{2} D^2 - D^2 = -\frac{1}{2} D^2 = -V_D \,, \quad V_D = \frac{1}{8} \sum_{ij} p_i p_j e^{(p_i+p_j)C} \phi_i^* \phi_i \phi_j^* \phi_j \,, \tag{5.30}$$

where we will refer to V_D as the D-term scalar potential in the following.

Next, we compile all terms featuring F_i and F_i^* in one common Lagrangian $\mathcal{L}_F^i$,

$$\begin{aligned}\mathcal{L}_F^i = \Bigg\{ W_i F_i + e^{p_i C} \Bigg[F_i^* F_i + p_i \left(-\frac{i}{2}\phi_i^* \left(M - iN\right) F_i + \frac{i}{\sqrt{2}}\bar{\psi}_i \bar{\chi} F_i \right) \\ + \frac{p_i^2}{2}\frac{1}{2}\phi_i^* \bar{\chi}^2 F_i \Bigg] + \text{h.c.} \Bigg\} - e^{p_i C} F_i^* F_i \,.\end{aligned} \tag{5.31}$$

The last term in Eq. (5.31) prevents us from double-counting $e^{p_i C} F_i^* F_i$, which appears twice within the curly brackets. $\mathcal{L}_F^i$ can be simplified by observing that

$$\mathcal{L}_F^i = \frac{\partial \mathcal{L}_F^i}{\partial F_i} F_i + \frac{\partial \mathcal{L}_F^i}{\partial F_i^*} F_i^* - e^{p_i C} F_i^* F_i \,. \tag{5.32}$$

The first two terms on the right-hand side of this relation vanish due the equations of motions of F_i and F_i^*, which provides us with a compact expression for $\mathcal{L}_F^i$,

$$\frac{\partial \mathcal{L}_F^i}{\partial F_i} = \frac{\partial \mathcal{L}_F^i}{\partial F_i^*} = 0 \,, \quad \mathcal{L}_F^i = -e^{p_i C} F_i^* F_i \,. \tag{5.33}$$

Written out explicitly, the equation of motion for F_i^* reads

$$\frac{\partial \mathcal{L}_F^i}{\partial F_i} = W_i + e^{p_i C} \left[F_i^* + p_i \left(-\frac{i}{2}\phi_i^* \left(M - iN\right) + \frac{i}{\sqrt{2}}\bar{\psi}_i \bar{\chi} \right) + \frac{p_i^2}{2}\frac{1}{2}\phi_i^* \bar{\chi}^2 \right] = 0 \,. \tag{5.34}$$

From this we obtain F_i^* as a function of W_i, $M - iN$ as well as fermionic expressions,

$$F_i^* = -\left[e^{-p_i C} W_i + p_i \left(-\frac{i}{2}\phi_i^* \left(M - iN\right) + \frac{i}{\sqrt{2}}\bar{\psi}_i \bar{\chi} \right) + \frac{p_i^2}{2}\frac{1}{2}\phi_i^* \bar{\chi}^2 \right] . \tag{5.35}$$

We may distinguish terms in $\mathcal{L}_F^i$ that are either proportional to $e^{-p_i C}$, 1, or $e^{p_i C}$,

$$\mathcal{L}_F^i = -e^{-p_i C} L_-^i - L_0^i - e^{p_i C} L_+^i \,. \tag{5.36}$$

Combining our results in Eq. (5.33) and (5.35), we find

$$L_-^i = W_i W_i^* \,, \tag{5.37}$$

$$L_0^i = W_i \left[p_i \left(\frac{i}{2}\phi_i \left(M + iN\right) - \frac{i}{\sqrt{2}}\psi_i \chi \right) + \frac{p_i^2}{2}\frac{1}{2}\phi_i \chi^2 \right] + \text{h.c.} \,, \tag{5.38}$$

$$\begin{aligned}L_+^i = \frac{p_i^4}{16}\phi_i^* \phi_i \chi^2 \bar{\chi}^2 + \frac{p_i^2}{2}\psi_i \chi \bar{\psi}_i \chi + \frac{p_i^2}{4}\phi_i^* \phi_i \left(M^2 + N^2\right) \\ + \left\{ -\frac{p_i^2}{2\sqrt{2}}\phi_i^* \psi_i \chi \left(M - iN\right) + \frac{i p_i^3}{8}\phi_i^* \phi_i \bar{\chi}^2 \left(M + iN\right) - \frac{i p_i^3}{4\sqrt{2}}\phi_i^* \bar{\chi}^2 \psi_i \chi + \text{h.c.} \right\} .\end{aligned} \tag{5.39}$$

All terms appearing in L_+^i already exist in $\mathcal{L}_K^i$. Due to the additional negative sign in Eq. (5.36), all of these terms drop out of the total Lagrangian! Eventually, we are therefore left with only one contribution $\mathcal{L}_{MN}$ to the total Lagrangian which still contains auxiliary fields other than C and χ, i.e. the auxiliary gauge fields M and N to be exact,

$$\mathcal{L}_{MN} = -\sum_i \left\{ \frac{i}{2} W_i p_i \phi_i \left(M + iN\right) + \text{h.c.} \right\} . \tag{5.40}$$

Thinking of the superpotential W as a function of the scalar fields ϕ_i, its variation δW under a gauge transformation, characterized by a rotation angle λ, can be directly related to the corresponding variations $\delta\phi_i$ of the scalar fields. The gauge invariance of the superpotential, $\delta W = 0$, then implies the vanishing of $\mathcal{L}_{MN}$,

$$0 = \delta W = \sum_i W_i \delta\phi_i = -\frac{i}{2}\lambda \sum_i W_i p_i \phi_i \,, \quad \mathcal{L}_{MN} = 0 \,. \tag{5.41}$$

The only remaining contributions to the total Lagrangian contained in $\mathcal{L}_F^i$ are thus those terms in L_-^i and L_0^i which do not involve any auxiliary fields except for C and χ,

$$\sum_i \mathcal{L}_F^i \supset -V_F - \sum_i \left\{ W_i \left[\frac{p_i^2}{4}\phi_i \chi^2 - \frac{i p_i}{\sqrt{2}}\psi_i \chi \right] + \text{h.c.} \right\} \,, \tag{5.42}$$

where we have introduced V_F to refer to the F-term scalar potential,

$$V_F = \sum_i e^{-p_i C} W_i^* W_i \,. \tag{5.43}$$

Field Redefinitions

Having integrated out F_i, M, N, and D, there is only one step left that separates us from writing down our final result for the total Lagrangian. As noted above, the auxiliary fields C and χ have mass dimension 0 and 1/2, respectively. To promote them to fields with canonical mass dimension, we rescale them as follows,[2]

$$C \to C' = \frac{p\tilde{v}}{\sqrt{2}} C \,, \quad \chi \to \chi' = \frac{p\tilde{v}}{\sqrt{2}} \chi \,. \tag{5.44}$$

Here, p denotes an arbitrary real constant, $p \in \mathbb{R}$, and $\tilde{v}$ is a spacetime-dependent auxiliary scalar field, $\tilde{v} = \tilde{v}\,(t, \vec{x})$, of mass dimension 1. The rescalings in Eq. (5.44) are such that C and χ acquire canonical kinetic terms, once a subset of scalar fields obtains nonzero VEVs $\langle \phi_i^* \phi_i \rangle$ and given that the product $p\tilde{v}$ is then identified as

$$p\tilde{v}(t) = \left(\sum_i p_i^2 \, \langle \phi_i^* \phi_i \rangle \right)^{1/2} \,. \tag{5.45}$$

This implies that, assuming the scalar VEVs not to vary over space, the mass scale $\tilde{v}$ is merely a function of time, $\tilde{v} = \tilde{v}(t)$, rather than a full-fledged scalar field. Furthermore, in the special case of only one scalar field ϕ_0 acquiring a nonvanishing VEV, which corresponds to the physical situation during the $B-L$ phase transition, Eq. (5.45) reduces to $p\tilde{v} = p_0 \, \langle \phi_0^* \phi_0 \rangle^{1/2}$, which suggests to identify p and $\tilde{v}$ with p_0 and $\langle \phi_0^* \phi_0 \rangle^{1/2}$, respectively.

[2] In the following, we will again omit the primes on C and χ and implicitly understand that from now on C and χ refer to the fields of the correct mass dimension.

5.1.2 General Lagrangian in Arbitrary Gauge

We are now ready to piece together the results which we have obtained so far in this section. The following five steps lead us to our final expression for $\mathcal{L}$, the total Lagrangian of the supersymmetric $U(1)$ gauge theory: we (i) add our results for $\mathcal{L}_G$ (cf. Eq. (5.7)), $\mathcal{L}_K$ (cf. Eqs. (5.10), (5.11), (5.19), (5.20), (5.25), (5.26), and (5.27)), and $\mathcal{L}_W$ (cf. Eq. (5.8)); (ii) remove all terms from this sum, which are contained in L_+^i (cf. Eq. (5.39)); (iii) set the auxiliary fields F_i, M, N, and D to zero; (iv) include by hand the terms in Eqs. (5.30) and (5.42); and (v) rescale the auxiliary fields C and χ according to Eq. (5.44). In the resultant Lagrangian, we of course recover all terms which one usually obtains in Wess-Zumino or complex gauge. But more importantly, besides that we obtain a further contribution $\mathcal{L}_{C\chi}$ to the total Lagrangian, featuring nonstandard couplings to C, $\partial_\mu C$ and χ,

$$\mathcal{L} = \mathcal{L}_{\text{WZ}} + \mathcal{L}_{C\chi}\,, \quad \mathcal{L}_{\text{WZ}} = \mathcal{L}_{\text{WZ}}^{\text{kin}} + \mathcal{L}_{\text{WZ}}^{\text{gauge}} + \mathcal{L}_{\text{WZ}}^{\text{ferm}} - V_F - V_D\,. \tag{5.46}$$

We distinguish five different contributions to $\mathcal{L}_{\text{WZ}}$, which are respectively given as

$$\begin{aligned}
\mathcal{L}_{\text{WZ}}^{\text{kin}} =& -\frac{1}{4}F_{\mu\nu}F^{\mu\nu} - i\bar{\xi}\bar{\sigma}^\mu\partial_\mu\xi \qquad (5.47)\\
&- \sum_i \exp\left(p_i\sqrt{2}C/(p\tilde{v})\right)\left(\partial_\mu\phi_i^*\partial^\mu\phi_i + i\bar{\psi}_i\bar{\sigma}^\mu\partial_\mu\psi_i\right)\,,\\
\mathcal{L}_{\text{WZ}}^{\text{gauge}} =& \sum_i \exp\left(p_i\sqrt{2}C/(p\tilde{v})\right)\left[\frac{p_i}{2}\left(i\phi_i^*\partial^\mu\phi_i - i\phi_i\partial^\mu\phi_i^* + \bar{\psi}_i\bar{\sigma}^\mu\psi_i\right)A_\mu \qquad (5.48)\right.\\
&\left.- \frac{p_i^2}{4}\phi_i^*\phi_i A_\mu A^\mu\right]\,,\\
\mathcal{L}_{\text{WZ}}^{\text{ferm}} =& \sum_i \exp\left(p_i\sqrt{2}C/(p\tilde{v})\right)\frac{ip_i}{\sqrt{2}}\phi_i^*\psi_i\xi - \frac{1}{2}\sum_{i,j}W_{ij}\psi_i\psi_j + \text{h.c.}\,, \qquad (5.49)\\
V_F =& \sum_i \exp\left(-p_i\sqrt{2}C/(p\tilde{v})\right)W_i^*W_i\,, \qquad (5.50)\\
V_D =& \frac{1}{8}\sum_{ij}p_ip_j\exp\left((p_i+p_j)\sqrt{2}C/(p\tilde{v})\right)\phi_i^*\phi_i\phi_j^*\phi_j\,. \qquad (5.51)
\end{aligned}$$

Expanding the exponential functions in $\mathcal{L}_{\text{WZ}}$ to leading order in the auxiliary field C, which is in fact equivalent to setting C to zero, yields the familiar Lagrangian in Wess-Zumino gauge. All terms of higher order in C, i.e. all terms involving at least one power of C at all, correspond to additional couplings that arise when performing a super-gauge transformation from Wess-Zumino to complex gauge. Meanwhile, the Lagrangian $\mathcal{L}_{C\chi}$ assumes the following form,

$$\begin{aligned}
\mathcal{L}_{C\chi} =& \sum_i \exp\left(p_i\sqrt{2}C/(p\tilde{v})\right)\left[\frac{p_i}{2\sqrt{2}}\phi_i^*\phi_i\Box\frac{C}{p\tilde{v}} - \frac{ip_i^2}{p\tilde{v}}\phi_i^*\bar{\chi}\bar{\sigma}^\mu\partial_\mu\frac{\phi_i\chi}{p\tilde{v}}\right. \qquad (5.52)\\
&\left.+\frac{p_i^3}{2(p\tilde{v})^2}\phi_i^*\phi_i\bar{\chi}\bar{\sigma}^\mu\chi A_\mu - \frac{p_i^2}{\sqrt{2}p\tilde{v}}\phi_i^*\phi_i\left(\chi\xi + \bar{\chi}\bar{\xi}\right)\right.
\end{aligned}$$

$$
\begin{aligned}
&+\frac{ip_i}{\sqrt{2}}\left(\frac{i}{2}\phi_i^*\partial_\mu\phi_i+\frac{i}{2}\phi_i\partial_\mu\phi_i^*-\bar{\psi}_i\bar{\sigma}_\mu\psi_i-\frac{p_i^2}{(p\tilde{v})^2}\phi_i^*\phi_i\bar{\chi}\bar{\sigma}_\mu\chi\right)\partial^\mu\frac{C}{p\tilde{v}}\\
&-\left\{\frac{p_i^2}{\sqrt{2}p\tilde{v}}\phi_i^*\bar{\chi}\bar{\sigma}^\mu\psi_i\partial_\mu\frac{C}{p\tilde{v}}+\frac{p_i}{p\tilde{v}}\phi_i^*\bar{\chi}\bar{\sigma}^\mu\partial_\mu\psi_i+\frac{ip_i^2}{2p\tilde{v}}\phi_i^*\bar{\chi}\bar{\sigma}^\mu\psi_iA_\mu+\text{h.c.}\right\}\Bigg]\\
&-\sum_i\left\{W_i\left(\frac{p_i^2}{2(p\tilde{v})^2}\phi_i\chi^2-\frac{ip_i}{p\tilde{v}}\psi_i\chi\right)+\text{h.c.}\right\}.
\end{aligned}
$$

In Wess-Zumino gauge the auxiliary fields C and χ are zero, implying that the Lagrangian $\mathcal{L}_{C\chi}$ vanishes in this gauge as well.

5.1.3 Gauge and Mass Eigenstates

The Abelian Higgs model of the $B-L$ phase transition corresponds to the supersymmetric $U(1)$ gauge theory featuring the chiral superfields Φ, S_1 and S_2 in combination with the superpotential W_{B-L} (cf. Eq. (3.8)),

$$
W_{B-L}=\frac{\sqrt{\lambda}}{2}\Phi\left(v_{B-L}^2-2S_1S_2\right).
$$

We thus readily obtain the Lagrangian governing the dynamics of the $B-L$ phase transition by applying the general result, which we computed in the previous section (cf. Eq. (5.46)), to the special case of $N=3$ chiral superfields $\Phi_i=\Phi,S_1,S_2$ whose interactions are determined by the superpotential in Eq. (3.8). Before actually writing down the Lagrangian of the Abelian Higgs model, we shall however discuss in more detail the $B-L$ Higgs superfields S_1 and S_2, in particular their relationship to each other in unitary gauge.

Gauge Eigenstates

S_1 and S_2 carry definite $B-L$ charges, $q_S=q_{S_2}=-q_{S_1}=2$ (cf. Sec. 3.1.1). In the following we will therefore refer to their scalar and fermionic components, $s_{1,2}$ and $\tilde{s}_{1,2}$, as the Higgs fields in the *gauge basis* or as the *gauge eigenstates*. Let us now calculate the scalar potential V for the scalar fields $s_{1,2}$. Before the spontaneous breaking of $B-L$, the gauge fields C and χ do not posses kinetic terms and are thus not dynamical. Prior to the $B-L$ phase transition, the *physical gauge* hence corresponds to the Wess-Zumino gauge, in which both C and χ vanish. In Wess-Zumino gauge, V is given as the the sum of V_F and V_D (cf. Eqs. (5.50) and (5.51)) after setting C to zero,

$$
\begin{aligned}
V&=V_F+V_D\,,\quad V_F=V_F^{(0)}+V_F^{(1)}+V_F^{(2)}+V_F^{(1,2)}\,,\\
V_F^{(0)}&=\frac{\lambda}{4}v_{B-L}^4\,,\quad V_F^{(1)}=\lambda\left|s_1\right|^2\left|\phi\right|^2\,,\quad V_F^{(2)}=\lambda\left|s_2\right|^2\left|\phi\right|^2\,,\\
V_F^{(1,2)}&=\lambda\left|s_1\right|^2\left|s_2\right|^2-\frac{\lambda}{2}v_{B-L}^2\left(s_1s_2+s_1^*s_2^*\right)\,,\quad V_D=\frac{p_S^2}{8}\left(\left|s_1\right|^2-\left|s_2\right|^2\right)^2\,.
\end{aligned}
\tag{5.53}
$$

Here, $\phi \in \Phi$ denotes the complex scalar contained in the inflaton superfield Φ and p_S is given as $p_S = 2gq_S$. This result for V as a function of ϕ, s_1 and s_2 illustrates two important aspects. (i) Due to the mass mixing term in $V_F^{(1,2)}$, the scalar fields $s_{1,2}$, and hence the chiral superfields $S_{1,2}$ as well, do not correspond to the physical mass eigenstates. (ii) In the supersymmetric true vacuum, V has to vanish, which, given our result for V_D, enforces $|s_1| = |s_2|$ at the end of the $B-L$ phase transition.

Mass Eigenstates

The scalar mass matrix of the $B-L$ Higgs sector is diagonalized by performing a unitary transformation on the scalar Higgs fields s_1 and s_2^*,

$$s_\pm = \frac{1}{\sqrt{2}} \left(s_1 \pm s_2^* \right) . \tag{5.54}$$

As s_1 and s_2^* are equally charged under the $U(1)_{B-L}$, the two superpositions $s_\pm$ also have definite and, in fact, equal $B-L$ charges. This has the particular virtue that all of the product operators $s_\pm^* s_\pm$ are gauge-invariant. In passing, we also mention that it is not feasible to perform the transformation in Eq. (5.54) directly on the level of the superfields $S_{1,2}$ in the superpotential. To see this, note that s_2^* is the scalar component of the conjugate superfield $S_2^\dagger$. But as the superpotential is supposed to be a holomorphic function, it must not contain $S_2^\dagger$ nor any other conjugate field. Applying now Eq. (5.54) to our result in Eq. (5.53) provides us with the scalar potential V as a function of the scalar fields ϕ and $s_\pm$,

$$\begin{aligned} V &= V_F + V_D \,, \quad V_F = V_F^{(+)} + V_F^{(-)} + V_F^{(\pm)} \,, \\ V_F^{(+)} &= \frac{\lambda}{4} \left(|s_+|^2 - v_{B-L}^2 \right)^2 + \lambda \, |s_+|^2 \, |\phi|^2 \,, \\ V_F^{(-)} &= \frac{\lambda}{4} \left(|s_-|^4 + 2 v_{B-L}^2 \, |s_-|^2 \right) + \lambda \, |s_-|^2 \, |\phi|^2 \,, \\ V_F^{(\pm)} &= -\frac{\lambda}{4} \left(s_+^2 s_-^{*2} + s_+^{*2} s_-^2 \right) \,, \quad V_D = \frac{p_S^2}{8} \left(s_+ s_-^* + s_+^* s_- \right)^2 . \end{aligned} \tag{5.55}$$

Evidently, the scalar fields $s_\pm$ represent indeed the physical mass eigenstates. As anticipated in Sec. 3.1.1, the scalar mass eigenvalues squared $m_{s_\pm}^2$ turn out to be,

$$m_{s_\pm}^2 = \frac{\lambda}{2} \left(\varphi^2 \mp v_{B-L}^2 \right) , \tag{5.56}$$

where we have used that $\phi = \varphi/\sqrt{2} e^{i\theta}$, with φ being the inflaton field. The scalars $s_\pm$ are accompanied by two massive higgsinos $\tilde{s}_\pm$ with Majorana masses $m_{\tilde{s}_\pm}$,

$$\tilde{s}_+ = \frac{i}{\sqrt{2}} e^{i\theta/2} \left(\tilde{s}_1 + \tilde{s}_2 \right) , \quad \tilde{s}_- = \frac{1}{\sqrt{2}} e^{i\theta/2} \left(\tilde{s}_1 - \tilde{s}_2 \right) , \quad m_{\tilde{s}_\pm} = \sqrt{\frac{\lambda}{2}} \varphi \,. \tag{5.57}$$

Together, the scalar and fermionic fields $s_\pm$ and $\tilde{s}_\pm$ constitute the Higgs fields in the *mass basis*. In contrast to $s_\pm$, the higgsino fields $\tilde{s}_\pm$ are constructed from oppositely charged gauge

eigenstates, which implies that they do not carry definite $B-L$ charges. Because of that, it is not sensible to combine the scalar and the fermionic Higgs mass eigenstates in common chiral superfields $S_\pm$. Finally, we recall that in Sec. 3.1.1 it was the mass splitting between the fields $s_\pm$ and $\tilde{s}_\pm$, which was after all responsible for the emergence of a nonvanishing contribution to the Colemann-Weinberg potential (cf. Eq. (3.11)).

The transition from the gauge to the mass basis allows us to identify which scalar DOF contained in $S_{1,2}$ actually corresponds to the real $B-L$ Higgs boson or waterfall field σ. As can be seen from Eq. (5.55), for inflaton field values below the critical point, $\varphi < \varphi_c$, the potential of the complex scalar $s_+ = \sigma_+/\sqrt{2}e^{i\zeta_+}$ has the shape of a *Mexican hat*. Its radial component σ_+ hence plays the role of the waterfall field of the $B-L$ phase transition.[3] Meanwhile, its angular component ζ_+ is one of the Goldstone bosons, which are absorbed into the vector multiplet in the course of $B-L$ breaking. Once the inflaton field φ drops below φ_c, the complex Higgs field s_+ acquires a nonzero VEV v, approaching v_{B-L} at large times,

$$v(t) = \left\langle s_+^* s_+ \right\rangle^{1/2} , \quad \lim_{t\to\infty} v(t) = v_{B-L} . \tag{5.58}$$

The fact that v goes precisely to v_{B-L} rather than to v_{B-L} times some numerical factor is due our specific normalization of the parameters in the superpotential (cf. Eq. (3.8)). In the literature [16, 17, 33, 34, 147], W_{B-L} is often defined as $W_{B-L} = \sqrt{\lambda}\Phi\left(v_{B-L}^2 - S_1 S_2\right)$, i.e. without any additional factors of 2, which results in the complex Higgs boson s_+ obtaining a VEV of $\sqrt{2}v_{B-L}$ or equivalently in the waterfall field σ_+ obtaining a VEV of $2v_{B-L}$. In this case, the actual scale of $B-L$ breaking, $\sqrt{2}v_{B-L}$, is larger than the dimensionful parameter in the superpotential, v_{B-L}, by a factor of $\sqrt{2}$.

Higgs Fields in Unitary Gauge

As soon as s_+ develops a nonvanishing VEV, $B-L$ is spontaneously broken, which is, *inter alia*, reflected in the vector multiplet V turning massive. Before $B-L$ breaking, the only physical gauge DOFs are one massless vector boson as well as one left-chiral gaugino. Now, during the $B-L$ phase transition, two further bosonic and two further fermionic DOFs, i.e. the particle content of one chiral multiplet, are absorbed into the vector multiplet, so that it henceforth consists of one massive vector boson, one real gauge scalar and one Dirac gaugino (cf. Sec. 5.2.2). In the physical gauge after $B-L$ breaking, i.e. in *unitary gauge*, the number of chiral multiplets is hence reduced by one. Figuratively speaking, we may say that one chiral multiplet is *eaten* by the massless vector multiplet for the purpose of rendering it massive. In the context of our Abelian Higgs model of the $B-L$ phase transition, we are able to eliminate one chiral multiplet by performing a super-gauge transformation, which maps S_1 and S_2 to

[3] As we intend to reserve the field name σ for the waterfall field in unitary gauge, we shall refer to the radial component of s_+ as σ_+. The real scalar σ_+ may then be regarded as the generalization of σ to arbitrary gauge.

the same chiral superfield S. At the same time, such a super-gauge transformation relates the vector superfield V in arbitrary gauge to its counterpart in unitary gauge Z,

$$S_{1,2} = \frac{1}{\sqrt{2}} S \exp\left(\pm i\Lambda\right) , \quad V = Z + \frac{i}{p_S}\left(\Lambda - \Lambda^\dagger\right) , \tag{5.59}$$

for some appropriate chiral superfield Λ. For clarity, we iterate once more: S and Z are the Higgs and the vector superfield in unitary gauge, in which the physical DOFs are manifest, $S_{1,2}$ and V are the respective fields in arbitrary gauge and Λ is the corresponding super-gauge transformation parameter, relating these two sets of fields to each other. After symmetry breaking, the Wess-Zumino gauge is no longer of any use, since it is only able to account for the dynamics of a massless vector multiplet. The special choice $\Lambda = 0$ corresponds to performing no super-gauge transformation at all and hence staying in unitary gauge,

$$S_{1,2} \text{ and } V \text{ in unitary gauge:} \qquad S_1 = S_2 = \frac{1}{\sqrt{2}} S , \quad V = Z . \tag{5.60}$$

The chiral superfields S and Λ contain the complex scalar fields $s = (\sigma + i\tau)/\sqrt{2}$ and $\lambda = (a + ib)/\sqrt{2}$. According to Eqs. (5.54) and (5.59), these are related to the scalar Higgs fields in the gauge and in the mass basis in the following way,

$$s_{1,2} = \frac{1}{\sqrt{2}}\, s\, e^{\pm i\lambda} , \quad s_\pm = \frac{1}{2}\left(s\, e^{i\lambda} \pm s^* e^{i\lambda^*}\right) . \tag{5.61}$$

In unitary gauge, λ is zero, which is reflected in the disappearance of the complex phases of the scalar fields in the mass basis, $s_+ = \sigma_+/\sqrt{2}e^{i\zeta_+}$ and $s_- = \sigma_-/\sqrt{2}e^{i\zeta_-}$,

$$\lambda = 0 : \quad s_+ = \frac{1}{2}\left(s + s^*\right) = \mathrm{Re}\left\{s\right\} = \frac{\sigma}{\sqrt{2}} , \quad s_- = \frac{1}{2}\left(s - s^*\right) = i\,\mathrm{Im}\left\{s\right\} = \frac{i\tau}{\sqrt{2}} . \tag{5.62}$$

Here, the result for s_+ directly implies that the real scalar σ has to be identified as the physical waterfall field in unitary gauge. Its relation to σ_+, the waterfall field in arbitrary gauge, also follows from Eq. (5.61). Expanding $s_\pm$, s and λ into their real components, the second identity in Eq. (5.61) allows us to express the real scalar Higgs DOFs in arbitrary gauge, $\sigma_\pm$ and $\zeta_\pm$, as functions of the real scalar Higgs DOFs in unitary gauge, σ and τ, as well as of the two super-gauge transformation parameters a and b,

$$\begin{aligned}
\sigma_+ &= \left[\sigma^2 \cosh^2\left(\frac{b}{\sqrt{2}}\right) + \tau^2 \sinh^2\left(\frac{b}{\sqrt{2}}\right)\right]^{1/2} , \\
\sigma_- &= \left[\sigma^2 \sinh^2\left(\frac{b}{\sqrt{2}}\right) + \tau^2 \cosh^2\left(\frac{b}{\sqrt{2}}\right)\right]^{1/2} , \\
\tan\zeta_+ &= \frac{\sigma \sin\left(a/\sqrt{2}\right)\cosh\left(b/\sqrt{2}\right) - \tau\cos\left(a/\sqrt{2}\right)\sinh\left(b/\sqrt{2}\right)}{\sigma\cos\left(a/\sqrt{2}\right)\cosh\left(b/\sqrt{2}\right) + \tau\sin\left(a/\sqrt{2}\right)\sinh\left(b/\sqrt{2}\right)} , \\
\tan\zeta_- &= \frac{\sigma \sin\left(a/\sqrt{2}\right)\sinh\left(b/\sqrt{2}\right) - \tau\cos\left(a/\sqrt{2}\right)\cosh\left(b/\sqrt{2}\right)}{\sigma\cos\left(a/\sqrt{2}\right)\sinh\left(b/\sqrt{2}\right) + \tau\sin\left(a/\sqrt{2}\right)\cosh\left(b/\sqrt{2}\right)} .
\end{aligned} \tag{5.63}$$

Restricting ourselves to ordinary gauge transformations, i.e. discarding the possibility of complex gauge transformations by setting the parameter b to 0, we find in particular,

$$\sigma_+ = |\sigma| \,, \quad \sigma_- = |\tau| \,, \quad \zeta_+ = \frac{a}{\sqrt{2}} + (1 - \mathrm{sgn}\,(\sigma))\,\frac{\pi}{2} \,, \quad \zeta_- = \frac{a}{\sqrt{2}} + \mathrm{sgn}\,(\tau)\,\frac{\pi}{2} \,, \tag{5.64}$$

where the shifts of ζ_+ and ζ_- relative to $a/\sqrt{2}$ ensure that, in unitary gauge, s_+ and s_-/i have the same sign as σ and τ, respectively. Acting with some ordinary gauge transformation on the complex Higgs fields s_+ and s_- in unitary gauge therefore results in

$$\begin{aligned} s_+ &= \frac{\sigma}{\sqrt{2}} \to \frac{(-1)^{(1-\mathrm{sgn}(\sigma))/2}\,|\sigma|}{\sqrt{2}}\, e^{ia/\sqrt{2}} = \frac{\sigma}{\sqrt{2}}\, e^{ia/\sqrt{2}} \,, \\ s_- &= \frac{i\tau}{\sqrt{2}} \to \frac{i^{\mathrm{sgn}(\tau)}\,|\tau|}{\sqrt{2}}\, e^{ia/\sqrt{2}} = \frac{i\tau}{\sqrt{2}}\, e^{ia/\sqrt{2}} \,, \end{aligned} \tag{5.65}$$

which illustrates that $s_\pm$ carry indeed equal $B-L$ charges (cf. the comment below Eq. (5.54)).

The complex scalar s is the only remaining Higgs boson in unitary gauge. It acquires the same VEV as s_+, one of the two complex Higgs bosons in arbitrary gauge (cf. Eq. (5.58)),

$$s = \frac{1}{\sqrt{2}}\,(\sigma + i\tau) \,, \quad \langle s^* s \rangle^{1/2} = \frac{1}{2}\,\langle \sigma^2 \rangle^{1/2} = \langle s_+^* s_+ \rangle^{1/2} = v(t) \,. \tag{5.66}$$

This demonstrates once more that σ, the real component of s, is the physical symmetry-breaking Higgs boson or waterfall field of the $B-L$ phase transition. τ, the imaginary component of s, remains by contrast massive and hence stabilized at $\tau = 0$ at all times. With the aid of Eqs. (5.55) and (5.62), we now readily obtain the scalar potential V as a function of σ and τ in the special case, in which the auxiliary field C vanishes,[4]

$$\begin{aligned} V &= V_F + V_D \,, \;\; V_F = V_F^{(\sigma)} + V_F^{(\tau)} + V_F^{(\sigma\tau)} \,, \;\; V_F^{(\sigma\tau)} = \frac{\lambda}{8}\sigma^2\tau^2 \,, \;\; V_D = 0 \,, \\ V_F^{(\sigma)} &= \frac{\lambda}{16}\left(\sigma^2 - 2v_{B-L}^2\right)^2 + \frac{1}{2}\lambda\sigma^2\,|\phi|^2 \,, \\ V_F^{(\tau)} &= \frac{\lambda}{16}\left(\tau^4 + 4v_{B-L}^2\tau^2\right) + \frac{1}{2}\lambda\tau^2\,|\phi|^2 \,. \end{aligned} \tag{5.67}$$

Restoring the complex scalar s, this result can be written in a more compact way,

$$\begin{aligned} V &= \frac{\lambda}{4}\left|v_{B-L}^2 - s^2\right|^2 + \lambda\,|s|^2\,|\phi|^2 \\ &= \frac{\lambda}{4}\left(v_{B-L}^2 - |s|^2\right)^2 + \frac{1}{2}\lambda v_{B-L}^2\tau^2 + \lambda\,|s|^2\,|\phi|^2 \,, \end{aligned} \tag{5.68}$$

which nicely illustrates how the complex field s is stabilized in the direction of its imaginary component τ by means of an additional mass term for this component.

[4] As σ and τ are fields in unitary gauge, one actually also has to take into account the auxiliary gauge scalar C in the calculation of their scalar potential (cf. Sec. 5.2.1).

5.2 During and After Spontaneous Symmetry Breaking

Building upon the results of the previous section, we are now able to (i) derive the Lagrangian of the Abelian Higgs model of the $B-L$ phase transition, (ii) identify the physical DOFs of our model and (iii) calculate all relevant decay rates.

5.2.1 Lagrangian of the SSB Sector in Unitary Gauge

We evaluate the Lagrangian in Eq. (5.46) for the special case of $N = 3$ chiral superfields $\Phi_i = \Phi, S_1, S_2$, interacting with each other via the superpotential W_{B-L} (cf. Eq. (3.8)), and perform a super-gauge transformation to unitary gauge (cf. Eq. (5.60)). Identifying p with $p_S = 2gq_S$ and denoting the scalar and fermionic components of S and Φ by $(s, \tilde{s})$ and $(\phi, \tilde{\phi})$, respectively, we find

$$\begin{aligned}
\mathcal{L}_{\text{WZ}}^{\text{kin}} = & -\frac{1}{4}F_{\mu\nu}F^{\mu\nu} - i\bar{\xi}\bar{\sigma}^{\mu}\partial_{\mu}\xi - \partial_{\mu}\phi^{*}\partial^{\mu}\phi - i\bar{\tilde{\phi}}\bar{\sigma}^{\mu}\partial_{\mu}\tilde{\phi} \\
& - \cosh\left(\sqrt{2}C/\tilde{v}\right)\left(\partial_{\mu}s^{*}\partial^{\mu}s + i\bar{\tilde{s}}\bar{\sigma}^{\mu}\partial_{\mu}\tilde{s}\right), \qquad (5.69) \\
\mathcal{L}_{\text{WZ}}^{\text{gauge}} = & \sinh\left(\sqrt{2}C/\tilde{v}\right)\left[\frac{p_S}{2}\left(is^{*}\partial^{\mu}s - is\partial^{\mu}s^{*} + \bar{\tilde{s}}\bar{\sigma}^{\mu}\tilde{s}\right)A_{\mu}\right] \\
& - \cosh\left(\sqrt{2}C/\tilde{v}\right)\frac{p_S^2}{4}\left|s\right|^2 A_{\mu}A^{\mu}, \qquad (5.70) \\
\mathcal{L}_{\text{WZ}}^{\text{ferm}} = & \sinh\left(\sqrt{2}C/\tilde{v}\right)\frac{ip_S}{\sqrt{2}}s^{*}\tilde{s}\xi + \frac{1}{2}\sqrt{\lambda}\phi\tilde{s}\tilde{s} + \sqrt{\lambda}s\tilde{\phi}\tilde{s} + \text{h.c.}, \qquad (5.71) \\
V_F = & \frac{\lambda}{4}|v_{B-L}^2 - s^2|^2 + \cosh\left(\sqrt{2}C/\tilde{v}\right)\lambda\left|s\right|^2\left|\phi\right|^2, \qquad (5.72) \\
V_D = & \frac{p_S^2}{8}\sinh^2\left(\sqrt{2}C/\tilde{v}\right)\left|s\right|^4. \qquad (5.73)
\end{aligned}$$

The Lagrangian taking care of the couplings of the gauge fields C and χ now reads

$$\begin{aligned}
\mathcal{L}_{C\chi} = & \sinh\left(\sqrt{2}C/\tilde{v}\right)\left[\frac{\left|s\right|^2}{2\sqrt{2}}\Box\frac{C}{\tilde{v}} + \frac{p_S\left|s\right|^2}{2\tilde{v}^2}\bar{\chi}\bar{\sigma}^{\mu}\chi A_{\mu} - \left\{\frac{s^{*}}{\tilde{v}}\bar{\chi}\bar{\sigma}^{\mu}\partial_{\mu}\tilde{s} + \text{h.c.}\right\}\right. \qquad (5.74) \\
& \left. + \frac{i}{\sqrt{2}}\left(\frac{i}{2}s^{*}\partial_{\mu}s + \frac{i}{2}s\partial_{\mu}s^{*} - \bar{\tilde{s}}\bar{\sigma}_{\mu}\tilde{s} - \frac{\left|s\right|^2}{\tilde{v}^2}\bar{\chi}\bar{\sigma}_{\mu}\chi\right)\partial^{\mu}\frac{C}{\tilde{v}}\right] \\
& - \cosh\left(\sqrt{2}C/\tilde{v}\right)\left[\frac{is^{*}}{\tilde{v}}\bar{\chi}\bar{\sigma}^{\mu}\partial_{\mu}\frac{s\,\chi}{\tilde{v}} + \frac{p_S\left|s\right|^2}{\sqrt{2}\tilde{v}}\left(\chi\xi + \bar{\chi}\bar{\xi}\right)\right. \\
& \left. + \left\{\frac{s^{*}}{\sqrt{2}\tilde{v}}\bar{\chi}\bar{\sigma}^{\mu}\tilde{s}\partial_{\mu}\frac{C}{\tilde{v}} + \frac{ip_S s^{*}}{2\tilde{v}}\bar{\chi}\bar{\sigma}^{\mu}\tilde{s}A_{\mu} + \text{h.c.}\right\}\right] + \left\{\frac{\sqrt{\lambda}s^2}{2\tilde{v}^2}\phi\chi^2 + \text{h.c.}\right\}.
\end{aligned}$$

We account for the spontaneous breaking of $B-L$ by shifting the complex Higgs field s around its time-dependent expectation value (cf. Eqs. (5.58) and (5.66)),

$$s \to v(t) + s = v(t) + \frac{1}{\sqrt{2}}\left(\sigma + i\tau\right), \quad \lim_{t\to\infty} v(t) = v_{B-L}. \qquad (5.75)$$

Up to now, we denoted with s and σ the fluctuations of the complex $B-L$ Higgs boson and of its real component around the origin, i.e. around the false vacuum. From now on, s and σ shall, however, refer to the respective fluctuations around the homogeneous Higgs background, i.e. eventually, once the $B-L$ phase transition is completed, around the true vacuum. The replacement in Eq. (5.75) induces mass terms for all particles, which are coupled to the Higgs boson s (cf. Sec. 5.2.2), and gives rise to kinetic terms for the gauge fields C and χ,

$$\mathcal{L}_{C\chi} \supset -\frac{1}{2}\frac{v^2}{\tilde{v}^2}\partial_\mu C \partial^\mu C - \frac{v^2}{\tilde{v}^2} i\bar{\chi}\bar{\sigma}^\mu \partial_\mu \chi \,. \tag{5.76}$$

As anticipated in Sec. 5.1.1, the mass scale $\tilde{v}$ has to be identified with the VEV v, in order to obtain canonically normalized kinetic terms (cf. Eq. (5.45)),

$$\tilde{v}(t) = v(t) = \left\langle s_+^* s_+ \right\rangle \,. \tag{5.77}$$

5.2.2 Physical Degrees of Freedom and Time-Dependent Masses

With the full Lagrangian of the Abelian Higgs model at our disposal, we are now ready to evaluate how the bosonic and fermionic DOFs, which we initially introduced through the superfields Φ, $S_{1,2}$ and V, are eventually distributed among the physical particles in the broken phase. In Fig. 5.1, we give an overview of the particle spectrum and indicate how the various particle species are respectively produced as well as how they respectively interact with each other.

Symmetry-Breaking Sector

Out of the four real scalar DOFs initially contained in $S_{1,2}$, only two DOFs remain as independent real scalar fields after the $B-L$ phase transition—the waterfall field σ as well as its partner τ. We can read off the masses of these two particles, m_σ and m_τ, from the F-term scalar potential (cf. Eqs. (5.67) and (5.72)),

$$V_F \supset \frac{\lambda}{16}\left[\left(\sqrt{2}v+\sigma\right)^2 - 2v_{B-L}^2\right]^2 + \frac{1}{2}\lambda\left(\sqrt{2}v+\sigma\right)^2|\phi|^2 \supset \frac{1}{2}m_\sigma^2\sigma^2 \,, \tag{5.78}$$

$$V_F \supset \frac{\lambda}{16}\left(\tau^4 + 4v_{B-L}^2\tau^2\right) + \frac{\lambda}{8}\left(\sqrt{2}v+\sigma\right)^2\tau^2 + \frac{1}{2}\lambda\tau^2|\phi|^2 \supset \frac{1}{2}m_\tau^2\tau^2 \,, \tag{5.79}$$

where m_σ and m_τ are given as

$$m_\sigma^2(t) = \frac{\lambda}{2}\left(3v^2(t) - v_{B-L}^2 + 2\left|\phi(t)\right|^2\right) \,, \tag{5.80}$$

$$m_\tau^2(t) = \frac{\lambda}{2}\left(v^2(t) + v_{B-L}^2 + 2\left|\phi(t)\right|^2\right) \,. \tag{5.81}$$

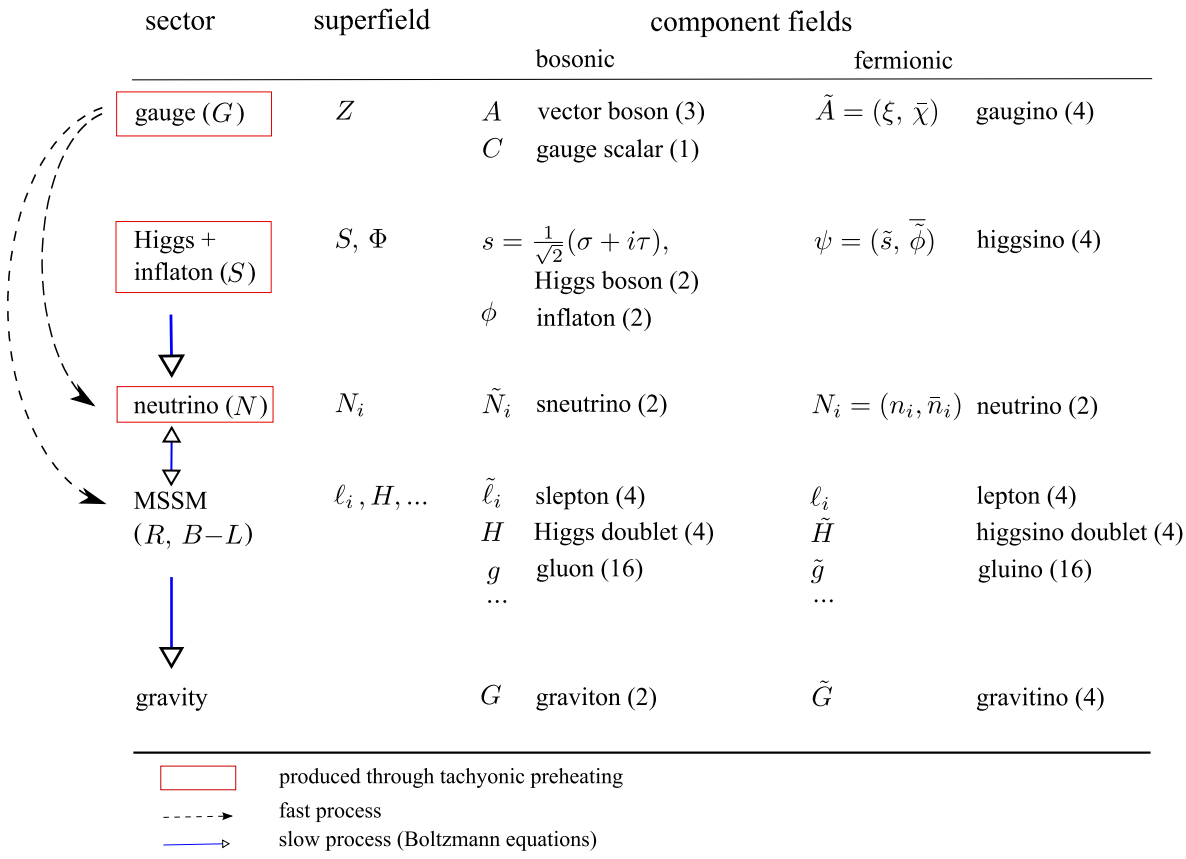

Figure 5.1: Physical particle spectrum as well as all relevant production and decay processes after the spontaneous breaking of $B-L$ symmetry. The Higgs field σ and all particles coupled to it are produced during tachyonic preheating (red boxes). The gauge DOFs then decay nearly instantaneously (black, dashed arrows), whereas the decay and production of the other particles can be described by Boltzmann equations (blue, solid arrows). The numbers in parentheses denote the respective internal DOFs.

In the supersymmetric true vacuum, ϕ vanishes and v has reached its final value,[5]

$$t \to \infty : \qquad v(t) = v_{B-L}\,, \quad \phi = 0\,, \quad m_\sigma^2(t) = m_\sigma^2(t) = \lambda v_{B-L}^2\,. \tag{5.82}$$

The real scalars σ and τ are accompanied by the complex scalar ϕ. Its mass m_ϕ can also be read off from the F-term scalar potential (cf. Eq. (5.72)),

$$V_F \supset \cosh\left(\sqrt{2}C/v\right)\lambda\,|v+s|^2\,|\phi|^2 \supset m_\phi^2\,|\phi|^2\,, \quad m_\phi^2(t) = \lambda v^2(t)\,. \tag{5.83}$$

Finally, the fermionic component $\tilde{s}$ of the superfield S pairs up with the fermionic component $\tilde{\phi}$ of the inflaton superfield Φ to form a Dirac fermion $\psi = \left(\tilde{s}, \bar{\tilde{\phi}}\right)^T$, the higgsino, which acquires a mass m_ψ in the course of $B-L$ breaking (cf. Eq. (5.71)),

$$\mathcal{L}_{\text{WZ}}^{\text{ferm}} \supset \sqrt{\lambda}(v+s)\,\tilde{\phi}\tilde{s} + \text{h.c.} \supset m_\psi\,\tilde{\phi}\tilde{s} + \text{h.c.}\,, \quad m_\psi(t) = \sqrt{\lambda}v(t)\,. \tag{5.84}$$

As required by supersymmetry, which is restored at the end of the $B-L$ phase transition, all particles originating from the chiral superfields Φ and $S_{1,2}$ end up having same mass in the true vacuum,

$$t \to \infty : \qquad m_\sigma(t) = m_\tau(t) = m_\phi(t) = m_\psi(t) = m_S = \sqrt{\lambda}v_{B-L}\,. \tag{5.85}$$

Gauge Sector

Next, we turn to the gauge sector. One key implication of the spontaneous breaking of $B-L$ is that it turns the massless vector multiplet into a full massive vector multiplet with four scalar and four fermionic DOFs. The mass m_A of the vector boson A can be read off from the Lagrangian $\mathcal{L}_{\text{WZ}}^{\text{gauge}}$ (cf. Eq. (5.70)),

$$\mathcal{L}_{\text{WZ}}^{\text{gauge}} \supset -\cosh\left(\sqrt{2}C/v\right)\frac{p_S^2}{4}\,|v+s|^2\,A_\mu A^\mu \supset -\frac{1}{2}m_A^2 A_\mu A^\mu\,. \tag{5.86}$$

where m_A now depends on $p_S = 2gq_S = 4g$ rather than the coupling constant λ,

$$m_A^2(t) = \frac{1}{2}p_S^2 v^2(t) = 2g^2 q_S^2 v^2(t) = 8g^2 v^2(t)\,. \tag{5.87}$$

Similarly to $\tilde{s}$ and $\tilde{\phi}$, the Weyl fermion ξ and the former auxiliary field χ consort with each other to form a Dirac fermion $\tilde{A} = \left(\xi, \bar{\chi}\right)^T$, the gaugino, which obtains a mass $m_{\tilde{A}}$ during the $B-L$ phase transition. The mass term for the gaugino is contained in $\mathcal{L}_{C\chi}$, which also features the kinetic terms for C and χ (cf. Eq. (5.74)),

$$\mathcal{L}_{C\chi} \supset -\cosh\left(\sqrt{2}C/v\right)\frac{p_S\,|v+s|^2}{\sqrt{2}v}\chi\xi + \text{h.c.} \supset -m_{\tilde{A}}\,\chi\xi + \text{h.c.}\,, \tag{5.88}$$

[5] In Sec. 6.2, when discussing the nonperturbative production of particles during tachyonic preheating, we will work in the *quench approximation*, in which the inflaton field ϕ is straight away set to zero as soon as the waterfall field becomes unstable. In the quench approximation, the terms proportional to $|\phi|^2$ in Eqs. (5.80) and (5.81) may hence be omitted from the beginning.

from which we infer that $m_{\tilde{A}} = m_A$ at all times (cf. Eq. (5.87)). As previously mentioned, the vector multiplet absorbs two real scalar DOFs, which initially belong to the Higgs superfields $S_{1,2}$—one ends up being the longitudinal component of the massive vector boson A, the other is to be identified with the gauge field C, which becomes dynamical as soon as $B-L$ is broken. During the $B-L$ phase transition, C acquires a mass m_C, which receives contributions from the D-term scalar potential (cf. Eq. (5.73)) as well as from the Lagrangian $\mathcal{L}_{C\chi}$ (cf. Eq. (5.74)),

$$\begin{aligned}\mathcal{L}_{C\chi} - V_D &\supset \sinh\left(\sqrt{2}C/v\right)\frac{|v+s|^2}{2\sqrt{2}}\Box\frac{C}{v} - \frac{p_S^2}{8}\sinh^2\left(\sqrt{2}C/v\right)|v+s|^4 \\ &\supset \frac{1}{2}m_C^2 C^2\,, \quad m_C^2 = \frac{1}{2}p_S^2 v^2 + v\frac{\partial^2}{\partial t^2}\frac{1}{v} = \frac{1}{2}p_S^2 v^2 + 2\frac{\dot{v}^2}{v^2} - \frac{\ddot{v}}{v}\,.\end{aligned} \tag{5.89}$$

The mass term in the Lagrangian $\mathcal{L}_{C\chi}$ relies on the fact that during the $B-L$ phase transition v is a function of time. Once v has reached its final value, it vanishes and m_C is solely accounted for by the mass term in V_D.

In order to assess the relative importance of the two contributions to the mass of the scalar C in the course of $B-L$ breaking, we need to know the time dependence of the VEV v. To this end, we expand the complex Higgs boson s_+ into momentum eigenfunctions $s_+(k,t)e^{-i\mathbf{kx}}$, where $k = |\mathbf{k}|$, and write v as an integral over the Higgs mode functions $s_+(k,t)$ (cf. Eq. (5.58)),

$$v^2(t) = \left\langle s_+^* s_+ \right\rangle = \int \frac{d^3k}{(2\pi)^3}\,|s_+(k,t)|^2\,. \tag{5.90}$$

Given the solutions to the mode equations for all wavenumbers k, this relation yields v as a function of time. Due to the quartic self-interaction of the field s_+ (cf. Eq. (5.55)), the equations of motion of the respective field modes are, however, nonlinear and thus require a numerical treatment. The authors of Ref. [35] perform a fully nonlinear lattice simulation to study the evolution of the Higgs VEV in the quench approximation and conclude that, apart from strongly damped oscillations after symmetry breaking, it is well approximated by a smooth step function interpolating between the false, $v = 0$, and the true vacuum, $v = v_{B-L}$,

$$v(t) \approx \frac{v_{B-L}}{2}\left[1 + \tanh\frac{m_S\,(t - t_{\mathrm{PH}})}{2}\right]\,, \quad m_S = \sqrt{\lambda}v_{B-L}\,. \tag{5.91}$$

Here, t_{PH} denotes the time at the end of tachyonic preheating and we fix the origin of the time axis by setting $t_{\mathrm{PH}} = 0$. Now, inserting the approximate expression for v in Eq. (5.91) into our result for m_C (cf. Eq. (5.89)), we obtain

$$m_C^2(t) \approx \left(\frac{1}{2}p_S^2 + \frac{\lambda}{1+\exp\left(m_S t\right)}\right)v^2(t) \approx \frac{1}{2}p_S^2 v^2(t)\,. \tag{5.92}$$

The contribution to m_C from the Lagrangian $\mathcal{L}_{C\chi}$ falls off exponentially fast and is hence always negligibly small at sufficiently late times. But even at early times, $t < 0$, it is outweighed by the contribution from the D-term scalar potential since, owing to perturbativity,

$\lambda \ll \frac{1}{2}p_S^2 \simeq 4\pi/3$ (cf. Sec. 3.2.2). On top of that, the extra mass term in $\mathcal{L}_{C\chi}$ significantly complicates the calculation describing the nonperturbative production of C quanta during tachyonic preheating (cf. Sec. 6.2). As our final results concerning the generation of entropy, baryon asymmetry and dark matter prove to be rather insensitive to the dynamics of the gauge sector in any case (cf. Ch. 7), we shall therefore ignore the contribution to m_C from the Lagrangian $\mathcal{L}_{C\chi}$ in the following and treat the gauge particles as if they had equal masses at all times, $m_C \approx m_{\tilde{A}} = m_A$. In the supersymmetric true vacuum, this approximation turns into an exact statement,

$$t \to \infty : \qquad m_A(t) = m_{\tilde{A}}(t) = m_C(t) = m_G = \frac{1}{\sqrt{2}} p_S v_{B-L} \,. \tag{5.93}$$

Neutrino Sector

So far, we have seen how the spontaneous breaking of $B-L$ causes the bosonic and fermionic DOFs initially contained in the superfields Φ, $S_{1,2}$ and V to assemble in new physical particles. For completeness, let us now also list all further particle species present in the broken phase.

The neutrino superfields n_i^c are coupled to the Higgs superfield S_1 via a common term in the seesaw superpotential (cf. Eq. (3.20)). In unitary gauge and after $B-L$ breaking, we have to replace S_1 by $\frac{1}{\sqrt{2}}(v+S)$ in this term (cf. Eq. (3.25)),

$$S_1 \to \frac{1}{\sqrt{2}}(v+S) \,, \quad W_{\text{Seesaw}} \supset \frac{1}{\sqrt{2}} h_i^n n_i^c n_i^c S_1 \to \frac{1}{2} h_i^n n_i^c n_i^c (v+S) \,. \tag{5.94}$$

In consequence of the new coupling to the homogeneous Higgs background, the fermionic components of the fields n_i^c and n_i combine into three heavy Majorana neutrinos N_i (cf. Eq. (3.26)). The superpartners of these neutrinos, the heavy sneutrinos $\tilde{N}_i$, are identified with the scalar components of the fields n_i^c. From Eq. (5.94) it directly follows that the heavy neutrinos share common masses M_i with their superpartners at all times,

$$M_i(t) = h_i^n v(t) \,. \tag{5.95}$$

MSSM and Gravitino

Finally, our model features the entire MSSM particle content as well as the gravity multiplet consisting of the graviton and the gravitino. We assume that supersymmetry is spontaneously broken before the end of inflation in some hidden sector. The mediation of supersymmetry breaking to the visible sector via, for instance, gravitational or loop-suppressed interactions then induces soft masses for all MSSM superparticles as well as for the gravitino (cf. Sec. 3.1.4). The soft masses, which are partly generated for the particles coupling to the $B-L$ Higgs boson s, are negligibly small compared to their masses generated in the course of $B-L$ breaking. Furthermore, as soon as a primordial thermal bath has emerged, all MSSM particles obtain

effective thermal masses due to their rapid gauge and Yukawa interactions. At the high temperatures reached during reheating after the $B-L$ phase transition, these thermal masses always exceed by far the corresponding soft masses. By contrast, all other particles interact too feebly with the thermal bath and thus do not obtain sizable thermal masses.

5.2.3 Decay Rates and Branching Ratios

A central result of the previous section is that the masses of all particles coupled to the Higgs boson s rapidly grow while the Higgs VEV v evolves from 0 to v_{B-L} (cf. Eq. (5.91)). This sudden change in inertia leads to the nonadiabatic production of these particles [35]. In Sec. 6.2, we will discuss the particle abundances generated during tachyonic preheating in more detail. For now, we merely state that all particles from the SSB, gauge and neutrino sectors are produced during the $B-L$ phase transition, *viz.* predominantly with momenta k much smaller than their respective masses, $k \ll m$. Next to a dominating abundance of nonrelativistic Higgs bosons, tachyonic preheating thus also gives rise to a gas of nonrelativistic higgsinos, inflatons, gauge particles, and heavy (s)neutrinos.

All of these particles are unstable and decay after preheating into lighter DOFs (cf. Fig. 5.1). To determine the relevant decay channels, we have to identify all renormalizable operators in the Lagrangian, which entail kinematically allowed two-body decays. Due to our particular choice of Froggatt-Nielsen flavour charges (cf. Eq. (3.75)), the mass spectrum of our model exhibits the following hierarchy,[6]

$$m_G \sim v_{B-L} \gg m_S \sim M_3 \sim M_2 \gg M_1 \gg v_{\mathrm{EW}} \,. \tag{5.96}$$

When identifying the relevant operators in the Lagrangian, we therefore have to look for terms that couple (i) one gauge particle to two particles from any other sector, (ii) one Higgs boson, higgsino, inflaton or (s)neutrino of the second or third generation to (s)neutrinos of the first generation or MSSM particles, or (iii) one (s)neutrino of the first generation to MSSM particles.

Gauge Sector

All operators which couple fields of the gauge sector to fields of the SSB sector contain at least two gauge fields. Real gauge particles, i.e. gauge particles on the mass shell, can thus not decay into Higgs bosons, higgsinos or inflatons. Meanwhile, the interactions of the heavy (s)neutrinos as well as of the MSSM particles with the $B-L$ vector boson A are accounted for by (cf. Eq. (5.48)),

$$\mathcal{L}_{\mathrm{WZ}}^{\mathrm{gauge}} \supset \sum_i \exp\left(p_i \sqrt{2} C/(p_S v)\right) \left[\frac{p_i}{2}\left(i\phi_i^* \partial^\mu \phi_i - i\phi_i \partial^\mu \phi_i^* + \bar{\psi}_i \bar{\sigma}^\mu \psi_i\right) A_\mu\right] , \tag{5.97}$$

[6] For definiteness, we will set $m_S = M_3 = M_2$ in Chs. 7 and 8.

from which one obtains the actual operator describing the two-body decays of the vector A as the lowest-order term when expanding the exponential in powers of C. The interactions with the gaugino are governed by (cf. Eq. (5.49))

$$\mathcal{L}_{\text{WZ}}^{\text{ferm}} \supset \sum_i \exp\left(p_i\sqrt{2}C/(p_S v)\right) \frac{ip_i}{\sqrt{2}}\phi_i^*\psi_i\xi + \text{h.c.} \supset \sum_i \frac{ip_i}{\sqrt{2}}\phi_i^*\psi_i\xi + \text{h.c.}\,. \tag{5.98}$$

As far as we restrict ourselves to renormalizable interactions, the gauge field C only decays into the scalar components ϕ_i of the heavy (s)neutrino and MSSM superfields. The strongest interaction between one C particle and two scalars derives from the D-term scalar potential (cf. Eqs. (5.51) and (5.73)),

$$\begin{aligned} V_D &= \frac{1}{8}\left[p_S \sinh\left(\sqrt{2}C/v\right)|v+s|^2 + \sum_i p_i \exp\left(p_i\sqrt{2}C/(p_S v)\right)|\phi_i|^2\right]^2 \\ &\supset \frac{p_S}{4}\sinh\left(\sqrt{2}C/v\right)|v+s|^2 \sum_i p_i \exp\left(p_i\sqrt{2}C/(p_S v)\right)|\phi_i|^2 \\ &\supset \frac{p_S}{4v}\sqrt{2}C\,|v+s|^2\sum_i p_i\,|\phi_i|^2 \supset \frac{v}{\sqrt{2}}C\sum_i \frac{1}{2}p_S p_i\,|\phi_i|^2\,. \end{aligned} \tag{5.99}$$

Beyond that, the F-term scalar potential contains an operator coupling the scalar C to two heavy sneutrinos $\tilde{N}_i$ (cf. Eq. (5.50)),

$$\begin{aligned} V_F &\supset \exp\left(-p_{n^c}\sqrt{2}C/(p_S v)\right)\sum_i W_{n_i^c}^* W_{n_i^c}\,,\; W_{n_i^c} = h_i^n \tilde{N}_i(v+s) + h_{ji}^\nu \tilde{\ell}_j H_u\,, \\ &\supset -\frac{p_{n^c}}{p_S v}\sqrt{2}C\,|v+s|^2\sum_i (h_i^n)^2\left|\tilde{N}_i\right|^2 \supset -\frac{v}{\sqrt{2}}C\sum_i (h_i^n)^2\left|\tilde{N}_i\right|^2\,, \end{aligned} \tag{5.100}$$

where we have used that the neutrino superfields n_i^c carry $B-L$ charge $q_{n^c} = 1$, such that $p_{n^c} = 2gq_{n_c} = p_S/2$. The strength of the interactions in Eqs. (5.99) and (5.100) is determined by the effective gauge couplings $\frac{1}{2}p_S p_i$ as well as by the Yukawa couplings $(h_i^n)^2$, respectively. Since $(h_i^n)^2 \ll \frac{1}{2}p_S\,|p_i|$ (cf. Sec. 3.2.2), we shall neglect the contribution from Eq. (5.100) to the decay rate for the process $C \to \tilde{N}_i\tilde{N}_i^*$ in the following.

Given the operators in Eqs. (5.97), (5.98) and (5.99), we are now able to calculate the tree-level decay rates and branching ratios of the particles A, $\tilde{A}$ and C by means of standard methods [261].[7] As it turns out, all three particles decay at the same total rate Γ_G^0,

$$\Gamma_A^0 = \Gamma_{\tilde{A}}^0 = \Gamma_C^0 = \Gamma_G^0 = \frac{g^2}{16\pi}m_G\sum_i q_i^2\left[1-(2m_i/m_G)^2\right]^{1/2}\,, \tag{5.101}$$

with the sum running over all heavy (s)neutrino and MSSM multiplets i carrying $B-L$ charges q_i. As m_G is much larger than all supersymmetry-breaking soft masses, we may treat the

[7] Note that the conventions for the spacetime metric $\eta_{\mu\nu}$ as well as for the sigma matrices σ^μ and $\bar{\sigma}^\mu$ employed in Ref. [261] differ from the conventions of Ref. [258]. Appendix A of Ref. [261], however, provides a manual for how to translate between these two different conventions.

MSSM particles as massless. Γ_G^0 can then be written as

$$\Gamma_G^0 = \frac{g^2}{16\pi} m_G \left(\sum_{\text{MSSM}} q_i^2 + \sum_i \left[1 - (2M_i/m_G)^2\right]^{1/2} \right), \quad \sum_{\text{MSSM}} q_i^2 = 13\,, \tag{5.102}$$

where the second sum now runs over the three heavy (s)neutrino multiplets $(N_i, \tilde{N}_i)$. Next, introducing the function R through the relation

$$R\,(q,m) = \frac{q^2 \left[1 - (2m/m_G)^2\right]^{1/2}}{13 + \sum_i \left[1 - (2M_i/m_G)^2\right]^{1/2}}\,, \tag{5.103}$$

allows us to state the branching ratios for the various final states into which the gauge particles A, $\tilde{A}$ and C are able to decay in a particularly convenient form,

$$\text{Br}\big(A \to N_i N_i\big) = \frac{2}{3} R(1, M_i)\,, \quad \text{Br}\big(A \to \psi_i \bar{\psi}_i\big) = \frac{2}{3} R(q_i, 0)\,, \tag{5.104}$$

$$\text{Br}\big(A \to \tilde{N}_i \tilde{N}_i^*\big) = \frac{1}{3} R(1, M_i)\,, \quad \text{Br}\big(A \to \phi_i \phi_i^*\big) = \frac{1}{3} R(q_i, 0)\,, \tag{5.105}$$

$$\text{Br}\big(\tilde{A} \to N_i \tilde{N}_i\big) = \quad R(1, M_i)\,, \quad \text{Br}\big(\tilde{A} \to \bar{\psi}_i \phi_i\big) = \quad R(q_i, 0)\,, \tag{5.106}$$

$$\text{Br}\big(C \to \tilde{N}_i \tilde{N}_i^*\big) = \quad R(1, M_i)\,, \quad \text{Br}\big(C \to \phi_i \phi_i^*\big) = \quad R(q_i, 0)\,. \tag{5.107}$$

Here, ϕ_i and ψ_i denote the components of an arbitrary MSSM matter multiplet.

Symmetry-Breaking Sector

The SSB sector only interacts with the gauge as well as with the heavy (s)neutrino sector. In addition, as a result of our specific mass spectrum (cf. Eq. (5.96)), the particles of the SSB sector are only allowed to decay into the (s)neutrinos of the first generation. All operators accounting for the decay of the Higgs boson, higgsino and inflaton hence derive from the following terms in the superpotential,[8]

$$\begin{aligned} W &\supset \frac{\sqrt{\lambda}}{2} \Phi \left[v_{B-L}^2 - (v+S)^2 \right] + \frac{1}{2} h_1^n n_1^c n_1^c (v+S) \\ &\supset -\sqrt{\lambda} v\, \Phi S + \frac{1}{2} h_1^n v\, n_1^c n_1^c + \frac{1}{2} h_1^n n_1^c n_1^c S\,. \end{aligned} \tag{5.108}$$

Inserting these terms into Eq. (5.49), we obtain the following Yukawa interactions,

$$\mathcal{L}_{\text{WZ}}^{\text{ferm}} \supset -\frac{1}{2} \sum_{i,j} W_{ij}\, \psi_i \psi_j + \text{h.c.} \supset -\frac{1}{2} h_1^n s\, \nu_{R,1} \nu_{R,1} - h_1^n \tilde{N}_1\, \nu_{R,1} \tilde{s} + \text{h.c.} \tag{5.109}$$

[8] If the decays into the second and third (s)neutrino generations were kinematically allowed, the calculation of the respective partial decay rates would be, of course, analogous.

The former of these two operators describes the decay of the scalars σ and τ into a pair of N_1 neutrinos, while the latter governs the decay of the higgsino ψ into an N_1 neutrino and an $\tilde{N}_1^*$ sneutrino. Moreover, the superpotential in Eq. (5.108) implies the following trilinear couplings in the F-term scalar potential (cf. Eq. (5.50)),

$$V_F = \sum_i \exp\left(-p_i\sqrt{2}C/(p_S v)\right) W_i^* W_i \supset W_{n_1^c}^* W_{n_1^c} + W_S^* W_S \tag{5.110}$$
$$\supset \left(h_1^n\right)^2 v\left|\tilde{N}_i\right|^2 s - \frac{1}{2}h_1^n\sqrt{\lambda}v\tilde{N}_1^*\tilde{N}_1^*\phi + \text{h.c.}\,,$$

which respectively describe the decay of the real component of s, i.e. of the scalar σ, into a $\tilde{N}_1\tilde{N}_1^*$ pair as well as the decay of the inflaton ϕ into two $\tilde{N}_1$ sneutrinos. Note that the coupling of the scalar τ to the sneutrino field product $\left|\tilde{N}_i\right|^2$ drops out of the F-term scalar potential, when adding the hermitian conjugate of the two terms explicitly stated in Eq. (5.110).[9]

With the operators in Eqs. (5.109) and (5.110) at hand, we are ready to calculate the tree-level decay rates and branching ratios of the particles σ, τ, ψ, and ϕ. Just as in the case of the gauge multiplet, all particles decay at the same total rate Γ_S^0,

$$\Gamma_\sigma^0 = \Gamma_\tau^0 = \Gamma_\psi^0 = \Gamma_\phi^0 = \Gamma_S^0 = \frac{1}{32\pi}\frac{M_1^2}{v_{B-L}^2}m_S\left[1-\left(2M_1^2/m_S\right)^2\right]^{1/2}. \tag{5.111}$$

The branching ratios for the respective final states turn out to be mostly trivial,

$$\text{Br}\left(\sigma\to N_1N_1\right) = 1-\left(2M_1^2/m_S\right)^2\,,\quad \text{Br}\left(\sigma\to\tilde{N}_1\tilde{N}_1^*\right) = \left(2M_1^2/m_S\right)^2\,, \tag{5.112}$$
$$\text{Br}\left(\tau\to N_1N_1\right) = 1\,,\quad \text{Br}\left(\psi\to N_1\tilde{N}_1^*\right) = 1\,,\quad \text{Br}\left(\phi\to\tilde{N}_1\tilde{N}_1\right) = 1\,. \tag{5.113}$$

Neutrino Sector

By now, we have encountered three different production mechanisms for heavy (s)neutrinos: tachyonic preheating (PH), the decay of the $B-L$ vector boson and its superpartners (G) and the decay of the particles from the SSB sector (S). Beyond that, heavy (s)neutrinos may also be thermally produced (th), i.e. through inverse decay processes in the thermal bath (cf. Sec. 7.1). All of these mechanisms yield heavy (s)neutrinos components $\left(N_i^{\text{x}},\tilde{N}_i^{\text{x}}\right)$, where $\text{x} = \text{PH}, G, S, \text{th}$, with different characteristic energies. Due to the effect of relativistic time dilatation, they thus all decay at different rates $\Gamma_{N_i}^{\text{x}}$,

$$\Gamma_{N_i}^{\text{x}} = \left\langle\frac{M_i}{E_{N_i}}\right\rangle_{\text{x}}\Gamma_{N_i}^0\,, \tag{5.114}$$

Here, $\Gamma_{N_i}^0$ denotes the zero-temperature (s)neutrino decay rate. It directly follows from the seesaw superpotential (cf. Eq. (3.28)) and is given by (cf. Eq. (3.40)),

$$\Gamma_{N_i}^0 = \frac{1}{4\pi}\frac{\widetilde{m}_i M_i}{v_u^2}M_i\,,$$

[9] In order to obtain a trilinear coupling of τ to two sneutrinos in the potential V_F, we would have to include an explicit mass term for the superfield S into the superpotential, $W \supset \frac{1}{2}mS^2$.

For completeness, let us also mention in passing the branching ratios for the various final states, into which the heavy (s)neutrinos can decay (cf. Eq. 3.39),

$$\mathrm{Br}\big(N_i \to \ell H_u\big) = \frac{1}{4}\,, \quad \mathrm{Br}\big(N_i \to \tilde{\ell}\tilde{H}_u\big) = \frac{1}{4}\,, \quad \mathrm{Br}\big(\tilde{N}_i \to \tilde{\ell} H_u\big) = \frac{1}{2}\,, \tag{5.115}$$

$$\mathrm{Br}\big(N_i \to \bar{\ell} H_u^*\big) = \frac{1}{4}\,, \quad \mathrm{Br}\big(N_i \to \tilde{\ell}^* \bar{\tilde{H}}_u\big) = \frac{1}{4}\,, \quad \mathrm{Br}\big(\tilde{N}_i \to \bar{\ell} \bar{\tilde{H}}_u\big) = \frac{1}{2}\,. \tag{5.116}$$

The prefactor of $\Gamma^0_{N_i}$ in Eq. (5.114) is the inverse time dilatation factor averaged over the momenta of all (s)neutrinos of a given component,

$$\left\langle \frac{M_i}{E_{N_i}} \right\rangle_{\mathrm{x}} = \frac{1}{n^{\mathrm{x}}_{N_i}} \frac{g_{N_i}}{(2\pi)^3} \int d^3p \frac{M_i}{E_{N_i}} f^{\mathrm{x}}_{N_i}(t,p)\,, \quad E_{N_i} = \sqrt{p^2 + M_i^2}\,, \tag{5.117}$$

with $n^{\mathrm{x}}_{N_i}$ and $f^{\mathrm{x}}_{N_i}$ being the number density and the phase space distribution function of the (s)neutrino species $\big(N_i^{\mathrm{x}}, \tilde{N}_i^{\mathrm{x}}\big)$, respectively (cf. Sec. 7.1). Typically, these two quantities exhibit a nontrivial time dependence and thus need to be determined by means of the Boltzmann equation for the (s)neutrinos under study.

Chapter 6

Nonperturbative Dynamics

The total decay rates and branching ratios which we derived from the Lagrangian of the supersymmetric Abelian Higgs model in the previous chapter are important ingredients to the study of the reheating process after the $B-L$ phase transition. Reheating is a *perturbative* process, which we will investigate by means of semiclassical Boltzmann equations in the next chapter. For now, we shall focus on the *nonperturbative* dynamics of the $B-L$ phase transition.

As the symmetry breaking at the end of hybrid inflation proceeds very rapidly and abruptly, it represents what is often referred to as a *waterfall* phase transition (cf. Sec. 3.1.1). It is accompanied by the production of local topological defects in the form of cosmic strings as well as the nonadiabatic production of particles coupled to the Higgs field s during tachyonic preheating. In this chapter, we will discuss these two nonperturbative processes in turn. First, we will estimate the amount of cosmic strings produced during the $B-L$ phase transition and use the current bound on the string tension to constrain the parameters of hybrid inflation, *viz.* the $B-L$ breaking scale v_{B-L} and the coupling constant λ (cf. Sec. 6.1). Subsequent to that, we will sketch the computation of the particle abundances generated during tachyonic preheating (cf. Sec. 6.2), which we will require as initial data for our study of the reheating process in the next chapter.

6.1 Production of Cosmic Strings

In the true vacuum of the Abelian Higgs model, the expectation value of the Higgs field $s_+ = \sigma_+/\sqrt{2}e^{i\zeta_+}$ equals the $B-L$ breaking scale, $\langle s_+^* s_+\rangle^{1/2} = v_{B-L}$. The vacuum manifold of the Abelian Higgs model is thus isomorphic to the circle and may be parametrized in terms of the Goldstone phase $\zeta_+ \in [0, 2\pi)$. Since the circle is not a simply connected manifold, i.e. since it exhibits a *nontrivial topology*, the classical field equations of the Abelian Higgs model admit solitonic solutions, which describe one-dimensional *topological defects* known as cosmic strings.[1]

In our case, the tension of a cosmic string equals its energy per unit length μ,

$$\mu = 2\pi v_{B-L}^2 B(\beta)\,, \quad B(\beta) \simeq \begin{cases} 1.04\,\beta^{0.195}\,, & 10^{-2} \lesssim \beta \ll 1\,, \\ 2.4/\ln(2/\beta)\,, & \beta \lesssim 10^{-2}\,, \end{cases} \tag{6.1}$$

where $\beta = \lambda/(8g^2)$. The characteristic distance ξ separating two strings at the moment of their formation is approximately given as [262],

$$\xi \approx (-\lambda\, v_{B-L}\, \dot{\varphi}_c)^{-1/3}\,, \tag{6.2}$$

with $\dot{\varphi}_c$ denoting the velocity of the inflaton field φ at the time when it reaches its critical value $\varphi_c = v_{B-L}$. We obtain $\dot{\varphi}_c$ directly from the Klein-Gordon equation, i.e. the equation of motion for the inflaton field (cf. Eq. (3.1)),

$$-\dot{\varphi}_c = \frac{1}{3H}\left(V' + \ddot{\varphi}\right)\,. \tag{6.3}$$

For small and intermediate values of the coupling constant, $\lambda \lesssim 10^{-3}$, inflation ends because of the tachyonic instability in the scalar potential (cf. Eq. (3.14)). The slow-roll approximation is then valid all the way until the onset of the $B-L$ phase transition (cf. Eq. (3.2)), so that we may neglect $\ddot{\varphi}$ in the calculation of $\dot{\varphi}_c$ and approximate the Hubble rate H by H_I (cf. Eq. (3.4)),

$$\lambda \lesssim 10^{-3} \;:\qquad -\dot{\varphi}_c \approx \frac{V'}{3H_I}\,. \tag{6.4}$$

By contrast, for large values of the coupling constant, $\lambda \gtrsim 10^{-3}$, inflation ends because the slow-roll condition $|\eta_V| \ll 1$ becomes violated at some inflaton field value $\varphi_{\rm sr} \gg \varphi_c$. In this case, we are hence not allowed to compute $\dot{\varphi}_c$ within the slow-roll approximation. The expression for $\dot{\varphi}_c$ in Eq. (6.4) remains, however, useful nonetheless, as it now provides us with an upper estimate of $\dot{\varphi}_c$,

$$\lambda \gtrsim 10^{-3} \;:\qquad -\dot{\varphi}_c < \frac{V'}{3H} < \frac{V'}{3H_I}\,, \tag{6.5}$$

[1] For reviews on cosmic strings, cf. for instance Refs. [30–32].

λ	10^{-8}	10^{-7}	10^{-6}	10^{-5}	10^{-4}	10^{-3}	10^{-2}
H^{-1}/ξ	5	10	20	50	100	200	$\lesssim 500$
$\rho_{\rm string}/\rho_0$ [%]	0.002	0.01	0.07	0.4	2	10	$\lesssim 80$

Table 6.1: Efficiency of the production of cosmic strings. H^{-1}/ξ, the ratio of the Hubble radius to the string separation scale, is a measure for the abundance of cosmic strings at the end of the $B-L$ phase transition, while $\rho_{\rm string}/\rho_0$, the string energy density relative to the initial false vacuum energy density, indicates the amount of energy stored in cosmic strings directly after symmetry breaking. The numbers shown in this table correspond to v_{B-L} kept fixed at $5 \times 10^{15}\,\text{GeV}$.

where we have used that $\ddot{\varphi} < 0$ and $H > H_I$. Note that for the range of v_{B-L} and λ values that we are interested in the only relevant contribution to the inflaton potential is the radiative Coleman-Weinberg correction $V_{\rm CW}$, while the terms induced by SUGRA are negligible [33, 263]. In summary, given the expressions for H_I and $V_{\rm CW}$ in Eqs. (3.4) and (3.11) and irrespectively of whether $|\eta_V| \ll 1$ or not, we find that the absolute value of $\dot{\varphi}_c$ cannot be larger than

$$\frac{V'}{3H_I} = \frac{\ln 4}{64\sqrt{6}\pi^{5/2}}\,\lambda^{3/2}\,M_P\,v_{B-L} \simeq \lambda^{3/2}\,v_{B-L}^2\left(\frac{6\times 10^{15}\,\text{GeV}}{v_{B-L}}\right)\,. \tag{6.6}$$

With the aid of Eqs. (6.1) and (6.2), the energy density $\rho_{\rm string}$ stored in cosmic strings just after the end of the $B-L$ phase transition can be calculated as

$$\rho_{\rm string} = \frac{\mu}{\xi^2}\,. \tag{6.7}$$

In the following, we will always employ the slow-roll expression for $\dot{\varphi}_c$ (cf. Eq. (6.6)) in the calculation of $\rho_{\rm string}$. For $\lambda \lesssim 10^{-3}$, our results for $\rho_{\rm string}$ will hence represent actual estimates of the string energy density, while for $\lambda \gtrsim 10^{-3}$, given Eq. (6.5) and the fact that $\rho_{\rm string}$ scales like $(-\dot{\varphi}_c)^{2/3}$, we will merely obtain upper bounds on the string energy density. As a first observation, we note that the fraction $\rho_{\rm string}/\rho_0$ of the total energy stored in cosmic strings directly after the $B-L$ phase transition monotonically increases with λ. This is because larger values of λ entail higher string tensions as well as shorter average distances between two strings. Some numerical results, illustrating the increasing efficiency of the production of cosmic strings for larger λ values, are listed in Tab. 6.1.[2]

Subsequent to their production, the cosmic strings may intercommute with each other, which leads to the formation of closed string loops next to the abundance of infinitely extended

[2] Including SUGRA corrections into the inflaton potential on condition of a canonical Kähler potential [145], these results remain practically unchanged. Given a nonminimal Kähler potential, inflation can no longer be successfully realized for $\lambda < \lambda_{\rm min}$, with $\lambda_{\rm min}$ depending on the coefficients of the noncanonical terms in the Kähler potential [34]. In this case, our results agree with the outcome of the full calculation, based on the complete potential, as long as $\lambda \gtrsim \lambda_{\rm min}$.

strings. These string loops oscillate, thereby loosing energy into gravitational waves as well as into the Higgs and gauge DOFs [264, 265]. After a relaxation time t_{string}, roughly given by the distance scale ξ [264], the cosmic string network enters the *scaling regime*, which is characterized by an abundance of only $\mathcal{O}(1)$ cosmic strings per Hubble volume and a string energy density ρ_{string} scaling like $H^2 M_P^2$. Relic cosmic strings are a possible source for primordial density fluctuations, gravitational lensing as well as gravitational waves. Hence, if cosmic strings are indeed generated during some phase transition in the early universe, they should reveal their existence in a variety of present-day cosmological observations. The fact that no effects related to cosmic strings have been observed so far implies an upper bound on the string tension [266–269]. The actual values quoted in the literature partly differ from each other. In this thesis, we will work with the following representative value,

$$G\mu \lesssim 5 \times 10^{-7} \,, \tag{6.8}$$

with $G = M_P^{-2}$ being Newton's constant. This constraint directly translates into an upper bound on v_{B-L}, which weakly depends on λ (cf. Eq. (6.1)),

$$v_{B-L} \lesssim 1.8 \times 10^{-4} \left(\ln \frac{16 g^2}{\lambda} \right)^{1/2} M_P \,. \tag{6.9}$$

We conclude that, for reasonable values of the coupling constant λ, the nonobservation of cosmic strings alone already excludes the possibility of $B-L$ breaking taking place *above* the GUT scale, i.e. $v_{B-L} \lesssim 1 \times 10^{16}$ GeV for $\lambda > 10^{-20}$.

Similarly to us, the authors of Ref. [34] also discuss the production of cosmic strings during the $B-L$ phase transition at the end of supersymmetric F-term hybrid inflation.[3] Combining the requirement of successful inflation with bounds on the parameter space inferred from the amplitude of the CMB power spectrum A_s (cf. Eq. (2.26)) as well as the nonobservation of cosmic strings [266], they find consistency among all observations for

$$3 \times 10^{15} \text{ GeV} \lesssim v_{B-L} \lesssim 7 \times 10^{15} \text{ GeV} \,, \quad 10^{-4} \lesssim \sqrt{\lambda} \lesssim 10^{-1} \,. \tag{6.10}$$

Note in particular that, up to a factor of $\mathcal{O}(1..10)$, the range of *viable* v_{B-L} values is compatible with the upper boundary of the range of *preferred* v_{B-L} values, which we found in our Monte-Carlo study of the Froggatt-Nielsen model (cf. Eq. (4.3)). The synopsis of our results in Eqs. (3.16), (4.3) and (6.10) hence leads to the conclusion that the flavour charge a, which controls the magnitude of v_{B-L} relative to mass scale M_0 (cf. Eq. (3.68)), should be zero. In addition to that, the results of Ref. [34] in Eq. (6.10) imply a proportionality factor of about 5 in Eq. (3.68),

$$a = 0 \,, \quad v_{B-L} \simeq 5 \times \eta^{2a} M_0 \simeq 5 \times 10^{15} \text{ GeV} \,. \tag{6.11}$$

[3] Cf. also the analyses in Refs. [33, 270, 271].

A factor of 5 can still be accounted for by the Froggatt-Nielsen model, since it is *triple* products of $\mathcal{O}(1)$ factors which enter into the calculation of v_{B-L} from the neutrino mass matrices M and m_D. Likewise, the viable range of λ values can be translated into constraints on the flavour charge d (cf. Eqs. (3.57) and (3.75)),

$$\sqrt{\lambda} \sim \eta^e \,, \quad e = 2(d-1) \,, \quad 1.4 \lesssim d \lesssim 2.6 \,, \tag{6.12}$$

and therefore, according to Eq. (3.68), also into constraints on the heavy-(s)neutrino mass M_1. The parameter space, which we shall investigate in this thesis, is hence defined by (cf. Eqs. (3.70), (6.11) and (6.12)),

$$\begin{aligned} &10^{-5}\,\mathrm{eV} \leq \widetilde{m}_1 \leq 1\,\mathrm{eV} \,, \\ &v_{B-L} = 5 \times 10^{15}\,\mathrm{GeV} \,, \\ &10^{9}\,\mathrm{GeV} \leq M_1 \leq 3 \times 10^{12}\,\mathrm{GeV} \,. \end{aligned} \tag{6.13}$$

The production and decay of cosmic strings can in principle have a large influence on the further evolution of the universe after the $B-L$ phase transition. However, as we will argue in the following, for our purposes it is not necessary to consider any processes related to cosmic strings in more detail as long as we restrict ourselves to the parameter space in Eq. (6.13). By means of Eq. (6.2), we find that for $\lambda \sim 10^{-3}..10^{-2}$ the number of cosmic strings per Hubble volume $N_s = \left(H^{-1}/\xi\right)^2$ is as large as $\mathcal{O}\left(10^5\right)$. For $\lambda \gtrsim 6 \times 10^{-3}$, the upper bound on the fractional string energy density exceeds 50 %. In the case of such large λ values, the cosmic string relaxation time, $t_{\mathrm{string}} \sim \xi \sim 10^{-3} H^{-1}$, is however much shorter than the Hubble time H^{-1}. Most of the string energy is hence converted back into Higgs and gauge DOFs before the reheating processes has really begun. The exact mechanism of energy loss of cosmic strings is not yet fully understood, which prompts us to refrain from attempting to precisely describe it. As an important result, we should, however, keep in mind that *at the very most* about half of the initial false vacuum energy density may be processed via an intermediate population of cosmic strings into the particles of the Higgs and gauge multiplets. Generically, the effects of cosmic strings are much less important. For $\lambda \lesssim 10^{-4}$, for instance, their relative energy contribution is at the level of at most $\mathcal{O}\left(1\,\%\right)$. Due to supersymmetry, the additional higgsinos produced in the decay of cosmic strings decay into the same supermultiplet, *viz.* n_1^c, as the Higgs bosons produced during tachyonic preheating (cf. Sec. 5.2.3). We thus expect that it should not make a qualitative difference, whether the extra higgsinos produced in string decays are taken into account in the description of the reheating process or not. Meanwhile, the extra gauge particles produced in string decays predominantly decay into radiation, which is subsequently quickly diluted during the phase of matter domination after preheating. We hence claim that the reheating process after the $B-L$ phase transition is, in fact, mostly insensitive to all string-induced modifications of its initial conditions. In a numerical study of the reheating process similar to the one discussed in

Ch. 7, we are able to confirm this claim. Considering the case of extremal string production, we shift half of the energy initially stored in the Higgs bosons at the end of preheating into the gauge DOFs and calculate the resulting abundances of entropy, baryon asymmetry and gravitino dark matter. We find no deviations from the results presented in Section 7.2 above the percent level. These findings serve us a justification to neglect all effects related to the production and decay of cosmic strings in the remainder of this thesis.

6.2 Tachyonic Preheating

Next to the production of cosmic strings, the decay of the false vacuum entails a second nonperturbative process, *viz.* tachyonic preheating [28, 29], which also results in particle production [35]. In this section, we shall first discuss tachyonic preheating, i.e. the transfer of the false vacuum energy into a gas of nonrelativistic Higgs bosons, and then the nonadiabatic particle production associated with it.

Energy Transfer from the False Vacuum to Nonrelativistic Higgs Bosons

When the inflaton field φ reaches its critical value $\varphi_c = v_{B-L}$, the scalar potential develops a tachyonic instability in the direction of the waterfall field σ. As we shall demonstrate now, this triggers the growth of the long-wavelength modes of the Higgs field $s_+ = \sigma_+/\sqrt{2}e^{i\zeta_+}$ at an exponential rate. Neglecting the expansion of the universe during the $B-L$ phase transition, the linearized equations of motion of the Higgs mode functions $s_+(k,t)$ are given by (cf. Eqs. (5.55) and (5.56)),

$$\ddot{s}_+(k,t) + \left(k^2 + m_{s_+}^2\right) s_+(k,t) = 0\,, \quad m_{s_+}^2 = \frac{\lambda}{2}\left(\varphi^2 - \varphi_c^2\right)\,, \quad \varphi \leq \varphi_c\,. \tag{6.14}$$

The solutions of these mode equations corresponding to momenta k which satisfy $k^2 < -m_{s_+}^2$ are indeed superpositions of a growing and a decaying exponential. For a fixed value of the inflaton field φ, for instance, we may explicitly write

$$s_+(k,t) = A(k)\exp\left(\omega_k t\right) + B(k)\exp\left(-\omega_k t\right)\,, \quad \omega_k = \sqrt{-m_{s_+}^2 - k^2}\,. \tag{6.15}$$

This spinodal growth of the long-wavelength modes directly translates into an exponential growth of the variance v^2 of the Higgs field (cf. Eq. (5.90)) as well as of the occupation numbers n_k of the respective modes [35],

$$v^2(t) = \left\langle s_+^* s_+ \right\rangle = \int \frac{d^3k}{(2\pi)^3}\left|s_+(k,t)\right|^2\,, \quad n_k(t) = \left|s_+^*(k,t)\dot{s}_+(k,t)\right| - \frac{1}{2}\,, \tag{6.16}$$

Tachyonic preheating continues, until the nonlinear term in the full mode equations, which is induced by the quartic Higgs self-coupling, begins to compensate for the negative mass

squared, i.e. when the curvature of the Higgs potential vanishes. As an important detail, note that, given the initial conditions $s_+ = \dot{s}_+ = 0$, the classical component of the Higgs field $\langle s_+ \rangle$ never acquires a VEV. This illustrates that the decay of the false vacuum is a purely quantum mechanical process, which is solely driven by the exponentially growing quantum fluctuations of the Higgs field. As anticipated in Sec. 2.2.3, the fact that $\langle s_+ \rangle = 0$ also implies that $B-L$ actually never becomes broken during the phase transition, but merely hidden.

At the end of preheating, the occupation numbers of the long-wavelength Higgs modes are exponentially large, which allows for a treatment of these modes as an ensemble of colliding *semiclassical waves* [272]. Another interpretation of the large occupation numbers at low momenta, the one which we will adopt in the following, is that after preheating the universe is filled by a dominating abundance of nonrelativistic Higgs bosons, i.e. *particles in coherent quantum states*. Finally, we recapitulate that the $B-L$ phase transition comes to an end once the Higgs VEV has become as large as the $B-L$ breaking scale, $\langle s_+^* s_+ \rangle^{1/2} = v_{B-L}$. To study the evolution of v at late times, when the nonlinear Higgs dynamics can no longer be neglected, one has to resort to numerical lattice simulations. In the quench approximation, for instance, matching the exponentially growing, analytic solution for v at early times with the numerical solution for v at late times, one finds that the time evolution of v is well described by the smooth step function in Eq. (5.91). This implies in particular that the energy transfer from the false vacuum into Higgs bosons is a very fast process, which typically completes within a single oscillation of the scalar field distribution.

Waterfall Conditions and Quench Approximation

For a broad range of parameters, the false vacuum decays almost instantaneously as soon as the inflaton field reaches its critical value. By definition, this is equivalent to the statement that the $B-L$ phase transition generically takes place in the *waterfall regime*. The realization of the waterfall regime is subject to two conditions, which were first formulated by Linde with respect to its original nonsupersymmetric version of hybrid inflation [10]. To ensure a rapid and abrupt vacuum decay, once the tachyonic instability in the scalar potential has appeared, two time scales, Δt_σ and Δt_ϕ, must be much shorter than the Hubble time,

$$\Delta t_\sigma,\, \Delta t_\phi \ll H_I^{-1}\,. \tag{6.17}$$

Δt_σ denotes the time it takes until the negative mass squared of the waterfall field has become sizable, so that the exponential growth of the Higgs quantum fluctuations sets in. Meanwhile, Δt_ϕ characterizes the time scale, on which the inflaton field value changes after the onset of symmetry breaking. It is hence also a measure for the time it takes for the inflaton to reach the minimum of the scalar potential. In Ref. [10], Linde translates the two requirements in Eq. (6.17) into relations among the parameters of his model, to which he refers as the two

waterfall conditions. We shall now extend Linde's results to the supersymmetric case and derive the two waterfall conditions for supersymmetric F-term hybrid inflation.

The relevant DOFs driving tachyonic preheating are the semiclassical infrared modes of the Higgs field s_+ (cf. Eq. (6.15)). Among all long-wavelength modes, the $k = 0$ mode grows in particular at the largest rate, $\omega_0 = \left|m_{s_+}\right|$. We may thus define Δt_σ as the time scale, on which the growth of this mode sets in, $\Delta t_\sigma = \omega_0^{-1}$. Expanding ω_0^2 in a Taylor series up to first order in Δt_σ around $\Delta t_\sigma = 0$ yields

$$\omega_0^2 = -m_{s_+}^2 = -\frac{\lambda}{2}\left(\varphi^2 - \varphi_c^2\right) \approx -\frac{\lambda}{2}\frac{d}{dt}\bigg|_{t_c} \varphi^2 \Delta t_\sigma\,, \quad \varphi\left(t_c\right) = \varphi_c\,. \tag{6.18}$$

Identifying ω_0^2 on the left-hand side of this relation with Δt_σ^{-2} and inserting the slow-roll expression for $\dot{\varphi}_c$ (cf. Eq. (6.6)), we obtain the first waterfall condition,

$$\Delta t_\sigma^{-3} \approx -\lambda \varphi_c \dot{\varphi}_c \gg H_I^3\,, \quad \sqrt[4]{\lambda} M_P \gg \frac{4\pi}{\sqrt[4]{3\ln 4}} v_{B-L}\,, \tag{6.19}$$

which may be cast into the form of a lower bound on the coupling constant λ,

$$\lambda \gg \frac{256\pi^4}{3\ln 3}\left(\frac{v_{B-L}}{M_P}\right)^4 \simeq 2 \times 10^{-10}\left(\frac{v_{B-L}}{5 \times 10^{15}\ \text{GeV}}\right)^4\,. \tag{6.20}$$

In the parameter space under study (cf. Eq. (6.13)), it is certainly fulfilled.

The time scale governing the inflaton dynamics is given by the time-dependent mass of the inflaton field which it acquires in the course of symmetry breaking, $\Delta t_\phi = m_\phi^{-1} = \left(\sqrt{\lambda} v\right)^{-1}$ (cf. Eq. (5.83)). Shortly after the onset of tachyonic preheating, the Higgs VEV v grows exponentially (cf. Eqs. (5.90) and (6.15)), so that the condition $\Delta t_\phi = m_\phi^{-1}$ is typically satisfied at rather early times, $\Delta t_\phi = C_\phi m_S^{-1}$, with C_ϕ being of $\mathcal{O}(10)$ [35]. The second waterfall condition then assumes the form of an upper bound on the possible values of the $B-L$ scale,

$$\Delta t_\phi^{-1} = \frac{m_S}{C_\phi} \gg H_I\,, \quad v_{B-L} \ll \sqrt{\frac{3}{2\pi}}\frac{M_P}{C_\phi} \simeq \frac{8}{C_\phi} \times 10^{18}\ \text{GeV}\,. \tag{6.21}$$

Also the second waterfall condition is clearly fulfilled in our parameter space. Moreover, the fact that $C_\phi \gg 1$ illustrates that the inflaton reaches the minimum of the scalar potential on a time scale much shorter than the actual duration of symmetry breaking, which only comes to an end once $m_\phi = m_S$.

In conclusion, we find that for the values of the parameters v_{B-L} and λ, which we shall consider in this thesis, (i) the negative mass squared of the waterfall field essentially pops up, once φ reaches its critical value, and that (ii) the inflaton field rapidly rolls down towards the minimum of the scalar potential. To simplify our investigation of tachyonic preheating, we may therefore henceforth work in the *quench approximation*, in which the inflaton field φ is straight away set to zero as soon as the waterfall field becomes unstable. This is to say that

we do not slowly turn on the negative mass squared $m_{s_+}^2$ of the waterfall field, but instead instantly introduce it with its largest possible absolute value,

$$\text{Quench approximation:} \qquad \varphi \leq \varphi_c \quad \rightarrow \quad m_{s_+}^2 = -\frac{\lambda}{2}\, v_{B-L}\,. \tag{6.22}$$

Physically, the quench approximation corresponds to the limiting case of a particularly rapid and abrupt waterfall transition. It is applicable, if v_{B-L} and λ clearly satisfy the two waterfall conditions, which is definitely guaranteed in our case. The fact that the quench approximation holds for the parameter values that we are interested in also serves as an *a posteriori* justification for the omission of the Hubble expansion in our discussion of tachyonic preheating (cf. Eq. (6.14)).

Nonadiabatic Particle Production During Tachyonic Preheating

The sudden change in the masses of the particles coupled to the Higgs field s_+ leads to the nonadiabatic production of these particles during tachyonic preheating, which can be studied using the formalism of quantum fields in strong backgrounds. In the quench approximation, employing the smooth step function in Eq. (5.91) to describe the time evolution of the Higgs VEV v, it is even feasible to derive analytic expressions for the occupation numbers n_k^B and n_k^F of the produced bosons and fermions [35]. One obtains n_k^B and n_k^F in three steps. First of all, one has to rewrite the mode equations of the bosonic and fermionic fields coupled to the Higgs field s_+ as oscillator equations with time-dependent and partly complex frequencies. Then, one needs to solve these oscillator equations in terms of hypergeometric functions. In the third and last step, one can use the solutions of the mode equations to compute the Bogoliubov coefficients, relating the mode functions in the asymptotic past to the mode functions in the asymptotic future. The Bogoliubov coefficients then directly yield the desired occupation numbers. For all bosons and fermions the masses of which increase linearly with the Higgs VEV, $m_B = h_B v$ and $m_F = h_F v$, one finds

$$\begin{aligned} n_k^B &= \frac{\cosh\left[\pi\sqrt{4\alpha^2-1}\right] - \cosh\left[2\pi\left(\omega_+ - \omega_-\right)/m_S\right]}{\sinh\left[2\pi\omega_-/m_S\right]\sinh\left[2\pi\omega_+/m_S\right]}\,, \\ n_k^F &= \frac{\cosh\left[2\pi\alpha\right] - \cosh\left[2\pi\left(\omega_+ - \omega_-\right)/m_S\right]}{2\sinh\left[2\pi\omega_-/m_S\right]\sinh\left[2\pi\omega_+/m_S\right]}\,. \end{aligned} \tag{6.23}$$

Here, $\alpha = m_i/m_S$ denotes the ratio of the mass m_i of the respective particle i in the true vacuum to the Higgs boson mass m_S. Meanwhile, ω_- and ω_+ are the asymptotic *in* and *out frequencies*, $\omega_- = k$ and $\omega_+ = \sqrt{k^2 + m_i^2}$. Apparently, n_k^B and n_k^F are largest for the low-momentum modes, $k \ll m_i$. We hence conclude that tachyonic preheating primarily entails the production of *nonrelativistic* particles.

According to our analysis in Sec. 5.2.2, the masses of the inflaton ϕ, the higgsino ψ as well as all particles from the gauge and neutrino sector increase linearly with the Higgs VEV v,

such that the formulae in Eq. (6.23) can be readily used to calculate the occupation numbers of these particles after preheating. The real Higgs scalar τ, however, represents an exception, which is not covered by the results in Eq. (6.23). As compared to, for instance, ϕ and ψ, the scalar τ comes with a constant contribution to its mass m_τ (cf. Eq. (5.81)), which directly derives from m_{s_-} in the quench approximation, $m_{s_-} = \sqrt{\lambda}/2\, v_{B-L}$ (cf. Eq. (5.56)). Note in particular that it is this constant mass term, which stabilizes the Higgs field s in the τ direction, so that the role of the waterfall direction is solely due to the Higgs field σ (cf. Eq. (5.68)). Neglecting the expansion of the universe, the linearized mode equation for the Higgs field τ takes the same form as the mode equations for all other scalars coupled to s_+,

$$\ddot{\tau}(t,k) + \left(k^2 + m_\tau^2(t)\right)\tau(t,k) = 0\,, \tag{6.24}$$

the only difference being the constant contribution to the mass squared, which is absent in the case of the other scalars. To restore the standard form of the mode equation, we simply absorb the constant mass term in the momentum k. In the language of Ref. [35], this is equivalent to a shift in the asymptotic *in* frequency,

$$k^2 \to k^2 + \lambda/2\, v_{B-L}^2\,, \quad \omega_-(k) = k \to \sqrt{k^2 + \lambda/2\, v_{B-L}^2}\,. \tag{6.25}$$

Performing this shift in the expression for n_k^B in Eq. (6.23) results in a drastic suppression of the τ occupation numbers. We find that, due to the large initial τ mass, the production of τ quanta during tachyonic preheating is less efficient by as much as four orders of magnitude for the smallest and hence most important momenta. This is physically intuitive, as the presence of a constant mass term already at the onset of symmetry breaking implies that a larger amount of energy is necessary to excite a given mode. On top of that, the only tree-level decay channel of the Higgs boson τ is into a pair of neutrinos N_1, whose production is vastly dominated by the decays of the much more abundant Higgs boson σ (cf. Sec. 5.2.3). Because of their low abundance as well as their inferiority to the σ bosons, we will completely neglect the τ particles in our analysis in Chs. 7 and 8.

For all other particles produced during tachyonic preheating, we will employ the following formulae for the final number and energy densities at $t = t_{\rm PH}$, which have been obtained by the authors of Ref. [35] by fitting the results of their nonlinear numerical lattice simulations to the function $f(\alpha,\gamma) = \sqrt{\alpha^2+\gamma^2} - \gamma$,[4]

$$\begin{aligned} n_B\left(t_{\rm PH}\right) &\simeq 1\times 10^{-3} g_i m_S^3 f(\alpha, 1.3)/\alpha\,, \\ n_F\left(t_{\rm PH}\right) &\simeq 3.6\times 10^{-4} g_i m_S^3 f(\alpha, 0.8)/\alpha\,, \\ \rho_B\left(t_{\rm PH}\right)/\rho_0 &\simeq 2\times 10^{-3}\, g_i\, \lambda\, f(\alpha, 1.3)\,, \\ \rho_F\left(t_{\rm PH}\right)/\rho_0 &\simeq 1.5\times 10^{-3}\, g_i\, \lambda\, f(\alpha, 0.8)\,, \end{aligned} \tag{6.26}$$

[4] The nonadiabatic production of particles during the $B-L$ phase transition can be significantly enhanced by quantum effects [273], which, however, require further investigations.

with g_i counting the internal DOFs of the respective particles (cf. Fig. 5.1). Just as the σ bosons themselves, these particles are mostly produced with very low momenta, i.e. non-relativistically. Furthermore, we observe that the total energy fraction transferred from the Higgs background into bosonic and fermionic DOFs typically ends up being quite small. The backreaction of the produced particles with the Higgs field is consequently expected to be insignificant, justifying *a posteriori* our procedure of first determining the time evolution of the Higgs VEV and then using this Higgs VEV as a homogeneous background in the mode equations. Another interesting consequence of Eq. (6.26) is that the decay of the gauge DOFs produced during tachyonic preheating yields equal amounts of scalar and fermionic particles, with regard to each matter multiplet into which the gauge DOFs can decay. This directly follows from combining the branching ratios in Eq. (5.104) with the fact that the number densities n_B and n_F are proportional to g_i.

Chapter 7

The Reheating Process

Tachyonic preheating after hybrid inflation and the subsequent decay of the $B-L$ gauge multiplet set the stage for the emergence of the hot early universe. As outlined in Sec. 3.2.1, the reheating process after the $B-L$ phase transition is driven by the decay of thermally and nonthermally produced heavy (s)neutrinos, which entails the generation of a primordial lepton asymmetry as a byproduct. Meanwhile, inelastic 2-to-2 scatterings in the thermal bath generate an abundance of gravitinos, which might either give rise to gravitino or WIMP dark matter.

In this chapter, we will now elaborate on the reheating process and demonstrate in particular that it is indeed capable of engendering the observed BAU η_B^{obs} (cf. Sec. 2.1.3) as well as the relic density of dark matter $\Omega_{\text{DM}}^{\text{obs}} h^2$ (cf. Sec. 2.1.4), i.e. successfully generating the initial conditions of the hot early universe. Postponing the discussion of WIMP dark matter to the next chapter, we will now take the gravitino to be the LSP and consider the possibility of gravitino dark matter. The appropriate tool to track the cosmic evolution after the $B-L$ phase transition quantitatively are the Boltzmann equations for the various particle species under study. After carefully deriving them (cf. Sec. 7.1), we will first solve these Boltzmann equations for a representative choice of parameter values (cf. Sec. 7.2). This will provide us with a detailed and time-resolved description of all particle abundances. Then, we will carry out a scan of the parameter space, which will allow us to determine relations between neutrino and superparticle masses (cf. Sec. 7.3).

The results presented in this chapter were first published in Refs. [57, 58, 60].

7.1 Boltzmann Equations

The relevant physical particles remaining after the decay of the gauge DOFs are: (i) the Higgs boson σ, the inflaton ϕ and the higgsino ψ, (ii) all three generations of heavy (s)neutrinos $\left(N_i, \tilde{N}_i\right)$, (iii) all MSSM particles, and (iv) the gravitino $\widetilde{G}$. In this section, we will successively derive the Boltzmann equations which respectively describe the evolution of these particle species in an expanding Friedmann-Lemaître background. The formalism of Boltzmann equations as well as our notational conventions are summarized in App. A.1. Depending on the particle species, we will either work with the actual Boltzmann equation for the respective phase space distribution function f_X or with the integrated Boltzmann equation for the respective comoving number density N_X, which counts the number of X particles in a comoving spatial volume of size a^3,

$$N_X(t) = a^3 n_X(t) = a^3 \frac{g_X}{(2\pi)^3} \int d^3p\, f_X(t,p)\,. \tag{7.1}$$

Here, n_X denotes the number density of particle species X (cf. Eq. A.6) and a is the cosmic scale factor, which accounts for the expansion of the universe in the Robertson-Walker metric. All physical observables are invariant under a rescaling of the scale factor. For convenience, we thus set $a_{\rm PH} = a\left(t_{\rm PH}\right) = 1$ in our analysis, where $t_{\rm PH} = 0$ corresponds to the time at the end of preheating (cf. Eq. (5.91)).[1]

The time-dependence of the scale factor a is controlled by the Friedmann equation. For a flat universe and a constant equation of state $\omega = \rho/p$ between some reference time $t_0 < t$ and time t, the Friedmann equation is solved by

$$a(t) = a(t_0)\left[1 + \frac{3}{2}(1+\omega)\left(\frac{8\pi}{3M_P^2}\rho_{\rm tot}(t_0)\right)^{1/2}(t-t_0)\right]^{\frac{2}{3(1+\omega)}}. \tag{7.2}$$

After preheating, the total energy density of the universe $\rho_{\rm tot}$ is dominated by the abundance of nonrelativistic Higgs bosons, i.e. $\omega = 0$. In the course of reheating, the initial Higgs boson energy is, however, gradually transferred into MSSM radiation. Eventually, we thus have $\omega = 1/3$. In the intervening time, the equation of state parameter ω changes continuously. We approximate this behaviour by working with a *piecewise constant*, *effective* equation of state with coefficients ω_i in the intervals $(t_i, t_{i+1}]$, where $a_{\rm PH} \leq a(t_i) < a(t_{i+1})$. We determine the ω_i iteratively by requiring self-consistency of the Friedmann equation, i.e. by numerically solving the following equation for all time intervals $(t_i, t_{i+1}]$, until we reach $\omega_i = 1/3$,

$$\frac{\rho_{\rm tot}(t_i)}{\rho_{\rm tot}(t_{i+1})} = \left(\frac{a(t_{i+1})}{a(t_i)}\right)^{3(1+\omega_i)}, \quad \rho_{\rm tot} \approx \rho_\sigma + \rho_{N_1}^S\,. \tag{7.3}$$

[1] The scale factor a actually has the unit of a length, $[a] = \mathrm{GeV}^{-1}$. For the ease of notation, we will, however, always omit the unit symbol, when stating values of a. Alternatively, all explicit values of a which we will state in the following may be understood as indicating the ratio $a/a_{\rm PH}$.

In the computation of the effective equation of state parameters ω_i, we approximate the total energy density ρ_{tot} by its two dominant components—the energy density of the Higgs bosons ρ_σ and the energy density of the neutrinos produced in Higgs, higgsino and inflaton decays $\rho^S_{N_1}$. For both densities we are able to derive analytical expressions (cf. Eqs. (7.18) and (7.45)), so that we can determine the time evolution of the scale factor *before* solving any Boltzmann equation numerically. In conclusion, we also note that in the following we will calculate the Hubble rate H as $\dot{a}/a$ using the piecewise defined scale factor in Eq. (7.2).

7.1.1 Symmetry-Breaking Sector

The particles of the SSB sector are solely produced during tachyonic preheating and exclusively decay into the heavy (s)neutrinos of the first generation (cf. Sec. 5.2.3). The Boltzmann equations for σ, ϕ and ψ read

$$\begin{aligned} \hat{\mathcal{L}} f_\sigma &= -C_\sigma(\sigma \to N_1 N_1) - C_\sigma(\sigma \to \tilde{N}_1 \tilde{N}_1^*)\,, \\ \hat{\mathcal{L}} f_\phi &= -C_\phi(\phi \to \tilde{N}_1 \tilde{N}_1)\,, \\ \hat{\mathcal{L}} f_\psi &= -C_\psi(\psi \to N_1 \tilde{N}_1^*)\,. \end{aligned} \tag{7.4}$$

In order to solve these equations, let us consider for a moment the general case of an arbitrary particle X which is produced at some time t_0 with an initial distribution function f_X^0, but which merely decays after its production into other particles $ij..$, not being replenished by other processes. The time evolution of f_X is then described by the following Boltzmann equation,

$$\hat{\mathcal{L}} f_X = \mathcal{C}_X = -\sum_{ij} C_X(X \to ij..)\,, \tag{7.5}$$

with the total collision $\mathcal{C}_X$ being given by

$$\mathcal{C}_X = -\sum_{ij..} \frac{1}{2g_X} \int d\Pi\,(X|i,j,..)\,(2\pi)^4\,\delta^{(4)} f_X\,|\mathcal{M}\,(X \to ij..)|^2\,. \tag{7.6}$$

By definition of the total zero-temperature decay rate Γ_X^0 of the particle X, this operator can be simplified to $\mathcal{C}_X = -m_X f_X \Gamma_X^0$, such that Eq. (7.5) turns into

$$\frac{1}{E_X}\,\hat{\mathcal{L}} f_X(t,p) = \left(\frac{\partial}{\partial t} - Hp\frac{\partial}{\partial p}\right) f_X(t,p) = \frac{d}{dt} f_X(t,p) = -\frac{m_X}{E_X}\Gamma_X^0 f_X(t,p)\,. \tag{7.7}$$

This is a linear homogeneous ordinary differential equation in time, which has a unique solution for each initial distribution function f_X^0,

$$f_X(t,p) = f_X^0(t,p)\exp\left[-\Gamma_X^0 \int_{t_0}^{t} dt' \frac{m_X}{\mathcal{E}_X\,(E_X;t,t')}\right]\,, \quad E_X = \sqrt{p^2 + m_X^2}\,. \tag{7.8}$$

where $\mathcal{E}_X$ denotes the energy of an X particle at time t_2 which at time t_1 has an energy E_1. Irrespectively of the time ordering of t_1 and t_2, we have

$$\mathcal{E}_X\left(E_1;t_1,t_2\right)=\left[\left(\frac{a_1}{a_2}\right)^2\left(E_1^2-m_X^2\right)+m_X^2\right]^{1/2}\,,\quad a_{1,2}=a\left(t_{1,2}\right)\,. \tag{7.9}$$

If the particle species X is exclusively produced with a particular initial momentum p_*, its initial distribution function is proportional to a delta function,

$$f_X^0(t,p)\propto\delta(p_0-p_*)\,,\quad p=\frac{a_0}{a}\,p_0\,,\quad a_0=a(t_0)\,. \tag{7.10}$$

Here, p_0 is the momentum of an X particle at time t_0, which evolves into a momentum p at time t. The correct normalization of the delta function in Eq. (7.10) is obtained from matching the integral of f_X^0 over $g_X d^3p/\left(2\pi\right)^3$ with the initial number density $n_X(t_0)$,

$$f_X^0(t,p)=\frac{2\pi^2}{g_X}n_X(t_0)\,\frac{\delta\left(p_0-p_*\right)}{p_0^2}=\frac{2\pi^2}{g_X}\left(\frac{a_0}{a}\right)^3 n_X(t_0)\,\frac{\delta\left(p-\left(a_0/a\right)p_*\right)}{p^2}\,. \tag{7.11}$$

The delta function contained in f_X^0 allows us to rewrite Eq. (7.8) as follows,

$$f_X(t,p)=f_X^0(t,p)\exp\left[-\Gamma_X^0\int_{t_0}^{t}dt'\frac{m_X}{\mathcal{E}_X\left(E_*;t_0,t'\right)}\right]\,,\quad E_*=\sqrt{p_*^2+m_X^2}\,. \tag{7.12}$$

This step has eliminated the nontrivial p dependence of f_X, so that we may now integrate it over $g_X d^3p/\left(2\pi\right)^3$ in order to calculate the number density n_X,

$$n_X(t)=\left(\frac{a_0}{a}\right)^3 n_X(t_0)\exp\left[-\Gamma_X^0\int_{t_0}^{t}dt'\frac{m_X}{\mathcal{E}_X\left(E_*;t_0,t'\right)}\right]\,. \tag{7.13}$$

In the case that $p_*=0$, the expressions for E_*, $\mathcal{E}_X$, f_X^0, f_X and n_X simplify to

$$\begin{aligned}&p_*=0\,,\quad E_*=\mathcal{E}_X=m_X\,,\quad f_X^0(t,p)=\frac{2\pi^2}{g_X}\left(\frac{a_0}{a}\right)^3 n_X(t_0)\,\frac{\delta\left(p\right)}{p^2}\\ &f_X(t,p)=f_X^0(t,p)\,e^{-\Gamma_X^0\left(t-t_0\right)}\,,\quad n_X(t)=\left(\frac{a_0}{a}\right)^3 n_X(t_0)\,e^{-\Gamma_X^0\left(t-t_0\right)}\,.\end{aligned} \tag{7.14}$$

Since σ, ϕ and ψ are mostly produced with very low momenta during tachyonic preheating (cf. Eq. (6.23)), it is justified to approximate their initial distribution functions by delta functions. Our results in Eq. (7.14) thus directly provide us with the solutions of the Boltzmann equations in Eq. (7.4),

$$f_X\left(t,p\right)=\frac{2\pi^2}{g_X}\left(\frac{a_{\rm PH}}{a}\right)^3 n_X\left(t_{\rm PH}\right)\,\frac{\delta\left(p\right)}{p^2}\,e^{-\Gamma_S^0\left(t-t_{\rm PH}\right)}\,,\qquad X=\sigma,\,\phi,\,\psi\,, \tag{7.15}$$

where we have used the fact that σ, ϕ and ψ all have the same total decay rate Γ_S^0 (cf. Eq. (5.111)). Recall that $N_X=a^3 n_X$ (cf. Eq. (7.1)). The comoving number densities N_X corresponding to these distribution functions f_X are then given by

$$N_X(t)=N_X(t_{\rm PH})\,e^{-\Gamma_S^0\left(t-t_{\rm PH}\right)}\,,\qquad X=\sigma,\,\phi,\,\psi\,. \tag{7.16}$$

Taking into account that $a_{\mathrm{PH}} = 1$, the initial comoving number densities $N_\phi(t_{\mathrm{PH}})$ and $N_\psi(t_{\mathrm{PH}})$ readily follow from Eq. (6.26). The initial comoving number density of Higgs bosons $N_\sigma(t_{\mathrm{PH}})$ can be deduced from the initial Higgs energy density $\rho_\sigma(t_{\mathrm{PH}})$, which in turn is given as the difference of the initial vacuum energy density ρ_0 and the energy densities of all particles produced during tachyonic preheating,

$$\begin{aligned} N_\sigma(t_{\mathrm{PH}}) = a_{\mathrm{PH}}^3\, n_\sigma(t_{\mathrm{PH}}) = n_\sigma(t_{\mathrm{PH}}) &= \frac{1}{m_S}\rho_\sigma(t_{\mathrm{PH}}) \\ &= \frac{\rho_0}{m_S}\left(1 - \sum_{\text{bosons}} \rho_B\left(t_{\mathrm{PH}}\right)/\rho_0 - \sum_{\text{fermions}} \rho_F\left(t_{\mathrm{PH}}\right)/\rho_0\right) . \end{aligned} \tag{7.17}$$

As σ, ϕ and ψ are all nonrelativistic, the energy densities ρ_X are trivially related to the comoving number densities N_X in Eq. (7.16),

$$\rho_X(t) = \frac{m_S}{a^3} N_X(t) = m_S\, n_X(t_{\mathrm{PH}}) \left(\frac{a_{\mathrm{PH}}}{a}\right)^3 e^{-\Gamma_S^0 (t - t_{\mathrm{PH}})} , \qquad X = \sigma,\, \phi,\, \psi\,. \tag{7.18}$$

7.1.2 Neutrino Sector

Heavy (S)neutrinos from Tachyonic Preheating

Next to the particles of the SSB sector, tachyonic preheating also entails the production of the gauge DOFs as well as of all three heavy (s)neutrino generations. Again, the respective initial comoving number densities $N_X\left(t_{\mathrm{PH}}\right) = n_X(t_{\mathrm{PH}})$ can be calculated employing our results in Eq. (6.26). In the following, we will label all quantities associated with the heavy (s)neutrino components $\left(N_i^{\mathrm{PH}}, \tilde{N}_i^{\mathrm{PH}}\right)$ produced during preheating with an upper index PH.

Heavy (S)neutrinos and Radiation from the Decay of the Gauge DOFs

Due to their strong coupling and their large mass, the gauge particles A, $\tilde{A}$ and C have a very short lifetime $t_G = t_{\mathrm{PH}} + 1/\Gamma_G^0$ (cf. Eq. (5.101)) and hence decay practically immediately after preheating. It is thus not necessary to explicitly resolve the time dependence of their number densities. Instead, we may simply approximate the comoving number densities of the gauge particles by step functions,

$$N_X(t) = N_X\left(t_{\mathrm{PH}}\right)\, \Theta\left(t_G - t\right) , \quad t \geq t_{\mathrm{PH}} , \quad X = A,\, \tilde{A},\, C\,. \tag{7.19}$$

Interpreting the comoving number densities N_X as functions of the scale factor, we would have to replace $\Theta\left(t_G - t\right)$ by $\Theta\left(a_G - a\right)$, where $a_G = a(t_G)$. As a technical detail, we note that we will use a_G as the initial value of the scale factor, when solving the Boltzmann equations numerically.

The decay of the gauge particles gives rise to further heavy (s)neutrino components $\left(N_i^G, \tilde{N}_i^G\right)$ as well as to an initial abundance of radiation.[2] This time, the respective initial comoving number densities are determined by $N_A\left(t_{\rm PH}\right)$, $N_{\tilde{A}}\left(t_{\rm PH}\right)$ and $N_C\left(t_{\rm PH}\right)$ as well as the branching ratios of the gauge particles (cf. Eq. (5.104)),

$$\begin{aligned}
N_{N_i}^G(t_G) &= 2\, N_A\left(t_{\rm PH}\right) \mathrm{Br}\big(A \to N_i N_i\big) + N_{\tilde{A}}\left(t_{\rm PH}\right) \mathrm{Br}\big(\tilde{A} \to N_i \tilde{N}_i\big)\,, \\
N_{\tilde{N}_i}^G(t_G) &= 2\, N_A\left(t_{\rm PH}\right) \mathrm{Br}\big(A \to \tilde{N}_i \tilde{N}_i^*\big) + N_{\tilde{A}}\left(t_{\rm PH}\right) \mathrm{Br}\big(\tilde{A} \to N_i \tilde{N}_i\big) \\
&\quad + 2\, N_C\left(t_{\rm PH}\right) \mathrm{Br}\big(C \to \tilde{N}_i \tilde{N}_i^*\big)\,, \\
N_R^G(t_G) &= 2\, N_A\left(t_{\rm PH}\right) \mathrm{Br}\big(A \to \mathrm{MSSM}\big) + 2\, N_{\tilde{A}}\left(t_{\rm PH}\right) \mathrm{Br}\big(\tilde{A} \to \mathrm{MSSM}\big) \\
&\quad + 2\, N_C\left(t_{\rm PH}\right) \mathrm{Br}\big(C \to \mathrm{MSSM}\big)\,,
\end{aligned} \tag{7.20}$$

where $\mathrm{Br}\big(A \to \mathrm{MSSM}\big)$, $\mathrm{Br}\big(\tilde{A} \to \mathrm{MSSM}\big)$ and $\mathrm{Br}\big(C \to \mathrm{MSSM}\big)$ are given by

$$\begin{aligned}
\mathrm{Br}\big(A \to \mathrm{MSSM}\big) &= \sum_{\mathrm{MSSM}} \left[\mathrm{Br}\big(A \to \psi_i \bar{\psi}_i\big) + \mathrm{Br}\big(A \to \phi_i \phi_i^*\big)\right]\,, \\
\mathrm{Br}\big(\tilde{A} \to \mathrm{MSSM}\big) &= \sum_{\mathrm{MSSM}} \mathrm{Br}\big(\tilde{A} \to \bar{\psi}_i \phi_i\big)\,, \\
\mathrm{Br}\big(C \to \mathrm{MSSM}\big) &= \sum_{\mathrm{MSSM}} \mathrm{Br}\big(C \to \phi_i \phi_i^*\big)\,.
\end{aligned} \tag{7.21}$$

Note that $N_{\tilde{N}_i}^G$ subsumes the comoving number densities of the $\tilde{N}_i$ sneutrinos and the $\tilde{N}_i^*$ antisneutrinos. We emphasize that, unless explicitly indicated otherwise, all further quantities associated with the heavy sneutrinos $\tilde{N}_i$ are meant to equally comprise the heavy sneutrinos $\tilde{N}_i$ *and* the heavy antisneutrinos $\tilde{N}_i^*$. Moreover, as already mentioned in Sec. 6.2, combining our results for the branching ratios of the gauge DOFs and the initial comoving number densities produced during preheating (cf. Eqs. (5.104) and (6.26)), one can easily show that $N_{N_i}^G(t_G) = N_{\tilde{N}_i}^G(t_G)$, which in turn implies that $N_{N_i}^G = N_{\tilde{N}_i}^G$ at all times (cf. Eq. (7.26)).

An important caveat applies to the comoving number density $N_R^G(t_G)$. As the MSSM particles produced in the decay of the gauge DOFs quickly thermalize after their production, $N_R^G(t_G)$ must not be used as the initial value of the comoving radiation number density, when solving the radiation Boltzmann equation. Instead, $N_R^G(t_G)$ merely provides us with the initial radiation energy density $\rho_R(t_G)$. Since the gauge particles are nonrelativistic at all times, their decay products are always equipped with an initial energy of $m_G/2$. Making use of the expressions for the radiation number and the radiation energy density in Eq. (A.16),

[2] Similarly to the heavy (s)neutrinos $\left(N_i^{\rm PH}, \tilde{N}_i^{\rm PH}\right)$, we will label all quantities associated with the heavy (s)neutrino produced in the decay of the gauge particles with an upper index G. This notational convention is consistently employed throughout this thesis. The lower index of a quantity such as a number density, decay rate, etc. always indicates the particle to which the respective quantity belongs, whereas its upper index always refers to the origin of this particle.

we find

$$\rho_R(t_G) = \frac{m_G}{2}\frac{N_R^G(t_G)}{a_G^3}\,, \quad T(t_G) = \left(\frac{30}{\pi^2 g_{*,\rho}}\rho_R(t_G)\right)^{1/4}\,, \tag{7.22}$$
$$N_R(t_G) = a_G^3\frac{\zeta(3)}{\pi^2}g_{*,n}T^3(t_G)\,.$$

Heavy (S)neutrinos of the Second and Third Generation

The heavy (s)neutrinos of the second and third generation are solely produced during preheating as well as in the decay of the gauge DOF and they exclusively decay into MSSM lepton-Higgs pairs. Their Boltzmann equations are hence of the same type as the template Boltzmann equation in Eq. (7.5),

$$\begin{aligned}\hat{\mathcal{L}} f_{N_{2,3}} &= -C_{N_{2,3}}\left(N_{2,3}\to \ell H_u, \bar{\ell}H_u^*, \tilde{\ell}\tilde{H}_u, \tilde{\ell}^*\bar{\tilde{H}}_u\right), \\ \hat{\mathcal{L}} f_{\tilde{N}_{2,3}} &= -C_{\tilde{N}_{2,3}}\left(\tilde{N}_{2,3}\to \tilde{\ell}H_u, \bar{\ell}\bar{\tilde{H}}_u\right) - C_{\tilde{N}^*_{2,3}}\left(\tilde{N}^*_{2,3}\to \tilde{\ell}^*H_u^*, \ell\tilde{H}_u\right).\end{aligned} \tag{7.23}$$

Consequently, $f_{N_{2,3}}$ and $f_{\tilde{N}_{2,3}}$, the solutions of the $N_{2,3}$ and $\tilde{N}_{2,3}$ Boltzmann equations, are of the same form as the distribution function in Eq. (7.8). Each of these solutions consists of two independently evolving parts, respectively accounting for the $\left(N_i^{\rm PH}, \tilde{N}_i^{\rm PH}\right)$ (s)neutrinos as well as for the $\left(N_i^G, \tilde{N}_i^G\right)$ (s)neutrinos,

$$f_X(t,p) = f_X^{\rm PH}(t,p) + \Theta\left(t-t_G\right) f_X^G(t,p)\,, \qquad X = N_i, \tilde{N}_i\,, \quad i=2,3\,, \tag{7.24}$$
$$f_X^{\rm PH}(t,p) = f_X^{\rm PH}(t_{\rm PH},p)\, e^{-\Gamma^0_{N_i}(t-t_{\rm PH})}\,,$$
$$f_X^G(t,p) = f_X^G(t_G,p)\exp\left[-\int_{t_G}^{t} dt' \frac{M_i\,\Gamma^0_{N_i}}{\mathcal{E}_X\left(m_G/2; t_G, t'\right)}\right]\,,$$

with the initial distribution functions $f_X^{\rm PH}(t_{\rm PH},p)$ and $f_X^G(t_G,p)$ being similar to those in Eqs. (7.14) and (7.11),

$$f_X^{\rm PH}(t_{\rm PH},p) = \frac{2\pi^2}{g_N}\frac{N_X^{\rm PH}(t_{\rm PH})}{a^3}\frac{\delta\left(p\right)}{p^2}\,, \qquad X = N_i, \tilde{N}_i\,, \quad i=2,3\,, \tag{7.25}$$
$$f_X^G(t_G,p) = \frac{2\pi^2}{g_N}\frac{N_X^G(t_G)}{a^3}\frac{\delta\left(p-(a_G/a)\,p_*\right)}{p^2}\,, \quad p_* = \sqrt{\left(\frac{m_G}{2}\right)^2 - M_i^2}\,.$$

Integrating the distribution functions in Eq. (7.24) over the heavy (s)neutrino momentum space yields the corresponding comoving number densities,

$$N_X(t) = N_X^{\rm PH}(t) + \Theta\left(t-t_G\right) N_X^G(t)\,, \qquad X = N_i, \tilde{N}_i\,, \quad i=2,3\,, \tag{7.26}$$
$$N_X^{\rm PH}(t) = N_X^{\rm PH}(t_{\rm PH})\, e^{-\Gamma^0_X(t-t_{\rm PH})}\,,$$
$$N_X^G(t) = N_X^G(t_G)\exp\left[-\int_{t_G}^{t} dt' \frac{M_i\,\Gamma^0_{N_i}}{\mathcal{E}_X\left(m_G/2; t_G, t'\right)}\right]\,.$$

Nonthermally Produced Heavy (S)neutrinos of the First Generation

Similarly to the two heavier (s)neutrino flavours, the heavy (s)neutrinos of the first generation are also produced during tachyonic preheating and in the decay of the gauge multiplet. On top of that, the abundances of the N_1 neutrinos and $\tilde{N}_1$ sneutrinos receive additional contributions from the decay of the Higgs boson σ, the inflaton ϕ and the higgsino ψ as well as from thermal production processes. The corresponding Boltzmann equations are consequently more involved,

$$\begin{aligned}\hat{\mathcal{L}} f_{N_1} &= 2\, C_{N_1}(\sigma \to N_1 N_1) + C_{N_1}(\psi \to N_1 \tilde{N}_1^*) \\ &+ \quad C_{N_1}\left(N_1 \leftrightarrow \ell H_u, \bar{\ell}\bar{H}_u^*, \tilde{\ell}\tilde{H}_u, \tilde{\ell}^*\bar{\tilde{H}}_u\right), \\ \hat{\mathcal{L}} f_{\tilde{N}_1} &= 2\, C_{\tilde{N}_1}(\sigma \to \tilde{N}_1 \tilde{N}_1^*) + 2\, C_{\tilde{N}_1}(\phi \to \tilde{N}_1 \tilde{N}_1) + C_{\tilde{N}_1}(\psi \to N_1 \tilde{N}_1^*) \\ &+ \quad C_{\tilde{N}_1}\left(\tilde{N}_1 \leftrightarrow \tilde{\ell} H_u, \bar{\tilde{\ell}}\bar{\tilde{H}}_u\right) + C_{\tilde{N}_1^*}\left(\tilde{N}_1^* \leftrightarrow \tilde{\ell}^* H_u^*, \ell \tilde{H}_u\right).\end{aligned} \tag{7.27}$$

Again, these Boltzmann equations are best tackled by decomposing the (s)neutrino distribution functions f_{N_1} and $f_{\tilde{N}_1}$ into independently evolving parts,

$$\begin{aligned}f_X(t,p) &= f_X^{\mathrm{nt}}(t,p) + f_X^{\mathrm{th}}(t,p), \qquad X = N_1, \tilde{N}_1, \\ &= f_X^{\mathrm{PH}}(t,p) + \Theta(t - t_G)\, f_X^G(t,p) + f_X^S(t,p) + f_X^{\mathrm{th}}(t,p).\end{aligned} \tag{7.28}$$

As the Boltzmann equations in Eq. (7.27) are linear in f_{N_1} and $f_{\tilde{N}_1}$, they may be rewritten as a set of independent *partial* Boltzmann equations, respectively describing the time evolution of one of the distribution functions f_X^{x}, where $X = N_1, \tilde{N}_1$ and $\mathrm{x} = \mathrm{PH}, G, S, \mathrm{th}$. Of course, the Boltzmann equations for f_X^{x} and N_X^{x}, with $X = N_1, \tilde{N}_1$ and $\mathrm{x} = \mathrm{PH}, G$ take exactly the same form as the Boltzmann equations for the two heavier (s)neutrino generations in Eq. (7.23). Our results for f_X^{x} and N_X^{x}, with $X = N_{2,3}, \tilde{N}_{2,3}$ and $\mathrm{x} = \mathrm{PH}, G$, in Eqs. (7.24) and (7.26) can thus readily be generalized to the first heavy (s)neutrino generation.

In order to solve the Boltzmann equations for $f_{N_1}^S$ and $f_{\tilde{N}}^S$, i.e. the heavy (s)neutrinos produced in the decay of particles from the SSB sector, let us consider for a moment the general case of an arbitrary particle X which is continuously produced in the decay of nonrelativistic particles i and which itself steadily decays into other particles $ab...$ The time evolution of f_X is then described by,

$$\hat{\mathcal{L}} f_X = \sum_{ij} (1 + \delta_{Xj})\, C_X(i \to Xj) - \sum_{ab..} C_X(X \to ab..). \tag{7.29}$$

Here, the Kronecker delta δ_{Xj} accounts for the fact that *two* X particles are produced in case of $j = X$. Just as in our discussion of the Boltzmann equation in Eq. (7.5), the sum over the decay operators $C_X(X \to ab..)$ can again be simplified to $m_X f_X \Gamma_X^0$ (cf. Eq. (7.7)). The production operators $C_X(i \to Xj)$ are given by

$$C_X(i \to Xj) = \frac{1}{2 g_X} \int d\Pi\,(X|i;j)\,(2\pi)^4\, \delta^{(4)} f_i\, |\mathcal{M}(i \to Xj)|^2 . \tag{7.30}$$

We shall restrict ourselves to particles i which are instantaneously produced at time t_0 with vanishing initial momentum. According to our results in Eq. (7.14), we are thus allowed to use the following expression for f_i,

$$f_i(t,p) = \frac{2\pi^2}{g_i} n_i(t) \frac{\delta(p)}{p^2} \,. \tag{7.31}$$

For a matrix element squared $|\mathcal{M}|^2$ which is independent of the momenta of the particles i and j the collision operator in Eq. (7.30) can then be rewritten as

$$C_X(i \to Xj) = \frac{1}{2g_X} \frac{2\pi^2}{g_i} n_i \left|\mathcal{M}\left(i \to Xj\right)\right|^2 \frac{S(i;X,j)\,\delta(p-p_*)}{8\pi\, m_i\, p_*} \,, \tag{7.32}$$

with $p_* = \left[(m_i/2)^2 - m_X^2\right]^{1/2}$. Employing the standard expression for the decay rate of a two-body decay, we are able to make the following substitution,

$$\frac{1}{2} \frac{S(i;X,j)}{8\pi\, m_i} \frac{1}{g_i} \left|\mathcal{M}\left(i \to Xj\right)\right|^2 = \frac{E_*}{p_*} \Gamma_i^0\left(i \to Xj\right) \,, \quad E_* = \frac{m_i}{2} \,. \tag{7.33}$$

The collision operator in Eq. (7.32) consequently turns into

$$C_X(i \to Xj) = E_* \frac{2\pi^2}{g_X} \gamma\left(i \to Xj\right) \frac{\delta(p-p_*)}{p_*^2} \,, \tag{7.34}$$

where we have used that $\gamma\left(i \to Xj\right) = n_i\, \Gamma_i^0\left(i \to Xj\right)$ for a nonrelativistic particle species i. The Boltzmann equation can now be brought into the following form

$$\frac{d}{dt} f_X(t,p) = \frac{2\pi^2}{g_X} \sum_{ij} (1+\delta_{Xj})\, \gamma\left(i \to Xj\right) \frac{\delta(p-p_*)}{p^2} - \frac{m_X}{E_X} \Gamma_X^0 f_X(t,p) \,. \tag{7.35}$$

Again, we end up with a linear homogeneous ordinary differential equation in time. Starting from zero initial abundance, $f_X^0 = 0$, its unique solution is given by

$$\begin{aligned} f_X(t,p) &= \frac{2\pi^2}{g_X} \sum_i \int_{t_0}^{t} dt'\, \gamma_{i,X}(t') \frac{\delta(p'-p_*)}{p'^2} \exp\left[-\int_{t'}^{t} dt'' \frac{m_X \Gamma_X^0}{\mathcal{E}_X(E_X;t,t'')}\right] \,, \\ \gamma_{i,X}(t) &= \sum_j (1+\delta_{Xj})\, \gamma\left(i \to Xj\right) \,, \quad p' = \frac{a}{a'} p \,, \quad a' = a(t') \,. \end{aligned} \tag{7.36}$$

Thanks to the delta function in the integral over dt', the energy $\mathcal{E}_X(E_X;t,t'')$ in the integral over dt'' can be replaced by $\mathcal{E}_X(m_i/2;t',t'')$. This eliminates the nontrivial momentum dependence of the distribution function f_X. The delta function itself can be rewritten as a function of p, the momentum of an X particle at time t,

$$\delta(p'-p_*) = \frac{a'}{a}\, \delta\left(p - (a'/a)\, p_*\right) \tag{7.37}$$

Our final result for the distribution function f_X then reads,

$$f_X(t,p) = \frac{2\pi^2}{g_X} \sum_i \int_{t_0}^{t} dt' \left(\frac{a'}{a}\right)^3 \gamma_{i,X}(t') \frac{\delta(p-(a'/a)\,p_*)}{p^2} \times \exp\left[-\int_{t'}^{t} dt'' \frac{m_X \Gamma_X^0}{\mathcal{E}_X(m_i/2;t',t'')}\right] . \tag{7.38}$$

Owing to the trivial momentum dependence of f_X, we can easily deduce the number, energy and interaction densities of the particle species X (cf. Eqs. (A.6), (A.7) and (A.9)). For the ease of notation, let us introduce $\delta n_X(t',t)$ to denote the number density at time t of those X particles which are produced at time t'. As we will see immediately, δn_X is given by

$$\delta n_X(t',t) = \sum_i \delta n_X^i(t',t) = \sum_i \left(\frac{a'}{a}\right)^3 \gamma_{i,X}(t') \exp\left[-\int_{t'}^{t} dt'' \frac{m_X \Gamma_X^0}{\mathcal{E}_X(m_i/2;t',t'')}\right] . \tag{7.39}$$

Indeed, with the aid of δn_X and δn_X^i, we are able to summarize our results as follows,

$$\begin{aligned}
f_X(t,p) &= \frac{2\pi^2}{g_X} \sum_i \int_{t_0}^{t} dt'\, \delta n_X^i(t',t) \frac{\delta(p-(a'/a)\,p_*)}{p^2} , \qquad (7.40)\\
n_X(t) &= \int_{t_0}^{t} dt'\, \delta n_X(t',t) = \sum_i \int_{t_0}^{t} dt'\, \delta n_X^i(t',t) = \sum_i n_X^i(t) ,\\
\rho_X(t) &= \sum_i \int_{t_0}^{t} dt'\, \mathcal{E}_X(m_i/2;t',t)\, \delta n_X^i(t',t)\\
\gamma_X(t) &= \gamma\,(X \to ab..) = \sum_i \int_{t_0}^{t} dt' \frac{m_X\, \Gamma_X^0}{\mathcal{E}_X(m_i/2;t',t)} \delta n_X^i(t',t) = \sum_i n_X^i(t)\, \Gamma_X^i(t) ,
\end{aligned}$$

where Γ_X^i represents the zero-temperature decay rate of the particle species X, weighted with the average inverse time dilatation factor for X particles produced in the decay of i particles (cf. Eqs. (5.114) and (5.117)),

$$\Gamma_X^i(t) = \left\langle \frac{m_X}{E_X} \right\rangle_i \Gamma_X^0 = \int_{t_0}^{t} dt' \frac{m_X}{\mathcal{E}_X(m_i/2;t',t)} \frac{\delta n_X^i(t',t)}{n_X^i(t)} \Gamma_X^0 . \tag{7.41}$$

The general expressions in Eqs. (7.39), (7.40) and (7.41) are readily applied to the heavy (s)neutrinos of the first generation, which are produced in the decay of particles from the SSB sector. To obtain the corresponding expressions for the N_1^S neutrinos and $\tilde{N}_1^S$ sneutrinos one merely has to perform the following substitutions,

$$\begin{aligned}
&t_0 \to t_{\rm PH} , \quad i \to \sigma,\phi,\psi , \quad m_i \to m_S , \quad X \to N_1^S, \tilde{N}_1^S , \quad g_X \to g_N \quad m_X \to M_1 , \qquad (7.42)\\
&\Gamma_X^0 \to \Gamma_{N_1}^0 , \quad \gamma_{i,X} \to \gamma_{S,N_1}, \gamma_{S,\tilde{N}_1} ,
\end{aligned}$$

with the interaction densities γ_{S,N_1} and $\gamma_{S,\tilde{N}_1}$ being defined as

$$\begin{aligned}
\gamma_{S,N_1}(t) &= 2\, n_\sigma(t)\, \Gamma^0(\sigma \to N_1 N_1) + n_\psi(t)\, \Gamma^0(\psi \to N_1 \tilde{N}_1^*) , \qquad (7.43)\\
\gamma_{S,\tilde{N}_1}(t) &= 2\, n_\sigma(t)\, \Gamma^0(\sigma \to \tilde{N}_1 \tilde{N}_1^*) + 2\, n_\phi(t)\, \Gamma^0(\phi \to \tilde{N}_1 \tilde{N}_1) + n_\psi(t)\, \Gamma^0(\psi \to N_1 \tilde{N}_1^*) .
\end{aligned}$$

To sum up, we find the following analytical results for the comoving number densities of the nonthermal heavy (s)neutrinos of the first generation,

$$N_X^{\rm nt}(t) = N_X^{\rm PH}(t) + N_X^G(t) + N_X^S(t)\,, \qquad X = N_1, \tilde{N}_1\,, \tag{7.44}$$

$$N_X^{\rm PH}(t) = N_X^{\rm PH}(t_{\rm PH})\, e^{-\Gamma^0_{N_1}(t-t_{\rm PH})}\,, \;\; N_X^G(t) = N_X^G(t_G)\, \exp\left[-\int_{t_G}^t dt' \frac{M_1\,\Gamma^0_{N_1}}{\mathcal{E}_X(m_G/2; t_G, t')}\right]\,,$$

$$N_X^S(t) = \int_{t_{\rm PH}}^t dt'\, a'^3\, \gamma_{S,X}(t') \exp\left[-\int_{t'}^t dt'' \frac{M_1\,\Gamma^0_{N_1}}{\mathcal{E}_X(m_S/2; t', t'')}\right]\,.$$

Meanwhile, the corresponding energy densities look as follows,

$$\rho_X^{\rm nt}(t) = \rho_X^{\rm PH}(t) + \rho_X^G(t) + \rho_X^S(t)\,, \qquad X = N_1, \tilde{N}_1\,, \tag{7.45}$$

$$\rho_X^{\rm PH}(t) = \frac{M_1}{a^3}\, N_X^{\rm PH}(t)\,, \;\; \rho_X^G(t) = \frac{\mathcal{E}_X(m_G/2; t_G, t)}{a^3}\, N_X^G(t)\,,$$

$$\rho_X^S(t) = \int_{t_{\rm PH}}^t dt'\, \frac{\mathcal{E}_X(m_S/2; t', t)}{a^3} a'^3\, \gamma_{S,X}(t') \exp\left[-\int_{t'}^t dt'' \frac{M_1\,\Gamma^0_{N_1}}{\mathcal{E}_X(m_S/2; t', t'')}\right]\,.$$

The expressions for the comoving number densities of the N_1 neutrinos and the $\tilde{N}_1$ sneutrinos in Eq. (7.44) only differ in terms of the interaction density $\gamma_{S,X}$. The time dependence of γ_{S,N_1} and $\gamma_{S,\tilde{N}_1}$ is however the same, so that the ratio $N^S_{\tilde{N}_1}/N^S_{N_1}$ is a constant at all times,

$$\gamma_{S,X}(t) \propto \frac{e^{-\Gamma^0_S(t-t_{\rm PH})}}{a^3}\,, \qquad \frac{N^S_{\tilde{N}_1}}{N^S_{N_1}} = \frac{2\,n_\sigma(t_{\rm PH})\,{\rm Br}(\sigma \to \tilde{N}_1 \tilde{N}_1^*) + 2\,n_\phi(t_{\rm PH}) + n_\psi(t_{\rm PH})}{2\,n_\sigma(t_{\rm PH})\,{\rm Br}(\sigma \to N_1 N_1) + n_\psi(t_{\rm PH})}\,, \tag{7.46}$$

where we have used that ${\rm Br}(\psi \to N_1 \tilde{N}_1^*) = {\rm Br}(\phi \to \tilde{N}_1 \tilde{N}_1) = 1$ (cf. Eq. (5.112)). According to the parametrization of our model, the ratio $N^S_{\tilde{N}_1}/N^S_{N_1}$ solely depends on the heavy (s)neutrino mass M_1. For those values of M_1 that we are interested in this dependence is, however, rather weak. Varying M_1 between 10^9 GeV and 3×10^{12} GeV (cf. Eq. (6.13)), the ratio $N^S_{\tilde{N}_1}/N^S_{N_1}$ only increases from roughly 4×10^{-5} to roughly 2×10^{-4}.

Thermally Produced Heavy (S)neutrinos of the First Generation

Unlike the two heavier (s)neutrino flavours, the (s)neutrinos of the first generation are also thermally produced through inverse decay processes in the bath. In the Boltzmann equations in Eq. (7.27), the production and the decay of the thermal (s)neutrinos are accounted for by the collision operators featuring an double arrow. The partial Boltzmann equations for the distribution functions $f^{\rm th}_{N_1}$ and $f^{\rm th}_{\tilde{N}_1}$ are hence of the following form,

$$\hat{\mathcal{L}} f_X = \mathcal{C}_X = \sum_{ij..} C_X(X \leftrightarrow ij..) = \frac{1}{2 g_X} \sum_{ij} \int d\Pi\,(X|i,j,..)\,(2\pi)^4\,\delta^{(4)} \tag{7.47}$$
$$\times \left[f_i f_j .. \left|\mathcal{M}\,(X \leftarrow ij..)\right|^2 - f_X \left|\mathcal{M}\,(X \to ij..)\right|^2\right]\,,$$

with $ij..$ denoting particles in thermal equilibrium. Neglecting any effects of CP violation in the decays and inverse decays of the X particles, we are able to identify $|\mathcal{M}\,(X \leftarrow ij..)|^2$ with $|\mathcal{M}\,(X \rightarrow ij..)|^2$. Furthermore, approximating the distributions functions $f_i, f_j, ..$ by Maxwell-Boltzmann distributions (cf. Eq. (A.14)), energy conservation implies,

$$f_i f_j .. = f_i^{\mathrm{eq}} f_j^{\mathrm{eq}} .. \approx e^{-E_i/T} e^{-E_j/T} .. = e^{-E_X/T} = f_X^{\mathrm{eq}} . \tag{7.48}$$

Employing the definition of the zero-temperature decay rate Γ_X^0 of the particle species X, the Boltzmann equation in Eq. (7.47) can therefore be rewritten as

$$\begin{aligned} \frac{d}{dt} f_X &= -\left(f_X - f_X^{\mathrm{eq}}\right) \frac{1}{2 g_X E_X} \sum_{ij..} \int d\Pi\,(X|i,j,..)\,(2\pi)^4\,\delta^{(4)}\,|\mathcal{M}\,(X \rightarrow ij..)|^2 \\ &= -\left(f_X - f_X^{\mathrm{eq}}\right) \frac{m_X}{E_X} \Gamma_X^0 \,. \end{aligned} \tag{7.49}$$

This Boltzmann equation equally describes the evolution of $f_{N_1}^{\mathrm{th}}$ as well as of $f_{\tilde{N}_1}^{\mathrm{th}}$. Thus, even before attempting to solve it, we already know that $f_{N_1}^{\mathrm{th}} = f_{\tilde{N}_1}^{\mathrm{th}}$ and hence $N_{N_1}^{\mathrm{th}} = N_{\tilde{N}_1}^{\mathrm{th}}$ at all times.[3] The exact distribution function of the thermal (s)neutrinos is given as the unique solution of Eq. (7.49) for vanishing initial conditions,

$$f_X^{\mathrm{th}}(t,p) = \int_{t_G}^{t} dt' \frac{M_1\,\Gamma_{N_1}^0}{\mathcal{E}_X(E_X;t,t')} f_X^{\mathrm{eq}}(t',p)\,\exp\left[-\int_{t'}^{t} dt'' \frac{M_1\,\Gamma_{N_1}^0}{\mathcal{E}_X(E_X;t,t'')}\right] , \quad X = N_1, \tilde{N}_1 \,. \tag{7.50}$$

As the thermal (s)neutrinos are produced within a broad range of energies $\mathcal{E}_X(E_X;t,t')$, the exact solution for f_X^{th} cannot be as easily integrated over momentum space as the nonthermal distribution function f_X in Eq. (7.40). However, since the thermal (s)neutrinos inherit their momentum distribution from the particles in the thermal bath, it is reasonable to assume that they are approximately in kinetic equilibrium (cf. Eq. (A.20)),

$$f_X^{\mathrm{th}}(t,p) \approx \frac{N_X^{\mathrm{th}}(t)}{N_X^{\mathrm{eq}}(t)} f_X^{\mathrm{eq}}(t,p) \,, \quad f_X^{\mathrm{eq}}(t,p) = e^{-E_X/T} \,, \qquad X = N_1, \tilde{N}_1 \,. \tag{7.51}$$

This approximation holds, if the quotient $f_X^{\mathrm{th}}/f_X^{\mathrm{eq}}$, with f_X^{th} taken from Eq. (7.50), is independent of the (s)neutrino momentum p. To be able to check whether this is indeed the case at all times, we need to know the temperature of the thermal bath T as a function of time. The temperature T, however, is determined from the solution of the radiation Boltzmann equation, which, as we will see further below, also contains terms involving the distribution function f_X^{th}. Consequently, we are only able to examine the *self-consistency* of our approximation in Eq. (7.51). Given a solution for T, we can check *a posteriori* how well the approximate distribution function in Eq. (7.51) coincides with the exact expression in Eq. (7.50), i.e. to which extent the exact solution f_X^{th} indeed exhibits the same momentum dependence as f_X^{eq}. Neglecting all effects due to supersymmetry and the decay of the gauge DOFs, we perform such

[3] This statement presupposes, of course, that both thermal neutrinos and thermal sneutrinos start out with the same initial distribution function, which, however, is certainly the case. At $t = t_G$, we have $f_{N_1}^{\mathrm{th}} = f_{\tilde{N}_1}^{\mathrm{th}} = 0$.

an analysis for a particular point in parameter space. A detailed discussion of our findings is given in Appendix B of Ref. [58]. Here, we merely remark that, in the case of the investigated parameter point, $f_X^{\mathrm{th}}/f_X^{\mathrm{eq}}$ turns out to depend, in general, only very weakly on the (s)neutrino momentum p. For particularly small and large momenta, the ratio $f_X^{\mathrm{th}}/f_X^{\mathrm{eq}}$ initially deviates from its mean value $\langle f_X^{\mathrm{th}}/f_X^{\mathrm{eq}}\rangle_p$ by as much as one order of magnitude. In the course of the reheating process, the momentum dependence of $f_X^{\mathrm{th}}/f_X^{\mathrm{eq}}$ then vanishes almost completely. This is to say that the distribution function of the thermal (s)neutrinos steadily converges towards the equilibrium distribution in Eq. (7.51). From this perspective, the approximation of kinetic equilibrium may hence be regarded as justified.

Inelastic 2-to-2 scatterings of the (s)thermal neutrinos involving MSSM (s)quark pairs speed up the equilibration of the (s)neutrino distribution function [274]. This results in a larger abundance of thermal (s)neutrinos at earlier times. On the other hand, these scatterings also tend to increase the efficiency of washout processes such that, after all, their impact on the final lepton asymmetry generated in the decay of the thermal (s)neutrinos is negligible for our purposes. Again restricting ourselves to the nonsupersymmetric case and omitting the decay of the gauge DOFs, we are able to numerically confirm this picture by solving the relevant set of Boltzmann equations [58].

Assuming that the thermal (s)neutrinos are in kinetic equilibrium throughout the reheating process, Eq. (7.49) is easily integrated over momentum space. Eventually, we obtain

$$aH\frac{d}{da}N_X^{\mathrm{th}} = -\Gamma_X^{\mathrm{th}}\left(N_X^{\mathrm{th}} - N_X^{\mathrm{eq}}\right), \qquad X = N_1, \tilde{N}_1\,. \tag{7.52}$$

Here, N_X^{eq} denotes the comoving number density of the thermal (s)neutrinos in thermal equilibrium (cf. Eq. (A.19)) and Γ_X^{th} stands for the zero-temperature decay rate of the thermal (s)neutrinos, weighted with the corresponding average inverse time dilatation factor,

$$\Gamma_X^{\mathrm{th}} = \left\langle \frac{M_1}{E_X}\right\rangle_{\mathrm{th}}\Gamma_X^0 = \frac{a^3}{N_X^{\mathrm{th}}}\frac{g_N}{(2\pi)^3}\int d^3p\frac{M_1}{E_X}f_x^{\mathrm{th}}\,\Gamma_X^0 = \frac{K_1(M_1/T)}{K_2(M_1/T)}\,\Gamma_X^0\,, \quad X = N_1, \tilde{N}_1\,, \tag{7.53}$$

where K_1 and K_2 are the modified Bessel functions of the second kind of order 1 and 2.

7.1.3 MSSM Degrees of Freedom

All three generations of heavy (s)neutrinos exclusively decay into the lepton-Higgs pairs of the MSSM. Due the strong standard model gauge interactions, the heavy-(s)neutrino decay products immediately thermalize, so that the energy of a decaying (s)neutrino is always quickly distributed among all MSSM DOFs. In this sense, the energy transfer from the heavy (s)neutrinos to the thermal bath represents the actual reheating process after the $B-L$ phase transition. The production of entropy during reheating is conveniently described by means of the Boltzmann equation for the comoving number density N_R of MSSM or radiation quanta. Meanwhile, the decay of the heavy (s)neutrinos also entails the generation of a primordial

lepton asymmetry. Before turning to the radiation Boltzmann equation, let us derive the Boltzmann equation for the comoving number density $N_L = N_\ell - N_{\bar{\ell}}$, which characterizes the excess of leptons ℓ over antileptons $\bar{\ell}$.

Lepton Asymmetry

The Boltzmann equation for the lepton asymmetry L directly follows from the respective equations for the lepton supermultiplet ℓ and the antilepton supermultiplet $\bar{\ell}$,

$$\begin{aligned} \hat{\mathcal{L}} f_L &= \hat{\mathcal{L}} f_\ell - \hat{\mathcal{L}} f_{\bar{\ell}} \,, \\ \hat{\mathcal{L}} f_\ell &= \sum_i \Big[C_\ell(\ell H_u \leftrightarrow N_i) + C_\ell(\tilde{\ell}\tilde{H}_u \leftrightarrow N_i) + C_\ell(\ell \tilde{H}_u \leftrightarrow \tilde{N}_i^*) + C_\ell(\tilde{\ell} H_u \leftrightarrow \tilde{N}_i) \Big] + 2\,\mathcal{C}_\ell^{\rm red} \,, \end{aligned} \tag{7.54}$$

with $\mathcal{C}_\ell^{\rm red}$ being the reduced collision operator for all 2-to-2 scattering processes with a heavy (s)neutrino in the intermediate state which result in a change of the total lepton number by two units, i.e. $\Delta L = 2$ scatterings processes with lepton-Higgs pairs in the external states,

$$\begin{aligned} \mathcal{C}_\ell^{\rm red} = {} & C_\ell^{\rm red}(\ell H_u \leftrightarrow \bar{\ell} H_u^*) + C_\ell^{\rm red}(\tilde{\ell}\tilde{H}_u \leftrightarrow \tilde{\ell}^* \bar{\tilde{H}}_u) + C_\ell^{\rm red}(\ell H_u \leftrightarrow \tilde{\ell}^* \bar{\tilde{H}}_u) \\ & + C_\ell^{\rm red}(\tilde{\ell}\tilde{H}_u \leftrightarrow \bar{\ell} H_u^*) + C_\ell^{\rm red}(\ell \tilde{H}_u \leftrightarrow \tilde{\ell}^* H_u^*) + C_\ell^{\rm red}(\tilde{\ell} H_u \leftrightarrow \bar{\ell} \bar{\tilde{H}}_u) \,. \end{aligned} \tag{7.55}$$

The Boltzmann equation for the antilepton multiplet $\bar{\ell}$ is readily obtained by CP-conjugating each term in the Boltzmann equation for the lepton multiplet ℓ.

The ordinary collision operators in Eq. (7.54), accounting for the decays and inverse decays of the heavy (s)neutrinos $\big(N_i, \tilde{N}_i\big)$, are able to mimic $\Delta L = 2$ scatterings with on-shell (s)neutrinos in the intermediate state. They, however, disregard off-shell scatterings, even though these equally affect the evolution of the lepton asymmetry. To remedy this flaw, we have to include the reduced collision operators $\mathcal{C}_\ell^{\rm red}$ and $\mathcal{C}_{\bar{\ell}}^{\rm red}$ in the Boltzmann equations for ℓ and $\bar{\ell}$, which incorporate the off-shell contributions to all relevant $\Delta L = 2$ scattering processes. For $M_1 \ll 10^{14}$ GeV, the CP-preserving parts of the reduced collision operators are negligibly small [275]. We thus discard them, keeping only their CP-violating contributions,

$$\mathcal{C}_X^{\rm red} = \mathcal{C}_{X,CP}^{\rm red} + \mathcal{C}_{X,\not{C}\!\not{P}}^{\rm red} \approx \mathcal{C}_{X,\not{C}\!\not{P}}^{\rm red} \,, \qquad X = \ell, \bar{\ell} \,. \tag{7.56}$$

The operators $\mathcal{C}_{X,\not{C}\!\not{P}}^{\rm red}$ can be computed by calculating the CP-violating contributions $\mathcal{C}_{X,\not{C}\!\not{P}}$ to the full collision operators $\mathcal{C}_X$ and then subtracting their on-shell parts $\mathcal{C}_{X,\not{C}\!\not{P}}^{\rm on}$,

$$\mathcal{C}_{X,\not{C}\!\not{P}}^{\rm red} = \mathcal{C}_{X,\not{C}\!\not{P}} - \mathcal{C}_{X,\not{C}\!\not{P}}^{\rm on} \,, \qquad X = \ell, \bar{\ell} \,. \tag{7.57}$$

As we prove in Appendix B, the unitarity and CPT invariance of the S matrix imply that the CP-violating operators $\mathcal{C}_{X,\not{C}\!\not{P}}$ vanish up to corrections of $\mathcal{O}\left((h^\nu)^4\right)$. Hence, the inclusion of the reduced collision operators $\mathcal{C}_{X,\not{C}\!\not{P}}^{\rm red}$ is practically equivalent to the subtraction of the operators $\mathcal{C}_{X,\not{C}\!\not{P}}^{\rm on}$, which describe $\Delta L = 2$ scatterings with real intermediate states,

$$\mathcal{C}_{X,\not{C}\!\not{P}}^{\rm red} = -\mathcal{C}_{X,\not{C}\!\not{P}}^{\rm on} + \mathcal{O}\left((h^\nu)^4\right) \,, \qquad X = \ell, \bar{\ell} \,. \tag{7.58}$$

The individual collision operators $C_X^{\rm on}$ contributing to $\mathcal{C}_X^{\rm on}$ may be rewritten as collision operators for inverse decays of MSSM lepton-Higgs pairs into *real* heavy (s)neutrinos,

$$C_X^{\rm on}\left(I \leftrightarrow \bar{F}\right) = \sum_i \left[\mathrm{Br}\left(R_i \to I\right) C_X^{\rm on}\left(\bar{F} \to R_i\right) - \mathrm{Br}\left(R_i \to \bar{F}\right) C_X^{\rm on}\left(I \to R_i\right)\right] , \tag{7.59}$$

$$X = \ell, \bar{\ell}\,, \quad R_i = N_i\,, \quad F = I, \tilde{I} \text{ for } I = \ell H_u, \tilde{\ell}\tilde{H}_u\,;$$

$$R_i = \tilde{N}_i\,, \quad F = \tilde{I} \text{ for } I = \tilde{\ell}H_u\,; \quad R_i = \tilde{N}_i^*\,, \quad F = \tilde{I} \text{ for } I = \ell\tilde{H}_u\,.$$

Here, $\bar{F}$ represents the pair of antiparticles corresponding to the pair of particles F. Similarly, $\tilde{I}$ is the pair of superparticles corresponding to the pair of particles I. Note that this relation equally applies to the CP-conserving parts $C_{X,CP}^{\rm on}$ of the collision operators $C_X^{\rm on}$ as well as to their CP-violating parts $C_{X,\not{CP}}^{\rm on}$. After rewriting all operators $C_{X,\not{CP}}^{\rm on}$ as operators for inverse decays, the Boltzmann equations for ℓ and $\bar{\ell}$ end up solely containing collision operators, all of which respectively look like one of the following two prototypes,

$$C_X^{\rm on}(Xj \to R_i) = \frac{1}{2g_X}\int d\Pi\left(X|j;R_i\right)(2\pi)^4\,\delta^{(4)}\, f_X f_j\,|\mathcal{M}\left(Xj \to R_i\right)|^2\,, \tag{7.60}$$

$$C_X^{\rm on}(R_i \to Xj) = \frac{1}{2g_X}\int d\Pi\left(X|R_i;j\right)(2\pi)^4\,\delta^{(4)}\, f_{R_i}\,|\mathcal{M}\left(R_i \to Xj\right)|^2\,.$$

The only amplitudes squared which we have to calculate are hence those describing the decays and inverse decays of heavy (s)neutrinos. Using the definition of the CP violation parameters ϵ_i as well as CPT invariance, the various partial amplitudes squared can be related to the tree-level amplitudes squared $|\mathcal{M}_i|^2$,

$$|\mathcal{M}_i|^2 = \left|\mathcal{M}\left(N_i \leftrightarrow \ell H_u, \bar{\ell}H_u^*, \tilde{\ell}\tilde{H}_u, \tilde{\ell}^*\bar{\tilde{H}}_u\right)\right|^2 = 8\left[\,(h^\nu)^\dagger\, h^\nu\right]_{ii} M_i^2\,. \tag{7.61}$$

Up to first order in the CP violation parameters ϵ_i, one finds [185],

$$\begin{aligned}
&|\mathcal{M}(N_i \to \ell H_u)|^2 = |\mathcal{M}(\bar{\ell}H_u^* \to N_i)|^2 = |\mathcal{M}(N_i \to \tilde{\ell}\tilde{H}_u)|^2 = |\mathcal{M}(\tilde{\ell}^*\bar{\tilde{H}}_u \to N_i)|^2 \\
&= |\mathcal{M}(\tilde{N}_i^* \to \ell\tilde{H}_u)|^2 = |\mathcal{M}(\bar{\ell}\bar{\tilde{H}}_u \to \tilde{N}_i)|^2 = |\mathcal{M}(\tilde{N}_i \to \tilde{\ell}H_u)|^2 = |\mathcal{M}(\tilde{\ell}^* H_u^* \to \tilde{N}_i^*)|^2 \\
&= \frac{1}{4}\left(1+\epsilon_i\right)|\mathcal{M}_i|^2\,, \\
&|\mathcal{M}(N_i \to \bar{\ell}H_u^*)|^2 = |\mathcal{M}(\ell H_u \to N_i)|^2 = |\mathcal{M}(N_i \to \tilde{\ell}^*\bar{\tilde{H}}_u)|^2 = |\mathcal{M}(\tilde{\ell}\tilde{H}_u \to N_i)|^2 \\
&= |\mathcal{M}(\tilde{N}_i \to \bar{\ell}\bar{\tilde{H}}_u)|^2 = |\mathcal{M}(\ell\tilde{H}_u \to \tilde{N}_i^*)|^2 = |\mathcal{M}(\tilde{N}_i^* \to \tilde{\ell}^* H_u^*)|^2 = |\mathcal{M}(\tilde{\ell}H_u \to \tilde{N}_i)|^2 \\
&= \frac{1}{4}\left(1-\epsilon_i\right)|\mathcal{M}_i|^2\,.
\end{aligned} \tag{7.62}$$

The relations in Eqs. (7.59), (7.60) and (7.62) enable us to compute the reduced collision operators in the Boltzmann equations for ℓ and $\bar{\ell}$. As we are only interested in the CP-violating contributions $\mathcal{C}_{X,\not{CP}}^{\rm red}$ to the operators $\mathcal{C}_X^{\rm red}$, we solely take into account those parts of the various amplitudes squared which are proportional to ϵ_i. Working up to leading order in ϵ_i, it is sufficient to employ the tree-level results for the (s)neutrino branching ratios (cf.

Eq. (5.115)) and to approximate the distribution functions of all particles in the lepton and Higgs multiplets by Maxwell-Boltzmann distributions. This latter simplification allows us in particular to replace the product $f_X f_j$ in $C_X^{\rm on}(Xj \to R_i)$ (cf. Eq. (7.60)) by the (s)neutrino equilibrium distribution function $f_{N_i}^{\rm eq}$ (cf. Eq. (7.48)). Up to corrections of $\mathcal{O}\left(\epsilon_i^2\right)$, we find

$$\mathcal{C}^{\rm red}_{X,\not{CP}} \approx -\mathcal{C}^{\rm on}_{X,\not{CP}} = \mp\frac{1}{2g_X}\sum_i \epsilon_i \int d\Pi\,(X|j;R_i)\,(2\pi)^4\,\delta^{(4)} f_{N_i}^{\rm eq}\,|\mathcal{M}_i|^2\,, \qquad X=\ell,\bar{\ell}\,. \tag{7.63}$$

The collision operators describing the decays and inverse decays of the heavy (s)neutrinos are of a similar form. In contrast to the reduced collision operators, we, however, do not take the (s)leptons to be in thermal equilibrium, when calculating these operators. Combining our results for all collision operators, the Boltzmann equations for ℓ and $\bar{\ell}$ finally read

$$\begin{aligned}\hat{\mathcal{L}} f_X = \frac{1}{2g_X}\sum_i \int d\Pi\,(X|j;R_i)\,(2\pi)^4\,\delta^{(4)}\frac{1}{4}\,|\mathcal{M}_i|^2 \\ \times\left[(1\pm\epsilon_i)(2f_{N_i}+f_{\tilde{N}_i}+f_{\tilde{N}_i^*})\mp 8\epsilon_i f_{N_i}^{\rm eq} - 2(1\mp\epsilon_i) f_X f_j^{\rm eq}\right], \qquad X=\ell,\bar{\ell}\,.\end{aligned} \tag{7.64}$$

The difference of these two equations yields the Boltzmann equation for the lepton asymmetry,

$$\begin{aligned}\hat{\mathcal{L}} f_L = \frac{1}{2g_L}\sum_i \int d\Pi\,(L|j;R_i)\,(2\pi)^4\,\delta^{(4)}\,|\mathcal{M}_i|^2 \\ \times\left[\epsilon_i(f_{N_i}-f_{N_i}^{\rm eq}) + \frac{\epsilon_i}{2}(f_{\tilde{N}_i}+f_{\tilde{N}_i^*}-2f_{N_i}^{\rm eq}) - \frac{f_{N_i}^{\rm eq}}{2N_\ell^{\rm eq}}N_L\right],\end{aligned} \tag{7.65}$$

where we have used the fact that the MSSM (s)leptons are in kinetic equilibrium,

$$f_L = f_\ell - f_{\bar{\ell}} = \frac{N_\ell}{N_\ell^{\rm eq}} f_\ell^{\rm eq} - \frac{N_{\bar{\ell}}}{N_{\bar{\ell}}^{\rm eq}} f_{\bar{\ell}}^{\rm eq} = \frac{N_L}{N_\ell^{\rm eq}} f_\ell^{\rm eq}\,, \quad f_L f_j^{\rm eq} = \frac{N_L}{N_\ell^{\rm eq}} f_{N_i}^{\rm eq}\,. \tag{7.66}$$

Just as in the case of the Boltzmann equations for the heavy (s)neutrinos, we again split the (s)neutrino distribution functions into independently evolving components. The integration of Eq. (7.65) over the lepton number momentum space then provides us with the Boltzmann equation for the comoving number density N_L. Up to corrections of $\mathcal{O}\left(\epsilon_i^2, (h^\nu)^4\right)$, we obtain

$$aH\frac{d}{da}N_L = aH\frac{d}{da}\left(N_L^{\rm nt}+N_L^{\rm th}\right), \quad aH\frac{d}{da}N_L^{\rm x} = \hat{\Gamma}_L^{\rm x} N_L^{\rm x} - \hat{\Gamma}_W N_L^{\rm x}\,, \quad {\rm x}={\rm nt},{\rm th}\,, \tag{7.67}$$

with the washout rate $\hat{\Gamma}_W$ and the effective (non)thermal production rates $\hat{\Gamma}_L^{\rm nt,th}$ given by

$$\hat{\Gamma}_W = \sum_i \frac{N_{N_i}^{\rm eq}}{2N_\ell^{\rm eq}}\Gamma_{N_i}^{\rm th} \approx \frac{N_{N_1}^{\rm eq}}{2N_\ell^{\rm eq}}\Gamma_{N_1}^{\rm th}\,, \tag{7.68}$$

$$\hat{\Gamma}_L^{\rm nt} = \left(N_L^{\rm nt}\right)^{-1}\left[\sum_{R_i}\epsilon_i\left(\Gamma_{R_i}^{\rm PH}N_{R_i}^{\rm PH}+\Gamma_{R_i}^{G}N_{R_i}^{G}\right)+\epsilon_1\left(\Gamma_{N_1}^{S}N_{N_1}^{S}+\Gamma_{\tilde{N}_1}^{S}N_{\tilde{N}_1}^{S}\right)\right],$$

$$\hat{\Gamma}_L^{\rm th} = \left(N_L^{\rm th}\right)^{-1}\sum_i \epsilon_i\,\Gamma_{N_i}^{\rm th}\left(N_{N_i}^{\rm th}+N_{\tilde{N}_i}^{\rm th}-2N_{N_i}^{\rm eq}\right) \approx \left(N_L^{\rm th}\right)^{-1}\epsilon_1\,\Gamma_{N_1}^{\rm th}\left(N_{N_1}^{\rm th}+N_{\tilde{N}_1}^{\rm th}-2N_{N_1}^{\rm eq}\right).$$

Here, all quantities labeled with an index $\tilde{N}_i$ equally comprise the heavy sneutrinos $\tilde{N}_i$ *and* the heavy antisneutrinos $\tilde{N}_i^*$. As for the washout rate $\hat{\Gamma}_W$ and the thermal production rate $\hat{\Gamma}_L^{\mathrm{th}}$, we only consider the contributions from the first heavy (s)neutrino generation. Since $M_3 \sim M_3 \gg M_1$, the thermal as well as equilibrium abundances of the two heavier (s)neutrino generations, $N_{N_i}^{\mathrm{th}}$, $N_{\tilde{N}_i}^{\mathrm{th}}$ and $N_{N_i}^{\mathrm{eq}}$, where $i = 2, 3$, are strongly suppressed, so that we can safely neglect the corresponding terms in the Boltzmann equations. The various decay rates $\Gamma_{R_i}^{\mathrm{x}}$ are computed according to Eqs. (5.114) and (5.117). Note that explicit expressions for the rates $\Gamma_{N_1}^S$, $\Gamma_{\tilde{N}_1}^S$ and $\Gamma_{N_1}^{\mathrm{th}}$ are given in Eqs. (7.41) and (7.53), respectively. Meanwhile, the remaining rates, i.e. $\Gamma_{R_i}^{\mathrm{PH}}$ and $\Gamma_{R_i}^G$, can be easily calculated using our results for the distribution functions $f_{R_i}^{\mathrm{PH}}$ and $f_{R_i}^G$ in Eq. (7.24). We remark that Eq. (7.68) nicely illustrates the connection between the decay rates $\Gamma_{R_i}^{\mathrm{x}}$ on the one hand and the effective production rates $\hat{\Gamma}_W$ and $\hat{\Gamma}_L^{\mathrm{nt,th}}$ on the other hand. The latter describe in particular the relative change in the lepton asymmetry due to a given process and can hence be directly compared to the Hubble rate H in order to assess the efficiency of the respective process.[4] Furthermore, we point out that we have introduced N_L^{nt} and N_L^{th} in Eq. (7.67) to denote the nonthermal and thermal contributions to the total lepton asymmetry $N_L = N_L^{\mathrm{nt}} + N_L^{\mathrm{th}}$, respectively. The comparison of the corresponding final baryon asymmetries η_B^{nt} and η_B^{th} will eventually allow us to identify the relative importance of nonthermal and thermal leptogenesis in different regions of parameter space (cf. Secs. 7.2 and 7.3). For the parameters ϵ_i, we employ the Froggatt-Nielsen estimates in Eq. (3.72). The final baryon asymmetry inferred from the solution of the Boltzmann equation in Eq. (7.67) then corresponds to the maximum possible baryon asymmetry, i.e. an upper bound on the actually produced asymmetry. As we have seen in Sec. 4.2, in the context of the Froggatt-Nielsen model, we should, however, expect that the actually produced asymmetry, corresponding to the actual value of ϵ_1, is only slightly smaller than this upper bound (cf. Eq. (4.14)).

Radiation

The progress of the reheating process after the $B-L$ phase transition is reflected in the time evolution of the temperature of the thermal bath T. In principle, the behaviour of T as a function of time t is determined by the following non-linear first-order differential equation, which directly follows from the covariant energy conservation,

$$\dot{\rho}_{\mathrm{tot}} + 3H\left(\rho_{\mathrm{tot}} + p_{\mathrm{tot}}\right) = 0\,. \tag{7.69}$$

We, however, choose to pursue a different approach and infer the temperature T from the comoving number density of radiation quanta, i.e. MSSM particles, N_R (cf. Eq. (A.16)),

$$N_R = a^3\,\frac{\zeta(3)}{\pi^2}\,g_{*,n}\,T^3\,, \quad T = \left(\frac{\pi^2}{g_{*,n}\,\zeta(3)}\,\frac{N_R}{a^3}\right)^{1/3}\,. \tag{7.70}$$

[4] This is a general feature of any effective production rate $\hat{\Gamma}_i$. To see this, note that the Boltzmann equation for the number density n_X of a species X can always be written as $\dot{n}_X/n_X = \left(\hat{\Gamma}/H - 3\right)H$, where $\hat{\Gamma} = \sum_i \hat{\Gamma}_i$.

Similarly to the comoving number densities of all other species, the time evolution of N_R may be studied by means of an appropriate Boltzmann equation. Hence, deducing the temperature T from N_R has the advantage that it allows us to consistently describe the reheating process exclusively in terms of a set of Boltzmann equations for comoving number densities N_X.

While the Boltzmann equation for the lepton asymmetry L corresponds to the difference of the respective equations for ℓ and $\bar{\ell}$ (cf. Eq. (7.64) and (7.65)), the Boltzmann equation for the distribution function f_R of MSSM particles is related to the sum of these two equations,

$$\hat{\mathcal{L}} f_R = \hat{r}_R \left(\hat{\mathcal{L}} f_\ell + \hat{\mathcal{L}} f_{\bar{\ell}} \right) . \tag{7.71}$$

Here, $\hat{r}_R$ counts the number of radiation quanta effectively added to the thermal bath in the decay of a heavy (s)neutrino. It has to be thought of as an operator acting on the various (s)neutrino distribution functions $f^{\mathrm{x}}_{R_i}$ contained in $\hat{\mathcal{L}} f_{\ell,\bar{\ell}}$ in the following way,

$$\hat{r}_R f^{\mathrm{x}}_{R_i} = r^{\mathrm{x}}_{R_i} f^{\mathrm{x}}_{R_i} , \quad R_i = N_i, \tilde{N}_i , \quad \mathrm{x} = \mathrm{PH}, G, S, \mathrm{th} , \tag{7.72}$$

with $r^{\mathrm{x}}_{R_i}$ denoting the effective increase of radiation quanta due to the decay of a heavy (s)neutrino R_i which originates from a production mechanism x. Let us now derive an explicit expression for $r^{\mathrm{x}}_{R_i}$. We consider a spatial volume V in which heavy (s)neutrinos R^{x}_i of average energy $\varepsilon^{\mathrm{x}}_{R_i}$ decay into MSSM lepton-Higgs pairs. The (s)neutrino decay products thermalize practically instantaneously after their production, so that we may neglect the cosmic expansion for the moment. Per decay, the energy density of the thermal bath is then increased by $\varepsilon^{\mathrm{x}}_{R_i}/V$ and a new thermal equilibrium at a slightly higher temperature is established right after the decay,

$$\rho_R \to \rho_R + \frac{\varepsilon^{\mathrm{x}}_{R_i}}{V} , \quad T \to T \left(1 + \frac{1}{\rho_R} \frac{\epsilon^{\mathrm{x}}_{R_i}}{V} \right)^{1/4} . \tag{7.73}$$

This increase in T corresponds to an increase in the number density n_R (cf. Eq. (A.16)),

$$n_R \to n_R \left(1 + \frac{1}{\rho_R} \frac{\epsilon^{\mathrm{x}}_{R_i}}{V} \right)^{3/4} \simeq n_R + \frac{3}{4} \frac{n_R}{\rho_R} \frac{\varepsilon^{\mathrm{x}}_{R_i}}{V} = n_R + \frac{r^{\mathrm{x}}_{R_i}}{V} , \quad r^{\mathrm{x}}_{R_i} = \frac{3\,\varepsilon^{\mathrm{x}}_{R_i}}{4\,\varepsilon_R} , \quad \varepsilon_R = \frac{\rho_R}{n_R} . \tag{7.74}$$

Note that, similarly to ε_R, the average (s)neutrino energy $\varepsilon^{\mathrm{x}}_{R_i}$ may also be obtained as the ratio of the corresponding energy density to the corresponding number density, $\varepsilon^{\mathrm{x}}_{R_i} = \rho^{\mathrm{x}}_{R_i}/n^{\mathrm{x}}_{R_i}$.

With these remarks on the operator $\hat{r}_R$ in mind, we are now ready to write down the radiation Boltzmann equation. Neglecting all effects of CP violation, we find

$$\hat{\mathcal{L}} f_R = \frac{1}{2 g_R} \sum_i \int d\Pi \, (R|j;R_i) \, (2\pi)^4 \, \delta^{(4)} \, |\mathcal{M}_i|^2 \, \hat{r}_R \Big[f_{N_i} + \frac{1}{2} f_{\tilde{N}_i} + \frac{1}{2} f_{\tilde{N}_i^*} - 2 f^{\mathrm{eq}}_{N_i} \Big] . \tag{7.75}$$

After decomposing the (s)neutrino distribution functions into their respective components, the integration of this equation over momentum space yields the Boltzmann equation for the comoving number density N_R of MSSM DOFs,

$$aH \frac{d}{da} N_R = aH \frac{d}{da} \left(N^{\mathrm{nt}}_R + N^{\mathrm{th}}_R \right) = \hat{\Gamma}_R N_R , \quad aH \frac{d}{da} N^{\mathrm{x}}_R = \hat{\Gamma}^{\mathrm{x}}_R N^{\mathrm{x}}_R , \quad \mathrm{x} = \mathrm{nt}, \mathrm{th} , \tag{7.76}$$

where the effective (non)thermal production rates $\hat{\Gamma}_R^{\mathrm{nt,th}}$ are given by

$$\hat{\Gamma}_R^{\mathrm{nt}} = \left(N_R^{\mathrm{nt}}\right)^{-1} \left[\sum_{R_i} \left(r_{R_i}^{\mathrm{PH}} \Gamma_{R_i}^{\mathrm{PH}} N_{R_i}^{\mathrm{PH}} + r_{R_i}^{G} \Gamma_{R_i}^{G} N_{R_i}^{G} \right) + \left(r_{N_1}^{S} \Gamma_{N_1}^{S} N_{N_1}^{S} + r_{\tilde{N}_1}^{S} \Gamma_{\tilde{N}_1}^{S} N_{\tilde{N}_1}^{S} \right) \right], \tag{7.77}$$

$$\hat{\Gamma}_R^{\mathrm{th}} = \left(N_R^{\mathrm{th}}\right)^{-1} \sum_i r_{R_i}^{\mathrm{th}} \, \Gamma_{N_i}^{\mathrm{th}} \left(N_{N_i}^{\mathrm{th}} + N_{\tilde{N}_i}^{\mathrm{th}} - 2N_{N_i}^{\mathrm{eq}} \right) \approx \left(N_R^{\mathrm{th}}\right)^{-1} r_{R_1}^{\mathrm{th}} \, \Gamma_{N_1}^{\mathrm{th}} \left(N_{N_1}^{\mathrm{th}} + N_{\tilde{N}_1}^{\mathrm{th}} - 2N_{N_1}^{\mathrm{eq}} \right).$$

We note that this result for the radiation Boltzmann equation is very similar in form to the Boltzmann equation for the lepton asymmetry in Eq. (7.67). The only differences are that Eq. (7.76) contains no washout but only production terms and that it features the factors $r_{R_i}^{\mathrm{x}}$ instead of the CP violation parameters ϵ_i. Moreover, we point out that the factor $r_{R_i}^{\mathrm{th}}$ can be equally used to count the number of radiation quanta produced in the decay of thermal neutrinos N_i^{th} as well as the quanta produced in the decay of thermal sneutrinos $\tilde{N}_i^{\mathrm{th}}$. Likewise, it also applies to heavy (s)neutrinos in thermal equilibrium (cf. Eq. (A.19)),

$$r_{R_i}^{\mathrm{th}} = r_{N_i}^{\mathrm{th}} = r_{\tilde{N}_i}^{\mathrm{th}} = r_{N_i}^{\mathrm{eq}} = r_{\tilde{N}_i}^{\mathrm{eq}} = \frac{3\,\varepsilon_{R_i}^{\mathrm{th}}}{4\,\varepsilon_R}, \quad \varepsilon_{R_i}^{\mathrm{th}} = \varepsilon_{R_i}^{\mathrm{eq}} = 3T + \frac{K_1(M_i/T)}{K_2(M_i/T)} M_i \,. \tag{7.78}$$

We also remark that we have introduced the total radiation production rate $\hat{\Gamma}_R$ in Eq. (7.76),

$$\hat{\Gamma}_R = N_R^{-1} \, aH \frac{dN_R}{da} = N_R^{-1} \frac{dN_R}{dt} = \frac{N_R^{\mathrm{nt}}}{N_R} \hat{\Gamma}_R^{\mathrm{nt}} + \frac{N_R^{\mathrm{th}}}{N_R} \hat{\Gamma}_R^{\mathrm{th}} \,. \tag{7.79}$$

$\hat{\Gamma}_R$ counts the relative increase in the comoving radiation number density N_R per unit time. It will prove to be a useful quantity in our discussion of the reheating process in Sec. 7.2.

7.1.4 Gravitinos

Gravitinos are predominantly produced through inelastic QCD 2-to-2 scattering processes in the thermal bath.[5] The integrated Boltzmann equation governing the time evolution of the comoving gravitino number density $N_{\widetilde{G}}$ reads

$$aH \frac{d}{da} N_{\widetilde{G}} = \hat{\Gamma}_{\widetilde{G}} N_{\widetilde{G}} \,. \tag{7.80}$$

In supersymmetric QCD, up to leading order in the strong gauge coupling g_s, one obtains the following expression for the total production rate $\hat{\Gamma}_{\widetilde{G}}$ [43],

$$\hat{\Gamma}_{\widetilde{G}}(T) = \frac{a^3}{N_{\widetilde{G}}} \left(1 + \frac{m_{\tilde{g}}^2(T)}{3m_{\widetilde{G}}^2} \right) \frac{54\,\zeta(3)\,g_s^2(T)}{\pi^2 M_P^2} \, T^6 \left[\ln\left(\frac{T^2}{m_g^2(T)} \right) + 0.8846 \right], \tag{7.81}$$

Here, $m_{\tilde{g}}$ denotes the energy scale-dependent gluino mass and m_g is the gluon plasma mass,

$$m_{\tilde{g}}(t) = \frac{g_s^2(T)}{g_s^2(\mu_0)} \, m_{\tilde{g}}(\mu_0) \,, \quad m_g(t) = \sqrt{\frac{3}{2}} \, g_s(T) \, T \,. \tag{7.82}$$

[5] Cf. Sec. 3.1.4 for a comprehensive discussion of all conceivable gravitino production mechanisms.

As reference scale μ_0, we choose the Z boson mass $M_Z \simeq 91.18\,\text{GeV}$, where the strong coupling constant is given by $\alpha_s(\mu_0) = g_s^2(\mu_0)/(4\pi) \simeq 0.118$ [2]. The scale dependence of g_s is controlled by the corresponding MSSM renormalization group equation, which is solved by

$$g_s(\mu(T)) = g_s(\mu_0)\left[1 + \frac{3}{8\pi^2}\, g_s^2(\mu_0)\, \ln\frac{\mu(T)}{\mu_0}\right]^{-1/2} . \tag{7.83}$$

with μ being the typical energy scale during reheating. It can be estimated as the average energy per relativistic particle in the thermal bath, $\mu(T) \simeq \varepsilon_R \simeq 3T$. For instance at temperatures $T = 10^8, 10^{10}, 10^{12}$ GeV, the strong coupling constant therefore takes the values $g_s = 0.90, 0.84, 0.80$. The gravitino mass $m_{\tilde{G}}$ and the gluino mass at the electroweak scale $m_{\tilde{g}} = m_{\tilde{g}}(\mu_0)$ remain as free parameters.

7.2 Time Evolution of the Particle Abundances

Combining the initial conditions set by the $B-L$ phase transition with the Boltzmann equations derived in the previous section poses an initial-value problem. Its solution allows us to quantitatively describe the generation of entropy, matter and dark matter due to the production and decay of heavy (s)neutrinos. We have numerically solved this problem for all values of the input parameters within the ranges specified in Eq. (6.13). In this section, we will first illustrate our findings for a representative choice of parameter values. In Sec. 7.3, we will then turn to the investigation of the parameter space.

The results presented in this section were first published in Ref. [60]. In this paper, in contrast to our earlier studies [57, 58], we take into account all (super)particles involved in the reheating process, in particular the gauge DOFs. This allows us to give a realistic, time-resolved description of the reheating process. Furthermore, compared to Refs. [57, 58], we consider a higher $B-L$ scale, $v_{B-L} = 5\times 10^{15}$ GeV, in Ref. [60], which renders reheating after the $B-L$ phase transition compatible with hybrid inflation and cosmic strings (cf. Sec. 6.1).

7.2.1 Particle Masses and Couplings

Let us study the evolution of the universe after inflation for

$$M_1 = 5.4\times 10^{10}\,\text{GeV}\,, \quad \widetilde{m}_1 = 4.0\times 10^{-2}\,\text{eV}\,, \quad m_{\widetilde{G}} = 100\,\text{GeV}\,, \quad m_{\tilde{g}} = 1\,\text{TeV}\,. \tag{7.84}$$

As we will see later in Sec. 7.3.3, requiring successful leptogenesis as well as the right gravitino abundance to explain dark matter typically forces M_1 to be close to 10^{11} GeV. Here, we adjust its explicit numerical value such that, given the values for $\widetilde{m}_1$ and $m_{\widetilde{G}}$, the gravitino abundance comes out right in order to account for dark matter. The choice for $\widetilde{m}_1$ represents the best-guess estimate in the context of the Froggatt-Nielsen flavour model, which we obtained in

our Monte-Carlo study in Ch. 4 (cf. Eq. (4.14)). In scenarios of gravity- or gaugino-mediated supersymmetry breaking, the gravitino often acquires a soft mass of $\mathcal{O}(100)\,\mathrm{GeV}$, which is why we set $m_{\widetilde{G}}$ to $100\,\mathrm{GeV}$. A gluino mass of $1\,\mathrm{TeV}$ is close to the current lower bounds from ATLAS [276] and CMS [277]. The values in Eq. (7.84) readily determine several further important model parameters:

$$\begin{aligned} m_S &= 1.6 \times 10^{13}\,\mathrm{GeV}\,, & M_{2,3} &= 1.6 \times 10^{13}\,\mathrm{GeV}\,, & & \\ \Gamma_S^0 &= 1.9 \times 10\,\mathrm{GeV}\,, & \Gamma_{N_{2,3}}^0 &= 2.1 \times 10^{10}\,\mathrm{GeV}\,, & \Gamma_{N_1}^0 &= 3.0 \times 10^{5}\,\mathrm{GeV}\,, \\ \lambda &= 1.0 \times 10^{-5}\,, & \epsilon_{2,3} &= -1.6 \times 10^{-3}\,, & \epsilon_1 &= 5.3 \times 10^{-6}\,. \end{aligned} \tag{7.85}$$

Here, we have chosen opposite signs for the CP parameters ϵ_1 and $\epsilon_{2,3}$, so that the sign of the total lepton asymmetry always indicates which contribution from the various (s)neutrino decays is the dominant one.

Fig. 7.1 presents the comoving number and energy densities of all relevant species as functions of the scale factor a. In both panels of this figure, some of the displayed curves subsume a number of closely related species. These combined curves are broken down into their respective components in the two panels of Fig. 7.2 and in the lower panel of Fig. 7.3. The upper panel of Fig. 7.3 presents the temperature of the thermal bath as function of a. In what follows, we will go through the various stages of the evolution depicted in Figs. 7.1, 7.2 and 7.3 step by step. Subsequent to that, we will, based on the plots in Fig. 7.4, discuss the impact of supersymmetry and the particles of the gauge sector on our results.

7.2.2 Decay of the Massive Particles

Initial conditions

Tachyonic preheating transfers the bulk of the initial vacuum energy into Higgs bosons, $\rho_\sigma\left(a_{\mathrm{PH}}\right)/\rho_0 \simeq 1.0$, and only small fractions of it into nonrelativistic higgsinos, inflatons, gauge DOFs and (s)neutrinos $\left(N_i^{\mathrm{PH}}, \tilde{N}_i^{\mathrm{PH}}\right)$. The particles in the gauge multiplet decay immediately afterwards around $a = a_G$, giving rise to relativistic (s)neutrinos $\left(N_i^G, \tilde{N}_i^G\right)$ and an initial abundance of radiation, which thermalizes right away. Initially, this thermal bath neither exhibits a lepton asymmetry, nor are there any gravitinos present in it. The cosmic expansion between preheating and the decay of the gauge DOFs is practically negligible, $a_G \simeq a_{\mathrm{PH}} \equiv 1$. Note that technically all plots in Figs. 7.1, 7.2 and 7.3 start at $a = a_G$.

Decay of the (S)neutrinos of the Second and Third Generation

Among all particles present at $a = a_G$, the heavy (s)neutrinos of the second and third generation have the shortest lifetimes (cf. Eq. (7.85)). Due to time dilatation, the relativistic

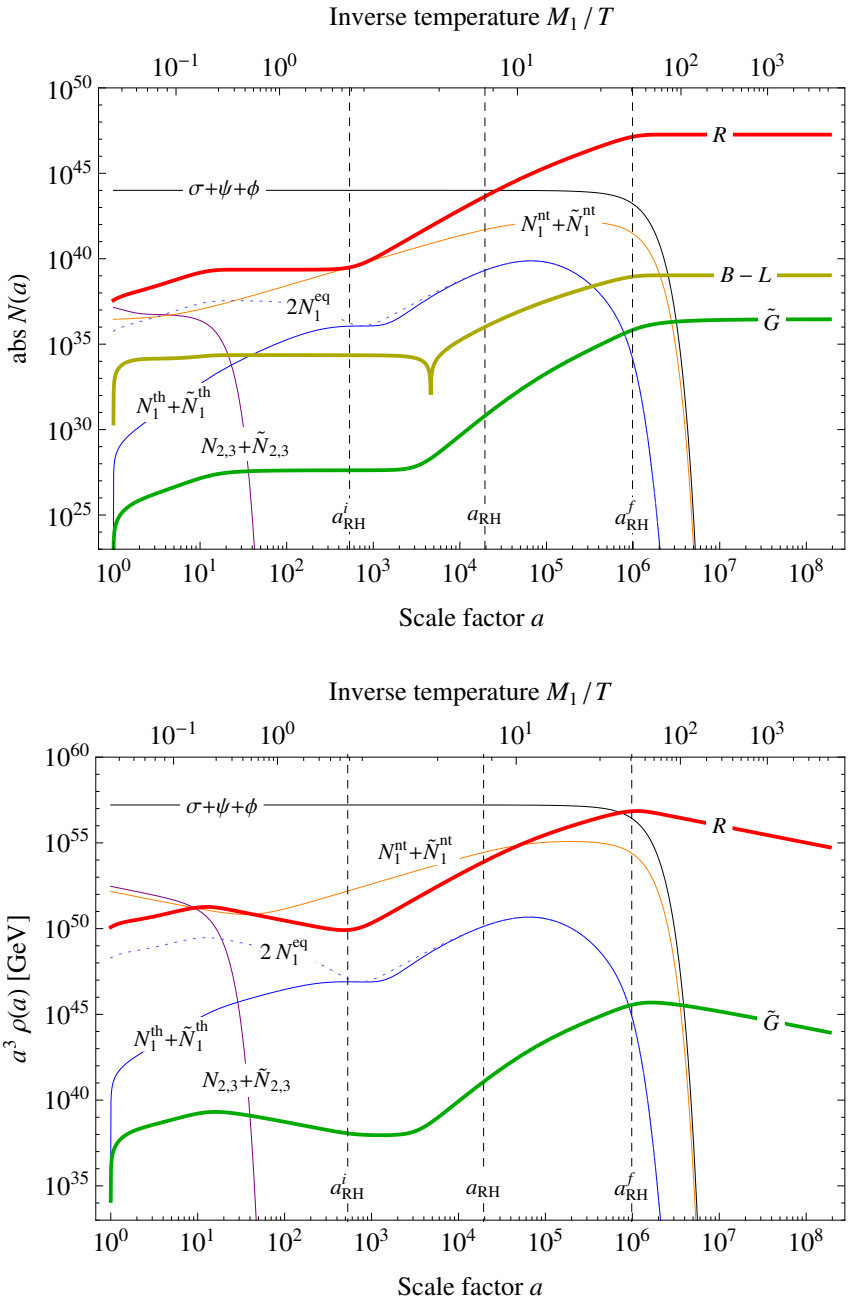

Figure 7.1: Comoving number densities **(upper panel)** and comoving energy densities **(lower panel)** for particles from the SSB sector (Higgs bosons σ + higgsinos ψ + inflatons ϕ), (non)thermally produced (s)neutrinos of the first generation ($N_1^{\rm th}+\tilde{N}_1^{\rm th}$, $N_1^{\rm nt}+\tilde{N}_1^{\rm nt}$), (s)neutrinos of the first generation in thermal equilibrium ($2N_1^{\rm eq}$, for comparison), (s)neutrinos of the second and third generation ($N_{2,3}+\tilde{N}_{2,3}$), the MSSM radiation (R), the lepton asymmetry ($B-L$), and gravitinos ($\widetilde{G}$) as functions of the scale factor a. The vertical lines labeled $a_{\rm RH}^i$, $a_{\rm RH}$ and $a_{\rm RH}^f$ mark the beginning, the middle and the end of the reheating process. The corresponding values for the input parameters are given in Eq. (7.84).

(s)neutrinos stemming from the decay of the gauge particles decay slower than the non-relativistic (s)neutrinos produced during preheating. The decay of the (s)neutrinos of the second and third generation is consequently responsible for an increase in the radiation number and energy densities on two slightly distinct time scales.

The gauge particles decay in equal shares into neutrinos and sneutrinos (cf. Sec. 7.1.2). Their number densities thus behave in exactly the same way, explaining the overlapping curves in Fig. 7.2. The production of radiation through the decay of these $N_{2,3}^G$ neutrinos and $\tilde{N}_{2,3}^G$ sneutrinos is efficient, as long as the radiation production rate $\hat{\Gamma}_R$ (cf. Eq. (7.79)) exceeds the Hubble rate H. At $a \simeq 11$, it drops below the Hubble rate, which roughly coincides with the value of the scale factor at which the comoving energy density of radiation reaches its first local maximum. The period between preheating and this first maximum of the radiation energy density can be regarded as the first stage of the reheating process. In the following, we shall refer to it as the stage of $N_{2,3}$ reheating.

Decay of the Particles of the Symmetry-Breaking Sector

The production of higgsinos and inflatons during preheating is roughly equally efficient, $N_\psi\left(a_{\mathrm{PH}}\right)/N_\phi\left(a_{\mathrm{PH}}\right) \simeq 1.0$. Taking into account the kinematic constraints resulting from the mass spectrum described in Sec. 3.2.2, all particles from the SSB sector exclusively decay into relativistic (s)neutrinos of the first generation $\left(N_1^S, \tilde{N}_1^S\right)$.

The majority of Higgs bosons, higgsinos and inflatons survives until $t_S = t_{\mathrm{PH}} + 1/\Gamma_S^0$ (cf. Eq. (5.111)), which corresponds to a scale factor of $a_S \simeq 7.2 \times 10^5$. Roughly up to this time, the main part of the total energy is stored in these particles. At later times, i.e. for $a \gtrsim a_S$, the energy budget is dominated by the energy in radiation.[6] Higgs bosons which decay earlier than the average lifetime are responsible for the generation of sizable abundances of N_1^S neutrinos and $\tilde{N}_1^S$ sneutrinos. The contributions from higgsino and inflaton decays to this process are essentially negligible.

Production and Decay of the Nonthermal (S)neutrinos of the First Generation

The decay of the particles from the SSB sector is the most important source for nonthermal (s)neutrinos. According to our discussion in Sec. 7.1.2, the ratio between the number densities of N_1^S neutrinos and $\tilde{N}_1^S$ sneutrinos is fixed to a constant value at all times (cf. Eq. (7.46)). For our choice of parameters, we find $N_{\tilde{N}_1}^S/N_{N_1}^S \simeq 4.4 \times 10^{-5}$. Moreover, the large hierarchy between the two decay rates $\Gamma_{N_1}^0$ and Γ_S^0 (cf. Eq. (7.85)) renders the N_1^S and $\tilde{N}_1^S$ number densities unable to exceed the number density of the Higgs bosons. From the perspective

[6] Note that in general the value of the scale factor at which the energy in radiation begins to dominate is determined by the lifetime of the most long-lived particle. In the case under study, the Higgs bosons have the longest lifetime. But for other parameter choices, it may be instead the (s)neutrinos of the first generation.

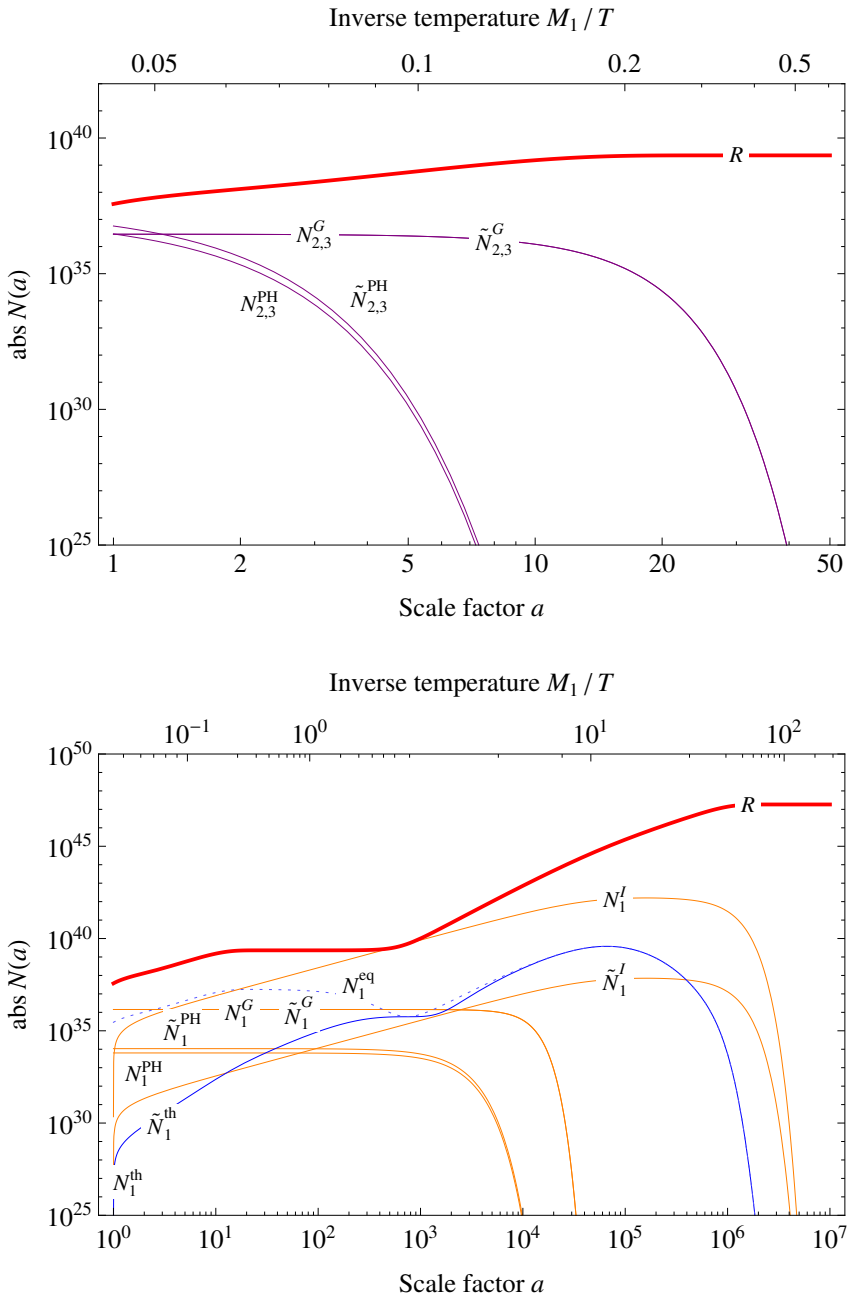

Figure 7.2: Breakdown of the comoving number densities shown in the upper panel of Fig. 7.1. The (s)neutrinos of the second and third generation ($N_{2,3}$+$\tilde{N}_{2,3}$) **(upper panel)** split into (s)neutrinos that are produced during preheating ($N_{2,3}^{\mathrm{PH}}$, $\tilde{N}_{2,3}^{\mathrm{PH}}$) and in the decay of the gauge DOFs ($N_{2,3}^{G}$, $\tilde{N}_{2,3}^{G}$). In all four cases, the sum of the contributions from both generations is shown. The (s)neutrinos of the first generation (N_1^{nt}+$\tilde{N}_1^{\mathrm{nt}}$, N_1^{th}+$\tilde{N}_1^{\mathrm{th}}$) **(lower panel)** split into (s)neutrinos that are produced during preheating (N_1^{PH}, $\tilde{N}_1^{\mathrm{PH}}$), in the decay of the gauge DOFs (N_1^{G}, $\tilde{N}_1^{G}$), in the decay of the particles from the SSB sector (N_1^{S}, $\tilde{N}_1^{S}$), and from the thermal bath (N_1^{th}, $\tilde{N}_1^{\mathrm{th}}$).

of the rather long-lived Higgs bosons, the (s)neutrinos essentially decay right after their production. As long as they are efficiently fueled by Higgs decays, the (s)neutrino number densities continue to rise. But once the supply of Higgs bosons is on the decline, they die out as well. The overall timescale of our scenario is hence controlled by the Higgs lifetime. However, as we will see below, the characteristic temperature of the reheating process is by contrast associated with the lifetime of the N_1^S neutrinos.

Further contributions to the abundances of nonthermal (s)neutrinos come from preheating as well as the decay of the gauge particles. Just as in the case of the second and third generation, the nonrelativistic (s)neutrinos produced during preheating decay at the fastest rate and the number densities of N_1^G neutrinos and $\tilde{N}_1^G$ sneutrinos are always the same.

7.2.3 Reheating and the Temperature of the Thermal Bath

Reheating through the Decay of N_1^S Neutrinos

The energy transfer from the nonthermal (s)neutrinos of the first generation to the thermal bath represents the actual reheating process. It is primarily driven by the decay of the N_1^S neutrinos, which soon exhibit the highest abundance among all (s)neutrino species. In analogy to the notion of $N_{2,3}$ reheating, we may now speak of N_1 reheating. This stage of reheating lasts as long as $\hat{\Gamma}_R \geq H$ (cf. Eq. (7.79)). Let us denote the two bounding values of the scale factor at which $\hat{\Gamma}_R = H$ by $a_{\rm RH}^i$ and $a_{\rm RH}^f$. In the case of our parameter example, we find $a_{\rm RH}^i \simeq 5.3 \times 10^2$ and $a_{\rm RH}^f \simeq 9.8 \times 10^5$. Between these two values of the scale factor, the comoving number density of radiation roughly grows like $N_R \propto a^3$. Around $a = a_{\rm RH}^i$, the comoving energy density of radiation reaches a local minimum and around $a = a_{\rm RH}^f$ a local maximum. Similarly, we observe that the end of reheating nearly coincides with the time at which the energy in radiation begins to dominate the total energy budget, $a_{\rm RH}^f \sim a_S$.

Plateau in the Evolution of the Temperature

The upper panel of Fig. 7.3 displays the temperature of the thermal bath T, calculated according to Eq. (7.70), as function of the scale factor a. As a key result of our analysis, we find that during N_1 reheating the temperature stays approximately constant. For a between $a_{\rm RH}^i$ and $a_{\rm RH}^f$, it varies by less than an order of magnitude. We thus conclude that in the first place $a_{\rm RH}^i$ and $a_{\rm RH}^f$ represent the limiting values for a plateau in the evolution of the radiation temperature. The origin of this plateau is the continuous production of N_1^S neutrinos during reheating. As long as these neutrinos are produced much faster than they decay, their comoving number density grows linearly in time, $N_{N_1}^S \propto \int_{t_{\rm PH}}^t dt'$ (cf. Eq. (7.44)). Taking into account that until $a \simeq a_S$ the expansion of the universe is driven by the energy in the Higgs bosons, i.e. nonrelativistic matter, this translates into $N_{N_1}^S \propto a^{3/2}$. The N_1^S number density

in turn controls the scaling behaviour on the right-hand side of the Boltzmann equation for radiation during N_1 reheating (cf. Eq. (7.76)). Using $H \propto a^{-3/2}$, we find

$$a_{\rm RH}^i \lesssim a \lesssim a_{\rm RH}^f : \quad aH\frac{d}{da}N_R \propto N_{N_1}^S \propto a^{3/2} , \quad N_R \propto a^3 , \quad T \approx \text{const.} \tag{7.86}$$

Reheating Temperature

The temperature at which the plateau in Fig. 7.3 is located sets the characteristic temperature scale of reheating. In addition, it represents the highest temperature that is ever reached in the thermal bath, as long as one restricts oneself to times at which the bath contains a significant fraction of the total energy budget of the universe (cf. lower panel of Fig. 7.1). To turn this qualitative understanding of the reheating temperature $T_{\rm RH}$ into a precise prescription for its calculation, we have to decide at which value of the scale factor $a_{\rm RH}$ we should read it off from the curve in Fig. 7.3. We choose the following intuitive definition: $a_{\rm RH}$ denotes the value of a when the decay of the N_1^S neutrinos into radiation is about to become efficient, which is the case once the Hubble rate H has dropped to the effective decay rate $\Gamma_{N_1}^S$,

$$\Gamma_{N_1}^S\left(a_{\rm RH}\right) = H\left(a_{\rm RH}\right) , \quad T_{\rm RH} = T\left(a_{\rm RH}\right) . \tag{7.87}$$

This prescription yields a temperature which is representative for the temperature plateau (cf. Fig. 7.3). For the chosen set of parameters, Eq. (7.87) has the following solution,

$$a_{\rm RH} \simeq 1.9 \times 10^4 , \quad H = \Gamma_{N_1}^S \simeq 3.5 \times 10^3 \text{ GeV} , \quad T_{\rm RH} \simeq 6.1 \times 10^9 \text{ GeV} . \tag{7.88}$$

In Figs. 7.1 and 7.4 as well as in the upper panel of Fig. 7.3, the three values of the scale factor marking the initial ($a_{\rm RH}^i$), characteristic intermediate ($a_{\rm RH}$) and final ($a_{\rm RH}^f$) point of the reheating process are indicated by dashed vertical lines.

Apart from the definition of the reheating temperature in Eq. (7.87), there are alternative ways to define the reheating temperature. For instance, we could use the temperature at the beginning ($a = a_{\rm RH}^i$) or the end of reheating ($a = a_{\rm RH}^f$) or the temperature when half of the total available energy has been transferred to radiation ($a \simeq a_S$ for the parameter example discussed in this section). In either case, although the respective value for $a_{\rm RH}$ may significantly vary, thanks to the temperature plateau during reheating, the resulting reheating temperature would not change much,

$$\frac{T\left(a_{\rm RH}^i\right)}{T_{\rm RH}} \simeq 1.5 , \quad \frac{T\left(a_S\right)}{T_{\rm RH}} \simeq \frac{1}{2.5} , \quad \frac{T\left(a_{\rm RH}^f\right)}{T_{\rm RH}} \simeq \frac{1}{3.0} . \tag{7.89}$$

Our definition of the reheating temperature may hence be regarded as a compromise between several more extreme approaches. But more important than that, it picks up on a physical feature that other definitions would miss. In Fig. 7.3, we observe that the temperature

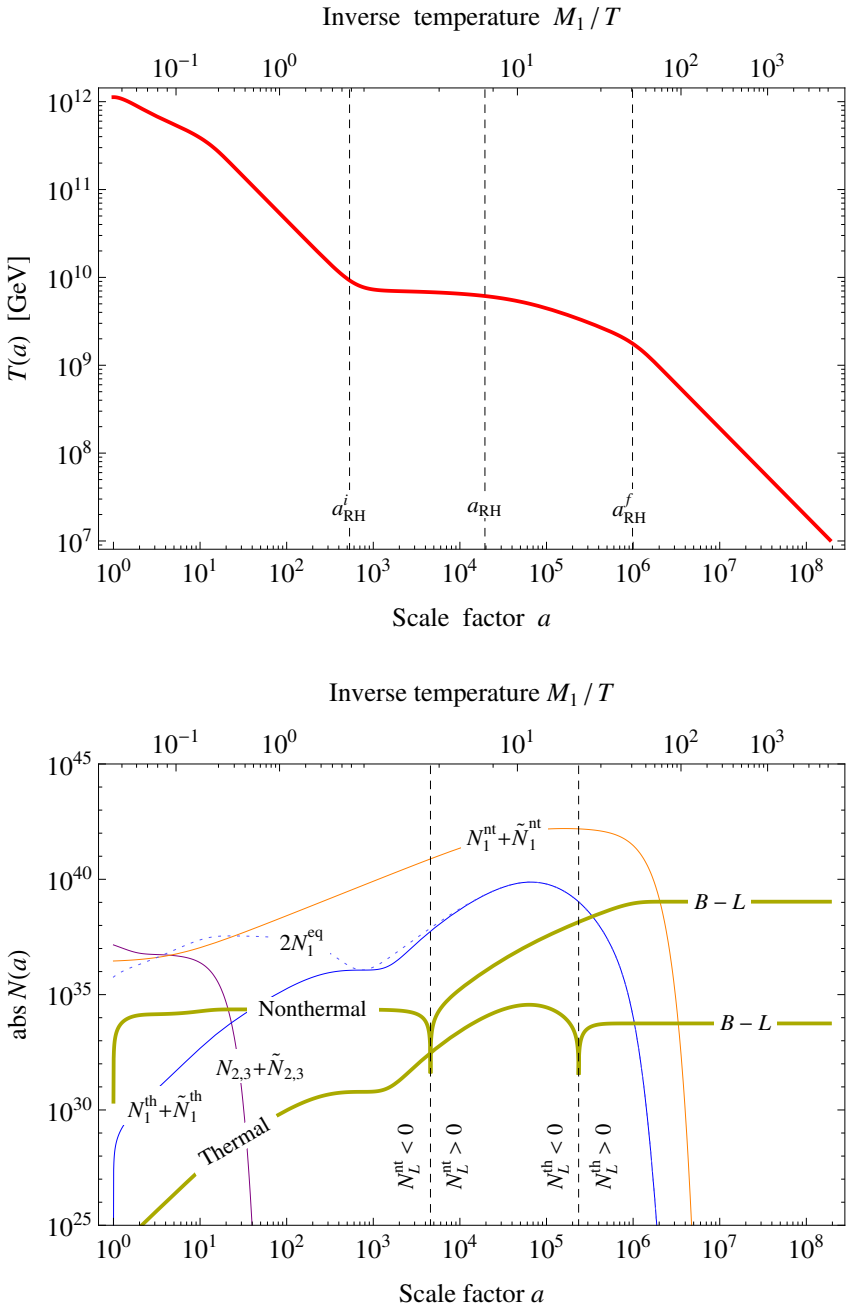

Figure 7.3: Temperature of the thermal bath T **(upper panel)** and comoving number densities for the nonthermal ($N_L^{\rm nt}$) and thermal ($N_L^{\rm th}$) contributions to the total lepton asymmetry as well as all (s)neutrino species ($N_1^{\rm nt}+\tilde{N}_1^{\rm nt}$, $N_1^{\rm th}+\tilde{N}_1^{\rm th}$, $2N_1^{\rm eq}$ for comparison, and $N_{2,3}+\tilde{N}_{2,3}$) **(lower panel)** as functions of the scale factor a. The vertical lines in the upper panel labeled $a^i_{\rm RH}$, $a_{\rm RH}$ and $a^f_{\rm RH}$ mark the beginning, the middle and the end of the reheating process. The vertical lines in the lower panel respectively mark the changes in the signs of the two components of the lepton asymmetry.

declines less during the first part of reheating, $a^i_{\rm RH} \leq a \leq a_{\rm RH}$, than during the second part, $a_{\rm RH} \leq a \leq a^f_{\rm RH}$. The stage of N_1 reheating evidently splits up into two phases, during the first of which the temperature is basically constant, whereas during the second one the temperature slightly decreases. The reason for this substructure in the temperature plateau is the following. As soon as the N_1^S neutrinos decay more efficiently, their comoving number density starts to grow slower than $a^{3/2}$. This diminishes the production rate of radiation. According to Eq. (7.86), a constant temperature can then no longer be maintained. The advantage of our definition for $T_{\rm RH}$ now is that we read it off from the curve in Fig. 7.3 at exactly that value of the scale factor at which the transition between these two phases of N_1 reheating takes place. Our definition thus yields a temperature which is both representative, as it mediates between several more extreme values, and especially singled out, as it is associated with a prominent feature in the temperature curve.

For completeness, we should however mention that for other parameter choices this picture may change. If the Higgs decay rate Γ_S^0 is, for instance, larger than the neutrino decay rate $\Gamma_{N_1}^S$, which can for example be achieved by going to lower values of the $B-L$ scale, the scaling behaviour of the N_1^S number density changes when the neutrino production efficiency begins to cease and not when the decays of the neutrinos themselves set in. The slight kink in the temperature plateau is then located at $a \simeq a_S$, which is in this case before the decay of the N_1^S neutrinos has become fully efficient. But the definition of the reheating temperature in Eq. (7.87) remains reasonable nonetheless. After all, if $\Gamma_S^0 > \Gamma_{N_1}^S$, the bulk of the total energy is first almost entirely accumulated in N_1^S neutrinos, before it is passed on to radiation. The energy in radiation thus receives its major contribution just when these neutrinos decay with a sufficient efficiency. The characteristic temperature at the time when this happens is then again obtained from Eq. (7.87). Further details on the reheating temperature in regions in parameter space in which $\Gamma_S^0 > \Gamma_{N_1}^S$ can be found in Ref. [58].

Evolution of the Temperature off the Plateau

During $N_{2,3}$ reheating, the temperature first increases up to a maximal value and then decreases like $a^{-1/2}$. The initial rise reflects the production of radiation through the decays of the (s)neutrinos of the second and third generation as long as the expansion of the universe is negligible. The subsequent decrease then follows from the Boltzmann equation for radiation (cf. Eq. (7.76)), using the fact that its right-hand side stays almost constant up to the end of $N_{2,3}$ reheating,

$$a_G \lesssim a \lesssim 11 : \quad aH\frac{d}{da}N_R \propto N^G_{N_{2,3}} \approx \text{const.}\,, \quad N_R \propto a^{3/2}\,, \quad T \propto a^{-1/2}\,. \tag{7.90}$$

Finally, we note that, between the two stages of reheating and after the end of reheating, the temperature drops off like a^{-1}. This is the usual adiabatic behaviour indicating that no

radiation, i.e. entropy, is being produced,

$$11 \lesssim a \lesssim a_{\mathrm{RH}}^{i} \text{ and } a_{\mathrm{RH}}^{f} \lesssim a : \quad aH\frac{d}{da}N_R \approx 0\,, \quad N_R \approx \text{const.}\,, \quad T \propto a^{-1}\,. \tag{7.91}$$

7.2.4 Small Departures from Thermal Equilibrium

Production and Decay of the Thermal (S)neutrinos of the First Generation

Unlike the two heavier (s)neutrino flavours, the (s)neutrinos of the first generation are also produced thermally $\left(N_i^{\mathrm{th}}, \tilde{N}_i^{\mathrm{th}}\right)$. Thanks to supersymmetry, the evolution of the N_1^{th} and $\tilde{N}_1^{\mathrm{th}}$ number densities is governed by exactly the same Boltzmann equation (cf. Eq. (7.52)), so that they are identical at all times. As both species inherit their momentum distribution from the thermal bath, they are always approximately in kinetic equilibrium.[7] Simultaneously, the interplay between decays and inverse decays drives them towards thermal equilibrium. Initially, there are no thermal (s)neutrinos present in the thermal bath and inverse decays result in a continuous rise of the thermal (s)neutrino number densities until $a \sim a_{\mathrm{RH}}^{i}$. Around this time, the temperature drops significantly below the mass M_1 and the thermal (s)neutrinos become nonrelativistic. The equilibrium number density $N_{N_1}^{\mathrm{eq}}$ begins to decrease due to Boltzmann suppression, until it almost reaches the actual number density of the thermal (s)neutrinos. The production of thermal (s)neutrinos can then no longer compete with the expansion of the universe and their comoving number densities do not continue to grow.

This picture, however, soon changes because reheating sets in. As the temperature remains almost perfectly constant until $a \sim a_{\mathrm{RH}}$, the equilibrium number density $N_{N_1}^{\mathrm{eq}}$ is not diminished due to Boltzmann suppression any further up to this time. Instead, it bends over and starts to increase like the volume, $N_{N_1}^{\mathrm{eq}} \propto a^3$. The number densities of the thermal (s)neutrinos subsequently follow this behaviour of the equilibrium number density. During the second phase of N_1 reheating, the temperature slightly decreases again, thereby reinforcing the Boltzmann factor in $N_{N_1}^{\mathrm{eq}}$. Consequently, the equilibrium number density stops growing and shortly afterwards starts to decline exponentially. An instant after it has passed its global maximum, the number densities of the thermal (s)neutrinos overshoot the equilibrium number density. Due to their numerical proximity, the two values of the scale factor at which $N_{N_1}^{\mathrm{eq}}$ and $N_{N_1}^{\mathrm{th}}$ respectively reach their global maxima cannot be distinguished from each other in Figs. 7.1. Both events occur close to $a = 6.6 \times 10^4$.

Generation of the Baryon Asymmetry

The out-of-equilibrium decays of the heavy (s)neutrinos violate L, C, and CP, thereby generating a lepton asymmetry in the thermal bath. A first nonthermal asymmetry is introduced

[7] For a more detailed discussion, cf. Sec. 7.1.2 and Appendix B of Ref. [58].

to the thermal bath during $N_{2,3}$ reheating. For $a_G \lesssim a \lesssim 2.2$, the decay of the (s)neutrinos stemming from preheating leads to an increase of the absolute value of the comoving number density $N_L^{\rm nt}$. In the interval $6.6 \lesssim a \lesssim 13$, the lepton asymmetry is slightly augmented through the decay of the (s)neutrinos which were produced in the decay of the gauge particles. The main part of the nonthermal asymmetry is, however, generated during N_1 reheating, while the scale factor takes values between $a \simeq 2.0 \times 10^3$ and $a \simeq 1.3 \times 10^6$. At all other times, the effective rate at which the nonthermal asymmetry is produced is at least half an order of magnitude smaller than the Hubble rate. Among all nonthermal (s)neutrinos of the first generation, only the N_1^S neutrinos contribute efficiently to the generation of the asymmetry. Their decay results in a positive nonthermal asymmetry that gradually overcompensates the negative asymmetry produced during $N_{2,3}$ reheating. At $a \simeq 4.6 \times 10^3$, the entire initial asymmetry has been erased and $N_L^{\rm nt}$ changes its sign.

Washout processes almost do not have any impact on the evolution of the nonthermal asymmetry. The rate $\hat{\Gamma}_W$, at which these processes occur (cf. Eq. (7.68)), is always smaller than the Hubble rate H by a factor of at least $\mathcal{O}(10)$. On top of that, at the time $\hat{\Gamma}_W$ is closest to H, which happens around $a \simeq 4.0 \times 10^4$ when $\hat{\Gamma}_W/H \simeq 0.12$, the production rate $\hat{\Gamma}_L^{\rm nt}$ is constantly larger than $\hat{\Gamma}_W$ by a factor of $\mathcal{O}(10)$, so that the effect of washout on the nonthermal asymmetry is indeed always negligible.

The decays and inverse decays of thermal (s)neutrinos of the first generation are responsible for the emergence of a thermal, initially negative asymmetry in the bath. As long as the abundance of thermal (s)neutrinos is far away from the one in thermal equilibrium, the absolute value of this asymmetry increases rapidly. Around $a \sim a_{\rm RH}^i$, this is not the case anymore, causing the production of the thermal asymmetry to stall for a short moment. At $a \simeq 6.3 \times 10^4$, the washout rate $\hat{\Gamma}_W$ overcomes the production rate $\hat{\Gamma}_L^{\rm th}$ of the thermal asymmetry and its absolute value begins to decline. Note that, at this time, the rates $\hat{\Gamma}_L^{\rm th}$ and $\hat{\Gamma}_W$ are smaller than H by roughly a factor 9. Shortly afterwards, at $a \simeq 6.6 \times 10^4$, the number density of thermal (s)neutrinos overshoots the equilibrium density, which results in the asymmetry being driven even faster towards zero. Already at $a \simeq 2.3 \times 10^5$, the initial thermal asymmetry is completely erased. Meanwhile, washout effects recede in importance. From $a \simeq 6.9 \times 10^4$ onwards, $\hat{\Gamma}_L^{\rm th}$ permanently dominates over $\hat{\Gamma}_W$, which is why, once the thermal asymmetry has turned positive, it does not decrease anymore. Instead, it freezes out at its maximal value around $a \simeq 4.5 \times 10^5$, which corresponds to the time when the ratio of $\Gamma_L^{\rm th}$ and the Hubble rate H drops below $1/\sqrt{10}$.

The final values of $N_L^{\rm nt,th}$ allow us to infer the present baryon asymmetry η_B as well as its composition in terms of a nonthermal ($\eta_B^{\rm nt}$) and a thermal ($\eta_B^{\rm th}$) contribution (cf. Eq. (2.34)),

$$\eta_B = \frac{n_B^0}{n_\gamma^0} = \eta_B^{\rm nt} + \eta_B^{\rm th}\,, \quad \eta_B^{\rm nt,th} = C_{\rm sph}\frac{g_{*,s}^0}{g_{*,s}}\,\frac{N_L^{\rm nt,th}}{N_\gamma}\bigg|_{a_f}\,. \tag{7.92}$$

Here, $C_{\mathrm{sph}} = 8/23$ denotes the sphaleron conversion factor (cf. Eq. (2.33)), $g_{*,s} = 915/4$ and $g^0_{*,s} = 43/11$ stand for the effective numbers of relativistic DOFs in the MSSM that enter the entropy density s_R of the thermal bath in the high- and low-temperature regime, respectively (cf. Eqs. (2.9) and (A.18)), and $N_\gamma = g_\gamma / g_{*,n}\, N_R$ is the comoving number density of photons. As final value for the scale factor, we use $a_f \simeq 1.9 \times 10^8$, which is the maximal value depicted in the two plots of Fig. 7.1. Since we are not able to predict the signs of the CP violation parameters ϵ_i in any case, we do not bother about the relative sign between the lepton and the baryon asymmetry and simply take η_B, η_B^{nt} and η_B^{th} to have the same signs as N_L, N_L^{nt} and N_L^{th}. In our parameter example, we then find

$$\eta_B \simeq 3.7 \times 10^{-9}\,, \quad \eta_B^{\mathrm{nt}} \simeq 3.7 \times 10^{-9}\,, \quad \eta_B^{\mathrm{th}} \simeq 1.9 \times 10^{-14}\,. \tag{7.93}$$

Recall that in Sec. 3.2.2, we set the CP asymmetry parameter ϵ_1 to its maximal value (cf. Eq. (3.72)). In this sense, the resulting values for the baryon asymmetry must be interpreted as upper bounds on the actually produced asymmetry and are thus perfectly compatible with the observed value for the baryon asymmetry, $\eta_B^{\mathrm{obs}} \simeq 6.2 \times 10^{-10}$ (cf. Sec. 2.1.3). We also recall that, in fact, the Froggatt-Nielsen model typically predicts values for ϵ_1 that are smaller than the maximal possible value by roughly a factor of $\mathcal{O}(10)$ (cf. Eq. (4.14)). Using a generic value for ϵ_1 according to the Froggatt-Nielsen model, rather than estimating ϵ_1 by means of its upper bound, would thus yield an excellent agreement between prediction and observation in the context of our parameter example, $\eta_B \simeq \eta_B^{\mathrm{obs}}$.

Furthermore, we find that in the case under study, it is the nonthermal contribution η_B^{nt} that lifts the total baryon asymmetry η_B above the observational bound. The thermal contribution η_B^{th} is smaller than η_B^{nt} by five orders of magnitude. If we discarded the entire idea of nonthermally produced (s)neutrinos being the main source of the lepton asymmetry and resorted to standard thermal leptogenesis, we would struggle to reproduce the observed asymmetry. For the chosen value of $\widetilde{m}_1$, standard leptogenesis would result in $\eta_B^{\mathrm{st}} \sim 10^{-10}$, which is almost an order of magnitude below the observed value (cf. Ref. [38] for details). By contrast, it is still much larger than our result for η_B^{th}. This has mainly two reasons. First, in our scenario, the decays of the nonthermal (s)neutrinos continuously increase the entropy of the thermal bath (cf. Figs. 7.1 and 7.3), which results in a nonstandard dilution of the thermal asymmetry during and after its production. Between, for instance, $a \simeq 6.3 \times 10^4$, which corresponds to the time when the production of the negative asymmetry is reversed and the absolute value of the asymmetry starts to decline, and $a = a_f$, the entropy of the thermal bath increases by a factor of $\mathcal{O}(100)$. Second, in consequence of the specific reheating mechanism at work, the generation of the thermal asymmetry is delayed in time, so that it takes place at a lower temperature than in the standard case. This implies a correspondingly smaller abundance of thermal (s)neutrinos, rendering our thermal mechanism for the generation of an asymmetry less efficient. We will resume this comparison of the thermal asymmetry η_B^{th} with the expectation from standard leptogenesis η_B^{st} in Sec. 7.3.2, where we will discuss the

respective dependences on the neutrino mass parameters $\widetilde{m}_1$ and M_1.

Production of Gravitino Dark Matter

Inelastic 2-to-2 scattering processes in the supersymmetric thermal plasma, mediated predominantly via the strong interaction, are responsible for the production of dark matter in the form of gravitinos. As the right-hand side of the gravitino Boltzmann equation (cf. Eq. (7.80)) scales like $a^3 T^6$, the efficiency of gravitino production in the course of reheating is directly controlled by the interplay between the expansion of the universe and the evolution of the temperature of the thermal bath.

During $N_{2,3}$ reheating, the temperature roughly declines as $T \propto a^{-1/2}$ (cf. Eq. (7.90)), such that in first approximation

$$aH\frac{d}{da}N_{\widetilde{G}} = \hat{\Gamma}_{\widetilde{G}} N_{\widetilde{G}} \propto a^3 T^6 \approx \text{const.}\,, \quad \hat{\Gamma}_{\widetilde{G}} \propto H \propto a^{-3/2}\,, \quad N_{\widetilde{G}} \propto a^{3/2}\,. \tag{7.94}$$

Once the decay of the (s)neutrinos of the second and third generation has ceased, the temperature decreases adiabatically, $T \propto a^{-1}$ or equivalently $a^3 T^6 \propto a^{-3}$ (cf. Eq. (7.91)). The rate of gravitino production $\hat{\Gamma}_{\widetilde{G}}$ then begins to decrease much faster than the Hubble rate, in fact, initially even slightly faster than a^{-3}, causing the comoving gravitino number density $N_{\widetilde{G}}$ to approach a constant value. The first stage of gravitino production is completed around $a \simeq 28$, which corresponds to the time when $\hat{\Gamma}_{\widetilde{G}}$ is half an order of magnitude smaller than H. From this time onwards, $\hat{\Gamma}_{\widetilde{G}}$ scales like a^{-3}, the production term in the Boltzmann equation is negligibly small and $N_{\widetilde{G}}$ is constant.

The decline of $\hat{\Gamma}_{\widetilde{G}}$ is reversed as soon as the temperature plateau characteristic for the phase of N_1 reheating is reached, such that approximately $a^3 T^6 \propto a^3$. While $\hat{\Gamma}_{\widetilde{G}} \ll H$, the gravitino density $N_{\widetilde{G}}$ continues to remain constant and $\hat{\Gamma}_{\widetilde{G}}$ increases almost as fast as a^3. At $a \simeq 1.9 \times 10^3$, it has nearly caught up again with the Hubble rate, i.e. the ratio $\hat{\Gamma}_{\widetilde{G}}/H$ reaches again a value of $1/\sqrt{10}$. This time marks the beginning of the second stage of gravitino production. The production term in the Boltzmann equation cannot be neglected any longer and, assuming for a moment an exactly constant temperature during N_1 reheating, we have

$$aH\frac{d}{da}N_{\widetilde{G}} = \hat{\Gamma}_{\widetilde{G}} N_{\widetilde{G}} \propto a^3 T^6 \propto a^3\,, \quad \hat{\Gamma}_{\widetilde{G}} \propto H \propto a^{-3/2}\,, \quad N_{\widetilde{G}} \propto a^{9/2}\,. \tag{7.95}$$

The gravitino density $N_{\widetilde{G}}$ hence begins to grow again, now even faster than during $N_{2,3}$ reheating. This terminates the rise of the rate $\hat{\Gamma}_{\widetilde{G}}$, turning it into a decline proportional to $a^{-3/2}$. We thus obtain the interesting result that, although the temperature evolves differently during $N_{2,3}$ and N_1 reheating, the rate $\hat{\Gamma}_{\widetilde{G}}$ always runs parallel to the Hubble rate during these two stages of the reheating process.

At the end of N_1 reheating, gravitino productions fades away in the same way as at the end of $N_{2,3}$ reheating. Around $a \simeq 3.5 \times 10^6$, when $\hat{\Gamma}_{\widetilde{G}}/H$ drops below $1/\sqrt{10}$, the gravitino

abundance freezes out. The final value of $N_{\widetilde{G}}$ then allows us to calculate $\Omega_{\widetilde{G}}h^2$, the present energy density of gravitinos $\rho^0_{\widetilde{G}}$ in units of ρ_c/h^2,

$$\Omega_{\widetilde{G}}h^2 = \frac{\rho^0_{\widetilde{G}}}{\rho_c/h^2} = \frac{m_{\widetilde{G}}n^0_\gamma}{\rho_c/h^2}\frac{g^0_{*,s}}{g_{*,s}}\left.\frac{N_{\widetilde{G}}}{N_\gamma}\right|_{a_f}, \tag{7.96}$$

where $\rho_c = 1.05 \times 10^{-5}\, h^2\,\mathrm{GeV\,cm^{-3}}$ denotes the critical energy density of the universe (cf. Eq. (2.3)), $h = 0.70$ the Hubble rate H in the units $H = h \times 100\,\mathrm{km\,s^{-1}\,Mpc^{-1}}$, $n^0_\gamma = 410\,\mathrm{cm^{-3}}$ the number density of the CMB photons (cf. Eq. (2.2)), and $g_{*,s}$, $g^0_{*,s}$, N_γ, and a_f are explained below Eq. (7.92). Recall that, after fixing $\widetilde{m}_1$, $m_{\widetilde{G}}$ and $m_{\tilde{g}}$, we adjusted the heavy neutrino mass, $M_1 = 5.4 \times 10^{10}$ GeV, such that we would obtain the right abundance of gravitinos to account for the relic density of dark matter, $\Omega^{\mathrm{obs}}_{\mathrm{DM}}h^2 \simeq 0.11$ (cf. Sec. 2.1.4). By construction, we thus now find in our parameter example

$$\Omega_{\widetilde{G}}h^2 \simeq 0.11\,. \tag{7.97}$$

In conclusion, we emphasize the intriguing simplicity of this mechanism for the generation of dark matter. Let us in particular focus on the physical picture behind the second stage of gravitino production. Initially, at the onset of N_1 reheating, the rate $\hat{\Gamma}_{\widetilde{G}}$ is still very small compared to the Hubble rate H. But, given the constant spacetime density of gravitino production $\gamma_{\widetilde{G}} = n_{\widetilde{G}}\hat{\Gamma}_{\widetilde{G}} \propto T^6$ during N_1 reheating and the rapid growth of the spatial volume due to the expansion, $\hat{\Gamma}_{\widetilde{G}}$ rapidly grows sufficiently large to set the production of gravitinos going. During the remaining time of N_1 reheating, this production can then proceed without further hindrance as the universe, although it is expanding, is filled by a thermal bath at a constant temperature. The continuous production of radiation nullifies the expansion and gravitinos are produced as in a static universe. In other words, one key feature of our scenario of reheating is that it turns the universe into a chemistry laboratory, in which the temperature is fixed at a certain value, so that dark matter can be cooked in it just to the right point.

7.2.5 Robustness against Theory Uncertainties

In the previous part of this chapter, we discussed in detail the emergence of the hot thermal universe after inflation. The successful explanation of reheating as well the generation of matter and dark matter by means of our scenario did, however, not rely on any fortunate coincidence between certain particulars, but was a direct consequence of the overall setup that we considered. The essential steps in the evolution after symmetry breaking were the following. Preheating results in an initial state the energy density of which is dominated by nonrelativistic Higgs bosons. These decay slowly into nonthermal neutrinos of the first generation, which in turn decay into radiation, thereby reheating the universe, generating a lepton asymmetry and setting the stage for the thermal production of gravitinos. At the

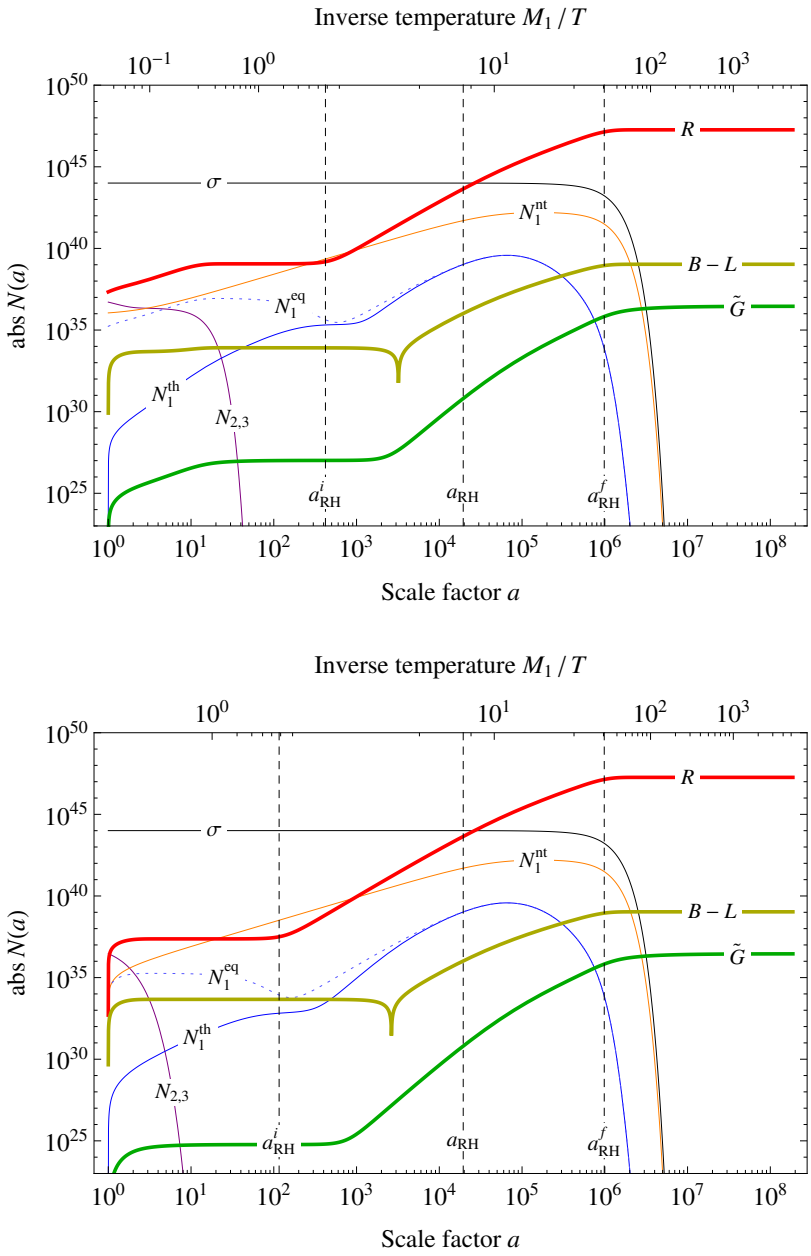

Figure 7.4: Comoving number densities after omitting all massive superparticles (**upper panel**) and in addition the $B-L$ vector boson (**lower panel**), to be compared with the result of the full analysis in Fig. 7.1. The individual curves show the comoving number densities of the Higgs bosons (σ), nonthermally and thermally produced neutrinos of the first generation ($N_1^{\rm nt}$, $N_1^{\rm th}$), neutrinos from the first generation in thermal equilibrium ($N_1^{\rm eq}$, for comparison), neutrinos of the second and third generation ($N_{2,3}$), the MSSM radiation (R), the lepton asymmetry ($B-L$), and gravitinos ($\tilde{G}$) as functions of the scale factor a. The vertical lines labeled $a_{\rm RH}^i$, $a_{\rm RH}$ and $a_{\rm RH}^f$ mark the beginning, the middle and the end of the reheating process. The corresponding values for the input parameters are given in Eq. (7.84).

same time, an additional contribution to the lepton asymmetry is generated by thermally produced (s)neutrinos. All further details which we took care of are, of course, important for a complete understanding of the physical picture, but merely have a small impact on the final outcome of our calculation. In particular, as we will illustrate in this section, the numerical results for the observables of interest, T_{RH}, η_B, and $\Omega_{\widetilde{G}}h^2$, remain unaffected if one neglects the superpartners of all massive particles or if one excludes the gauge particles from the analysis (cf. Fig. 7.4, in which we plot the corresponding comoving number densities of all remaining species as functions of the scale factor). This observation renders our scenario of reheating robust against uncertainties in the underlying theoretical framework and opens up the possibility to connect it to other models of inflation and preheating as long as these provide similar initial conditions as spontaneous $B-L$ breaking after hybrid inflation. In addition to that, the robustness of our scenario justifies to crudely simplify its technical description. If one is solely interested in the parameter dependence of the observables and less in the exact evolution during reheating, one may simply omit effects due to the gauge DOFs and supersymmetry, as we have done it in Refs. [57] and [58].

Nonsupersymmetric Analysis Including the Gauge Multiplet

In a first step, in order to assess the impact of supersymmetry on the reheating process, we neglect the superpartners of all massive particles, i.e. the gauge scalar C, the gaugino $\tilde{A}$, the higgsino ψ as well as all heavy sneutrinos $\tilde{N}_i$. Technically, this renders the inflaton ϕ stable, as it can only decay into a pair of $\tilde{N}_1$ sneutrinos. To avoid overclosure of the universe, we thus also omit the inflaton. By contrast, we keep the full particle spectrum of the MSSM and the gravitino because we still wish to account for dark matter by thermally produced gravitinos. All in all, these simplifications imply drastically simpler Boltzmann equations and induce small changes to the corresponding decay and production rates.

Again we solve the set of Boltzmann equations in combination with the initial conditions set by preheating and the decay of the gauge DOFs. For our key observables, we obtain

$$\begin{aligned} T_{\mathrm{RH}} &\simeq 6.1\times 10^{9}\,\mathrm{GeV}\,, \quad \eta_B \simeq 3.7\times 10^{-9}\,, \quad \eta_B^{\mathrm{nt}} \simeq 3.7\times 10^{-9}\,, \\ \eta_B^{\mathrm{th}} &\simeq 9.7\times 10^{-15}\,, \quad \Omega_{\widetilde{G}}h^2 \simeq 0.11\,. \end{aligned} \tag{7.98}$$

With regard to their first two digits, these results for T_{RH}, η_B, η_B^{nt} and $\Omega_{\widetilde{G}}h^2$ are the same as in the full analysis. The result for η_B^{th} is smaller by a factor 2, reflecting the missing contribution from the thermal sneutrinos of the first generation. In the upper panel of Fig. 7.4, we present the corresponding comoving number densities. They behave very similarly to the original densities in the upper panel of Fig. 7.1, the only minor differences being the following. At early times, all densities but the one of the Higgs bosons are a bit smaller, at most by a factor of $\mathcal{O}(10)$. In turn, the density of the Higgs bosons is technically a bit larger. But the relative change is of $\mathcal{O}\left(10^{-4}\right)$ and thus not visible in Fig. 7.4. The fact that initially more energy

remains in the Higgs bosons has two reasons. First, there are now simply less particle species present into which the initial vacuum energy could be distributed. Second, particles coupling to the gauge sector are produced in smaller numbers after preheating due to the absence of the superpartners of the $B-L$ vector boson. A direct consequence of the densities being initially slightly smaller is that they become sensitive to the decays of the nonthermal N_1^S neutrinos a bit earlier. The onset of reheating and the inversion of the lepton asymmetry, for instance, take place at $a_{\rm RH}^i \simeq 4.2 \times 10^2$ and $a \simeq 3.2 \times 10^3$, respectively, while these events occur later, at $a_{\rm RH}^i \simeq 5.3 \times 10^2$ and $a \simeq 4.6 \times 10^3$, if supersymmetry is fully included. However, as soon as the R and $B-L$ abundances are dominated by the decay products of the N_1^S neutrinos, the differences between the two plots in the upper panels of Figs. 7.1 and 7.4 begin to vanish. From $a \sim 10^4$ onwards, they are, apart from a factor 2 between the curves for the thermal (s)neutrinos, at or below the percent level.

It is easy to understand why the omission of the heavy superparticles does not have any effect on our final results. According to Eq. (6.26), the initial energy densities of the gauge scalar C, the gaugino $\tilde{A}$, the higgsino ψ, the inflaton ϕ as well as the heavy sneutrinos $\tilde{N}_i$ are monotonic functions of the Higgs-inflaton coupling λ. Setting λ to its maximal value, $\lambda = 10^{-2}$, we obtain upper bounds on these densities,

$$\left.\frac{\rho_{\tilde{A}}}{\rho_0}\right|_{a_{\rm PH}} \lesssim \mathcal{O}\left(10^{-2}\right) , \quad \left.\frac{\rho_{C,\psi,\phi,\tilde{N}_{2,3}}}{\rho_0}\right|_{a_{\rm PH}} \lesssim \mathcal{O}\left(10^{-3}\right) , \quad \left.\frac{\rho_{\tilde{N}_1}}{\rho_0}\right|_{a_{\rm PH}} \lesssim \mathcal{O}\left(10^{-8}\right) . \tag{7.99}$$

We thus conclude that no matter how the dynamics of the above species look like in detail, their influence on the reheating process will always be outweighed sooner or later by the decay of the much more abundant Higgs bosons. Hence, ignoring these particles does not affect the outcome of our calculation. Similarly, we can show that only the fermionic decays of the Higgs bosons are relevant for reheating. The ratio of $\tilde{N}_1^S$ sneutrinos to N_1^S neutrinos increases monotonically with the mass M_1 (cf. Eq. (7.46)). Our upper bound on this mass, $M_1 = 3 \times 10^{12}$ GeV, then translates into $N_{\tilde{N}_1}^S / N_{N_1}^S \lesssim \mathcal{O}\left(10^{-4}\right)$. The nonthermal $\tilde{N}_1^S$ sneutrinos can therefore also be safely neglected. In conclusion, our numerical results in Eqs. (7.99) in combination with the upper bound on $N_{\tilde{N}_1}^S / N_{N_1}^S$ substantiate our introductory comment at the beginning of this section. The essential feature of our scenario of reheating is the Higgs boson decay chain, $\sigma \to N_1^S \to R$. From the point of view of the final results for the observables, the inclusion of the full supersymmetric particle spectrum is rather a matter of theoretical consistency than a numerical necessity.

Nonsupersymmetric Analysis Neglecting the Gauge Multiplet

Finally, we wish to demonstrate that one is also free to neglect the decay of the gauge particles, if one is only interested in numerical results for the observables. In addition to all massive superparticles, we now also exclude the $B-L$ vector boson from our analysis. Consequently,

particle production in the decay of gauge particles does not take place any longer, which simplifies our set of Boltzmann equations once more. This time we find for our key observables

$$\begin{aligned} T_{\mathrm{RH}} &\simeq 6.1 \times 10^{9}\,\mathrm{GeV}\,, \quad \eta_B \simeq 3.7 \times 10^{-9}\,, \quad \eta_B^{\mathrm{nt}} \simeq 3.7 \times 10^{-9}\,, \\ \eta_B^{\mathrm{th}} &\simeq 9.7 \times 10^{-15}\,, \quad \Omega_{\widetilde{G}} h^2 \simeq 0.11\,. \end{aligned} \tag{7.100}$$

With regard to their first two digits, these results exactly match those in Eq. (7.98). The lower panel of Fig. 7.4 displays the corresponding comoving number densities, again to be compared with the original densities in the upper panel of Fig. 7.1. The absence of (s)neutrinos of the second and third generation produced through the decay of gauge particles now results in a slightly smaller initial lepton asymmetry and, more importantly, in drastically shorter $N_{2,3}$ reheating. While this first stage of reheating still lasted until $a \simeq 11$ in our complete analysis (cf. Sec. 7.2.2), it now comes to an end already at $a \simeq 1.7$. Before the onset of N_1 reheating, the abundances of radiation, thermal neutrinos and gravitinos are hence significantly reduced. For instance, at $a = 50$ the respective comoving number densities are suppressed by factors of the following orders of magnitude,

$$B\!-\!L \,:\, \mathcal{O}\left(10^{-1}\right)\,, \quad R\,,\, N_1^{\mathrm{th}}\,,\, N_1^{\mathrm{eq}} \,:\, \mathcal{O}\left(10^{-2}\right)\,, \quad \widetilde{G} \,:\, \mathcal{O}\left(10^{-3}\right)\,. \tag{7.101}$$

As before, due to this initial suppression, these densities are earlier sensitive to the decay of the N_1^S neutrinos. Now the onset of N_1 reheating and the inversion of the lepton asymmetry take place at $a_{\mathrm{RH}}^i \simeq 1.2\times 10^2$ and $a \simeq 2.6\times 10^3$, which is even earlier than in our nonsupersymmetric analysis including the gauge multiplet. However, during N_1 reheating the differences between the two plots in the upper panel of Fig. 7.1 and the lower panel of Fig. 7.4 vanish again. From $a \sim 10^4$ onwards, they are, apart from the factor 2 between the curves for the thermal (s)neutrinos, at or below the percent level. In conclusion, we find that including the gauge DOFs has a great impact on the dynamics at early times shortly after preheating, but turns out be nonessential when calculating the final numerical results.

7.3 Scan of the Parameter Space

The value of the Boltzmann equations derived in Sec. 7.1 is twofold. On the one hand, as we have seen in the last section, they are the basis for a detailed time-resolved description of the dynamics during reheating. On the other hand, as we will demonstrate in this section, solving them in the entire parameter space allows one to study the quantitative dependence of our key quantities, T_{RH}, η_B, and $\Omega_{\widetilde{G}} h^2$, on the parameters in the Lagrangian.

The relevant parameters of our model are the scale of $B\!-\!L$ breaking v_{B-L}, the heavy neutrino mass M_1, the effective neutrino mass $\widetilde{m}_1$, the gravitino mass $m_{\widetilde{G}}$, and the gluino mass $m_{\tilde{g}}$. Requiring consistency with hybrid inflation and the production of cosmic strings fixes the $B\!-\!L$ breaking scale, $v_{B-L} = 5 \times 10^{15}\,\mathrm{GeV}$, and limits the range of possible M_1

values (cf. Sec. 6.1). According to the Froggatt-Nielsen flavour model, $\widetilde{m}_1$ should be close to $\overline{m}_\nu \simeq 3 \times 10^{-2}\,\text{eV}$. However, in order to account for the uncertainties of the flavour model, we vary it between $10^{-5}\,\text{eV}$ and $1\,\text{eV}$ (cf. Eq. (6.13)). For the gravitino mass we consider typical values, as they arise in scenarios of gravity- or gaugino-mediated supersymmetry breaking,

$$30\,\text{MeV} \leq m_{\tilde{G}} \leq 700\,\text{GeV}\,. \tag{7.102}$$

As for the gluino, we stick without loss of generality to the mass that we used in the parameter example discussed in Sec. 7.2, $m_{\tilde{g}} = 1\,\text{TeV}$. The generalization to different choices for $m_{\tilde{g}}$ is straightforward (cf. App. C) and simply amounts to a rescaling of all values for the gravitino mass. Gravitino masses as large as 700 GeV are, in fact, inconsistent with unified gaugino masses at the GUT scale. If the gluino and the bino had the same mass at the GUT scale, the different running of the respective renormalization group equations would then entail a mass ratio of roughly 6 at low energies. The gravitino, which we assume to be the LSP, would then have to be lighter than the bino, resulting in an upper bound of $m_{\widetilde{G}} \lesssim 170\,\text{GeV}$. We however leave open the question whether gaugino mass unification takes place at the GUT scale and work in the following with the full gravitino mass range specified in Eq. (7.102).

At each point of the parameter space defined by the above restrictions, we solve the Boltzmann equations and record all important numerical results, which we now discuss in turn. In Sections 7.3.1 and 7.3.2, we study the parameter dependence of the reheating temperature and the final baryon asymmetry, respectively. In doing so, we devote particular attention to the composition of the asymmetry in terms of a nonthermal and a thermal contribution. By imposing the condition that the maximal possible baryon asymmetry be larger than the observed one, we identify the region in parameter space that is consistent with leptogenesis (cf. the comment below Eq. (7.93)),

$$\eta_B = \eta_B^{\text{nt}} + \eta_B^{\text{th}} \geq \eta_B^{\text{obs}} \simeq 6.2 \times 10^{-10}\,. \tag{7.103}$$

In Sec. 7.3.3, we then turn to the generation of dark matter in the form of gravitinos. Requiring the final gravitino abundance to match the observed density of dark matter,

$$\Omega_{\widetilde{G}} h^2 = \Omega_{\text{DM}}^{\text{obs}} h^2 \simeq 0.11\,, \tag{7.104}$$

we are able to derive relations between the neutrino parameters M_1 and $\widetilde{m}_1$ and the superparticle masses $m_{\widetilde{G}}$ and $m_{\tilde{g}}$. Combining the two conditions in Eqs. (7.103) and (7.104), we are eventually even able to set a lower bound on $m_{\widetilde{G}}$ in terms of $\widetilde{m}_1$.

Note that in all plots in this section (cf. Figs. 7.5, 7.6 and 7.7) the position of the parameter point which we investigated in Sec. 7.2 is marked by a small white circle.

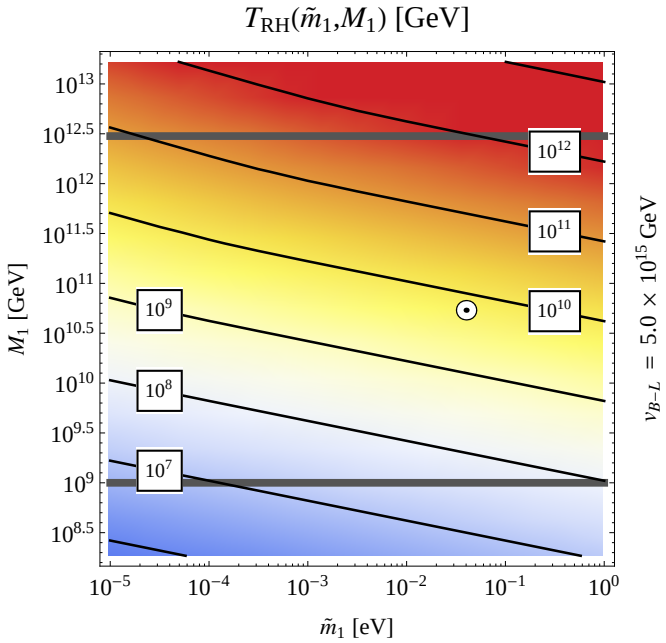

Figure 7.5: Contour plot of the reheating temperature T_{RH} as a function of the effective neutrino mass $\widetilde{m}_1$ and the heavy neutrino mass M_1. The reheating temperature is calculated according to Eq. (7.87) after solving the Boltzmann equations, cf. Sec. 7.2.3 for a comparison of our definition of the reheating temperature with other common approaches. The thick horizontal gray lines represent the lower and the upper bound on M_1, respectively, which arise from requiring consistency with hybrid inflation and the production of cosmic strings during the $B-L$ phase transition (cf. Eq. (6.13)). The small white circle marks the position of the parameter point discussed in Sec. 7.2.

7.3.1 Reheating Temperature

The process of reheating after the $B-L$ phase transition is accompanied by an intermediate plateau in the decline of the temperature, which determines the characteristic temperature scale of reheating. In Sec. 7.2.3, we concretized this intuitive notion and defined the reheating temperature T_{RH} as the temperature of the thermal bath at the moment when the decay of the N_1^S neutrinos into radiation is about to become efficient (cf. Eq. (7.87)),

$$\Gamma_{N_1}^S\left(a_{\mathrm{RH}}\right) = H\left(a_{\mathrm{RH}}\right) , \quad T_{\mathrm{RH}} = T\left(a_{\mathrm{RH}}\right) .$$

We also argued in Sec. 7.2.3 that this definition is particularly convenient compared to alternative approaches, because it is not only representative for the temperature plateau during reheating, but also associated with a physical feature in the temperature curve.

Having the solutions of the Boltzmann equations for all allowed values of $\widetilde{m}_1$ and M_1 at hand, Eq. (7.87) enables us to determine the reheating temperature as a function of these

two parameters, $T_{\mathrm{RH}} = T_{\mathrm{RH}}\left(\widetilde{m}_1, M_1\right)$. As the reheating process is solely controlled by Higgs and neutrino decays, T_{RH} obviously does not depend on the gravitino or gluino mass. In Fig. 7.5, we present the result of our analysis. We find that, within the considered range of neutrino parameters, the reheating temperature varies by almost five orders of magnitude. For $\widetilde{m}_1 = 10^{-4}\,\mathrm{eV}$ and $M_1 = 10^9\,\mathrm{GeV}$, we have, for instance, $T_{\mathrm{RH}} \sim 10^7\,\mathrm{GeV}$, while for $\widetilde{m}_1 = 10^{-1}\,\mathrm{eV}$ and $M_1 = 10^{12}\,\mathrm{GeV}$ we obtain $T_{\mathrm{RH}} \sim 3 \times 10^{11}\,\mathrm{GeV}$. Remarkably, the reheating temperature never exceeds the neutrino mass M_1. Instead, it is typically smaller than M_1 by one or even two orders of magnitude. As the ratio M_1/T_{RH} controls the strength of washout processes during reheating, we conclude that the effect of washout on the generation of the lepton asymmetry is in most cases negligible (cf. Sec. 7.3.2, where we will come back to this observation).

The reheating temperature increases monotonically with both neutrino parameters, $\widetilde{m}_1$ and M_1, with the dependence on M_1 being much more pronounced than the dependence on $\widetilde{m}_1$. In the following, we will derive a simple semianalytical approximation for T_{RH}, by means of which this behaviour can be easily understood. A more detailed discussion can be found in Appendix C of Ref. [58]. By definition, T_{RH} corresponds to the decay temperature of N_1 neutrinos decaying with the effective rate $\Gamma^S_{N_1}$. To first approximation, we may thus write

$$T_{\mathrm{RH}} \approx \left(\frac{90}{8\pi^3 g_{*,\rho}}\right)^{1/4} \sqrt{\Gamma^S_{N_1} M_P} = \gamma^{-1/2} \left(\frac{90}{8\pi^3 g_{*,\rho}}\right)^{1/4} \sqrt{\Gamma^0_{N_1} M_P}\,, \tag{7.105}$$

where $\gamma = \gamma\left(\widetilde{m}_1, M_1\right)$ denotes the Lorentz factor relating $\Gamma^S_{N_1}$ to the zero-temperature decay rate $\Gamma^0_{N_1}$ evaluated at $a = a_{\mathrm{RH}}$. This first estimate of the reheating temperature fails to accurately reproduce our numerical results because of two imprecisions. First, Eq. (7.105) is based on the assumption that, at $a = a_{\mathrm{RH}}$, the dominant contribution to the total energy is contained in radiation. This is, however, never the case. At $a = a_{\mathrm{RH}}$, the decays of the N_1^S neutrinos have just set in, so that at this time a significant fraction of the total energy is hence always still stored in these neutrinos. On top of that, for $\Gamma^0_S \ll \Gamma^S_{N_1}$, which is the case in almost the entire parameter space, the Higgs bosons have not decayed yet at $a = a_{\mathrm{RH}}$, so that in the end they dominate the total energy density at the time of reheating. To remedy this first imprecision, we have to multiply Eq. (7.105) by $\alpha^{-1/4}$, where $\alpha = \alpha\left(\widetilde{m}_1, M_1\right) = \rho_{\mathrm{tot}}\left(a_{\mathrm{RH}}\right)/\rho_R\left(a_{\mathrm{RH}}\right)$. The second imprecision is related to the fact that we do not explicitly solve the Friedmann equation to determine the Hubble parameter, but rather calculate it as $\dot{a}/a$ with the scale factor a being constructed as described in Sec. 7.1 (cf. Eq. (7.2)). As a consequence of this procedure, H does not always exactly fulfill the Friedmann equation. We account for this technical imprecision by multiplying Eq. (7.105) by $\beta^{-1/2}$, where $\beta = \beta\left(\widetilde{m}_1, M_1\right)$ relates $\dot{a}/a$ to the exact solution of the Friedmann equation at $a = a_{\mathrm{RH}}$. For appropriate functions α, β and γ, we can then write T_{RH} as

$$T_{\mathrm{RH}} = \alpha^{-1/4}\beta^{-1/2}\gamma^{-1/2} \left(\frac{90}{8\pi^3 g_{*,\rho}}\right)^{1/4} \sqrt{\Gamma^0_{N_1} M_P} \tag{7.106}$$

$$= 7.1 \times 10^{11}\,\text{GeV} \times \alpha^{-1/4}\beta^{-1/2}\gamma^{-1/2} \left(\frac{\widetilde{m}_1}{0.04\,\text{eV}}\right)^{1/2} \left(\frac{M_1}{10^{11}\,\text{GeV}}\right) .$$

The dependence of α, β and γ on $\widetilde{m}_1$ and M_1 follows from the solutions of the Boltzmann equations. Restricting ourselves to the region in parameter space in which $\Gamma^0_{N_1}/\Gamma^0_S \gtrsim \mathcal{O}(100)$, we find that β and γ are basically constant. We obtain $\beta \simeq 0.99$ and $\gamma \simeq 85$ with deviations around these values of a few percent. The dependence of the correction factor α on $\widetilde{m}_1$ and M_1 is well described by

$$\alpha \simeq 1.2 \times 10^3 \times \left(\frac{\widetilde{m}_1}{0.04\,\text{eV}}\right) \left(\frac{10^{11}\,\text{GeV}}{M_1}\right) . \tag{7.107}$$

Such a behaviour directly follows from the interplay of the decay rates $\Gamma^0_{N_1}$ and Γ^0_S. For large $\Gamma^0_{N_1}$ and small Γ^0_S, reheating takes place quite early, at a time when most Higgs bosons have not decayed yet. For small $\Gamma^0_{N_1}$ and large Γ^0_S, reheating takes place later and not as many Higgs bosons are present anymore at $a = a_{\text{RH}}$. The magnitude of α is hence controlled by the ratio $\Gamma^0_{N_1}/\Gamma^0_S$ which scales like $\widetilde{m}_1/M_1$. This explains the parameter dependence in Eq. (7.107). Putting all these results together yields a fitting formula for T_{RH} that reproduces our numerical results with an error of less than a percent in almost the entire parameter space,

$$T_{\text{RH}} \simeq 1.3 \times 10^{10}\,\text{GeV} \left(\frac{\widetilde{m}_1}{0.04\,\text{eV}}\right)^{1/4} \left(\frac{M_1}{10^{11}\,\text{GeV}}\right)^{5/4} . \tag{7.108}$$

7.3.2 Baryon Asymmetry

Based on the solutions of the Boltzmann equations, we calculate the nonthermal and thermal contributions to the final baryon asymmetry (cf. Eq. (7.92)) for all values of the neutrino parameters $\widetilde{m}_1$ and M_1. We present the result of this analysis in Fig. 7.6. The parameter regions in Fig. 7.6 where the nonthermal and thermal baryon asymmetries η_B^{nt} and η_B^{th} are consistent with the observational bound η_B^{obs} are shaded in bright green and gray green, respectively. The overlap of these two regions is coloured in dark green. In the white patch around $\widetilde{m}_1 \sim 0.3\,\text{eV}$ and $M_1 \sim 10^{12}\,\text{GeV}$, the total asymmetry $\eta_B = \eta_B^{\text{nt}} + \eta_B^{\text{th}}$ is larger than η_B^{obs}, but neither of its two contributions is. Below the solid blue line in Fig. 7.6, the nonthermal asymmetry dominates over the thermal one. Above the solid blue line, it is the other way around. We conclude that in the part of parameter space that we are interested in the thermal asymmetry is almost always outweighed by its nonthermal counterpart. Especially in the region in which leptogenesis is consistent with gravitino dark matter, where M_1 is typically of $\mathcal{O}\left(10^{11}\right)$ GeV (cf. Sec. 7.3.3), the thermal asymmetry is negligibly small.

In most of the parameter space the nonthermal asymmetry is insensitive to $\widetilde{m}_1$ and thus solely controlled by M_1. Only for large values of $\widetilde{m}_1$ and M_1, it depends on both neutrino mass parameters. This behaviour is directly related to the efficiency of the washout processes in the respective parameter regions. Let us suppose for a moment that washout does not take

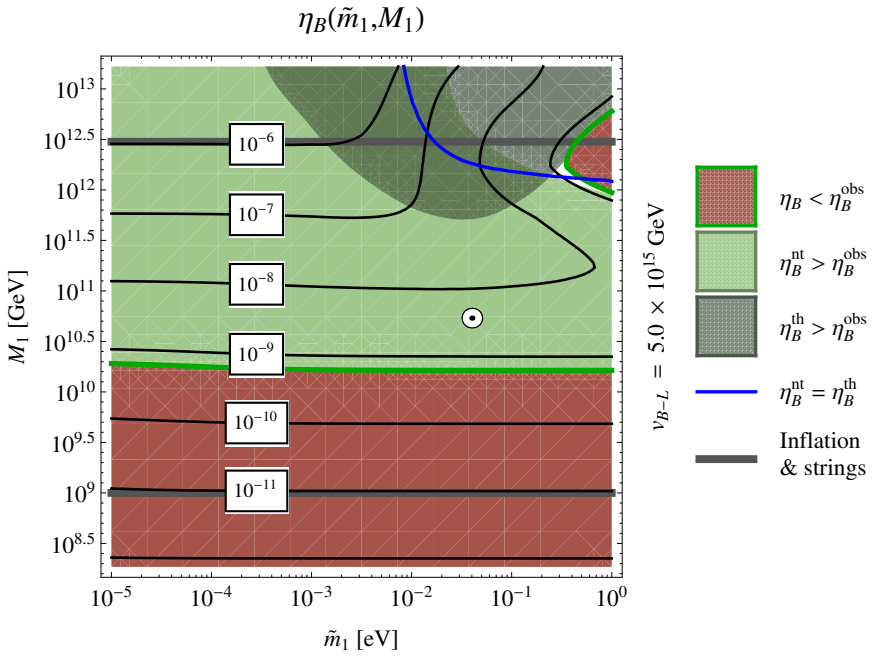

Figure 7.6: Contour plot of the baryon asymmetry η_B as a function of the effective neutrino mass $\widetilde{m}_1$ and the heavy neutrino mass M_1. The baryon asymmetry is calculated according to Eq. (7.92) after solving the Boltzmann equations. In the bright green (gray green) region the nonthermal (thermal) asymmetry is consistent with the observed asymmetry. In the red region the total asymmetry falls short of the observational bound. Below (above) the thin blue line the nonthermal (thermal) asymmetry dominates over the thermal (nonthermal) asymmetry. The thick horizontal gray lines represent the lower and the upper bound on M_1, respectively, which arise from requiring consistency with hybrid inflation and the production of cosmic strings during the $B-L$ phase transition (cf. Eq. (6.13)). The small white circle marks the position of the parameter point discussed in Sec. 7.2.

place. The final nonthermal asymmetry then only depends on the total number of (s)neutrinos produced during reheating and the amount of CP violation per (s)neutrino decay. Neither of these two quantities is, however, affected by changes in $\widetilde{m}_1$, so that the asymmetry, indeed, ends up being a function of M_1 only. From this perspective, the insensitivity of $\eta_B^{\rm nt}$ to $\widetilde{m}_1$ signals that the effect of washout on the generation of the asymmetry is negligible for most values of the neutrino parameters. This result is consistent with our findings for the reheating temperature and in particular the ratio $M_1/T_{\rm RH}$ as a function of $\widetilde{m}_1$ and M_1 (cf. Sec. 7.3.1). To see this, note that, for temperatures $T \lesssim M_1$, the effective washout rate $\hat{\Gamma}_W$ decreases exponentially when raising the ratio M_1/T,

$$T \lesssim M_1 : \quad \hat{\Gamma}_W = \frac{N_{N_1}^{\rm eq}}{2N_\ell^{\rm eq}} \Gamma_{N_1}^{\rm th} \propto \left(\frac{M_1}{T}\right)^{3/2} e^{-M_1/T}\, \Gamma_{N_1}^0 \,, \tag{7.109}$$

which readily follows from Eqs. (7.53) and (A.19). The fact that $M_1/T_{\rm RH}$ is of $\mathcal{O}(10)$ or

even larger for most parameter values then explains why the impact of washout is typically vanishingly small. In turn, Eq. (7.109) also illustrates the importance of washout at very large values of $\widetilde{m}_1$ and M_1, for which the ratio $M_1/T_{\rm RH}$ approaches values of $\mathcal{O}(1)$. Comparing our results for the reheating temperature and the baryon asymmetry in Figs. 7.5 and 7.6, respectively, we find that washout only plays a significant role if $M_1/T_{\rm RH} \lesssim 10$ and $M_1 \gtrsim 10^{11}$ GeV. Interestingly, the parameter region defined by these two conditions covers the entire range of parameters, in which the thermal asymmetry exceeds the observed asymmetry.

If washout is negligible, the nonthermal asymmetry can be reproduced to good approximation by assuming that all N_1^S neutrinos decay instantaneously at time $t_1 = t_S + 1/\Gamma^0_{N_1}$ into radiation. The resultant baryon asymmetry is then given by

$$\eta_B^{\rm nt} \approx \frac{3\pi^4 g^0_{*,s}}{90\zeta(3) g_\gamma} C_{\rm sph}\, \epsilon_1 \left.\frac{T}{\varepsilon^S_{N_1}}\right|_{t=t_1} , \tag{7.110}$$

where $\varepsilon^S_{N_1}$ denotes the average energy per N_1^S neutrino. The ratio $T/\varepsilon^S_{N_1}$ is proportional to $N^S_{N_1}/N_R$, the number density of N_1^S neutrinos at the time when these decay normalized to the radiation number density. It directly follows from the solutions of the Boltzmann equations and is well described by

$$\left.\frac{T}{\varepsilon^S_{N_1}}\right|_{t=t_1} \simeq 3.7 \times 10^{-4} \left(\frac{M_1}{10^{11}\,\text{GeV}}\right)^{1/2} . \tag{7.111}$$

Together with the expression for ϵ_1 in Eq. (3.72), this yields the following fitting formula for the nonthermal asymmetry in the case of weak washout,

$$\eta_B^{\rm nt} \simeq 6.7 \times 10^{-9} \left(\frac{M_1}{10^{11}\,\text{GeV}}\right)^{3/2} . \tag{7.112}$$

It reproduces our numerical results for $\eta_B^{\rm nt}$ within a factor of 2 for most values of M_1.

The requirement that the maximal possible asymmetry be larger than the observed one constrains the allowed range of M_1 values. Fig. 7.6 implies the following lower bound,

$$\eta_B \geq \eta_B^{\rm obs} \simeq 6.2 \times 10^{-10} \quad \longrightarrow \quad M_1 \geq M_1^{\rm min} \simeq 1.7 \times 10^{10}\,\text{GeV} , \tag{7.113}$$

where we have averaged out the slight dependence on $\widetilde{m}_1$. If M_1 is chosen below this minimal value, the asymmetry falls below the observational bound for two reasons. On the one hand, small M_1 implies a small CP parameter ϵ_1 (cf. Eq.(3.72)). On the other hand, according to Eq. (7.111), a small M_1 value also entails a small ratio $T/\varepsilon^S_{N_1}$, i.e. a small abundance of (s)neutrinos at the time the asymmetry is generated. The combination of both effects then renders the successful generation of the lepton asymmetry impossible.

The thermal asymmetry has, to first approximation, the same parameter dependence as the asymmetry generated in standard leptogenesis. It increases monotonically with M_1. If

M_1 is kept fixed at some value $M_1 \gtrsim 10^{12}\,\mathrm{GeV}$, it is largest for $\widetilde{m}_1$ values of $\mathcal{O}\left(10^{-2}\right)$ eV. The monotonic behaviour in M_1 is a direct consequence of the fact that the CP parameter ϵ_1 scales linearly with M_1. The preference for intermediate values of $\widetilde{m}_1$ has the same reason as in the standard case. Large $\widetilde{m}_1$ corresponds to strong washout, at least for the high values of M_1 at which the thermal generation of the asymmetry carries weight. Small $\widetilde{m}_1$ results in a low temperature and a small neutrino decay rate $\Gamma^0_{N_1}$, such that the thermal production of (s)neutrinos is suppressed. Especially in the parameter region in which the thermal asymmetry dominates over the nonthermal asymmetry, the expectation from standard leptogenesis η_B^{st} approximates our numerical results reasonably well,

$$\eta_B^{\mathrm{th}} \approx \eta_B^{\mathrm{st}} = \frac{3}{4}\frac{g^0_{*,s}}{g_{*,s}} C_{\mathrm{sph}} \epsilon_1 \kappa_f\left(\widetilde{m}_1\right). \tag{7.114}$$

Here, $\kappa_f = \kappa_f\left(\widetilde{m}_1\right)$ denotes the final efficiency factor. In the strong washout regime, $\widetilde{m}_1 \gg 10^{-3}\,\mathrm{eV}$, it is inversely proportional to $\widetilde{m}_1$ and independent of the initial conditions at high temperatures [38],

$$\kappa_f(\widetilde{m}_1) \simeq 2 \times 10^{-2} \left(\frac{10^{-2}\,\mathrm{eV}}{\widetilde{m}_1}\right)^{1.1}. \tag{7.115}$$

Combining Eqs. (7.114) and (7.115) with the expression for ϵ_1 in (3.71), we obtain

$$\eta_B^{\mathrm{th}} \simeq 7.0 \times 10^{-10} \left(\frac{0.1\,\mathrm{eV}}{\widetilde{m}_1}\right)^{1.1} \left(\frac{M_1}{10^{12}\,\mathrm{GeV}}\right). \tag{7.116}$$

In the region in parameter space where $\eta_B^{\mathrm{th}} > \eta_B^{\mathrm{nt}}$, this fitting formula reproduces our numerical results within a factor of 2.

Despite these similarities it is, however, important to note that our thermal mechanism for the generation of the lepton asymmetry differs from the standard scenario in two important aspects. First, our variant of thermal leptogenesis is accompanied by continuous entropy production, while one assumes an adiabatically expanding thermal bath in the case of standard leptogenesis. Consequently, our thermal asymmetry experiences an additional dilution during and after its generation (cf. the comment on page 145). Second, our scenario of reheating implies a particular relation between the temperature at which leptogenesis takes place, which is basically T_{RH} in our case, and the neutrino mass parameters (cf. Sec. 7.3.1) that differs drastically from the corresponding relation implied by standard leptogenesis. This translates into a different parameter dependence of the ratio M_1/T as a function of $\widetilde{m}_1$ and M_1, which in turn alters the efficiency of washout process and the production of thermal (s)neutrinos from the bath in the respective regions of parameter space. In the end, our thermal asymmetry therefore rather corresponds to a distorted version of the asymmetry generated by standard leptogenesis. As we have remarked above, in the parameter region where the thermal asymmetry is larger than the nonthermal asymmetry, η_B^{th} hardly deviates from η_B^{st}. But as soon as

we go to smaller values of $\widetilde{m}_1$ and M_1, the difference between the two asymmetries grows. The minimal value of M_1 for which the thermal asymmetry is still able to exceed the observational bound, for instance, turns out to be much larger in our scenario than in standard leptogenesis. We find an absolute lower bound on M_1 of roughly $5.1 \times 10^{11}\,\mathrm{GeV}$ at an effective neutrino mass $\widetilde{m}_1 \simeq 3.3 \times 10^{-2}\,\mathrm{eV}$, while standard leptogenesis only constrains M_1 to values larger than $M_1 \sim 10^9\,\mathrm{GeV}$. Lowering M_1 below $5.1 \times 10^{11}\,\mathrm{GeV}$ either implies a larger ratio M_1/T_{RH} or a larger effective neutrino mass $\widetilde{m}_1$ (cf. Fig. 7.5). In either case the thermal asymmetry is reduced, so that it drops below the observed value.

In conclusion, we emphasize that the generation of the lepton asymmetry is typically dominated by the decay of the nonthermal (s)neutrinos. Only in the parameter region of strong washout, which is characterized by a small ratio M_1/T_{RH}, the nonthermal asymmetry is suppressed and the thermal asymmetry has the chance to dominate. Related to that, we find that the viable region in parameter space governed by the nonthermal mechanism is significantly larger than the corresponding region for the thermal mechanism. Independently of $\widetilde{m}_1$, the neutrino mass M_1 can be as small as $M_1^{\mathrm{min}} \simeq 1.7 \times 10^{10}\,\mathrm{GeV}$, which is an order of magnitude below the bound of $5.1 \times 10^{11}\,\mathrm{GeV}$ which one obtains in the purely thermal case.

7.3.3 Gravitino Dark Matter

The final abundance of gravitinos $\Omega_{\widetilde{G}}h^2$ depends on three parameters: the reheating temperature T_{RH} as well as the two superparticle masses $m_{\widetilde{G}}$ and $m_{\tilde{g}}$. A key result of our reheating scenario is that T_{RH} is determined by the neutrino mass parameters $\widetilde{m}_1$ and M_1. As we keep the gluino mass fixed at 1 TeV, the gravitino abundance thus ends up being a function of $\widetilde{m}_1$, M_1 and $m_{\widetilde{G}}$. Based on the solutions of the Boltzmann equations, we calculate $\Omega_{\widetilde{G}}h^2$ according to Eq. (7.96) for all values of these three masses. By imposing the condition that gravitinos be the constituents of dark matter, we can then eliminate one of the free mass parameters, for instance the neutrino mass M_1,

$$\Omega_{\widetilde{G}}h^2\left(\widetilde{m}_1, M_1, m_{\widetilde{G}}\right) = \Omega_{\mathrm{DM}}^{\mathrm{obs}}h^2 \quad \longrightarrow \quad M_1 = M_1\left(\widetilde{m}_1, m_{\widetilde{G}}\right) . \tag{7.117}$$

The physical picture behind this step is the following. For given $m_{\widetilde{G}}$, the reheating temperature has to have one specific value, so that the abundance of gravitinos comes out right. Each choice for $\widetilde{m}_1$ then implies one particular value of M_1 for which this desired reheating temperature is obtained. Solving Eq. (7.117) for M_1 yields this value as a function of $\widetilde{m}_1$ and $m_{\widetilde{G}}$. The corresponding reheating temperature follows immediately,

$$T_{\mathrm{RH}} = T_{\mathrm{RH}}\left(\widetilde{m}_1, M_1\left(\widetilde{m}_1, m_{\widetilde{G}}\right)\right) \quad \longrightarrow \quad T_{\mathrm{RH}} = T_{\mathrm{RH}}\left(\widetilde{m}_1, m_{\widetilde{G}}\right) . \tag{7.118}$$

In summary, combining the requirement that gravitinos make up the dark matter with the fact that the reheating temperature is determined by neutrino parameters allows us to infer

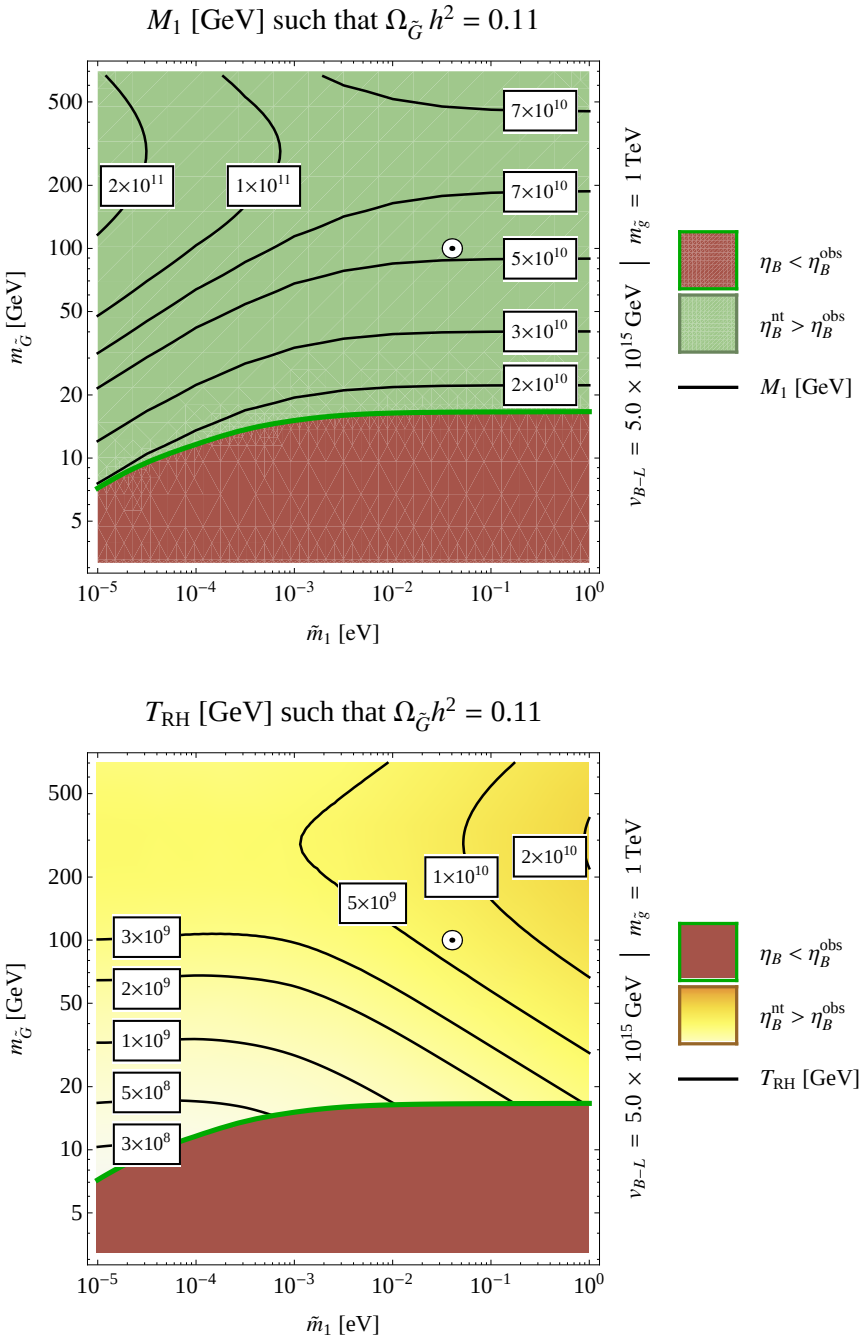

Figure 7.7: Contour plots of the heavy neutrino mass M_1 **(upper panel)** and the reheating temperature $T_{\rm RH}$ **(lower panel)** as functions of the effective neutrino mass $\widetilde{m}_1$ and the gravitino mass $m_{\widetilde{G}}$, such that the relic density of dark matter is accounted for by gravitinos (cf. Eqs. (7.117) and (7.118)). In the red region, the lepton asymmetry generated by leptogenesis is smaller than the observed one, providing us with a lower bound on the gravitino mass in dependence on $\widetilde{m}_1$. The colour code is the same as in Figs. 7.5 and 7.6. The small white circles mark the position of the parameter point discussed in Sec. 7.2.

relations between these neutrino parameters and superparticle masses. The lower bound on M_1 induced by leptogenesis (cf. Eq. (7.113)) can then be translated into a constraint on the mass parameters $\widetilde{m}_1$ and $m_{\widetilde{G}}$.

$$\eta_B = \eta_B\left(\widetilde{m}_1, M_1\left(\widetilde{m}_1, m_{\widetilde{G}}\right)\right) \geq \eta_B^{\text{obs}} \quad \longrightarrow \quad \eta_B = \eta_B\left(\widetilde{m}_1, m_{\widetilde{G}}\right) \geq \eta_B^{\text{obs}}\,. \tag{7.119}$$

We present our results for the functions $M_1\left(\widetilde{m}_1, m_{\widetilde{G}}\right)$ and $T_{\text{RH}}\left(\widetilde{m}_1, m_{\widetilde{G}}\right)$ in the two panels of Fig. 7.7, respectively. Furthermore, we indicate in both plots the constraint arising from the requirement of successful leptogenesis.

We observe the following trends in the two plots of Fig. 7.7. Both quantities, M_1 and T_{RH}, show a stronger dependence on the gravitino mass than on the effective neutrino mass. For $\widetilde{m}_1 \lesssim 10^{-3}\,\text{eV}$, the reheating temperature is almost completely insensitive to $\widetilde{m}_1$. The neutrino mass M_1 slightly increases, when lowering the value of $\widetilde{m}_1$. For large values of the effective neutrino mass, $\widetilde{m}_1 \gtrsim 10^{-3}\,\text{eV}$, the exact opposite is the case. M_1 does not depend on $\widetilde{m}_1$ anymore and T_{RH} slightly rises when increasing $\widetilde{m}_1$. In the following, we will construct semianalytical approximations for M_1 and T_{RH}, which will allow us to get some intuition for this behaviour. The final gravitinos abundance $\Omega_{\widetilde{G}}h^2$ can be parametrized as (cf. App. C)

$$\Omega_{\widetilde{G}}h^2 = \varepsilon\, C_1 \left(\frac{T_{\text{RH}}}{10^{10}\,\text{GeV}}\right)\left[C_2\left(\frac{m_{\widetilde{G}}}{100\,\text{GeV}}\right) + \left(\frac{100\,\text{GeV}}{m_{\widetilde{G}}}\right)\left(\frac{m_{\tilde{g}}}{1\,\text{TeV}}\right)^2\right]. \tag{7.120}$$

Here, the two coefficient functions $C_{1,2} = C_{1,2}\left(T_{\text{RH}}\right)$ subsume all factors contributing to $\Omega_{\widetilde{G}}h^2$ which can be taken care of analytically,

$$\begin{aligned} C_1 &= 10^{14}\,\text{GeV}^2\,\frac{n_\gamma^0}{\rho_c/h^2}\frac{g_{*,s}^0}{g_{*,s}}\left(\frac{90}{8\pi^3 g_{*,\rho}}\right)^{1/2}\frac{18 g_s^6\left(T_{\text{RH}}\right)}{g_\gamma g_s^4\left(\mu_0\right) M_P}\left[\log\left(\frac{T_{\text{RH}}^2}{m_{\tilde{g}}^2\left(T_{\text{RH}}\right)}\right) + 0.8846\right], \\ C_2 &= \frac{3 g_s^4\left(\mu_0\right)}{100 g_s^4\left(T_{\text{RH}}\right)}, \end{aligned} \tag{7.121}$$

They both depend only very weakly on the reheating temperature, so that for our purposes it will suffice to treat them as constants, $C_1 \simeq 0.26$ and $C_2 \simeq 0.13$. The factor ε parametrizes all effects that cannot be accounted for analytically in the derivation of Eq. (7.120), i.e. the amount of energy in radiation at $a = a_{\text{RH}}$, the ratio $\hat{\Gamma}_{\widetilde{G}}/H$ at $a = a_{\text{RH}}$ as well as the increase in the comoving number densities of gravitinos and radiation after $a = a_{\text{RH}}$. In principle, it depends on all mass parameters. In practice, after solving the Boltzmann equations, we find that it is mainly controlled by $\widetilde{m}_1$,

$$\varepsilon\left(\widetilde{m}_1\right) \simeq 1.2\left(\frac{10^{-3}\,\text{eV}}{\widetilde{m}_1}\right)^c, \tag{7.122}$$

where the exponent c is $c \simeq 0.21$ for $\widetilde{m}_1 \gtrsim 10^{-3}\,\text{eV}$ and $c \simeq -0.01$ for $\widetilde{m}_1 \lesssim 10^{-3}\,\text{eV}$. We insert our results for $C_{1,2}$ and ε into Eq. (7.120), set $\Omega_{\widetilde{G}}h^2$ to $\Omega_{\text{DM}}^{\text{obs}}h^2$ and solve for T_{RH},

$$T_{\text{RH}} \simeq 3.5\times 10^9\,\text{GeV}\left(\frac{\widetilde{m}_1}{10^{-3}\,\text{eV}}\right)^c\left[0.13\left(\frac{m_{\widetilde{G}}}{100\,\text{GeV}}\right) + \left(\frac{100\,\text{GeV}}{m_{\widetilde{G}}}\right)\right]^{-1}. \tag{7.123}$$

The corresponding expression for M_1 can then be obtained by exploiting Eq. (7.108),

$$M_1 \simeq 7.2 \times 10^{10}\,\text{GeV}\left(\frac{\widetilde{m}_1}{10^{-3}\,\text{eV}}\right)^d \left[0.13\left(\frac{m_{\widetilde{G}}}{100\,\text{GeV}}\right) + \left(\frac{100\,\text{GeV}}{m_{\widetilde{G}}}\right)\right]^{-4/5}\,, \tag{7.124}$$

where the exponent d is given as $4c/5-1/5$, so that $d \simeq -0.03$ for $\widetilde{m}_1 \gtrsim 10^{-3}$ eV and $d \simeq -0.20$ for $\widetilde{m}_1 \lesssim 10^{-3}$ eV. These two fitting formulae reproduce our numerical results with deviations of $\mathcal{O}(10\%)$ and nicely illustrate the different dependence of T_{RH} and M_1 on $\widetilde{m}_1$ for small and large values of $\widetilde{m}_1$, respectively. As expected, they show that the dependence on $\widetilde{m}_1$ is always very mild and solely stems from the factor ε, i.e. corrections beyond the purely analytical result for $\Omega_{\widetilde{G}}h^2$. If we were to omit these corrections and set ε to 1, the reheating temperature required for gravitino dark matter would be a function of $m_{\widetilde{G}}$ only, $T_{\text{RH}} = T_{\text{RH}}\left(\widetilde{m}_G\right)$, in accordance with the fact that the only parameters entering the gravitino production rate $\hat{\Gamma}_{\widetilde{G}}$ are the masses of the gravitino and the gluino.

Another interesting feature of the two plots in Fig. 7.7 is that for fixed $\widetilde{m}_1$ the neutrino mass as well as the reheating temperature always reach their respective maximal values around gravitino masses of 280 GeV. The extremal values of M_1 and T_{RH} depend on the corresponding choice for $\widetilde{m}_1$, but are typically of order 10^{11} GeV and 10^{10} GeV, respectively. The fact that both M_1 and T_{RH} increase with $m_{\widetilde{G}}$ at small gravitino mass and decrease with $m_{\widetilde{G}}$ at large gravitino mass is also reflected in our two fitting functions in Eqs. (7.123) and (7.124). The expressions in these two equations have their respective maxima at $m_{\widetilde{G}} = 0.13^{-1/2} \times 100\,\text{GeV} \simeq 280\,\text{GeV}$. The physical origin of this behaviour and also the reason why $\Omega_{\widetilde{G}}h^2$ in Eq. (7.120) receives two contributions, one of which is proportional to $m_{\widetilde{G}}$ and the other of which is inversely proportional to $m_{\widetilde{G}}$, is the composition of the gravitino in terms of two transverse DOFs, corresponding to helicity $\pm\frac{3}{2}$ states, and two goldstino DOFs, corresponding to helicity $\pm\frac{1}{2}$ states. Recall that the rate $\hat{\Gamma}_{\widetilde{G}}$ contains the following factor (cf. Eq. (7.81)),

$$\hat{\Gamma}_{\widetilde{G}} = \hat{\Gamma}_{\widetilde{G}}\left(T, m_{\widetilde{G}}, m_{\tilde{g}}\right) \propto \left(1 + \frac{m_{\tilde{g}}^2(T)}{3m_{\widetilde{G}}^2}\right)\,. \tag{7.125}$$

The first term in this factor accounts for the production of the transverse gravitino components, the second for the production of the goldstino components. For $m_{\widetilde{G}} \lesssim m_{\tilde{g}}\left(T\right)/\sqrt{3}$, goldstino production dominates. An increase in $m_{\widetilde{G}}$ then has to be compensated by an appropriately larger temperature, so that the final gravitino abundance remains constant. For $m_{\widetilde{G}} \gtrsim m_{\tilde{g}}\left(T\right)/\sqrt{3}$, mainly states with helicity $\pm\frac{3}{2}$ are populated, turning the rate $\hat{\Gamma}_{\widetilde{G}}$ into a function of the temperature only. In such a case the final gravitino abundance $\Omega_{\widetilde{G}}h^2$ simply scales linearly with $m_{\widetilde{G}}$ (cf. Eq. (7.96)) and larger gravitino masses have to be balanced by smaller temperatures. The particular gravitino mass which separates the two regimes of gravitino production directly follows from the gluino mass at $T \sim 10^{10}$ GeV (cf. Eq. (7.82)),

$$m_{\widetilde{G}} \simeq \frac{m_{\tilde{g}}\left(T\right)}{\sqrt{3}} = \frac{g_s^2\left(T\right)}{g_s^2\left(\mu_0\right)}\frac{m_{\tilde{g}}}{\sqrt{3}} \simeq 480/\sqrt{3}\,\text{GeV} \simeq 280\,\text{GeV}\,. \tag{7.126}$$

The relation between the gravitino mass and the neutrino parameters $\widetilde{m}_1$ and M_1 translates the lower bound on M_1 imposed by the requirement of successful leptogenesis (cf. Eq. (7.113)) into a lower bound on $m_{\widetilde{G}}$. As we can read off from Fig. 7.7, $m_{\widetilde{G}}$ must be at least of $\mathcal{O}(10)\,\mathrm{GeV}$ to obtain consistency between leptogenesis and gravitino dark matter. In fact, the bound on $m_{\widetilde{G}}$ slightly varies with $\widetilde{m}_1$. For $\widetilde{m}_1$ values between $10^{-5}\,\mathrm{eV}$ and $10^{-2}\,\mathrm{eV}$, it monotonically increases from roughly $7\,\mathrm{GeV}$ to $17\,\mathrm{GeV}$, from $\widetilde{m}_1 \sim 10^{-2}\,\mathrm{eV}$ onwards it remains at $m_{\widetilde{G}} \simeq 17\,\mathrm{GeV}$. For such low gravitino masses, the first term in the brackets on the right-hand side of Eq. (7.124) is negligibly small,[8] so that the fitting formula for M_1 can be easily solved for $m_{\widetilde{G}}$,

$$m_{\widetilde{G}} \simeq 8\,\mathrm{GeV}\left(\frac{M_1}{10^{10}\,\mathrm{GeV}}\right)^{5/4}\left(\frac{\widetilde{m}_1}{10^{-3}\,\mathrm{eV}}\right)^{1/4-c}. \tag{7.127}$$

Imposing the condition that M_1 be larger than $M_1^{\min} \simeq 1.7\times 10^{10}\,\mathrm{GeV}$ (cf. Eq. (7.113)) provides us with an analytical expression for the lower bound on $m_{\widetilde{G}}$,

$$m_{\widetilde{G}} \geq m_{\widetilde{G}}^{\min} \simeq 16\,\mathrm{GeV}\left(\frac{\widetilde{m}_1}{10^{-3}\,\mathrm{eV}}\right)^{1/4-c}. \tag{7.128}$$

This estimate reproduces our numerical results with a precision at the level of $\mathcal{O}(10\%)$. Physically, the connection between the bounds on $m_{\widetilde{G}}$ and M_1 is the following. For gravitino masses below $\mathcal{O}(10)$ GeV, a reheating temperature $T_{\mathrm{RH}} \lesssim \mathcal{O}\left(10^{8..9}\right)$ GeV is required to avoid overproduction of gravitinos. According to our reheating mechanism, such low reheating temperatures are associated with comparatively small values of the neutrino mass, $M_1 \lesssim \mathcal{O}\left(10^{10}\right)$ GeV. The low temperature and low mass then entail a small abundance of (s)neutrinos at the time the asymmetry is generated as well as a small CP parameter ϵ_1 (cf. Eqs. (7.111) and (3.71), respectively). Both effects combine and result in an insufficient lepton asymmetry, rendering dark matter made of gravitinos with a mass below $\mathcal{O}(10)$ GeV inconsistent with leptogenesis.

In conclusion, we find that our scenario of reheating can be easily realized in a large fraction of parameter space. The two conditions of successful leptogenesis and gravitino dark matter, in combination with constraints from hybrid inflation and the production of cosmic strings, allow us to interconnect parameters of the neutrino and supergravity sector. In particular, we are able to determine the neutrino mass M_1 and the reheating temperature T_{RH} as functions of the the effective neutrino mass $\widetilde{m}_1$ and the gravitino mass $m_{\widetilde{G}}$. Furthermore, the consistency between all ingredients of our scenario indicates preferences for M_1 and T_{RH}, namely M_1 values close to $10^{11}\,\mathrm{GeV}$ and T_{RH} values close to $3\times 10^9\,\mathrm{GeV}$. Finally, we obtain a lower bound on the gravitino mass of roughly $10\,\mathrm{GeV}$.

[8] In physical terms this means that for small gravitino masses mainly the goldstino DOFs of the gravitino rather than its transverse DOFs are excited.

Chapter 8

WIMP Dark Matter from Heavy Gravitino Decays

In Ch. 7, we have demonstrated that the $B-L$ phase transition, in combination with the subsequent reheating process, is indeed capable of generating the initial conditions for the hot early universe. In the context of the supersymmetric Abelian Higgs model, which we discussed in Ch. 5, and with $B-L$ breaking taking place at the GUT scale, an initial phase of unbroken $B-L$ yields hybrid inflation, ending in tachyonic preheating in the course of which $B-L$ is spontaneously broken. If the gravitino is the LSP, the entropy of the thermal bath, the baryon asymmetry as well as gravitino dark matter are successfully produced during reheating.

In this chapter we now point out that the spontaneous breaking of $B-L$ can also ignite the thermal phase of the universe, if the gravitino is the *heaviest* superparticle. This possibility is realized in anomaly mediation [227, 228] and has recently been reconsidered in the case of wino [229], higgsino [230] and bino [231] LSP, motivated by hints of the LHC experiments ATLAS and CMS that the Higgs boson may have a mass of about 125 GeV [51, 52]. It is known that a gravitino heavier than about 10 TeV can be consistent with primordial nucleosynthesis and leptogenesis [45, 53, 54] (cf. Sec. 3.1.4). In the following we shall investigate the restrictions on the mass of a WIMP as LSP, which are imposed by the consistency of hybrid inflation, leptogenesis, BBN and the dark matter density. As a preparation for our analysis, we first discuss the mechanisms contributing to the relic LSP abundance (cf. Sec. 8.1). Then, we present our results and illustrate how the bounds on the various parameters under study are related to each other (cf. Sec. 8.2). Lastly, we comment very briefly on the prospects for the experimental confirmation of our scenario (cf. Sec. 8.3).

The results presented in this chapter were first published in Ref. [61].

8.1 Thermal and Nonthermal Neutralino Production

During the radiation dominated era, WIMPs are produced through inelastic scatterings in the thermal bath as well as in gravitino decays. Let us now discuss in turn the thermal and nonthermal contributions to the final WIMP abundance.

Thermal Freeze-Out

The WIMP abundance from thermal freeze-out strongly depends on the nature of the LSP. Motivated by anomaly mediation and the present hints for the Higgs boson mass from LHC, we shall assume in this chapter that the superparticle mass spectrum exhibits the following characteristic hierarchy [229–231],

$$m_{\rm LSP} \ll m_{\rm squark,slepton} \ll m_{\widetilde{G}}\,. \tag{8.1}$$

Due to this hierarchy, the LSP is typically a *pure* gaugino or higgsino. It is well known that in this situation the thermal abundance of a bino LSP is generically too large, which is therefore disfavoured. Hence, the case of a light wino [229] or higgsino [230] is preferred.[1] A pure neutral wino ($\widetilde{w}$) or higgsino ($\widetilde{h}$) is almost mass degenerate with a chargino belonging to the same $SU(2)$ multiplet. The current lower bound on chargino masses [2] thus also applies to the LSP. The thermal abundance of a pure wino[2] or higgsino LSP becomes only significant for masses above 1 TeV, where it is well approximated by [279]

$$\Omega^{\rm th}_{\widetilde{w},\widetilde{h}} h^2 = c_{\widetilde{w},\widetilde{h}} \left(\frac{m_{\widetilde{w},\widetilde{h}}}{1\,\text{TeV}}\right)^2, \quad c_{\widetilde{w}} = 0.014\,, \quad c_{\widetilde{h}} = 0.10\,. \tag{8.2}$$

Heavy Gravitino Decay

In this chapter, we shall consider gravitino masses in the range from 10 TeV to 10^3 TeV, as they are suggested by anomaly mediation. The gravitino lifetime is then given by (cf. Eq. (3.49))

$$\tau_{\widetilde{G}} = \left[\frac{1}{4}\left(n_v + \frac{n_m}{12}\right)\frac{m^3_{\widetilde{G}}}{M_P^2}\right]^{-1} \simeq 24\left(\frac{10\,\text{TeV}}{m_{\widetilde{G}}}\right)^3 \text{sec}\,, \tag{8.3}$$

which corresponds to a gravitino decay temperature $T_{\widetilde{G}}$ of (cf. Eq. (2.23))

$$T_{\widetilde{G}} = \left(\frac{90\,M_P^2}{32\pi^3\, g_{*,\rho}(T_{\widetilde{G}})\,\tau^2_{\widetilde{G}}}\right)^{1/4} \simeq 0.24\left(\frac{43/4}{g_{*,\rho}(T_{\widetilde{G}})}\right)^{1/4}\left(\frac{m_{\widetilde{G}}}{10\,\text{TeV}}\right)^{3/2}\text{MeV}\,. \tag{8.4}$$

[1] Note that a *pure* higgsino also occurs as next-to-lightest superparticle along with multi-TeV coloured particles in hybrid gauge-gravity mediation, however with the gravitino as LSP [278].

[2] Compared to Ref. [279], we have reduced the thermal wino abundance $\Omega^{\rm th}_{\widetilde{w}} h^2$ by 30 % to account for the Sommerfeld enhancement effect [280, 281].

For gravitino masses between 10 TeV to 10^3 TeV, the temperature $T_{\widetilde{G}}$ varies between 0.2 MeV and 200 MeV, i.e. roughly between the temperatures of BBN (cf. Sec. 2.2.2) and the QCD phase transition (cf. Sec. 2.2.3). In this temperature range, the entropy increase due to gravitino decays and hence the corresponding dilution of the baryon asymmetry are negligible.

For such heavy gravitinos as we consider them in this chapter, the gravitino production rate $\hat{\Gamma}_{\widetilde{G}}$ becomes independent of the gravitino mass (cf. Eq. (7.81)). The present-day gravitino number density $n^0_{\widetilde{G}} \propto \Omega^0_{\widetilde{G}} h^2 / m_{\widetilde{G}}$ is hence solely determined by the reheating temperature T_{RH}. Solving the Boltzmann equations governing the reheating process (cf. Sec. 7.1) for a heavy gravitino, $m_{\widetilde{G}} \gg 1\,\mathrm{TeV}$, and neutrino mass parameters $\widetilde{m}_1$ and M_1 which result in reheating temperatures $T_{\mathrm{RH}} = 10^8..10^{11}$ GeV we find

$$\left(\frac{100\,\mathrm{GeV}}{m_{\widetilde{G}}}\right) \Omega^0_{\widetilde{G}} h^2 \simeq 2.7 \times 10^{-2} \left(\frac{T_{\mathrm{RH}}\,(\widetilde{m}_1, M_1)}{10^{10}\,\mathrm{GeV}}\right) . \tag{8.5}$$

Note that the rate $\hat{\Gamma}_{\widetilde{G}}$ of thermal gravitino production, and thus also the numerical prefactor on the right-hand of this relation, has a theoretical uncertainty of at least a factor of 2 (cf. App. C for an analytical reconstruction of Eq. (8.5)). The decay of a heavy gravitino, $m_{\widetilde{G}} \gg m_{\mathrm{LSP}}$, produces approximately one LSP. This yields the nonthermal contribution to the WIMP abundance $\Omega^{\widetilde{G}}_{\mathrm{LSP}} h^2$. Assuming that the gravitinos are thermally produced during reheating, i.e. employing the relation in Eq. (8.5), we obtain

$$\Omega^{\widetilde{G}}_{\mathrm{LSP}} h^2 = \frac{m_{\mathrm{LSP}}}{m_{\widetilde{G}}}\, \Omega_{\widetilde{G}} h^2 \simeq 2.7 \times 10^{-2} \left(\frac{m_{\mathrm{LSP}}}{100\,\mathrm{GeV}}\right) \left(\frac{T_{\mathrm{RH}}\,(\widetilde{m}_1, M_1)}{10^{10}\,\mathrm{GeV}}\right) . \tag{8.6}$$

For LSP masses below 1 TeV, which are most interesting for the LHC as well as for direct searches, the total LSP abundance,

$$\Omega_{\widetilde{w},\widetilde{h}} h^2 = \Omega^{\widetilde{G}}_{\widetilde{w},\widetilde{h}} h^2 + \Omega^{\mathrm{th}}_{\widetilde{w},\widetilde{h}} h^2 , \tag{8.7}$$

is thus dominated by the contribution from gravitino decay.

Finally, we point out that due to the large mass hierarchy, $m_{\widetilde{G}} \gg m_{\mathrm{LSP}}$, the LSPs are produced relativistically. They thus form *warm* dark matter, which can affect structure formation on small scales. A straightforward calculation yields the free-streaming length λ_{FS},

$$\lambda_{\mathrm{FS}} = \int_{\tau_{\widetilde{G}}}^{t_0} dt\, \frac{v_{\mathrm{LSP}}}{a} \simeq \left(\frac{3}{4}\right)^{2/3} \frac{m_{\widetilde{G}}}{2\, m_{\mathrm{LSP}}} \left(\tau_{\widetilde{G}}\, t_{\mathrm{eq}}\right)^{1/2} \left(\frac{t_0}{t_{\mathrm{eq}}}\right)^{2/3} \left[\ln \frac{16\, t_{\mathrm{eq}}\, m^2_{\mathrm{LSP}}}{\tau_{\widetilde{G}}\, m^2_{\widetilde{G}}} + 4\right] , \tag{8.8}$$

where v_{LSP} denotes the time-dependent absolute value of the three-velocity of an LSP which is produced in the decay of a heavy gravitino at time $\tau_{\widetilde{G}}$. Furthermore, t_{eq} and t_0 are the time of radiation-matter equality and the age of the universe, respectively (cf. Eq. (2.22)). For the gravitino and LSP masses that we consider in this chapter, one finds $\lambda_{\mathrm{FS}} \lesssim 0.1\,\mathrm{Mpc}$, which is below the scales relevant for structure formation [282].

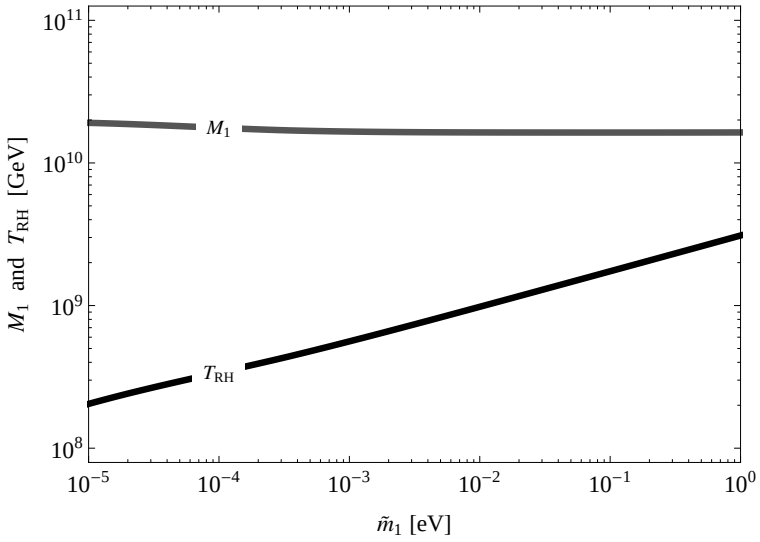

Figure 8.1: Lower bounds on the heavy (s)neutrino mass M_1 and the reheating temperature $T_{\rm RH}$ as functions of the effective neutrino mass $\widetilde{m}_1$ from successful leptogenesis.

8.2 Relations between Neutralino, Gravitino and Neutrino Masses

Requiring consistency between all ingredients of our scenario, we are able to deduce (i) constraints on the reheating temperature as well as bounds on the neutralino and the gravitino mass, which (ii) mutually depend on each other and (iii) also vary as functions of the effective neutrino mass $\widetilde{m}_1$. We shall now discuss these results one after another.

Bounds on the Reheating Temperature

Successful leptogenesis implies a lower bound on the heavy (s)neutrino mass M_1, which slightly depends on $\widetilde{m}_1$ (cf. Fig. 7.6). After averaging out the dependence on $\widetilde{m}_1$, we already stated the rough magnitude of this bound in Eq. (7.113). Now we fully present its behaviour as a function of $\widetilde{m}_1$ in Fig. 8.1. As each pair of $\widetilde{m}_1$ and M_1 values corresponds to a specific value of the reheating temperature $T_{\rm RH}$ (cf. Fig. 7.5), the lower bound on M_1 is readily translated into a lower bound on $T_{\rm RH}$, which is also displayed in Fig. 8.1.

The LSP has to be heavier than 94 GeV, the current lower bound on chargino masses [2]. From the requirement of LSP dark matter, i.e. $\Omega_{\rm LSP}h^2 = \Omega_{\rm DM}h^2 \simeq 0.11$, one then obtains an upper bound on the reheating temperature, $T_{\rm RH} < 4.2\times10^{10}$ GeV. For gravitino masses below 40 TeV, primordial nucleosynthesis provides a more stringent upper bound on the reheating temperature [131]. In Fig. 8.2, we compare upper and lower bounds on the reheating temperature from dark matter density, nucleosynthesis and leptogenesis, respectively, as functions of

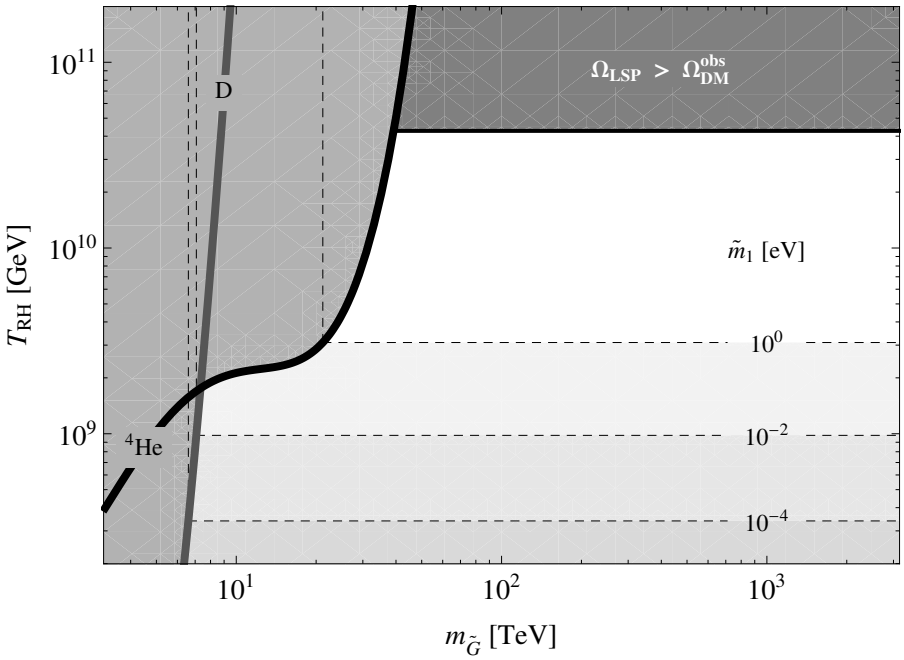

Figure 8.2: Upper and lower bounds on the reheating temperature as functions of the gravitino mass. The horizontal dashed lines denote lower bounds imposed by successful leptogenesis for different values of the effective neutrino mass $\widetilde{m}_1$, cf. Fig. 8.1. The curves labeled ^{4}He and D denote upper bounds originating from the primordial helium-4 and deuterium abundances created during BBN, which are taken from [131] (case 2, which gives the most conservative bounds). The vertical dashed lines represent the absolute lower bounds on the gravitino mass for fixed effective neutrino mass $\widetilde{m}_1$ and minimal reheating temperature. The shaded region marked $\Omega_{\rm LSP} > \Omega_{\rm DM}^{\rm obs}$ is excluded, as it corresponds to overproduction of dark matter, taking into account that the LSP mass is bounded from below, $m_{\rm LSP} \geq 94\,\text{GeV}$.

the gravitino mass. It is remarkable that for the entire mass range, 10 TeV $\lesssim m_{\widetilde{G}} \lesssim 10^3$ TeV, nucleosynthesis, dark matter and leptogenesis can be consistent.

Relation between the Neutralino and the Gravitino Mass

The dark matter constraint $\Omega_{\rm LSP}h^2 = \Omega_{\rm DM}h^2 \simeq 0.11$, with $\Omega_{\rm LSP}h^2$ calculated according to Eqs. (8.2), (8.6) and Eq. (8.7), establishes a one-to-one connection between LSP masses and values of the reheating temperature. This relation maps the viable region in the $(m_{\widetilde{G}}, T_{\rm RH})$-plane for a given effective neutrino mass $\widetilde{m}_1$ into the corresponding viable region in the $(m_{\widetilde{G}}, m_{\rm LSP})$-plane. We present our results for higgsino and wino LSP in the two panels of Fig. 8.3, respectively. The upper bound on the LSP mass is a consequence of the lower bound on the reheating temperature from leptogenesis, which is why it depends on the effective

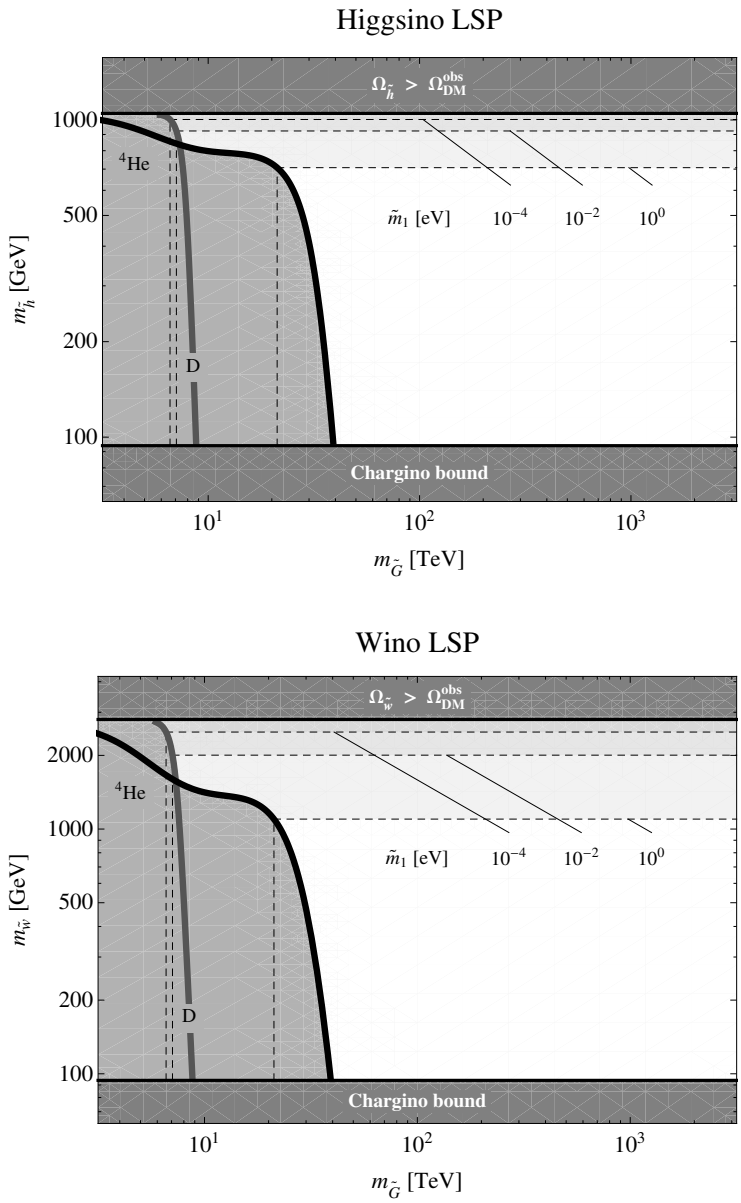

Figure 8.3: Upper and lower bounds on the LSP mass in the higgsino and wino case, respectively, and lower bounds on the gravitino mass. These bounds are in one-to-one correspondence with the bounds on the reheating temperature and the gravitino mass in Fig. 8.2. The horizontal dashed lines denote the upper bounds on the LSP mass imposed by successful leptogenesis for different values of the effective neutrino mass $\widetilde{m}_1$. The curves labeled ^{4}He and D denote lower bounds on the LSP as well as on the gravitino mass originating from the primordial helium-4 and deuterium abundances created during BBN. The vertical dashed lines represent the absolute lower bounds on the gravitino mass for fixed effective neutrino mass $\widetilde{m}_1$ and maximal LSP mass. The dark shaded regions on the upper edge of the plots correspond to thermal overproduction of dark matter and are hence excluded. We do not consider LSP masses below 94 GeV due to the present lower bound on the chargino mass.

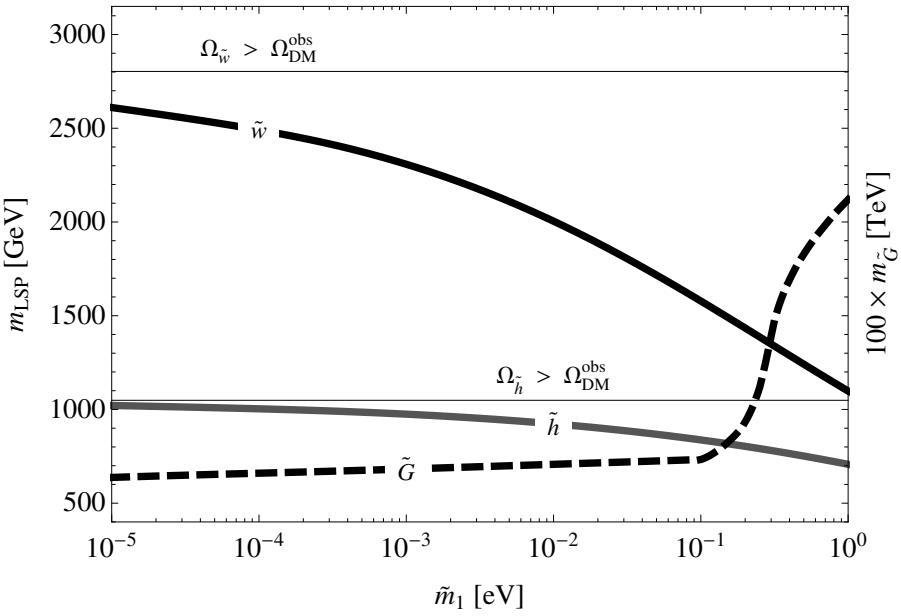

Figure 8.4: Upper bounds on wino ($\widetilde{w}$) and higgsino ($\widetilde{h}$) LSP masses imposed by successful leptogenesis as well as absolute lower bound on the gravitino mass according to BBN as functions of the effective neutrino mass $\widetilde{m}_1$. Note that in Fig. 8.3 these bounds are indicated by horizontal and vertical dashed lines, respectively, for different value for $\widetilde{m}_1$. Wino masses larger than 2.8 TeV and higgsino masses larger than 1.0 TeV result in thermal overproduction.

neutrino mass $\widetilde{m}_1$. The lower bound on the LSP mass corresponds to the upper bound on the reheating temperature from BBN and hence depends on the gravitino mass $m_{\widetilde{G}}$. This latter relation between $m_{\rm LSP}$ and $m_{\widetilde{G}}$ can also be interpreted the other way around. As each LSP mass is associated with a certain reheating temperature, we find for each value of $m_{\rm LSP}$ a lower bound on the gravitino mass. For given $\widetilde{m}_1$, we then obtain an absolute lower bound on the gravitino mass by raising the LSP mass to its maximal possible value.

Dependence on the Effective Neutrino Mass

The upper bound on the LSP mass as well as the absolute lower bound on the gravitino mass both depend on the effective neutrino mass $\widetilde{m}_1$. In Fig. 8.4, we now finally show the explicit dependence of these bounds on $\widetilde{m}_1$. The upper bound on the LSP mass imposed by successful leptogenesis increases when lowering $\widetilde{m}_1$, i.e. when extending the range of allowed reheating temperatures to lower values. For very small $\widetilde{m}_1$, it approaches the upper bound on the LSP mass above which thermal freeze-out leads to an overabundance of LSPs. At large values of $\widetilde{m}_1$, the bound on the LSP mass from leptogenesis becomes stronger. Furthermore, we find that the absolute lower bound on the gravitino mass is rather insensitive to the effective

neutrino mass for $\widetilde{m}_1 \lesssim 10^{-1}$ eV, but rapidly increases as a function of $\widetilde{m}_1$ for larger values of $\widetilde{m}_1$. This reflects the fact that small values of $\widetilde{m}_1$ correspond to low reheating temperatures, for which the allowed range of gravitino masses, being determined by the BBB abundance of deuterium, hardly changes when varying the temperature. It turn, when the allowed range of gravitino masses is determined by the BBN abundance of helium-4, which is the case for very large $\widetilde{m}_1$, the absolute lower bound on $m_{\widetilde{G}}$ increases with $\widetilde{m}_1$.

8.3 Prospects for Direct Detection and Collider Experiments

We conclude with a few remarks on the prospects for the confirmation of our scenario in direct detection and/or collider experiments.

Direct Detection Experiments

For pure wino and higgsino LSPs, the exchange of the lightest Higgs boson yields at tree level for the spin-independent elastic scattering cross section [283]

$$\sigma_{\rm SI}^{\widetilde{w}} \sim 2 \times 10^{-43}\,{\rm cm}^2 \left(\frac{125\,{\rm GeV}}{m_{h^0}}\right)^4 \left(\frac{100\,{\rm GeV}}{m_{\widetilde{h}}}\right)^2 \left(\sin 2\beta + \frac{m_{\widetilde{w}}}{m_{\widetilde{h}}}\right)^2 , \tag{8.9}$$

$$\sigma_{\rm SI}^{\widetilde{h}} \sim 7 \times 10^{-44}\,{\rm cm}^2 \left(\frac{125\,{\rm GeV}}{m_{h^0}}\right)^4 \left(\frac{100\,{\rm GeV}}{m_{\widetilde{w}}}\right)^2 ,$$

where m_{h^0} is the mass of the lightest Higgs boson. For the hierarchical mass spectrum of Eq. (8.1), one has $r_{\widetilde{w}} \equiv m_{\widetilde{w}}/m_{\widetilde{h}} \ll 1$ for wino LSP and $r_{\widetilde{h}} \equiv m_{\widetilde{h}}/m_{\widetilde{w}} \ll 1$ for higgsino LSP, respectively. Hence, the spin-independent scattering cross sections are significantly below the present experimental sensitivity for LSP masses below 1 TeV.

Collider Signatures

For the considered hierarchy of superparticle masses, gluinos and squarks are heavy. Hence, the characteristic missing energy signature of events with LSPs in the final state may be absent and the discovery of winos or higgsinos therefore very challenging.[3] In both cases the neutral LSP is almost mass degenerate with a chargino, which increases the discovery potential. One may hope for macroscopic charged tracks of the produced charginos. A generic prediction is also the occurrence of monojets caused by the Drell-Yan production of higgsino/wino pairs in association with initial state gluon radiation.

[3] For recent discussions, cf. for instance Refs. [284–286].

Chapter 9

Conclusions and Outlook

Cosmological phase transitions might be common events in the history of the hot early universe. Extrapolating the evolution of the universe back in time beyond primordial nucleosynthesis, we expect for instance the QCD as well as the electroweak phase transition to take place at temperatures around the QCD and the electroweak scale, respectively. In this thesis, we have now proposed the idea that also the very origin of the hot early universe as well as the generation of its initial conditions are connected to a phase transition, *viz.* the $B-L$ phase transition, which represents the cosmological realization of spontaneous $B-L$ breaking.

The false vacuum phase of unbroken $B-L$ symmetry drives a stage of hybrid inflation, which ends in a waterfall transition that is accompanied by tachyonic preheating and the production of topological defects in the form of cosmic strings. Successful inflation and the nonobservation of cosmic strings require the $B-L$ phase transition to occur at the GUT scale, which strengthens the supposition that the breaking of $B-L$ at the end of inflation might be embedded in the breaking scheme of some more comprehensive theory of grand unification. Tachyonic preheating, the decay of the $B-L$ gauge DOFs, the decay of the $B-L$ Higgs bosons and its superpartners as well as thermal processes produce an abundance of heavy (s)neutrinos. These (s)neutrinos decay into the lepton-Higgs pairs of the supersymmetric standard model, which reheats the universe and generates a primordial lepton asymmetry. At the same time, inelastic scattering processes in the thermal bath unavoidably lead to a thermal abundance of gravitinos. The initial conditions of the hot thermal phase of the early universe hence end up being completely determined by the parameters of the fundamental Lagrangian which governs the dynamics of the $B-L$ phase transition as well as the interactions of the heavy (s)neutrinos. This is to say that the temperature scale of reheating, the primordial baryon asymmetry as well as the thermal gravitino abundance are no longer unknown cosmological parameters. Instead, they are related to the masses and couplings of elementary particles, which can in principle be measured in particle physics experiments and astrophysical observations.

We have studied the $B-L$ phase transition in the full supersymmetric Abelian Higgs model and given a detailed time-resolved description of the reheating process based on the complete set of Boltzmann equation. A notable result of our analysis is that the competition of cosmic expansion and entropy production leads to an intermediate plateau of constant temperature, during which baryon asymmetry and gravitinos are produced. Remarkably, the final asymmetry as well as gravitino abundance are rather insensitive to many of the theoretical uncertainties associated with the $B-L$ phase transition and the subsequent reheating process. We have explicitly checked that the final outcomes of our calculations are robust against modifications of the theoretical framework pertaining to (i) the production and relaxation of cosmic strings, (ii) the massive superparticles, and (iii) the $B-L$ gauge DOFs. For instance, even if 50 % of the false vacuum energy density is initially stored in strings, they quickly loose most of their energy and the effect on the final baryon asymmetry and gravitino abundance is negligible. This robustness is due to the fact that after all most of the energy of the false vacuum is transferred to the $B-L$ Higgs bosons, whose slow decay, via heavy (s)neutrinos, dominates the reheating process.

In order to circumvent the cosmological gravitino problems, we have considered two, in a sense quite opposite superparticle mass spectra. In our first scenario, we took the gravitino to be the LSP. In this case, the requirement of consistency between hybrid inflation, leptogenesis and gravitino dark matter provided us with relations between neutrino and superparticle masses. For a gluino with a mass of 1 TeV, we a find a lower bound on the gravitino mass of about 10 GeV. The mass of the lightest of the heavy neutrinos M_1 typically has to have a value of order 10^{11} GeV. For a wide range of light neutrino masses, this results in a reheating temperature of order $10^9..10^{10}$ GeV. Our second scenario was motivated by hints for a 125 GeV Higgs boson at the LHC and featured the gravitino as the heaviest superparticle along with WIMP dark matter in the form of pure wino or higgsino LSPs. In this scenario, heavy gravitinos, which are thermally produced during reheating, decay at some time between the QCD phase transition and BBN into LSPs, thereby nonthermally generating the dark matter. This time, the requirement of consistency between hybrid inflation, leptogenesis, WIMP dark matter and BBN allowed us to derive upper and lower bounds on the LSP mass as well as lower bounds on the gravitino mass, all of which depend on the lightest neutrino mass.

On the way towards these phenomenological results, we completed a number of technical tasks, some of which deserve particular attention. First of all, we derived the Lagrangian of a general supersymmetric Abelian gauge theory in arbitrary gauge and concretized it for the Abelian Higgs model of the $B-L$ phase transition in unitary gauge. Furthermore, we gave a detailed discussion of the nonperturbative dynamics during the $B-L$ phase transition and generalized Linde's waterfall conditions for hybrid inflation to the supersymmetric case. Next, we devoted ourselves to the Boltzmann equations governing the reheating process. Partly, we were able to solve these equations analytically. Apart from that, we developed techniques

for the treatment of (i) the various contributions to the heavy (s)neutrino abundances, (ii) the evolution of the gravitational background, and (iii) the evolution of the temperature of the thermal bath. Finally, we addressed several important technical issues in the appendices such as the CP violation in 2-to-2 scatterings with intermediate (s)neutrino states or the generalization of our analysis to other gluino masses.

Besides its cosmological consequences, we have also studied the implications of the $B-L$ phase transition for the standard model neutrino sector. The breaking of $B-L$ during the decay of the false vacuum sets the stage for the seesaw mechanism. Upon the seesaw model we imposed a flavour structure of the Froggatt-Nielsen type, which naturally accounts for the measured quark and lepton mass hierarchies and the large neutrino mixing angles. Combining this flavour structure with the present knowledge on neutrino parameters, we were able to derive precise predictions for yet unknown observables, in particular the smallest mixing angle θ_{13}, the smallest neutrino mass m_1, and the Majorana phase α_{21}. This statement is based on a Monte-Carlo study: treating unspecified $\mathcal{O}(1)$ parameters of the considered Froggatt-Nielsen model as random variables, we found that the observables of interest are sharply peaked around certain central values.

In this thesis, we have made use of the fact that, in the context of supersymmetric hybrid inflation, the amplitude of the scalar power spectrum requires the $B-L$ breaking scale to be of order the GUT scale (cf. Eqs. (3.16) and (6.13)). However, one may also ignore this requirement and merely assume that the inflationary dynamics being responsible for the primordial scalar perturbations are in fact more complicated than in the simple hybrid inflation model considered in the present case. Under this assumption, the $B-L$ phase transition may equally take place at a scale much below the GUT scale. In Ref. [58], we investigate this possibility in more detail and arrive at the result that lower values of the $B-L$ breaking scale entail weaker bounds on the gravitino mass. If the $B-L$ phase transition occurs for instance at a scale $v_{B-L} \sim 10^{12}\,\mathrm{GeV}$, the gravitino could have a mass of $\mathcal{O}(100)\,\mathrm{MeV}$. Similarly, for a lower $B-L$ breaking scale, reheating would occur at a higher temperature because of faster Higgs decays. This would result in a stronger washout of the lepton asymmetry generated in (s)neutrino decays. Small v_{B-L} hence implies an upper bound on the effective neutrino mass $\widetilde{m}_1$ of about $0.1\,\mathrm{eV}$. In this thesis, we have by contrast demonstrated that, if the $B-L$ phase transition takes place at the GUT scale, this restriction does no longer apply, rendering the proposed reheating mechanism viable for all reasonable masses of the light neutrinos. On the other hand, reducing the gravitino mass from $\mathcal{O}(10)\,\mathrm{GeV}$ to $\mathcal{O}(100)\,\mathrm{MeV}$ significantly shortens the lifetime of the NLSP, which may soften the bound on the NLSP mass imposed by the requirement that the late-time decays of the NLSP must not spoil the success of BBN (cf. Sec. 3.1.4). A lower $B-L$ breaking scale thus possibly entails a simple solution to the NLSP decay problem, albeit at the cost of a more complicated inflationary sector.

An interesting alternative to supersymmetric F-term hybrid inflation is supersymmetric D-term hybrid inflation. In this inflationary model, inflation ends in the same manner as in the F-term model discussed in this thesis. The $B-L$ phase transition is in particular still required to occur at the GUT scale. But, allowing for noncanonical terms in the Kähler potential, the D-term variant of hybrid inflation may possibly improve upon its F-term sibling in terms of the predicted value for the scalar spectral index (cf. Sec. 3.1.1). In an ongoing research project, we currently consider a model in which the structure of the nonminimal Kähler potential is determined by the requirement that the superconformal invariance inherent in the superpotential of D-term hybrid inflation be only slightly broken during inflation.[1]

Further important questions which have remained unanswered in this thesis concern the role of the inflaton field during tachyonic preheating, if one goes beyond the quench approximation. In particular, it is necessary to investigate how the false vacuum energy is distributed among the waterfall and the inflaton field when oscillations in field configuration space in the direction of the inflaton field are also taken into account. Moreover, one may introduce a further constant term W_0 in the superpotential, which might unavoidably arise in the course of spontaneous supersymmetry breaking [34],

$$W_0 = m_{\widetilde{G}} M_P^2 \,. \tag{9.1}$$

This superpotential induces a mass mixing term for the waterfall and the inflaton field, which may partly affect the details of the reheating process. However, as the waterfall and the inflaton field both decay into the same chiral multiplet, *viz.* the heavy (s)neutrinos of the first generation, we do not expect this mass mixing and in fact the entire superpotential W_0 to lead to any qualitative changes of the overall picture presented in this thesis. Related to the occurrence of the term W_0 in the superpotential, one may also ask whether there potentially is a connection between the spontaneous breaking of $B-L$ at the end of hybrid inflation and the spontaneous breaking of supersymmetry. Assuming that the NLSP decay problem is avoided due to a small amount of R-parity breaking, this question equally applies to the mechanism for the breaking of R parity.

One may also address the production of gravitational waves during the $B-L$ phase transition. In an ongoing research project, we currently attempt to calculate the spectrum of gravitational waves that is generated during the decay of the false vacuum.[2] Finally, we point out that the warm WIMP dark matter scenario which we discussed in Ch. 8 might after all have interesting consequences for the formation of matter structures on small scales. It seems worthwhile to go further into this question as well.

In summary, we conclude that the decay of a false vacuum of unbroken $B-L$ symmetry represents indeed an intriguing possibility to implement the transition between inflation and

[1] As of July 2013, the work on this project has been completed; its results have been published in Ref. [287].

[2] As of July 2013, this project is almost complete; a preprint summarizing our results is available online [288].

the hot thermal phase of the early universe. Tachyonic preheating after hybrid inflation and the dynamics of the $B-L$ gauge DOFs set the stage for a matter dominated phase, whose evolution towards a hot thermal state is described by means of Boltzmann equations. We have carefully studied this process, putting particular emphasis on the various nonthermal and thermal contributions to the abundances of the heavy (s)neutrinos, and eventually arrived at a consistent picture of the early universe, whose properties are largely determined by the parameters of the neutrino sector. Measurements of the absolute neutrino mass scale and superparticle masses consistent with our predictions would hence provide important indirect evidence for the $B-L$ phase transition as the origin of the hot early universe.

Acknowledgements

In the first place, I wish to express my gratitude to Wilfried Buchmüller, who opened the door for me into particle cosmology. Having always been enthusiastic about cosmology and particle physics, I consider myself fortunate to have been given the opportunity to work with him on the physics of the early universe. He has been an excellent advisor, teacher and mentor.

I am also especially grateful to Valerie Domcke and Gilles Vertongen for their collaboration at different stages of the work presented in this thesis. Furthermore, I would like to thank Guido Altarelli, Torsten Bringmann, Felix Brümmer, Laura Covi, Kohei Kamada, Graham Ross, Fuminobu Takahashi, David Wark, Walter Winter, and Tsutomu Yanagida for helpful discussions and comments. My sincere gratitude goes to Jan Louis and Günter Sigl for agreeing to act as referees of my disputation and my dissertation, respectively. Moreover, I acknowledge support by the German Science Foundation (DFG) within the Collaborative Research Center (SFB) 676 "Particles, Strings and the Early Universe".

I highly appreciate the fact that DESY is a unique research facility offering doctoral candidates in particle physics a stimulating and inspiring environment. I benefited countless times from the high level of expertise which can be found everywhere at DESY and I am thankful to all people at DESY who helped and supported me in the course of the last three years. Many thanks go out to all members of the DESY Theory Group for the pleasant time and in particular to my office mates Jasper Hasenkamp, Michael Grefe, Vladimir Mitev, Sebastian Schmidt, and Václav Tlapák for the enjoyable atmosphere in our office. My time at DESY would not have been the same without Kranzzeit and our common lunch seminars.

Finally, I wish to thank my friends and fellows Sergei Bobrovskyi, Martin Krasny, Falk Lindner, and Markus Rummel, who stood by me through all ups and downs. It is thanks to them that my time in Hamburg became a once-in-a-lifetime experience and I am excited to see how our story continues. The same holds true for my friends and my family in and from Berlin. Throughout the years, I could always count on my fellow students Christopher Bronner, Frank Essenberger, Max Hoffmann, Kai Kornhuber, and Andreas Linscheid, on my friends Monia Gläske and Wolfgang Hasse as well as on my brother, my sisters and my parents.

Appendix A

Statistical Thermodynamics

In Ch. 7, we derive and solve the coupled system of semiclassical Boltzmann equations describing the cosmic evolution after the $B-L$ phase transition. As a supplement to this analysis, we summarize the underlying formalism of Boltzmann equations in this appendix (cf. Sec. A.1). In addition to that, we also discuss the properties of particle species in kinetic or thermal equilibrium (cf. Sec. A.2).

A.1 Kinetic Theory in the Expanding Universe

The Boltzmann equation for a particle species X describes the time evolution of its phase space distribution function f_X in the one-particle phase space Φ_X [62]. The distribution function f_X is defined such that $f_X d\Phi_X$ gives the average number of X particles in the phase space volume $d\Phi_X$ at time t. In general, f_X is a function of time t as well as of all phase space coordinates. But imposing homogeneity and isotropy of spacetime, f_X ends up solely depending on time t and the absolute value p of the physical three-momentum $\mathbf{p}$. In the Friedmann-Lemaître framework, the Boltzmann equation for f_X reads

$$\hat{\mathcal{L}} f_X(t,p) = E_X \left(\frac{\partial}{\partial t} - Hp \frac{\partial}{\partial p} \right) f_X(t,p) = \mathcal{C}_X \,, \quad E_X = \sqrt{p^2 + m_X^2} \,, \tag{A.1}$$

where $\hat{\mathcal{L}}$ denotes the Liouville operator, $\mathcal{C}_X$ stands for the total collision operator, H is the Hubble rate and m_X the mass of an X particle. $\mathcal{C}_X$ keeps track of changes in f_X due to elastic and inelastic interactions and may be decomposed into individual collision operators C_X, respectively accounting for all the different processes through which an X particle may interact with other particles $a, b, ..$ and $i, j, ..$,

$$\mathcal{C}_X = \sum_{ab..} \sum_{ij..} C_X(Xab.. \leftrightarrow ij..) = \sum_{ij..} C_X(X \leftrightarrow ij..) + \sum_{a} \sum_{ij..} C_X(Xa \leftrightarrow ij..) + \ldots \tag{A.2}$$

The operators C_X are obtained from integrating quantum mechanical transition probabilities $(2\pi)^4 \delta^{(4)} |\mathcal{M}|^2$ over the multi-particle phase space,

$$\begin{aligned} C_X(Xab.. \leftrightarrow ij..) = \frac{1}{2g_X} \int d\Pi \, (X|a,b,..;i,j,..) \, (2\pi)^4 \, \delta^{(4)} \left(\sum p_{\text{out}} - \sum p_{\text{in}}\right) \\ \times \left[f_i f_j .. \left(1 \pm f_X\right) \left(1 \pm f_a\right) \left(1 \pm f_b\right) .. \left|\mathcal{M}\left(ij.. \to Xab..\right)\right|^2 \right. \\ \left. - f_X f_a f_b .. \left(1 \pm f_i\right) \left(1 \pm f_j\right) .. \left|\mathcal{M}\left(Xab.. \to ij..\right)\right|^2 \right], \end{aligned} \tag{A.3}$$

where g_X is the number of internal DOFs of X and $d\Pi$ subsumes all Lorentz-invariant momentum space elements $d\tilde{p} = (2\pi)^{-3} \, d^3p/2E$ along with a statistical factor S, preventing us from double counting in the case of identical particles,

$$d\Pi(X|a,b,..;i,j,..) = S(X,a,b,..;i,j,..) d\tilde{p}_a d\tilde{p}_b .. d\tilde{p}_i d\tilde{p}_j .. \,. \tag{A.4}$$

The amplitudes squared $|\mathcal{M}|^2$ are understood to be summed over all internal DOFs of the particles in the initial and in the final state. $(1+f)$ and $(1-f)$ are quantum statistical factors, respectively implementing the effects of the Bose enhancement and Pauli blocking.[1] These factors are expected to have only a minor impact on the evolution of the distribution function [274]. In particular, their influence may partly be canceled by other quantum corrections like off-shell effects [289]. We shall thus neglect the quantum statistical factors in this thesis. Finally, we note that the operators C_X may be split into two parts, respectively accounting for the two directions in which the corresponding processes may proceed,

$$C_X(Xab.. \leftrightarrow ij..) = C_X(ij.. \to Xab..) - C_X(Xab.. \to ij..) \,. \tag{A.5}$$

The number density n_X of the particle species X follows from integrating its distribution function f_X over the momentum space element $g_X d^3p_X / (2\pi)^3$,

$$n_X(t) = \frac{g_X}{(2\pi)^3} \int d^3p \; f_X(t,p) \,. \tag{A.6}$$

Similarly, the corresponding energy density ρ_X is given as the integral over $E_X f_X$,

$$\rho_X(t) = \frac{g_X}{(2\pi)^3} \int d^3p \; E_X f_X(t,p) \,. \tag{A.7}$$

Dividing the Boltzmann equation in Eq. (A.1) by E_X on both sides and again integrating over $g_X d^3p_X / (2\pi)^3$ yields the first moment of the Boltzmann equation or simply the *integrated Boltzmann equation* for the number density n_X,

$$\dot{n}_X + 3Hn_X = \hat{\gamma}_X = \sum_{ab..} \sum_{ij..} \gamma(Xab.. \leftrightarrow ij..) \,, \tag{A.8}$$

[1] The Boltzmann equation is actually a *classical* evolution equation for f_X. However, using quantum mechanical S matrix elements as well as including the quantum statistical factors $(1 \pm f)$ in the calculation of the actually *classical* collision operators C_X renders it *semiclassical*.

with $\hat{\gamma}$ being the total spacetime density of inelastic interaction events involving particles of species X. The individual interaction densities γ are defined as

$$\gamma(Xab.. \leftrightarrow ij..) = \frac{g_X}{(2\pi)^3} \int \frac{d^3p}{E_X} C_X(Xab.. \leftrightarrow ij..) \,. \tag{A.9}$$

The Boltzmann equation in Eq. (A.8) can alternatively be written as an equation for the comoving number density $N_X = a^3 n_X$ as a function of the scale factor a,

$$aH \frac{d}{da} N_X = a^3 \hat{\gamma}_X = a^3 \sum_{ab..} \sum_{ij..} \gamma(Xab.. \leftrightarrow ij..) = \hat{\Gamma}_X N_X \,, \tag{A.10}$$

where we have introduced $\hat{\Gamma}_X$ as the total effective production rate of X particles,

$$\hat{\Gamma}_X = \frac{\hat{\gamma}_X}{n_X} = \frac{1}{N_X} a^3 \hat{\gamma}_X = \frac{1}{N_X} a^3 \sum_{ab..} \sum_{ij..} \gamma(Xab.. \leftrightarrow ij..) \,. \tag{A.11}$$

A.2 Kinetic and Thermal Equilibrium

The phase distribution function of a bosonic particle species X in kinetic equilibrium is given by the Bose-Einstein distribution (-1), whereas the phase distribution function of a fermionic particle species X in kinetic equilibrium corresponds to the Fermi-Dirac distribution ($+1$),

$$f_X(t,p) = \frac{1}{e^{(E_X - \mu_X)/T_X} \pm 1} \,. \tag{A.12}$$

Here, μ_X denotes the chemical potential of the particle species X and T_X is its equilibrium temperature. If the interactions between X particles and photons are fast enough, the temperature T_X coincides with the photon temperature T, i.e. the temperature of the thermal bath. The chemical potentials of the MSSM particles are an important ingredient to the calculation of the sphaleron conversion factor C_{sph} (cf. Eq. 2.32). If inelastic processes between different particle species are sufficiently fast, their respective chemical potentials are related to each other and the involved species are said to be in chemical equilibrium. For each independently conserved particle number, there exists in particular one independent chemical potential. Conversely, if there are no constraints on the number of X particles enforced by conservation laws, the chemical potential of species X vanishes. In this thesis, we refer to a collection of particle species with negligibly small chemical potentials that is in chemical equilibrium as being in thermal equilibrium. The phase space distribution function of a bosonic or fermionic species X in thermal equilibrium is therefore given as

$$f_X^{\mathrm{eq}}(t,p) \approx \frac{1}{e^{E_X/T_X} \pm 1} \,. \tag{A.13}$$

Furthermore, for all particles acquiring a mass in the course of $B-L$ breaking, we approximate the respective distributions in kinetic and thermal equilibrium, f_X and f_X^{eq}, by classical

Maxwell-Boltzmann distributions,

$$f_X(t,p) \approx e^{-(E_X-\mu_X)/T_X}\,, \quad f_X^{\rm eq}(t,p) \approx e^{-E_X/T_X}\,. \tag{A.14}$$

The number and energy densities of *massless* bosons and fermions in thermal equilibrium are readily obtained from Eqs. (A.6), (A.7) and (A.13),

$$\begin{aligned} \text{Bosons:} \qquad & n_X^{\rm eq} = \quad g_X \frac{\zeta(3)}{\pi^2} T_X^3\,, \quad \rho_X^{\rm eq} = \quad g_X \frac{\pi^2}{30} T_X^4\,, \\ \text{Fermions:} \qquad & n_X^{\rm eq} = \frac{3}{4}\, g_X \frac{\zeta(3)}{\pi^2} T_X^3\,, \quad \rho_X^{\rm eq} = \frac{7}{8}\, g_X \frac{\pi^2}{30} T_X^4\,, \end{aligned} \tag{A.15}$$

where ζ is the Riemann zeta function. With the aid of these expressions, we are able to write down n_R and ρ_R, the number and the energy density of MSSM radiation quanta in the thermal bath,

$$n_R = g_{*,n} \frac{\zeta(3)}{\pi^2} T^3\,, \quad \rho_R = g_{*,\rho} \frac{\pi^2}{30} T^4\,, \tag{A.16}$$

with $g_{*,n}$ and $g_{*,\rho}$ being the corresponding effective sums of relativistic DOFs,

$$\begin{aligned} g_{*,n} &= \sum_{\rm bosons} g_X \left(\frac{T_X}{T}\right)^3 + \frac{3}{4} \sum_{\rm fermions} g_X \left(\frac{T_X}{T}\right)^3\,, \\ g_{*,\rho} &= \sum_{\rm bosons} g_X \left(\frac{T_X}{T}\right)^4 + \frac{7}{8} \sum_{\rm fermions} g_X \left(\frac{T_X}{T}\right)^4\,. \end{aligned} \tag{A.17}$$

Setting all equilibrium temperatures T_X to the photon temperature T, the MSSM values of $g_{*,n}$ and $g_{*,\rho}$ turn out to be $427/2$ and $915/4$, respectively. From the result for ρ_R in Eq. (A.16), we can easily deduce an expression for the radiation entropy density s_R. Making use of the equation of state of radiation, $\omega_R = p_R/\rho_R = 1/3$, where p_R is the radiation pressure, we find

$$\begin{aligned} s_R &= \frac{\rho_R + p_R}{T} = \frac{4}{3}\frac{\rho_R}{T} = g_{*,s} \frac{2\pi^2}{45} T^4\,, \\ g_{*,s} &= \sum_{\rm bosons} g_X \left(\frac{T_X}{T}\right)^3 + \frac{7}{8} \sum_{\rm fermions} g_X \left(\frac{T_X}{T}\right)^3\,. \end{aligned} \tag{A.18}$$

With all equilibrium temperatures T_X coinciding with the photon temperature T, $g_{*,s}$ equals $g_{*,\rho}$. In the MSSM, we then have $g_{*,s} = 915/4$. For *massive* particles in thermal equilibrium, now employing the approximation in Eq. (A.14), we obtain,

$$n_X^{\rm eq} = g_X \frac{m_X^3}{2\pi^2 z_X} K_2(z_X)\,, \quad \rho_X^{\rm eq} = g_X \frac{m_X^4}{2\pi^2} \left[\frac{1}{z_X} K_1(z_X) + \frac{3}{z_X^2} K_2(z_X)\right]\,. \tag{A.19}$$

Here, $z_X = m_X/T_X$ represents the inverse temperature in units of m_X^{-1}, while K_n denotes the modified Bessel function of the second kind of order n.

Finally, we note that, approximating the distribution functions f_X and f_X^{eq} by Maxwell-Boltzmann distributions as in Eq. (A.14), implies that f_X is proportional to f_X^{eq},

$$f_X(t,p) = R_X(t) f_X^{\mathrm{eq}}(t,p)\,, \quad R_X(t) = e^{\mu_X/T_X}\,, \tag{A.20}$$

According to Eq. (A.6), R_X is nothing but the ratio of n_X to the number density in thermal equilibrium, $R_X = n_X/n_X^{\mathrm{eq}}$. Here, the number density n_X may have any value. Furthermore, one can easily show that R_X also corresponds to the ratio of the energy density ρ_X and the corresponding energy density in thermal equilibrium ρ_X^{eq},

$$\rho_X = R_X(t)\rho_X^{\mathrm{eq}} = \frac{n_X}{n_X^{\mathrm{eq}}}\rho_X^{\mathrm{eq}}\,. \tag{A.21}$$

This relation shows in particular that, within the Maxwell-Boltzmann approximation, the average energy per particle $\varepsilon_X = \rho_X/n_X$ in kinetic equilibrium is the same as in thermal equilibrium.

Appendix B

CP Violation in 2-to-2 Scattering Processes

The Boltzmann equation for the lepton asymmetry L corresponds to the difference of the respective equations for the lepton multiplet ℓ and the antilepton multiplet $\bar{\ell}$ (cf. Eq. (7.54)). The ordinary collision operators in the Boltzmann equations for ℓ and $\bar{\ell}$ account for the decays and inverse decays of heavy (s)neutrinos *on the mass shell*. In the Boltzmann equation for the lepton asymmetry, these collision operators induce terms of $\mathcal{O}(\epsilon_i)$. In addition to that, it turns out that $\Delta L = 2$ scatterings with MSSM lepton-Higgs pairs in the external states and *off-shell* (s)neutrinos in the intermediate state yield contributions of the same order in the CP violation parameters ϵ_i to the Boltzmann equation for the lepton asymmetry. To consistently calculate the lepton asymmetry up to first order in the parameters ϵ_i, one therefore has to add the reduced collision operators $\mathcal{C}_{\ell}^{\mathrm{red}}$ and $\mathcal{C}_{\bar{\ell}}^{\mathrm{red}}$ to the equations for ℓ and $\bar{\ell}$ (cf. Eq. (7.55)). These operators incorporate the off-shell contributions to all relevant $\Delta L = 2$ scatterings and are hence related to the full 2-to-2 scattering operators in the following way,

$$\mathcal{C}_X = \mathcal{C}_X^{\mathrm{on}} + \mathcal{C}_X^{\mathrm{red}}\,, \qquad X = \ell, \bar{\ell}\,, \tag{B.1}$$

where $\mathcal{C}_X^{\mathrm{on}}$ are the on-shell collision operators accounting for scattering processes with real intermediate states. In the derivation of the Boltzmann equation for the lepton asymmetry in Sec. 7.1.3, we neglect the CP-preserving parts of all operators in Eq. (B.1) (cf. Eq. (7.56)) and make use of the fact that the CP-violating parts of $\mathcal{C}_X$ vanish up to corrections of $\mathcal{O}\left((h^{\nu})^4\right)$ (cf. Eq. (7.58)). The purpose of this appendix is to show that this is indeed the case,

$$\mathcal{C}_{X,\not{CP}} = 0 + \mathcal{O}\left((h^{\nu})^4\right)\,. \tag{B.2}$$

For the nonsupersymmetric case, a prove of this statement is given in Refs. [186] and [290]. In this appendix we shall now extent it to the supersymmetric case.

The full 2-to-2 scattering operator $\mathcal{C}_X$ is composed of individual collision operators C_X, which are all of the following form,

$$\begin{aligned} C_X(I \leftrightarrow \bar{F}) &= C_X(\bar{F} \to I) - C_X(I \to \bar{F}) \\ C_X(I \to \bar{F}) &= \frac{1}{2g_X} \int d\Pi\left(X|a;ij\right) f_X f_a \left(2\pi\right)^4 \delta^{(4)} \left|M\left(Xa \to \bar{i}\bar{j}\right)\right|^2 , \\ C_X(\bar{F} \to I) &= \frac{1}{2g_X} \int d\Pi\left(X|a;ij\right) f_{\bar{i}} f_{\bar{j}} \left(2\pi\right)^4 \delta^{(4)} \left|M\left(\bar{i}\bar{j} \to Xa\right)\right|^2 . \end{aligned} \tag{B.3}$$

Here, I denotes the pair of initial state particles, $I = Xa = \ell H_u, \tilde{\ell}\tilde{H}_u, \tilde{\ell}H_u, \ell\tilde{H}_u$, while F stands for the pair of antiparticles corresponding to the pair of final state particles $\bar{F}$. For $I = \ell H_u, \tilde{\ell}\tilde{H}_u$, we have $F = I, \tilde{I}$, where $\tilde{I}$ is the pair of superparticles corresponding to the pair of particles I, while for $I = \tilde{\ell}H_u, \ell\tilde{H}_u$, the only possibility is $F = \tilde{I}$. Note that each pair of particles I, F implicitly carries a weak isospin as well as a flavour index. The matrix element squared $|M|^2$ is understood to be summed over all internal DOFs of the particles in the external states. It is directly related to the corresponding S matrix element squared,

$$\left|S\left(Xa \to ij\right)\right|^2 = \left(2\pi\right)^4 \delta^{(4)} \left|M\left(Xa \to ij\right)\right|^2 , \tag{B.4}$$

where $|S|^2$ represents the probability per spacetime unit volume for the occurrence of the process $Xa \to ij$. In the case of distinct particles in the initial and final state, the matrix element squared $|M|^2$ reduce to the ordinary transition amplitude squared $|\mathcal{M}|^2$ (cf. Sec. A.1).

To prove Eq. (B.2), it is sufficient to show that the CP-violating contribution to the sum over all operators $C_X(I \to \bar{F})$ vanishes up to corrections of $\mathcal{O}\left((h^\nu)^4\right)$. In order to do so, we demonstrate that difference between the sum over all operators $C_X(I \to \bar{F})$ and the CP conjugate of this sum vanishes up to corrections of $\mathcal{O}\left((h^\nu)^4\right)$,

$$\sum_{I,F} \left[C_X(I \to \bar{F}) - C_X(\bar{I} \to F)\right] = 0 + \mathcal{O}\left((h^\nu)^4\right) . \tag{B.5}$$

If we manage to confirm this statement, we have simultaneously shown that the CP-violating contribution to the sum over all operators $C_X(\bar{F} \to I)$ vanishes up to $\mathcal{O}\left((h^\nu)^4\right)$, since

$$\sum_{F,I} \left[C_X(\bar{F} \to I) - C_X(F \to \bar{I})\right] = -\sum_{I,F} \left[C_X(I \to \bar{F}) - C_X(\bar{I} \to F)\right] . \tag{B.6}$$

The combination of Eqs. (B.5) and (B.6) then entails that $\mathcal{C}_{X,\not{CP}}$ is of the same order of magnitude as the sum over all operators $C_X(I \to \bar{F})$, i.e. zero up to corrections of $\mathcal{O}\left((h^\nu)^4\right)$.

To show that Eq. (B.5) holds, we first rewrite the operators C_X in Eq. (B.5) as integrals over S matrix elements squared. In a self-explanatory shorthand notation, we may write

$$\sum_{I,F} \left[C_X(I \to \bar{F}) - C_X(\bar{I} \to F)\right] = \sum_{I,F} \int \frac{d\Pi\left(X|a;ij\right)}{2g_X} \left[(ff)_I \left|S_{I\bar{F}}\right|^2 - (ff)_{\bar{I}} \left|S_{\bar{I}F}\right|^2\right] . \tag{B.7}$$

The CPT invariance of the S matrix implies that $|S_{IF}|^2 = |S_{\bar{F}\bar{I}}|^2$. Similarly, the fact that, up to corrections of $\mathcal{O}(\epsilon_i)$, all particles in the MSSM lepton and Higgs multiplets are in thermal equilibrium provides us with $(ff)_I \approx (ff)_{\bar{F}}$. In fact, as we are eventually interested in the CP-violating parts of the S matrix elements squared, which are of $\mathcal{O}(\epsilon_i)$ themselves, it is for our purposes sufficient to work with $(ff)_I = (ff)_{\bar{F}}$ in the following. We then find[1]

$$\sum_{I,F} C_X(I \to F) = \sum_{I,F} C_X(\bar{F} \to \bar{I}) = \sum_{I,F} C_X(\bar{I} \to \bar{F})\,, \tag{B.8}$$

which allows us to include the collision operators into the sum in Eq. (B.7) that account for the lepton number-conserving processes $I \to F$ and $\bar{I} \to \bar{F}$,

$$\begin{aligned}\sum_{I,F} \left[C_X(I \to \bar{F}) - C_X(\bar{I} \to F)\right] &= \frac{1}{2g_X} \sum_{I,F} \int d\Pi\,(X|a;ij) \\ \times \left[(ff)_I\,|S_{I\bar{F}}|^2 + (ff)_I\,|S_{IF}|^2 - (ff)_{\bar{I}}\,|S_{\bar{I}F}|^2 - (ff)_{\bar{I}}\,|S_{\bar{I}\bar{F}}|^2\right]&,\end{aligned} \tag{B.9}$$

Owing to the unitary of the S matrix, the integration of the S matrix elements squared for a fixed initial state I over all possible final-state configurations F and $\bar{F}$ yields unity,

$$\sum_F \int d\Pi\,(ij) \left[|S_{I\bar{F}}|^2 + |S_{IF}|^2\right] = \sum_F \int d\Pi\,(ij) \left[|S_{\bar{I}F}|^2 + |S_{\bar{I}\bar{F}}|^2\right] = 1 + \mathcal{O}\left((h^\nu)^4\right)\,. \tag{B.10}$$

Since we only integrate over all possible *two-particle* final states and hence omit all possible *multi-particle* final states, we obtain corrections to the exact result of $\mathcal{O}\left((h^\nu)^4\right)$. The leading corrections are due to four-particle final states, which are of $\mathcal{O}\left((h^\nu)^8\right)$, if the heavy (s)neutrino in the intermediate state is off-shell [290]. Close to the resonance pole, the corrections due to processes with four particles in the final state are enhanced, so that they reach a magnitude of $\mathcal{O}\left((h^\nu)^4\right)$ [38, 185]. This observation concludes our argument. Substituting Eq. (B.10) back into Eq. (B.9), we end up with the statement in Eq. (B.5), which we intended to prove.

In the literature, the fact that the CP-violating contributions to the collision operator $\mathcal{C}_X$ vanish up to corrections of $\mathcal{O}\left((h^\nu)^4\right)$ is often formulated in terms of other quantities, which are closely related to $\mathcal{C}_X$. To facilitate the comparison of our analysis with other works, we point out that the collision operators C_X contained in $\mathcal{C}_X$ can also be written as momentum space integrals over reduced cross sections $\hat{\sigma}$,

$$\begin{aligned}C_X(I \to \bar{F}) &= \frac{1}{2g_X} \int d\Pi\,(X|a)\, f_X f_a\, \hat{\sigma}\,(Xa \to \bar{i}\bar{j})\,, \\ \hat{\sigma}\,(Xa \to \bar{i}\bar{j}) &= \int d\Pi\,(ij)\,(2\pi)^4\,\delta^{(4)}\,|M\,(Xa \to \bar{i}\bar{j})|^2 = \int d\Pi\,(ij)\,|S\,(Xa \to \bar{i}\bar{j})|^2\,.\end{aligned} \tag{B.11}$$

[1] The scattering processes with heavy *neutrinos* in the intermediate state feature different initial and final states I and F than the processes with heavy *sneutrinos* or heavy *antisneutrinos* in the intermediate state. The entire discussion in this appendix would hence remain valid, if we were to restrict ourselves solely to scattering processes with either only *neutrinos*, *sneutrinos* or *antisneutrinos* in the intermediate state.

These reduced cross sections $\hat{\sigma}$ are related to the ordinary cross sections σ as follows,

$$\hat{\sigma}\left(Xa \to \bar{i}\bar{j}\right) = 2s\,\lambda^{1/2}\left(1, m_X^2/2, m_a^2/s\right) g_X g_a\,\sigma\left(Xa \to \bar{i}\bar{j}\right) , \tag{B.12}$$

where s is the Mandelstam variable corresponding to the square of the center-of-mass energy, while λ is given as $\lambda(a,b,c) = a^2 + b^2 + c^2 - 2ab - 2ac - 2bc$. The collision operators C_X may hence also be written as

$$C_X(I \to \bar{F}) = g_a \int d\Pi\left(X|a\right) f_X f_a\, s\,\lambda^{1/2}\left(1, m_X^2/2, m_a^2/s\right)\,\sigma\left(Xa \to \bar{i}\bar{j}\right) . \tag{B.13}$$

Finally, integrating over $g_X/E_X\, d^3p/\left(2\pi\right)^3$ yields the interaction densities γ (cf. Eq. (A.9)),

$$\begin{aligned}
\gamma(I \to \bar{F}) &= \frac{g_X}{(2\pi)^3}\int \frac{d^3p}{E_X}\, C_X\left(I \to \bar{F}\right), \qquad (B.14)\\
&= \int d\Pi\left(Xa; ij\right) f_X f_a\left(2\pi\right)^4 \delta^{(4)}\left|M\left(Xa \to \bar{i}\bar{j}\right)\right|^2 ,\\
&= \int d\Pi\left(Xa; ij\right) f_X f_a \left|S\left(Xa \to \bar{i}\bar{j}\right)\right|^2 ,\\
&= \int d\Pi\left(Xa\right) f_X f_a\,\hat{\sigma}\left(Xa \to \bar{i}\bar{j}\right) ,\\
&= 2 g_X g_a \int d\Pi\left(Xa\right) f_X f_a\, s\,\lambda^{1/2}\left(1, m_X^2/2, m_a^2/s\right)\,\sigma\left(Xa \to \bar{i}\bar{j}\right) .
\end{aligned}$$

In conclusion, we summarize the central implication of our result in Eq. (B.2), which we require in the derivation of the Boltzmann equation for the lepton asymmetry. From the combination of Eqs. (B.1) and (B.2), we directly infer that (cf. Eq. (7.58))

$$\mathcal{C}^{\text{red}}_{X,\not{C}\not{P}} = -\mathcal{C}^{\text{on}}_{X,\not{C}\not{P}} + \mathcal{O}\left((h^\nu)^4\right) ,$$

which implies that

$$\begin{aligned}
&\sum_{I,F} C^{\text{red}}_{X,\not{C}\not{P}}(I \to \bar{F}) = \sum_{I,F}\sum_i \text{Br}(V_i \to \bar{F})\, C^{\text{red}}_{X,\not{C}\not{P}}(I \to V_i) = \qquad (B.15)\\
-&\sum_{I,F} C^{\text{on}}_{X,\not{C}\not{P}}(I \to \bar{F}) = \sum_{I,F}\sum_i \text{Br}(R_i \to \bar{F})\, C^{\text{on}}_{X,\not{C}\not{P}}(I \to R_i) + \mathcal{O}\left((h^\nu)^4\right) ,
\end{aligned}$$

with R_i and V_i denoting real and virtual heavy (s)neutrinos in the intermediate state. For $I = \ell H_u, \tilde{\ell}\tilde{H}_u$, we have $R_i, V_i = N_i$, while for $I = \tilde{\ell}H_u$ and $I = \ell\tilde{H}_u$, the intermediate states are given by $R_i, V_i = \tilde{N}_i$ and by $R_i, V_i = \tilde{N}_i^*$, respectively. The branching ratios summed over all final states $\bar{F}$ cancel on both sides, so that we end up with

$$\sum_I\sum_i C^{\text{red}}_{X,\not{C}\not{P}}(I \to V_i) = -\sum_I\sum_i C^{\text{on}}_{X,\not{C}\not{P}}(I \to R_i) + \mathcal{O}\left((h^\nu)^4\right) . \tag{B.16}$$

Hence, thanks to the fact the on- and off-shell contributions to $\mathcal{C}_{X,\not{C}\not{P}}$ cancel each other up to $\mathcal{O}\left((h^\nu)^4\right)$, *adding* the *off-shell* operators $C^{\text{red}}_{X,\not{C}\not{P}}$ to the Boltzmann equations for ℓ and $\bar{\ell}$ is equivalent to *subtracting* the *on-shell* operators $C^{\text{on}}_{X,\not{C}\not{P}}$.

Appendix C

Thermal Gravitino Production

In Sec. 7.3.3, in the derivation of approximate formulae for the reheating temperature $T_{\rm RH}$ and the heavy (s)neutrino mass M_1 as functions of the effective neutrino mass $\widetilde{m}_1$ and the gravitino mass $m_{\widetilde{G}}$, we require an analytical expression for the thermal gravitino abundance $\Omega^0_{\widetilde{G}} h^2$ generated in the course of reheating (cf. Eq. (7.120)). Similarly, in Sec. 8.1, we make use of a fit formula for $\Omega^0_{\widetilde{G}} h^2$ as a function of $T_{\rm RH}$, when computing the nonthermal LSP abundance produced in gravitino decays (cf. Eq. (8.5)). In this appendix, we now explicitly derive the expression for $\Omega^0_{\widetilde{G}} h^2$ in Eq. (7.120), which automatically provides us with an analytical approximation for the numerical relation in Eq. (8.5). Our quantitative analysis in Secs. 7.2 and 7.3 is based on the assumption of a gluino mass of 1 TeV. In this appendix, we therefore also illustrate how our results are easily generalized to other values of the gluino mass.

In the current epoch, gravitinos are nonrelativistic. Their present contribution to the energy density of the universe is hence given by

$$\Omega^0_{\widetilde{G}} h^2 = \Omega^0_{\widetilde{G}} h^2(\widetilde{m}_1, M_1, m_{\widetilde{G}}, m_{\tilde{g}}) = m_{\widetilde{G}}\, \eta^0_{\widetilde{G}}\, n^0_\gamma\, h^2/\rho^0_c\,, \quad \eta^0_{\widetilde{G}} = n^0_{\widetilde{G}}/n^0_\gamma\,. \tag{C.1}$$

In order to relate the gravitino-to-photon ratio $\eta^0_{\widetilde{G}}$ to the corresponding number densities during reheating, we make two simplifying assumptions. First, we assume that after $a = a_{\rm RH}$ the entropy of the thermal bath is not increased much further, which leads us to

$$n^0_\gamma = \delta_1 \left(\frac{a_{\rm RH}}{a_0}\right)^3 \frac{g_{*,s}}{g^0_{*,s}}\, n_\gamma(a_{\rm RH})\,. \tag{C.2}$$

Second, we assume that at $a = a_{\rm RH}$ the gravitino production becomes inefficient such that at later times not many further gravitinos are produced,

$$n^0_{\widetilde{G}} = \delta_2 \left(\frac{a_{\rm RH}}{a_0}\right)^3 n_{\widetilde{G}}(a_{\rm RH})\,. \tag{C.3}$$

This second assumption also implies that at $a = a_{\rm RH}$ the gravitino production rate $\hat{\Gamma}_{\widetilde{G}}$ is of

the same order of magnitude as the Hubble rate H,

$$\hat{\Gamma}_{\widetilde{G}}(a_{\rm RH}) = \frac{\gamma_{\widetilde{G}}(a_{\rm RH})}{n_{\widetilde{G}}(a_{\rm RH})} = \delta_3^{-1} H(a_{\rm RH})\,, \quad n_{\widetilde{G}}(a_{\rm RH}) = \delta_3\,\frac{\gamma_{\widetilde{G}}(a_{\rm RH})}{H(a_{\rm RH})}\,. \tag{C.4}$$

The three correction factors $\delta_1 \gtrsim 1$, $\delta_2 \gtrsim 1$ and $\delta_3 \sim \mathcal{O}(1)$, introduced in Eqs. (C.2), (C.3) and (C.4), respectively, quantify the deviations of the actual values of n_γ^0, $n_{\widetilde{G}}^0$ and $n_{\widetilde{G}}(a_{\rm RH})$ from our approximations. Combining them into one factor $\delta = \delta_2\delta_3/\delta_1$, we may write for $\eta_{\widetilde{G}}^0$

$$\eta_{\widetilde{G}}^0 = \delta\,\frac{g_{*,s}^0}{g_{*,s}}\frac{\gamma_{\widetilde{G}}(a_{\rm RH})}{n_\gamma(a_{\rm RH})H(a_{\rm RH})}\,, \tag{C.5}$$

where $n_\gamma(a_{\rm RH})$, $\gamma_{\widetilde{G}}(a_{\rm RH})$ and $H(a_{\rm RH})$ directly follow from Eqs. (A.15), (7.81) and the Friedmann equation (cf. Sec. 7.3.1). Inserting Eq. (C.5) back into Eq. (C.1), we find for $\Omega_{\widetilde{G}}^0 h^2$

$$\Omega_{\widetilde{G}}^0 h^2 = \varepsilon f_{\widetilde{G}}(T_{\rm RH})\left(m_{\widetilde{G}} + \frac{m_{\tilde{g}}^2(T_{\rm RH})}{3m_{\widetilde{G}}}\right)T_{\rm RH}\,, \quad \varepsilon = \alpha^{-1/2}\beta^{-1}\delta\,, \tag{C.6}$$

where $f_{\widetilde{G}}(T_{\rm RH})$ stands for

$$f_{\widetilde{G}}(T_{\rm RH}) = \frac{n_\gamma^0}{\rho_c/h^2}\frac{g_{*,s}^0}{g_{*,s}}\left(\frac{90}{8\pi^3 g_{*,\rho}}\right)^{1/2}\frac{54\,g_s^2(T_{\rm RH})}{g_\gamma M_p}\left[\ln\left(\frac{T_{\rm RH}^2}{m_{\tilde{g}}^2(T_{\rm RH})}\right) + 0.8846\right]\,. \tag{C.7}$$

Eq. (C.6) may conveniently be rewritten as

$$\Omega_{\widetilde{G}} h^2 = \varepsilon\, C_1\left(\frac{T_{\rm RH}}{10^{10}\ {\rm GeV}}\right)\left[C_2\left(\frac{m_{\widetilde{G}}}{100\ {\rm GeV}}\right) + \left(\frac{100\ {\rm GeV}}{m_{\widetilde{G}}}\right)\left(\frac{m_{\tilde{g}}}{1\ {\rm TeV}}\right)^2\right]\,. \tag{C.8}$$

with C_1 and C_2 being defined as

$$\begin{aligned} C_1 &= 10^{14}\ {\rm GeV}^2\,\frac{n_\gamma^0}{\rho_c/h^2}\frac{g_{*,s}^0}{g_{*,s}}\left(\frac{90}{8\pi^3 g_{*,\rho}}\right)^{1/2}\frac{18 g_s^6\,(T_{\rm RH})}{g_\gamma g_s^4\,(\mu_0)\,M_P}\left[\log\left(\frac{T_{\rm RH}^2}{m_{\tilde{g}}^2\,(T_{\rm RH})}\right) + 0.8846\right]\,,\\ C_2 &= \frac{3 g_s^4\,(\mu_0)}{100 g_s^4\,(T_{\rm RH})}\,. \end{aligned} \tag{C.9}$$

The expressions for $\Omega_{\widetilde{G}} h^2$, C_1 and C_2 in Eqs. (C.8) and (C.9) are exactly those which we employ in our analysis in Sec. 7.3.3. A fit formula for the correction factor ε, which we are not able to determine analytically, is provided in Eq. (7.122). The dependence of C_1 and C_2 on the reheating temperature is presented in Fig. C.1. We find that $C_2 \ll 1$, which means that for $m_{\widetilde{G}} \ll m_{\tilde{g}}$ the term linear in $m_{\widetilde{G}}$ in Eq. (C.8) can usually be neglected. Notice that doing so and setting $\varepsilon = 1$ turns Eq. (C.8) into Eq. (3.47).

Finally, our results may be easily generalized to gluino masses other than 1 TeV. In fact, for given values of $\widetilde{m}_1$, M_1 and $m_{\widetilde{G}}$, it is possible to keep η_B^0 and $\Omega_{\widetilde{G}}^0 h^2$ constant when changing $m_{\tilde{g}}$ by simply rescaling the gravitino mass,

$$m_{\widetilde{G}}^0 \to m_{\widetilde{G}} = m_{\widetilde{G}}\left(m_{\tilde{g}}, m_{\widetilde{G}}^0\right)\,, \qquad m_{\widetilde{G}}\left(1\ {\rm TeV}, m_{\widetilde{G}}^0\right) = m_{\widetilde{G}}^0\,. \tag{C.10}$$

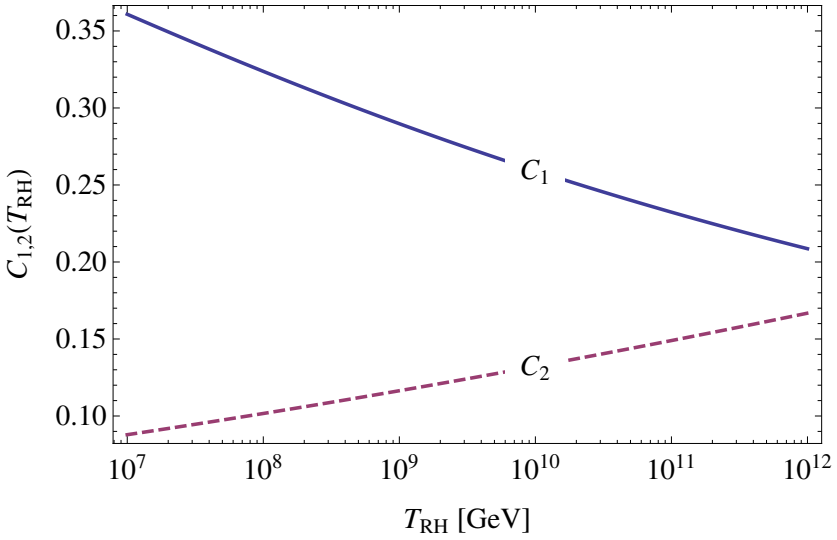

Figure C.1: The coefficients C_1 and C_2 as functions of the reheating temperature $T_{\rm RH}$.

As for the baryon asymmetry, this is a trivial consequence of the fact that η_B^0 is a function of $\widetilde{m}_1$ and M_1 only. In the case of the gravitino abundance, we observe that for fixed reheating temperature, $T_{\rm RH} = T_{\rm RH}\,(\widetilde{m}_1, M_1)$, $\Omega_{\widetilde{G}}^0 h^2$ remains constant as long as $m_{\widetilde{G}}\big(m_{\tilde{g}}, m_{\widetilde{G}}^0\big)$ is chosen such that the term in square brackets in Eq. (C.8) does not change,

$$\left[C_2\left(\frac{m_{\widetilde{G}}^0}{100\,\text{GeV}}\right) + \left(\frac{100\,\text{GeV}}{m_{\widetilde{G}}^0}\right)\right] = \left[C_2\left(\frac{m_{\widetilde{G}}}{100\,\text{GeV}}\right) + \left(\frac{100\,\text{GeV}}{m_{\widetilde{G}}}\right)\left(\frac{m_{\tilde{g}}}{1\,\text{TeV}}\right)^2\right] . \quad \text{(C.11)}$$

From this condition, we can determine the rescaled gravitino mass $m_{\widetilde{G}}$ as a function of the rescaled gluino mass $m_{\tilde{g}}$ and the original gravitino mass $m_{\widetilde{G}}^0$. As Eq. (C.11) is a quadratic equation in $m_{\widetilde{G}}$, it generically has two solutions $m_{\widetilde{G}}^{\pm}$, one of which is typically closer to the original gravitino mass than the other. $m_{\widetilde{G}}^0$ lies right in between $m_{\widetilde{G}}^-$ and $m_{\widetilde{G}}^+$ once the two terms in square brackets in Eq. (C.8) are of equal size, i.e. when gravitinos in helicity $\pm\frac{1}{2}$ states contribute exactly as much to the total abundance as gravitinos in helicity $\pm\frac{3}{2}$ states. One easily sees that this is the case when $m_{\widetilde{G}}^0 \simeq 280\,\text{GeV}$ (cf. Eq. (7.126)). When going to values of $m_{\tilde{g}}$ larger than 1 TeV, we have $m_{\widetilde{G}}^0 \gtrsim m_{\widetilde{G}}^+ \gg m_{\widetilde{G}}^-$ above 280 GeV and $m_{\widetilde{G}}^0 \lesssim m_{\widetilde{G}}^- \ll m_{\widetilde{G}}^+$ below 280 GeV. At $m_{\tilde{g}}$ smaller than 1 TeV, we always find $m_{\widetilde{G}}^- < m_{\widetilde{G}}^0 < m_{\widetilde{G}}^+$.

If the gravitino mass is much smaller than the gluino mass, almost only the goldstino part of the gravitino is produced and the term linear in $m_{\widetilde{G}}$ in Eq. (C.8) can be neglected. The scaling behaviour of the gravitino mass then becomes trivial,

$$m_{\widetilde{G}}^0 \ll m_{\tilde{g}} : \qquad m_{\widetilde{G}} = m_{\widetilde{G}}^0 \left(\frac{m_{\tilde{g}}}{1\,\text{TeV}}\right)^2 . \quad \text{(C.12)}$$

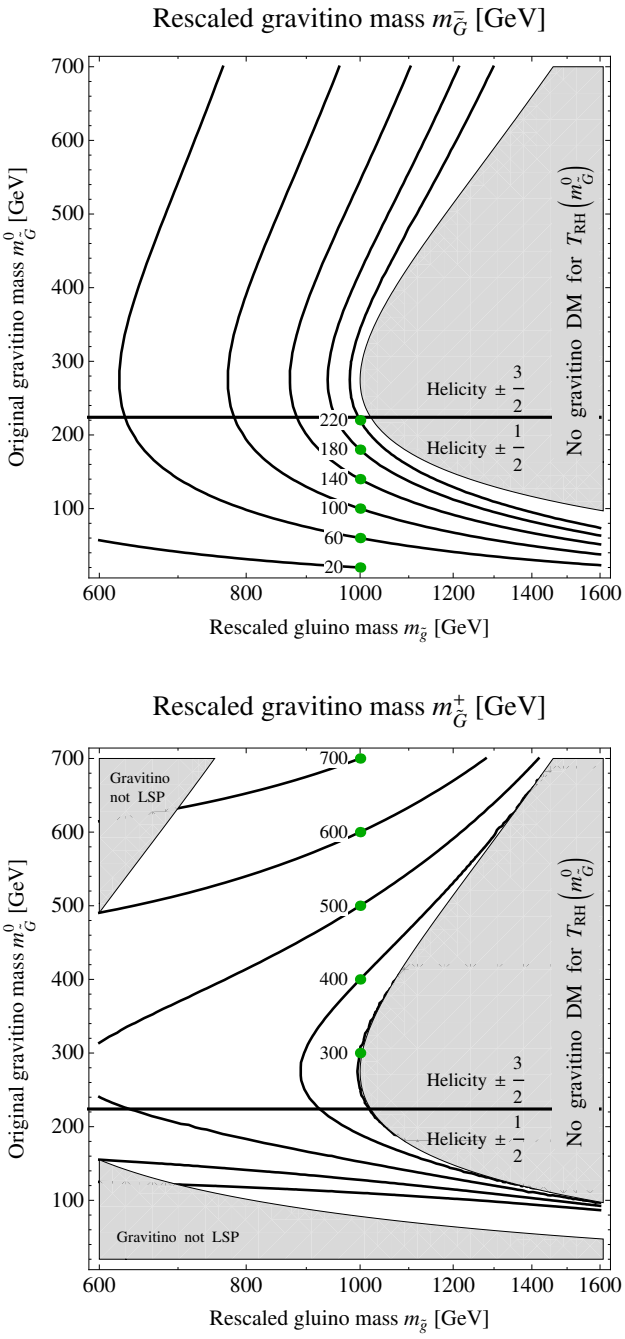

Figure C.2: Contour plots of the two solutions $\left(m_{\widetilde{G}}^{\pm}\right)$ of Eq. (C.11) for the rescaled gravitino mass $m_{\widetilde{G}}$ as a function of the rescaled gluino mass $m_{\tilde{g}}$ and the original gravitino mass $m_{\widetilde{G}}^{0}$. The black solid contours correspond to constant values of $m_{\widetilde{G}}$ (given next to the green dots). They serve as level curves that allow a determination of $m_{\widetilde{G}}$ for arbitrary points in the $\left(m_{\tilde{g}}, m_{\widetilde{G}}^{0}\right)$-plane. They can also be regarded as function graphs of $m_{\widetilde{G}}^{0}$ as a function of $m_{\tilde{g}}$ for constant $m_{\widetilde{G}}$. We restrict ourselves to the interval $20\,\mathrm{GeV} \leq m_{\widetilde{G}}^{0} \leq 700\,\mathrm{GeV}$ in this figure. Below 20 GeV, Eq. (C.12) provides an excellent approximation.

Actually, the rescaled gravitino mass $m_{\widetilde{G}}$ also is a function of T_{RH}, as it depends on the coefficient $C_2(T_{\mathrm{RH}})$. As apparent from Fig. 7.7 and Eq. (7.123), this dependence on T_{RH} directly translates into a dependence on the effective neutrino mass $\widetilde{m}_1$. In order to solve Eq. (C.11), we set $\widetilde{m}_1$ to 0.04 eV and compute T_{RH} according to Eq. (7.123) as a function of the input gravitino mass, $T_{\mathrm{RH}} = T_{\mathrm{RH}}\big(m^0_{\widetilde{G}}\big)$. Our solutions $m^{\pm}_{\widetilde{G}}$ for the rescaled gravitino mass are presented in the two panels of Fig. C.2, respectively. In the gray shaded regions, there are either no real solutions of Eq. (C.11) or the rescaled gravitino mass is larger than the corresponding gluino mass, $m_{\widetilde{G}} > m_{\tilde{g}}$. The former case implies that it is impossible to keep the gravitino abundance constant, when going to larger $m_{\tilde{g}}$ while sticking to the reheating temperature $T_{\mathrm{RH}}\big(m^0_{\widetilde{G}}\big)$. In the latter case, the gravitino would not be the LSP any longer.

Bibliography

[1] E. Komatsu *et. al.* [WMAP Collaboration], *Seven-Year WMAP Observations: Cosmological Interpretation*, *Astrophys.J.Suppl.* **192** (2011) 18.

[2] K. Nakamura *et. al.* [Particle Data Group], *Review of particle physics*, *J.Phys.G* **G37** (2010) 075021.

[3] W. J. Percival *et. al.* [SDSS Collaboration], *Baryon Acoustic Oscillations in the Sloan Digital Sky Survey Data Release 7 Galaxy Sample*, *Mon.Not.Roy.Astron.Soc.* **401** (2010) 2148–2168.

[4] S. Fukuda *et. al.* [Super-Kamiokande Collaboration], *Tau neutrinos favored over sterile neutrinos in atmospheric muon-neutrino oscillations*, *Phys.Rev.Lett.* **85** (2000) 3999–4003 [hep-ex/0009001].

[5] Q. Ahmad *et. al.* [SNO Collaboration], *Measurement of the rate of* $\nu_e + d \to p + p + e^-$ *interactions produced by* ^8B *solar neutrinos at the Sudbury Neutrino Observatory*, *Phys.Rev.Lett.* **87** (2001) 071301 [nucl-ex/0106015].

[6] A. H. Guth, *The Inflationary Universe: A Possible Solution to the Horizon and Flatness Problems*, *Phys.Rev.* **D23** (1981) 347–356.

[7] A. D. Linde, *A New Inflationary Universe Scenario: A Possible Solution of the Horizon, Flatness, Homogeneity, Isotropy and Primordial Monopole Problems*, *Phys.Lett.* **B108** (1982) 389–393.

[8] A. Albrecht and P. J. Steinhardt, *Cosmology for Grand Unified Theories with Radiatively Induced Symmetry Breaking*, *Phys.Rev.Lett.* **48** (1982) 1220–1223.

[9] A. D. Linde, *Axions in inflationary cosmology*, *Phys.Lett.* **B259** (1991) 38–47.

[10] A. D. Linde, *Hybrid inflation*, *Phys.Rev.* **D49** (1994) 748–754 [astro-ph/9307002].

[11] W. Buchmuller, C. Greub and P. Minkowski, *Neutrino masses, neutral vector bosons and the scale of* $B-L$ *breaking*, *Phys.Lett.* **B267** (1991) 395–399.

[12] G. 't Hooft, *Symmetry Breaking Through Bell-Jackiw Anomalies*, *Phys.Rev.Lett.* **37** (1976) 8–11.

[13] G. 't Hooft, *Computation of the Quantum Effects Due to a Four-Dimensional Pseudoparticle*, *Phys.Rev.* **D14** (1976) 3432–3450.

[14] K. Babu and R. Mohapatra, *Is there a connection between quantization of electric charge and a Majorana neutrino?*, *Phys.Rev.Lett.* **63** (1989) 938.

[15] K. Babu and R. N. Mohapatra, *Quantization of electric charge from anomaly constraints and a Majorana neutrino*, *Phys.Rev.* **D41** (1990) 271.

[16] E. J. Copeland, A. R. Liddle, D. H. Lyth, E. D. Stewart and D. Wands, *False vacuum inflation with Einstein gravity*, *Phys.Rev.* **D49** (1994) 6410–6433 [astro-ph/9401011].

[17] G. Dvali, Q. Shafi and R. K. Schaefer, *Large scale structure and supersymmetric inflation without fine tuning*, *Phys.Rev.Lett.* **73** (1994) 1886–1889 [hep-ph/9406319].

[18] S. Dimopoulos and H. Georgi, *Softly Broken Supersymmetry and $SU(5)$*, *Nucl.Phys.* **B193** (1981) 150.

[19] G. R. Farrar and P. Fayet, *Phenomenology of the Production, Decay, and Detection of New Hadronic States Associated with Supersymmetry*, *Phys.Lett.* **B76** (1978) 575–579.

[20] H. Pagels and J. R. Primack, *Supersymmetry, Cosmology and New TeV Physics*, *Phys.Rev.Lett.* **48** (1982) 223.

[21] H. Goldberg, *Constraint on the Photino Mass from Cosmology*, *Phys.Rev.Lett.* **50** (1983) 1419.

[22] J. R. Ellis, J. Hagelin, D. V. Nanopoulos, K. A. Olive and M. Srednicki, *Supersymmetric Relics from the Big Bang*, *Nucl.Phys.* **B238** (1984) 453–476.

[23] P. Minkowski, *$\mu \to e\gamma$ at a Rate of One Out of 10^9 Muon Decays?*, *Phys.Lett.* **B67** (1977) 421.

[24] T. Yanagida, *Horizontal symmetry and masses of neutrinos*, *Conf.Proc.* **C7902131** (1979) 95.

[25] S. Glashow, *The future of elementary particle physics*, *NATO Adv.Study Inst.Ser.B Phys.* **59** (1980) 687.

[26] M. Gell-Mann, P. Ramond and R. Slansky, *Complex spinors and unified theories*, *Conf.Proc.* **C790927** (1979) 315–321.

[27] R. N. Mohapatra and G. Senjanovic, *Neutrino Mass and Spontaneous Parity Violation*, *Phys.Rev.Lett.* **44** (1980) 912.

[28] G. N. Felder, J. Garcia-Bellido, P. B. Greene, L. Kofman, A. D. Linde *et. al.*, *Dynamics of symmetry breaking and tachyonic preheating*, *Phys.Rev.Lett.* **87** (2001) 011601 [hep-ph/0012142].

[29] G. N. Felder, L. Kofman and A. D. Linde, *Tachyonic instability and dynamics of spontaneous symmetry breaking*, *Phys.Rev.* **D64** (2001) 123517 [hep-th/0106179].

[30] A. Vilenkin, *Cosmic Strings and Domain Walls*, *Phys.Rept.* **121** (1985) 263.

[31] M. Hindmarsh and T. Kibble, *Cosmic strings*, *Rept.Prog.Phys.* **58** (1995) 477–562 [hep-ph/9411342].

[32] M. Hindmarsh, *Signals of Inflationary Models with Cosmic Strings*, *Prog.Theor.Phys.Suppl.* **190** (2011) 197–228 [1106.0391].

[33] R. A. Battye, B. Garbrecht and A. Moss, *Constraints on Supersymmetric Models of Hybrid Inflation*, *JCAP* **0609** (2006) 007 [astro-ph/0607339].

[34] K. Nakayama, F. Takahashi and T. T. Yanagida, *Constraint on the gravitino mass in hybrid inflation*, *JCAP* **1012** (2010) 010 [1007.5152].

[35] J. Garcia-Bellido and E. Ruiz Morales, *Particle production from symmetry breaking after inflation*, *Phys.Lett.* **B536** (2002) 193–202 [hep-ph/0109230].

[36] M. Fukugita and T. Yanagida, *Baryogenesis Without Grand Unification*, *Phys.Lett.* **B174** (1986) 45.

[37] M. Plumacher, *Baryon asymmetry, neutrino mixing and supersymmetric $SO(10)$ unification*, *Nucl.Phys.* **B530** (1998) 207–246 [hep-ph/9704231].

[38] W. Buchmuller, P. Di Bari and M. Plumacher, *Leptogenesis for pedestrians*, *Annals Phys.* **315** (2005) 305–351 [hep-ph/0401240].

[39] G. Lazarides and Q. Shafi, *Origin of matter in the inflationary cosmology*, *Phys.Lett.* **B258** (1991) 305–309.

[40] T. Asaka, K. Hamaguchi, M. Kawasaki and T. Yanagida, *Leptogenesis in inflaton decay*, *Phys.Lett.* **B464** (1999) 12–18 [hep-ph/9906366].

[41] T. Asaka, K. Hamaguchi, M. Kawasaki and T. Yanagida, *Leptogenesis in inflationary universe*, *Phys.Rev.* **D61** (2000) 083512 [hep-ph/9907559].

[42] F. Hahn-Woernle and M. Plumacher, *Effects of reheating on leptogenesis*, *Nucl.Phys.* **B806** (2009) 68–83 [0801.3972].

[43] M. Bolz, A. Brandenburg and W. Buchmuller, *Thermal production of gravitinos*, *Nucl.Phys.* **B606** (2001) 518–544 [hep-ph/0012052].

[44] J. Pradler and F. D. Steffen, *Thermal gravitino production and collider tests of leptogenesis*, *Phys.Rev.* **D75** (2007) 023509 [hep-ph/0608344].

[45] S. Weinberg, *Cosmological Constraints on the Scale of Supersymmetry Breaking*, *Phys.Rev.Lett.* **48** (1982) 1303.

[46] J. R. Ellis, D. V. Nanopoulos and S. Sarkar, *The Cosmology of Decaying Gravitinos*, *Nucl.Phys.* **B259** (1985) 175.

[47] M. Kawasaki, K. Kohri and T. Moroi, *Hadronic decay of late-decaying particles and Big-Bang Nucleosynthesis*, *Phys.Lett.* **B625** (2005) 7–12 [astro-ph/0402490].

[48] M. Kawasaki, K. Kohri and T. Moroi, *Big-Bang nucleosynthesis and hadronic decay of long-lived massive particles*, *Phys.Rev.* **D71** (2005) 083502 [astro-ph/0408426].

[49] K. Jedamzik, *Big bang nucleosynthesis constraints on hadronically and electromagnetically decaying relic neutral particles*, *Phys.Rev.* **D74** (2006) 103509 [hep-ph/0604251].

[50] M. Bolz, W. Buchmuller and M. Plumacher, *Baryon asymmetry and dark matter*, *Phys.Lett.* **B443** (1998) 209–213 [hep-ph/9809381].

[51] G. Aad *et. al.* [ATLAS Collaboration], *Combined search for the Standard Model Higgs boson using up to* $4.9\,fb^{-1}$ *of pp collision data at* $\sqrt{s} = 7\,TeV$ *with the ATLAS detector at the LHC*, *Phys.Lett.* **B710** (2012) 49–66 [1202.1408].

[52] S. Chatrchyan *et. al.* [CMS], *Combined results of searches for the standard model Higgs boson in pp collisions at* $\sqrt{s} = 7\,TeV$, *Phys. Lett.* **B710** (2012) 26–48 [1202.1488].

[53] T. Gherghetta, G. F. Giudice and J. D. Wells, *Phenomenological consequences of supersymmetry with anomaly induced masses*, *Nucl.Phys.* **B559** (1999) 27–47 [hep-ph/9904378].

[54] M. Ibe, R. Kitano, H. Murayama and T. Yanagida, *Viable supersymmetry and leptogenesis with anomaly mediation*, *Phys.Rev.* **D70** (2004) 075012 [hep-ph/0403198].

[55] W. Buchmuller and T. Yanagida, *Quark lepton mass hierarchies and the baryon asymmetry*, *Phys.Lett.* **B445** (1999) 399–402.

[56] C. Froggatt and H. B. Nielsen, *Hierarchy of Quark Masses, Cabibbo Angles and CP Violation*, *Nucl.Phys.* **B147** (1979) 277.

[57] W. Buchmuller, K. Schmitz and G. Vertongen, *Matter and Dark Matter from False Vacuum Decay*, *Phys.Lett.* **B693** (2010) 421–425 [1008.2355].

[58] W. Buchmuller, K. Schmitz and G. Vertongen, *Entropy, Baryon Asymmetry and Dark Matter from Heavy Neutrino Decays*, *Nucl.Phys.* **B851** (2011) 481–532 [1104.2750].

[59] W. Buchmuller, V. Domcke and K. Schmitz, *Predicting θ_{13} and the Neutrino Mass Scale from Quark Lepton Mass Hierarchies*, *JHEP* **1203** (2012) 008 [1111.3872].

[60] W. Buchmuller, V. Domcke and K. Schmitz, *Spontaneous $B-L$ Breaking as the Origin of the Hot Early Universe*, *Nucl.Phys.* **B862** (2012) 587–632 [1202.6679].

[61] W. Buchmuller, V. Domcke and K. Schmitz, *WIMP Dark Matter from Gravitino Decays and Leptogenesis*, *Phys.Lett.* **B713** (2012) 63–67 [1203.0285].

[62] E. W. Kolb and M. S. Turner, *The Early universe*, *Front.Phys.* **69** (1990) 1–547.

[63] S. Dodelson, *Modern cosmology*, *Amsterdam, Netherlands: Academic Pr.* (2003) 440 p.

[64] V. Mukhanov, *Physical foundations of cosmology*, *Cambridge, UK: Univ. Pr.* (2005) 421 p.

[65] M. Trodden and S. M. Carroll, *TASI lectures: Introduction to cosmology*, astro-ph/0401547.

[66] V. Rubakov, *Introduction to cosmology*, *PoS* **RTN2005** (2005) 003.

[67] A. G. Riess, L. Macri, S. Casertano, M. Sosey, H. Lampeitl *et. al.*, *A Redetermination of the Hubble Constant with the Hubble Space Telescope from a Differential Distance Ladder*, *Astrophys.J.* **699** (2009) 539–563 [0905.0695].

[68] M. Hicken, W. Wood-Vasey, S. Blondin, P. Challis, S. Jha *et. al.*, *Improved Dark Energy Constraints from 100 New CfA Supernova Type Ia Light Curves*, *Astrophys.J.* **700** (2009) 1097–1140 [0901.4804].

[69] R. Kessler, A. Becker, D. Cinabro, J. Vanderplas, J. A. Frieman *et. al.*, *First-year Sloan Digital Sky Survey-II (SDSS-II) Supernova Results: Hubble Diagram and Cosmological Parameters*, *Astrophys.J.Suppl.* **185** (2009) 32–84 [0908.4274].

[70] M. Kowalski *et. al.* [Supernova Cosmology Project], *Improved Cosmological Constraints from New, Old and Combined Supernova Datasets*, *Astrophys.J.* **686** (2008) 749–778 [0804.4142].

[71] J. C. Mather, E. Cheng, D. Cottingham, R. Eplee, D. Fixsen *et. al.*, *Measurement of the Cosmic Microwave Background spectrum by the COBE FIRAS instrument*, *Astrophys.J.* **420** (1994) 439–444.

[72] J. C. Mather, D. Fixsen, R. Shafer, C. Mosier and D. Wilkinson, *Calibrator design for the COBE far infrared absolute spectrophotometer (FIRAS)*, *Astrophys.J.* **512** (1999) 511–520 [astro-ph/9810373].

[73] G. F. Smoot, C. Bennett, A. Kogut, E. Wright, J. Aymon *et. al.*, *Structure in the COBE differential microwave radiometer first year maps*, *Astrophys.J.* **396** (1992) L1–L5.

[74] D. Fixsen, *The Temperature of the Cosmic Microwave Background*, *Astrophys.J.* **707** (2009) 916–920 [0911.1955].

[75] M. Archidiacono, E. Calabrese and A. Melchiorri, *The Case for Dark Radiation*, *Phys.Rev.* **D84** (2011) 123008 [1109.2767].

[76] C. A. Egan and C. H. Lineweaver, *A Larger Estimate of the Entropy of the Universe*, *Astrophys.J.* **710** (2010) 1825–1834 [0909.3983].

[77] A. Ringwald, *Prospects for the direct detection of the cosmic neutrino background*, *Nucl.Phys.* **A827** (2009) 501C–506C [0901.1529].

[78] S. Hannestad, *Primordial neutrinos*, *Ann.Rev.Nucl.Part.Sci.* **56** (2006) 137–161 [hep-ph/0602058].

[79] T. L. Smith, S. Das and O. Zahn, *Constraints on neutrino and dark radiation interactions using cosmological observations*, *Phys.Rev.* **D85** (2012) 023001.

[80] W. Hu, D. J. Eisenstein and M. Tegmark, *Weighing neutrinos with galaxy surveys*, *Phys.Rev.Lett.* **80** (1998) 5255–5258 [astro-ph/9712057].

[81] J. Lesgourgues and S. Pastor, *Massive neutrinos and cosmology*, *Phys.Rept.* **429** (2006) 307–379 [astro-ph/0603494].

[82] S. A. Thomas, F. B. Abdalla and O. Lahav, *Upper Bound of* 0.28 *eV on the Neutrino Masses from the Largest Photometric Redshift Survey*, *Phys.Rev.Lett.* **105** (2010) 031301 [0911.5291].

[83] M. Fukugita and P. E. Peebles, *The Cosmic energy inventory*, *Astrophys.J.* **616** (2004) 643–668 [astro-ph/0406095].

[84] R. Cen and J. P. Ostriker, *Where are the baryons?*, *Astrophys.J.* **514** (1999) 1 [astro-ph/9806281].

[85] W. Buchmuller, R. Peccei and T. Yanagida, *Leptogenesis as the origin of matter*, *Ann.Rev.Nucl.Part.Sci.* **55** (2005) 311–355 [hep-ph/0502169].

[86] G. Steigman, *When Clusters Collide: Constraints On Antimatter On The Largest Scales*, *JCAP* **0810** (2008) 001 [0808.1122].

[87] A. G. Cohen, A. De Rujula and S. Glashow, *A Matter-antimatter universe?*, *Astrophys.J.* **495** (1998) 539–549 [astro-ph/9707087].

[88] G. Bertone, D. Hooper and J. Silk, *Particle dark matter: Evidence, candidates and constraints*, *Phys.Rept.* **405** (2005) 279–390 [hep-ph/0404175].

[89] J. Einasto, *Dark Matter*, 0901.0632.

[90] D. Hooper, *TASI 2008 Lectures on Dark Matter*, 0901.4090.

[91] G. Bertone (ed.), *Particle dark matter: Observations, models and searches*, *Cambridge, UK: Univ. Pr.* (2010) 738 p.

[92] M. Milgrom, *A Modification of the Newtonian dynamics as a possible alternative to the hidden mass hypothesis*, *Astrophys.J.* **270** (1983) 365–370.

[93] J. D. Bekenstein, *Relativistic gravitation theory for the MOND paradigm*, *Phys.Rev.* **D70** (2004) 083509 [astro-ph/0403694].

[94] V. C. Rubin and J. Ford, W.Kent, *Rotation of the Andromeda Nebula from a Spectroscopic Survey of Emission Regions*, *Astrophys.J.* **159** (1970) 379–403.

[95] S. Faber and R. Jackson, *Velocity dispersions and mass to light ratios for elliptical galaxies*, *Astrophys.J.* **204** (1976) 668.

[96] R. Catena and P. Ullio, *A novel determination of the local dark matter density*, *JCAP* **1008** (2010) 004 [0907.0018].

[97] F. Zwicky, *Die Rotverschiebung von extragalaktischen Nebeln*, *Helvetica Physica Acta* **6** (1933) 110–127.

[98] D. Clowe, M. Bradac, A. H. Gonzalez, M. Markevitch, S. W. Randall *et. al.*, *A direct empirical proof of the existence of dark matter*, *Astrophys.J.* **648** (2006) L109–L113 [astro-ph/0608407].

[99] M. Viel, J. Lesgourgues, M. G. Haehnelt, S. Matarrese and A. Riotto, *Constraining warm dark matter candidates including sterile neutrinos and light gravitinos with WMAP and the Lyman-alpha forest*, *Phys.Rev.* **D71** (2005) 063534 [astro-ph/0501562].

[100] K. Jedamzik, M. Lemoine and G. Moultaka, *Gravitino, axino, Kaluza-Klein graviton warm and mixed dark matter and reionisation*, *JCAP* **0607** (2006) 010 [astro-ph/0508141].

[101] B. Paczynski, *Gravitational microlensing by the galactic halo*, *Astrophys.J.* **304** (1986) 1–5.

[102] P. Tisserand *et. al.* [EROS-2 Collaboration], *Limits on the Macho Content of the Galactic Halo from the EROS-2 Survey of the Magellanic Clouds*, *Astron.Astrophys.* **469** (2007) 387–404 [astro-ph/0607207].

[103] F. De Paolis, G. Ingrosso, P. Jetzer and M. Roncadelli, *A Case for a baryonic dark halo*, *Phys.Rev.Lett.* **74** (1995) 14–17 [astro-ph/9410016].

[104] A. G. Riess *et. al.* [Supernova Search Team], *Observational evidence from supernovae for an accelerating universe and a cosmological constant*, *Astron.J.* **116** (1998) 1009–1038 [astro-ph/9805201].

[105] S. Perlmutter *et. al.* [Supernova Cosmology Project], *Measurements of Omega and Lambda from 42 high redshift supernovae*, *Astrophys.J.* **517** (1999) 565–586 [astro-ph/9812133]. The Supernova Cosmology Project.

[106] B. Ratra and P. Peebles, *Cosmological Consequences of a Rolling Homogeneous Scalar Field*, *Phys.Rev.* **D37** (1988) 3406.

[107] C. Wetterich, *Cosmology and the Fate of Dilatation Symmetry*, *Nucl.Phys.* **B302** (1988) 668.

[108] C. Armendariz-Picon, V. F. Mukhanov and P. J. Steinhardt, *Essentials of k essence*, *Phys.Rev.* **D63** (2001) 103510 [astro-ph/0006373].

[109] B. Jain and P. Zhang, *Observational Tests of Modified Gravity*, *Phys.Rev.* **D78** (2008) 063503 [0709.2375].

[110] T. Clifton, P. G. Ferreira, A. Padilla and C. Skordis, *Modified Gravity and Cosmology*, *Phys.Rept.* **513** (2012) 1–189.

[111] S. Weinberg, *The Cosmological Constant Problem*, *Rev.Mod.Phys.* **61** (1989) 1–23.

[112] I. Zlatev, L.-M. Wang and P. J. Steinhardt, *Quintessence, cosmic coincidence, and the cosmological constant*, *Phys.Rev.Lett.* **82** (1999) 896–899 [astro-ph/9807002].

[113] R. Dicke, P. Peebles, P. Roll and D. Wilkinson, *Cosmic Black-Body Radiation*, *Astrophys.J.* **142** (1965) 414–419.

[114] W. Hu and S. Dodelson, *Cosmic microwave background anisotropies*, *Ann.Rev.Astron.Astrophys.* **40** (2002) 171–216 [astro-ph/0110414].

[115] D. Samtleben, S. Staggs and B. Winstein, *The Cosmic microwave background for pedestrians: A Review for particle and nuclear physicists*, *Ann.Rev.Nucl.Part.Sci.* **57** (2007) 245–283 [0803.0834].

[116] R. Sachs and A. Wolfe, *Perturbations of a cosmological model and angular variations of the microwave background*, *Astrophys.J.* **147** (1967) 73–90.

[117] E. F. Bunn, A. R. Liddle and . White, Martin J., *Four year COBE normalization of inflationary cosmologies*, *Phys.Rev.* **D54** (1996) 5917–5921 [astro-ph/9607038].

[118] K. A. Olive, G. Steigman and T. P. Walker, *Primordial nucleosynthesis: Theory and observations*, *Phys.Rept.* **333** (2000) 389–407 [astro-ph/9905320].

[119] F. Iocco, G. Mangano, G. Miele, O. Pisanti and P. D. Serpico, *Primordial Nucleosynthesis: from precision cosmology to fundamental physics*, *Phys.Rept.* **472** (2009) 1–76.

[120] R. V. Wagoner, W. A. Fowler and F. Hoyle, *On the Synthesis of elements at very high temperatures*, *Astrophys.J.* **148** (1967) 3–49.

[121] R. H. Cyburt, B. D. Fields and K. A. Olive, *The NACRE thermonuclear reaction compilation and big bang nucleosynthesis*, *New Astron.* **6** (2001) 215–238 [astro-ph/0102179].

[122] R. H. Cyburt, B. D. Fields and K. A. Olive, *An Update on the big bang nucleosynthesis prediction for Li-7: The problem worsens*, *JCAP* **0811** (2008) 012 [0808.2818].

[123] G. Steigman, D. Schramm and J. Gunn, *Cosmological Limits to the Number of Massive Leptons*, *Phys.Lett.* **B66** (1977) 202–204.

[124] G. Mangano, G. Miele, S. Pastor, T. Pinto, O. Pisanti *et. al.*, *Relic neutrino decoupling including flavor oscillations*, *Nucl.Phys.* **B729** (2005) 221–234 [hep-ph/0506164].

[125] J. Bernstein, L. S. Brown and G. Feinberg, *Cosmological helium production simplified*, *Rev.Mod.Phys.* **61** (1989) 25.

[126] G. Mangano and P. D. Serpico, *A robust upper limit on $N_{\rm eff}$ from BBN, circa 2011*, *Phys.Lett.* **B701** (2011) 296–299 [1103.1261].

[127] M. Kawasaki, K. Kohri and N. Sugiyama, *Cosmological constraints on late time entropy production*, *Phys.Rev.Lett.* **82** (1999) 4168 [astro-ph/9811437].

[128] S. Hannestad, *What is the lowest possible reheating temperature?*, *Phys.Rev.* **D70** (2004) 043506 [astro-ph/0403291].

[129] R. H. Cyburt, J. R. Ellis, B. D. Fields and K. A. Olive, *Updated nucleosynthesis constraints on unstable relic particles*, *Phys.Rev.* **D67** (2003) 103521 [astro-ph/0211258].

[130] M. Pospelov, *Particle physics catalysis of thermal Big Bang Nucleosynthesis*, *Phys.Rev.Lett.* **98** (2007) 231301 [hep-ph/0605215].

[131] M. Kawasaki, K. Kohri, T. Moroi and A. Yotsuyanagi, *Big-Bang Nucleosynthesis and Gravitino*, *Phys.Rev.* **D78** (2008) 065011 [0804.3745].

[132] N. Manton, *Topology in the Weinberg-Salam Theory*, *Phys.Rev.* **D28** (1983) 2019.

[133] F. R. Klinkhamer and N. Manton, *A Saddle Point Solution in the Weinberg-Salam Theory*, *Phys.Rev.* **D30** (1984) 2212.

[134] V. Kuzmin, V. Rubakov and M. Shaposhnikov, *On the Anomalous Electroweak Baryon Number Nonconservation in the Early Universe*, *Phys.Lett.* **B155** (1985) 36.

[135] P. B. Arnold and L. D. McLerran, *Sphalerons, Small Fluctuations and Baryon Number Violation in Electroweak Theory*, *Phys.Rev.* **D36** (1987) 581.

[136] H. Klapdor-Kleingrothaus, S. Kolb and V. Kuzmin, *Light lepton number violating sneutrinos and the baryon number of the universe*, *Phys.Rev.* **D62** (2000) 035014 [hep-ph/9909546].

[137] P. B. Arnold and L. G. Yaffe, *Nonperturbative dynamics of hot nonAbelian gauge fields: Beyond leading log approximation*, *Phys.Rev.* **D62** (2000) 125013 [hep-ph/9912305].

[138] S. Y. Khlebnikov and M. Shaposhnikov, *The Statistical Theory of Anomalous Fermion Number Nonconservation*, *Nucl.Phys.* **B308** (1988) 885–912.

[139] D. H. Lyth and A. Riotto, *Particle physics models of inflation and the cosmological density perturbation*, *Phys.Rept.* **314** (1999) 1–146 [hep-ph/9807278].

[140] A. D. Linde, *Particle physics and inflationary cosmology*, hep-th/0503203.

[141] R. M. Wald, *Asymptotic behavior of homogeneous cosmological models in the presence of a positive cosmological constant*, *Phys.Rev.* **D28** (1983) 2118–2120.

[142] P. Binetruy and G. Dvali, *D term inflation*, *Phys.Lett.* **B388** (1996) 241–246 [hep-ph/9606342].

[143] E. Halyo, *Hybrid inflation from supergravity D terms*, *Phys.Lett.* **B387** (1996) 43–47 [hep-ph/9606423].

[144] S. R. Coleman and E. J. Weinberg, *Radiative Corrections as the Origin of Spontaneous Symmetry Breaking*, *Phys.Rev.* **D7** (1973) 1888–1910.

[145] A. D. Linde and A. Riotto, *Hybrid inflation in supergravity*, *Phys.Rev.* **D56** (1997) 1841–1844 [hep-ph/9703209].

[146] B. Garbrecht, *Ultraviolet Regularisation in de Sitter Space*, *Phys.Rev.* **D74** (2006) 043507 [hep-th/0604166].

[147] M. Bastero-Gil, S. King and Q. Shafi, *Supersymmetric Hybrid Inflation with Non-Minimal Kahler potential*, *Phys.Lett.* **B651** (2007) 345–351 [hep-ph/0604198].

[148] K. Eguchi *et. al.* [KamLAND Collaboration], *First results from KamLAND: Evidence for reactor anti-neutrino disappearance*, *Phys.Rev.Lett.* **90** (2003) 021802 [hep-ex/0212021].

[149] M. Ahn *et. al.* [K2K Collaboration], *Measurement of Neutrino Oscillation by the K2K Experiment*, *Phys.Rev.* **D74** (2006) 072003 [hep-ex/0606032].

[150] D. Michael *et. al.* [MINOS Collaboration], *Observation of muon neutrino disappearance with the MINOS detectors and the NuMI neutrino beam*, *Phys.Rev.Lett.* **97** (2006) 191801.

[151] R. Mohapatra, S. Antusch, K. Babu, G. Barenboim, M.-C. Chen *et. al.*, *Theory of neutrinos: A White paper*, *Rept.Prog.Phys.* **70** (2007) 1757–1867 [hep-ph/0510213].

[152] M. Gonzalez-Garcia and M. Maltoni, *Phenomenology with Massive Neutrinos*, *Phys.Rept.* **460** (2008) 1–129 [0704.1800].

[153] J. R. Ellis and M. K. Gaillard, *Fermion Masses and Higgs Representations in $SU(5)$*, *Phys.Lett.* **B88** (1979) 315.

[154] E. Witten, *Dynamical Breaking of Supersymmetry*, *Nucl.Phys.* **B188** (1981) 513.

[155] T. Yamashita, *Doublet-Triplet Splitting in an $SU(5)$ Grand Unification*, *Phys.Rev.* **D84** (2011) 115016.

[156] G. R. Farrar and M. Losada, *SUSY and the electroweak phase transition*, *Phys.Lett.* **B406** (1997) 60–65 [hep-ph/9612346].

[157] T. Takagi, *On an algebraic problem related to an analytic theorem of Carathéodory and Fejer and on an allied theorem of Landau*, *Japan J.Math.* **1** (1925) 83.

[158] S. Weinberg, *Baryon and Lepton Nonconserving Processes*, *Phys.Rev.Lett.* **43** (1979) 1566–1570.

[159] B. Pontecorvo, *Mesonium and anti-mesonium*, *Sov.Phys.JETP* **6** (1957) 429.

[160] B. Pontecorvo, *Inverse beta processes and nonconservation of lepton charge*, *Sov.Phys.JETP* **7** (1958) 172–173.

[161] Z. Maki, M. Nakagawa and S. Sakata, *Remarks on the unified model of elementary particles*, *Prog.Theor.Phys.* **28** (1962) 870–880.

[162] A. Sakharov, *Violation of CP Invariance, C Asymmetry, and Baryon Asymmetry of the Universe*, *Pisma Zh.Eksp.Teor.Fiz.* **5** (1967) 32–35.

[163] M. Shaposhnikov, *Structure of the High Temperature Gauge Ground State and Electroweak Production of the Baryon Asymmetry*, *Nucl.Phys.* **B299** (1988) 797.

[164] K. Kajantie, M. Laine, K. Rummukainen and M. E. Shaposhnikov, *Is there a hot electroweak phase transition at m(H) larger or equal to m(W)?*, *Phys.Rev.Lett.* **77** (1996) 2887–2890 [hep-ph/9605288].

[165] M. Carena, G. Nardini, M. Quiros and C. Wagner, *The Baryogenesis Window in the MSSM*, *Nucl.Phys.* **B812** (2009) 243–263 [0809.3760].

[166] D. Curtin, P. Jaiswal and P. Meade, *Excluding Electroweak Baryogenesis in the MSSM*, *JHEP* **1208** (2012) 005 [1203.2932].

[167] J. R. Espinosa, T. Konstandin and F. Riva, *Strong Electroweak Phase Transitions in the Standard Model with a Singlet*, *Nucl.Phys.* **B854** (2012) 592–630.

[168] J. R. Espinosa, B. Gripaios, T. Konstandin and F. Riva, *Electroweak Baryogenesis in Non-minimal Composite Higgs Models*, *JCAP* **1201** (2012) 012 [1110.2876].

[169] M. Yoshimura, *Unified Gauge Theories and the Baryon Number of the Universe*, *Phys.Rev.Lett.* **41** (1978) 281–284.

[170] A. Y. Ignatiev, N. Krasnikov, V. Kuzmin and A. Tavkhelidze, *Universal CP Noninvariant Superweak Interaction and Baryon Asymmetry of the Universe*, *Phys.Lett.* **B76** (1978) 436–438.

[171] S. Weinberg, *Cosmological Production of Baryons*, *Phys.Rev.Lett.* **42** (1979) 850–853.

[172] I. Affleck and M. Dine, *A New Mechanism for Baryogenesis*, *Nucl.Phys.* **B249** (1985) 361.

[173] S. Davidson, E. Nardi and Y. Nir, *Leptogenesis*, *Phys.Rept.* **466** (2008) 105–177 [0802.2962].

[174] G. Giudice, A. Notari, M. Raidal, A. Riotto and A. Strumia, *Towards a complete theory of thermal leptogenesis in the SM and MSSM*, *Nucl.Phys.* **B685** (2004) 89–149 [hep-ph/0310123].

[175] S. M. Bilenky, J. Hosek and S. Petcov, *On Oscillations of Neutrinos with Dirac and Majorana Masses*, *Phys.Lett.* **B94** (1980) 495.

[176] W. Rodejohann, *Neutrino-less Double Beta Decay and Particle Physics*, *Int.J.Mod.Phys.* **E20** (2011) 1833–1930 [1106.1334].

[177] H. Murayama, H. Suzuki, T. Yanagida and J. Yokoyama, *Chaotic inflation and baryogenesis by right-handed sneutrinos*, *Phys.Rev.Lett.* **70** (1993) 1912–1915.

[178] J. R. Ellis, M. Raidal and T. Yanagida, *Sneutrino inflation in the light of WMAP: Reheating, leptogenesis and flavor violating lepton decays*, *Phys.Lett.* **B581** (2004) 9–18 [hep-ph/0303242].

[179] S. Antusch, M. Bastero-Gil, S. F. King and Q. Shafi, *Sneutrino hybrid inflation in supergravity*, *Phys.Rev.* **D71** (2005) 083519 [hep-ph/0411298].

[180] S. Antusch, J. P. Baumann, V. F. Domcke and P. M. Kostka, *Sneutrino Hybrid Inflation and Nonthermal Leptogenesis*, *JCAP* **1010** (2010) 006 [1007.0708].

[181] K. Hamaguchi, H. Murayama and T. Yanagida, *Leptogenesis from N dominated early universe*, *Phys.Rev.* **D65** (2002) 043512 [hep-ph/0109030].

[182] H. Murayama and T. Yanagida, *Leptogenesis in supersymmetric standard model with right-handed neutrino*, *Phys.Lett.* **B322** (1994) 349–354 [hep-ph/9310297].

[183] M. Dine, L. Randall and S. D. Thomas, *Baryogenesis from flat directions of the supersymmetric standard model*, *Nucl.Phys.* **B458** (1996) 291–326 [hep-ph/9507453].

[184] M. Fujii, K. Hamaguchi and T. Yanagida, *Leptogenesis with almost degenerate majorana neutrinos*, *Phys.Rev.* **D65** (2002) 115012 [hep-ph/0202210].

[185] L. Covi, E. Roulet and F. Vissani, *CP violating decays in leptogenesis scenarios*, *Phys.Lett.* **B384** (1996) 169–174 [hep-ph/9605319].

[186] W. Buchmuller and M. Plumacher, *CP asymmetry in Majorana neutrino decays*, *Phys.Lett.* **B431** (1998) 354–362 [hep-ph/9710460].

[187] S. Davidson and A. Ibarra, *A Lower bound on the right-handed neutrino mass from leptogenesis*, *Phys.Lett.* **B535** (2002) 25–32 [hep-ph/0202239].

[188] S. P. Martin, *A Supersymmetry primer*, hep-ph/9709356.

[189] J. R. Ellis, A. D. Linde and D. V. Nanopoulos, *Inflation Can Save the Gravitino*, *Phys.Lett.* **B118** (1982) 59.

[190] D. V. Nanopoulos, K. A. Olive and M. Srednicki, *After Primordial Inflation*, *Phys.Lett.* **B127** (1983) 30.

[191] M. Y. Khlopov and A. D. Linde, *Is It Easy to Save the Gravitino?*, *Phys.Lett.* **B138** (1984) 265–268.

[192] V. S. Rychkov and A. Strumia, *Thermal production of gravitinos*, *Phys.Rev.* **D75** (2007) 075011 [hep-ph/0701104].

[193] A. H. Chamseddine, R. L. Arnowitt and P. Nath, *Locally Supersymmetric Grand Unification*, *Phys.Rev.Lett.* **49** (1982) 970.

[194] R. Barbieri, S. Ferrara and C. A. Savoy, *Gauge Models with Spontaneously Broken Local Supersymmetry*, *Phys.Lett.* **B119** (1982) 343.

[195] L. E. Ibanez, *Locally Supersymmetric $SU(5)$ Grand Unification*, *Phys.Lett.* **B118** (1982) 73.

[196] D. E. Kaplan, G. D. Kribs and M. Schmaltz, *Supersymmetry breaking through transparent extra dimensions*, *Phys.Rev.* **D62** (2000) 035010 [hep-ph/9911293].

[197] Z. Chacko, M. A. Luty, A. E. Nelson and E. Ponton, *Gaugino mediated supersymmetry breaking*, *JHEP* **0001** (2000) 003 [hep-ph/9911323].

[198] L. Covi, J. E. Kim and L. Roszkowski, *Axinos as cold dark matter*, *Phys.Rev.Lett.* **82** (1999) 4180–4183 [hep-ph/9905212].

[199] J. L. Feng, A. Rajaraman and F. Takayama, *Superweakly interacting massive particles*, *Phys.Rev.Lett.* **91** (2003) 011302 [hep-ph/0302215].

[200] J. L. Feng, S. Su and F. Takayama, *Supergravity with a gravitino LSP*, *Phys.Rev.* **D70** (2004) 075019 [hep-ph/0404231].

[201] F. D. Steffen, *Dark Matter Candidates - Axions, Neutralinos, Gravitinos, and Axinos*, *Eur.Phys.J.* **C59** (2009) 557–588 [0811.3347].

[202] R. Kallosh, L. Kofman, A. D. Linde and A. Van Proeyen, *Gravitino production after inflation*, *Phys.Rev.* **D61** (2000) 103503 [hep-th/9907124].

[203] G. Giudice, I. Tkachev and A. Riotto, *Nonthermal production of dangerous relics in the early universe*, *JHEP* **9908** (1999) 009 [hep-ph/9907510].

[204] T. Moroi, H. Murayama and M. Yamaguchi, *Cosmological constraints on the light stable gravitino*, *Phys.Lett.* **B303** (1993) 289–294.

[205] A. de Gouvea, T. Moroi and H. Murayama, *Cosmology of supersymmetric models with low-energy gauge mediation*, *Phys.Rev.* **D56** (1997) 1281–1299 [hep-ph/9701244].

[206] L. Covi, J. Hasenkamp, S. Pokorski and J. Roberts, *Gravitino Dark Matter and general neutralino NLSP*, *JHEP* **0911** (2009) 003 [0908.3399].

[207] C. F. Berger, L. Covi, S. Kraml and F. Palorini, *The Number density of a charged relic*, *JCAP* **0810** (2008) 005 [0807.0211].

[208] M. Kusakabe, T. Kajino, T. Yoshida and G. J. Mathews, *Effect of Long-lived Strongly Interacting Relic Particles on Big Bang Nucleosynthesis*, *Phys.Rev.* **D80** (2009) 103501 [0906.3516].

[209] R. H. Cyburt, J. R. Ellis, B. D. Fields, K. A. Olive and V. C. Spanos, *Bound-State Effects on Light-Element Abundances in Gravitino Dark Matter Scenarios*, *JCAP* **0611** (2006) 014.

[210] T. Kanzaki, M. Kawasaki, K. Kohri and T. Moroi, *Cosmological constraints on gravitino LSP scenario with sneutrino NLSP*, *Phys.Rev.* **D75** (2007) 025011.

[211] W. Buchmuller, K. Hamaguchi, M. Ibe and T. Yanagida, *Eluding the BBN constraints on the stable gravitino*, *Phys.Lett.* **B643** (2006) 124–126 [hep-ph/0605164].

[212] J. Hasenkamp and J. Kersten, *Leptogenesis, Gravitino Dark Matter and Entropy Production*, *Phys.Rev.* **D82** (2010) 115029 [1008.1740].

[213] A. De Simone, M. Garny, A. Ibarra and C. Weniger, *Supersymmetric Leptogenesis with a Light Hidden Sector*, *JCAP* **1007** (2010) 017 [1004.4890].

[214] C. Cheung, J. Mardon, Y. Nomura and J. Thaler, *A Definitive Signal of Multiple Supersymmetry Breaking*, *JHEP* **1007** (2010) 035 [1004.4637].

[215] W. Buchmuller, L. Covi, K. Hamaguchi, A. Ibarra and T. Yanagida, *Gravitino Dark Matter in R-Parity Breaking Vacua*, *JHEP* **0703** (2007) 037.

[216] F. Takayama and M. Yamaguchi, *Gravitino dark matter without R-parity*, *Phys.Lett.* **B485** (2000) 388–392 [hep-ph/0005214].

[217] G. Bertone, W. Buchmuller, L. Covi and A. Ibarra, *Gamma-Rays from Decaying Dark Matter*, *JCAP* **0711** (2007) 003 [0709.2299].

[218] K. Ishiwata, S. Matsumoto and T. Moroi, *High Energy Cosmic Rays from the Decay of Gravitino Dark Matter*, *Phys.Rev.* **D78** (2008) 063505 [0805.1133].

[219] A. Ibarra and D. Tran, *Antimatter Signatures of Gravitino Dark Matter Decay*, *JCAP* **0807** (2008) 002 [0804.4596].

[220] L. Covi, M. Grefe, A. Ibarra and D. Tran, *Unstable Gravitino Dark Matter and Neutrino Flux*, *JCAP* **0901** (2009) 029.

[221] W. Buchmuller, K. Hamaguchi, M. Ratz and T. Yanagida, *Supergravity at colliders*, *Phys.Lett.* **B588** (2004) 90–98 [hep-ph/0402179].

[222] J. R. Ellis, A. R. Raklev and O. K. Oye, *Gravitino dark matter scenarios with massive metastable charged sparticles at the LHC*, *JHEP* **0610** (2006) 061 [hep-ph/0607261].

[223] S. Bobrovskyi, W. Buchmuller, J. Hajer and J. Schmidt, *Broken R-Parity in the Sky and at the LHC*, *JHEP* **1010** (2010) 061 [1007.5007].

[224] S. Bobrovskyi, W. Buchmuller, J. Hajer and J. Schmidt, *Quasi-stable neutralinos at the LHC*, *JHEP* **1109** (2011) 119 [1107.0926].

[225] M. Kawasaki and T. Moroi, *Gravitino decay into a neutrino and a sneutrino in the inflationary universe*, *Phys.Lett.* **B346** (1995) 27–34 [hep-ph/9408321].

[226] J. Hasenkamp, *Dark radiation from the axino solution of the gravitino problem*, *Phys.Lett.* **B707** (2012) 121–128.

[227] G. F. Giudice, M. A. Luty, H. Murayama and R. Rattazzi, *Gaugino mass without singlets*, *JHEP* **9812** (1998) 027 [hep-ph/9810442].

[228] L. Randall and R. Sundrum, *Out of this world supersymmetry breaking*, *Nucl.Phys.* **B557** (1999) 79–118 [hep-th/9810155].

[229] M. Ibe and T. T. Yanagida, *The Lightest Higgs Boson Mass in Pure Gravity Mediation Model*, *Phys.Lett.* **B709** (2012) 374–380 [1112.2462].

[230] K. S. Jeong, M. Shimosuka and M. Yamaguchi, *Light Higgsino in Heavy Gravitino Scenario with Successful Electroweak Symmetry Breaking*, *JHEP* **1209** (2012) 050 [1112.5293].

[231] S. Krippendorf, H. P. Nilles, M. Ratz and M. W. Winkler, *The heterotic string yields natural supersymmetry*, *Phys.Lett.* **B712** (2012) 87–92 [1201.4857].

[232] S. Raby, *SUSY GUT Model Building*, *Eur.Phys.J.* **C59** (2009) 223–247 [0807.4921].

[233] Y. Grossman and M. Neubert, *Neutrino masses and mixings in nonfactorizable geometry*, *Phys.Lett.* **B474** (2000) 361–371 [hep-ph/9912408].

[234] T. Gherghetta and A. Pomarol, *Bulk fields and supersymmetry in a slice of AdS*, *Nucl.Phys.* **B586** (2000) 141–162 [hep-ph/0003129].

[235] W. Buchmuller, K. Hamaguchi, O. Lebedev and M. Ratz, *Supersymmetric Standard Model from the Heterotic String (II)*, *Nucl.Phys.* **B785** (2007) 149–209 [hep-th/0606187].

[236] J. Sato and T. Yanagida, *Large lepton mixing in a coset space family unification on* $E_7/SU(5) \times U(1)^3$, *Phys.Lett.* **B430** (1998) 127–131 [hep-ph/9710516].

[237] N. Irges, S. Lavignac and P. Ramond, *Predictions from an anomalous* $U(1)$ *model of Yukawa hierarchies*, *Phys.Rev.* **D58** (1998) 035003 [hep-ph/9802334].

[238] W. Buchmuller, D. Delepine and L. T. Handoko, *Neutrino mixing and flavor changing processes*, *Nucl.Phys.* **B576** (2000) 445–465 [hep-ph/9912317].

[239] F. Vissani, *Large mixing, family structure, and dominant block in the neutrino mass matrix*, *JHEP* **9811** (1998) 025 [hep-ph/9810435].

[240] L. J. Hall, H. Murayama and N. Weiner, *Neutrino mass anarchy*, *Phys.Rev.Lett.* **84** (2000) 2572–2575 [hep-ph/9911341].

[241] J. Sato and T. Yanagida, *Low-energy predictions of lopsided family charges*, *Phys.Lett.* **B493** (2000) 356–365.

[242] F. Vissani, *Expected properties of massive neutrinos for mass matrices with a dominant block and random coefficients order unity*, *Phys.Lett.* **B508** (2001) 79–84 [hep-ph/0102236].

[243] G. Cowan, *Statistical data analysis*, *Oxford, UK: Clarendon* (1998) 197 p.

[244] K. Abe *et. al.* [T2K Collaboration], *Indication of Electron Neutrino Appearance from an Accelerator-produced Off-axis Muon Neutrino Beam*, *Phys.Rev.Lett.* **107** (2011) 041801 [1106.2822].

[245] P. Adamson *et. al.* [MINOS Collaboration], *Improved search for muon-neutrino to electron-neutrino oscillations in MINOS*, *Phys.Rev.Lett.* **107** (2011) 181802.

[246] Y. Abe *et. al.* [DOUBLE-CHOOZ Collaboration], *Indication for the disappearance of reactor electron antineutrinos in the Double Chooz experiment*, *Phys.Rev.Lett.* **108** (2012) 131801.

[247] F. An *et. al.* [DAYA-BAY Collaboration], *Observation of electron-antineutrino disappearance at Daya Bay*, *Phys.Rev.Lett.* **108** (2012) 171803.

[248] J. Ahn *et. al.* [RENO collaboration], *Observation of Reactor Electron Antineutrino Disappearance in the RENO Experiment*, *Phys.Rev.Lett.* **108** (2012) 191802 [1204.0626].

[249] [Planck Collaboration], *The Scientific programme of planck*, astro-ph/0604069.

[250] M. Beck [KATRIN Collaboration], *The KATRIN Experiment*, *J.Phys.Conf.Ser.* **203** (2010) 012097 [0910.4862].

[251] H. Klapdor-Kleingrothaus, A. Dietz, H. Harney and I. Krivosheina, *Evidence for neutrinoless double beta decay*, *Mod.Phys.Lett.* **A16** (2001) 2409–2420 [hep-ph/0201231].

[252] G. Meierhofer [GERDA Collaboration], *GERDA: A new neutrinoless double beta experiment using Ge-76*, *J.Phys.Conf.Ser.* **312** (2011) 072011.

[253] G. Altarelli, F. Feruglio and I. Masina, *Models of neutrino masses: Anarchy versus hierarchy*, *JHEP* **0301** (2003) 035 [hep-ph/0210342].

[254] I. Masina and C. A. Savoy, *On power and complementarity of the experimental constraints on seesaw models*, *Phys.Rev.* **D71** (2005) 093003 [hep-ph/0501166].

[255] F. Plentinger, G. Seidl and W. Winter, *The Seesaw mechanism in quark-lepton complementarity*, *Phys.Rev.* **D76** (2007) 113003 [0707.2379].

[256] F. Plentinger, G. Seidl and W. Winter, *Systematic parameter space search of extended quark-lepton complementarity*, *Nucl.Phys.* **B791** (2008) 60–92 [hep-ph/0612169].

[257] T. Asaka, W. Buchmuller and L. Covi, *Quarks and leptons between branes and bulk*, *Phys.Lett.* **B563** (2003) 209–216 [hep-ph/0304142].

[258] J. Wess and J. Bagger, *Supersymmetry and supergravity*, *Princeton, USA: Univ. Pr.* (1992) 259 p.

[259] D. Bailin and A. Love, *Supersymmetric gauge field theory and string theory*, *Bristol, UK: IOP* (1994) 322 p.

[260] S. Weinberg, *The quantum theory of fields. Vol. 3: Supersymmetry*, *Cambridge, UK: Univ. Pr.* (2000) 419 p.

[261] H. K. Dreiner, H. E. Haber and S. P. Martin, *Two-component spinor techniques and Feynman rules for quantum field theory and supersymmetry*, *Phys.Rept.* **494** (2010) 1–196 [0812.1594].

[262] E. J. Copeland, S. Pascoli and A. Rajantie, *Dynamics of tachyonic preheating after hybrid inflation*, *Phys.Rev.* **D65** (2002) 103517 [hep-ph/0202031].

[263] W. Buchmuller, L. Covi and D. Delepine, *Inflation and supersymmetry breaking*, *Phys.Lett.* **B491** (2000) 183–189 [hep-ph/0006168].

[264] M. Hindmarsh, S. Stuckey and N. Bevis, *Abelian Higgs Cosmic Strings: Small Scale Structure and Loops*, *Phys.Rev.* **D79** (2009) 123504 [0812.1929].

[265] J.-F. Dufaux, D. G. Figueroa and J. Garcia-Bellido, *Gravitational Waves from Abelian Gauge Fields and Cosmic Strings at Preheating*, *Phys.Rev.* **D82** (2010) 083518 [1006.0217].

[266] R. Battye and A. Moss, *Updated constraints on the cosmic string tension*, *Phys.Rev.* **D82** (2010) 023521 [1005.0479].

[267] J. Dunkley, R. Hlozek, J. Sievers, V. Acquaviva, P. Ade *et. al.*, *The Atacama Cosmology Telescope: Cosmological Parameters from the 2008 Power Spectra*, *Astrophys.J.* **739** (2011) 52 [1009.0866].

[268] J. Urrestilla, N. Bevis, M. Hindmarsh and M. Kunz, *Cosmic string parameter constraints and model analysis using small scale Cosmic Microwave Background data*, *JCAP* **1112** (2011) 021 [1108.2730].

[269] C. Dvorkin, M. Wyman and W. Hu, *Cosmic String constraints from WMAP and the South Pole Telescope*, *Phys.Rev.* **D84** (2011) 123519 [1109.4947].

[270] R. Battye, B. Garbrecht and A. Moss, *Tight constraints on F- and D-term hybrid inflation scenarios*, *Phys.Rev.* **D81** (2010) 123512 [1001.0769].

[271] R. Jeannerot and M. Postma, *Confronting hybrid inflation in supergravity with CMB data*, *JHEP* **0505** (2005) 071 [hep-ph/0503146].

[272] J. Garcia-Bellido, M. Garcia Perez and A. Gonzalez-Arroyo, *Symmetry breaking and false vacuum decay after hybrid inflation*, *Phys.Rev.* **D67** (2003) 103501 [hep-ph/0208228].

[273] J. Berges, D. Gelfand and J. Pruschke, *Quantum theory of fermion production after inflation*, *Phys.Rev.Lett.* **107** (2011) 061301 [1012.4632].

[274] F. Hahn-Woernle, M. Plumacher and Y. Wong, *Full Boltzmann equations for leptogenesis including scattering*, *JCAP* **0908** (2009) 028 [0907.0205].

[275] W. Buchmuller, P. Di Bari and M. Plumacher, *Cosmic microwave background, matter - antimatter asymmetry and neutrino masses*, *Nucl.Phys.* **B643** (2002) 367–390 [hep-ph/0205349].

[276] G. Aad *et. al.* [ATLAS Collaboration], *Search for supersymmetry in final states with jets, missing transverse momentum and one isolated lepton in* $\sqrt{s} = 7\ TeV$ *pp collisions using* $1\,fb^{-1}$ *of ATLAS data*, *Phys.Rev.* **D85** (2012) 012006 [1109.6606].

[277] S. Chatrchyan *et. al.* [CMS Collaboration], *Search for Supersymmetry at the LHC in Events with Jets and Missing Transverse Energy*, *Phys.Rev.Lett.* **107** (2011) 221804 [1109.2352].

[278] F. Brummer and W. Buchmuller, *Light Higgsinos as Heralds of Higher-Dimensional Unification*, *JHEP* **1107** (2011) 010 [1105.0802].

[279] N. Arkani-Hamed, A. Delgado and G. Giudice, *The Well-tempered neutralino*, *Nucl.Phys.* **B741** (2006) 108–130 [hep-ph/0601041].

[280] J. Hisano, S. Matsumoto, M. Nagai, O. Saito and M. Senami, *Non-perturbative effect on thermal relic abundance of dark matter*, *Phys.Lett.* **B646** (2007) 34–38 [hep-ph/0610249].

[281] M. Cirelli, A. Strumia and M. Tamburini, *Cosmology and Astrophysics of Minimal Dark Matter*, *Nucl.Phys.* **B787** (2007) 152–175 [0706.4071].

[282] F. Borzumati, T. Bringmann and P. Ullio, *Dark matter from late decays and the small-scale structure problems*, *Phys.Rev.* **D77** (2008) 063514 [hep-ph/0701007].

[283] J. Hisano, S. Matsumoto, M. M. Nojiri and O. Saito, *Direct detection of the Wino and Higgsino-like neutralino dark matters at one-loop level*, *Phys.Rev.* **D71** (2005) 015007 [hep-ph/0407168].

[284] H. Baer, V. Barger and P. Huang, *Hidden SUSY at the LHC: the light higgsino-world scenario and the role of a lepton collider*, *JHEP* **1111** (2011) 031 [1107.5581].

[285] S. Bobrovskyi, F. Brummer, W. Buchmuller and J. Hajer, *Searching for light higgsinos with b-jets and missing leptons*, *JHEP* **1201** (2012) 122 [1111.6005].

[286] T. Moroi and K. Nakayama, *Wino LSP detection in the light of recent Higgs searches at the LHC*, *Phys.Lett.* **B710** (2012) 159–163 [1112.3123].

[287] W. Buchmller, V. Domcke and K. Schmitz, *Superconformal D-Term Inflation*, *JCAP* **1304** (2013) 019 [1210.4105].

[288] W. Buchmuller, V. Domcke, K. Kamada and K. Schmitz, *The Gravitational Wave Spectrum from Cosmological B-L Breaking*, 1305.3392.

[289] A. Anisimov, W. Buchmuller, M. Drewes and S. Mendizabal, *Quantum Leptogenesis I*, *Annals Phys.* **326** (2011) 1998–2038 [1012.5821].

[290] E. Roulet, L. Covi and F. Vissani, *On the CP asymmetries in Majorana neutrino decays*, *Phys.Lett.* **B424** (1998) 101–105 [hep-ph/9712468].